Entropy Generation Effects During Flow And Heat Transfer Processes

By

Adnan Saeed Butt

DEPARTMENT OF MATHEMATICS
QUAID-I-AZAM UNIVERSITY
ISLAMABAD, PAKISTAN

2017

Entropy Generation Effects During Flow And Heat Transfer Processes

By

Adnan Saeed Butt

Supervised By

Dr. Asif Ali

DEPARTMENT OF MATHEMATICS

QUAID-I-AZAM UNIVERSITY

ISLAMABAD, PAKISTAN

2017

Entropy Generation Effects During Flow And Heat Transfer Processes

By

Adnan Saeed Butt

A THESIS SUBMITTED IN THE PARTIAL FULFILLMENT OF THE REQUIREMENTS FOR THE DEGREE OF

DOCTOR OF PHILOSOPHY

IN

MATHEMATICS

Supervised by

Dr. Asif Ali

DEPARTMENT OF MATHEMATICS
QUAID-I-AZAM UNIVERSITY
ISLAMABAD, PAKISTAN
2017

Dedication

To my parents
for their enthusiasm,
compassion,
and patience

Acknowledgement

Praise is to Allah Almighty, Creator and Sustainer of the heavens and the earth, and everything between them, Lord of lords, who gave me the potential and ability to complete this dissertation. All of my respect and veneration goes to the Holy Prophet Muhammad (Peace be upon him) who showed humanity the right path, brought the message of peace and love and emphasized the necessity and importance of knowledge. Respect is due for his family, friends, companions and all followers (peace be upon all of them).

I owe my deepest gratitude to Prof. Dr. Asif Ali who not only supervised this dissertation but always has been a source of stimulation for me. He always encouraged me to set prodigious goals and to find own ways to achieve them. His stimulating suggestions, conscious guidance and superb planning abetted me in the completion of this thesis. This dissertation could not have been completed without generous support and guidance of Dr Ahmer Mehmood and Dr Sufian Munawar. Their fabulous provision, valuable suggestions and careful readings are extremely accredited in the completion of this work. I am also grateful to Prof. Dr. Tasawar Hayat, chair department of Mathematics, for providing research oriented environment and excellent facilities at the department. I would always be indebted to all my teachers of Quaid-i-Azam University by whom I gained marvelous skills and knowledge. The financial support from Higher Education Commission (HEC) of Pakistan is highly acknowledged without which this research work could not be accomplished definitely.

I gratefully acknowledge the marvelous company of my closest friends Attaullah, Sajjad Shaukat, Dr. Nazim Tufail, Dr. Awais Yousaf, Dr. Abdur Razaq, Dr. Sabir Ali Shahzad, Dr. Qasim, Dr. Aqeel, Dr. Amanullah Dar, Dr. Syed Muhammad Imran, Dr. Azeem, Dr. Saira, Muhammad Nasir, Muhammad Raees, Tariq Nawaz, Mughees, Atif Khan and Ifzan Arshad who have continuously supported me during the Ph.D. We spend delightful moments together at QAU. I am thankful to my colleagues, my seniors and juniors for their moral support and good wishes. Moreover, I am thankful to all those numerous well-wishers who prayed for my success, I am not being able to mention here all of them.

Finally, my sincere gratitude goes to my parents who supported me indirectly with great concern, generous support, love and prayers for my achievements. Words are countless to say thank to those benevolent hands that sincerely raised me with gentle love, care and patience. Without their prayers

and sacrifices I could not be able to successfully complete whole of my educational career. May almighty Allah reward all of them with great honor in this world and the world hereafter.

Adnan Saeed Butt

Abstract

Entropy is a useful, measurable quantity which is widely used in the field of fluid mechanics and heat transfer to study the energy losses that cannot be reversed. Entropy based analysis of flow and heat transfer phenomena helps to identify the factors that are responsible for the entropy production. Knowing about the causes of entropy generation is essential because large amount of irreversible energy losses do affect the efficiency of thermo-mechanical devices in practical applications.

In this dissertation, entropy generation effects have been inspected in the boundary layer flow and heat transfer of viscous fluid due to stretching surfaces. Different geometrical configurations of flat and curved stretchable sheets as well as channels with stretching walls have been considered and the effects of presence of magnetic field, porous medium and slip effects on entropy production are examined. The problems have been investigated theoretically by using appropriate models that are derived from the laws of conservation of mass, momentum and energy. Moreover, second law of thermodynamics is applied for the examination of entropy generation in the considered thermal processes.

Analytical and numerical methods have been employed to obtain the solutions of the governing non-linear equations. Homotopy Analysis Method (HAM) has been used to obtain the analytic solution and shooting technique has been utilized for the numerical computations. The accuracy and validity of the obtained analytical and numerical solutions have been proved by comparing them with available results under limiting conditions or by comparing the analytical and numerical values with each other.

The studies carried out in this thesis reveal that entropy generation effects are more significant near the stretching surfaces. Furthermore, the magnetic field is also a strong source of entropy production. The viscous dissipation effects are also observed to be responsible for entropy generation. It is also noted that the entropy generation is more pronounced in the case of curved stretching surface.

Author's Declaration

I **Adnan Saeed Butt** hereby state that my PhD thesis titled **Entropy Generation Effects During Flow and Heat Transfer Processes** is my own work and has not been submitted previously by me for taking any degree from the Quaid-i-Azam University Islamabad, Pakistan or anywhere else in the country/world.

At any time if my statement is found to be incorrect even after my graduate the university has the right to withdraw my PhD degree.

Student/Author's Signature: 

Name of Student: **Adnan Saeed Butt**

Date: **10-05-2017**

Plagiarism Undertaking

I solemnly declare that research work presented in the thesis titled "**Entropy Generation Effects During Flow and Heat Transfer Processes**" is solely my research work with no significant contribution from any other person. Small contribution/help wherever taken has been duly acknowledged and that complete thesis has been written by me.

I understand the zero tolerance policy of the HEC and **Quaid-i-Azam University** towards plagiarism. Therefore, I as an Author of the above titled thesis declare that no portion of my thesis has been plagiarized and any material used as reference is properly referred/cited.

I undertake that if I am found guilty of any formal plagiarism in the above titled thesis even afterward of PhD degree, the University reserves the rights to withdraw/revoke my PhD degree and that HEC and the University has the right to publish my name on the HEC/University Website on which names of students are placed who submitted plagiarized thesis.

Student/Author Signature: 

Name: Adnan Saeed Butt

Entropy Generation Effects During Flow and Heat Transfer Processes

By

Adnan Saeed Butt

CERTIFICATE

A THESIS SUBMITTED IN THE PARTIAL FULFILLMENT OF THE REQUIREMENTS FOR THE DEGREE OF DOCTOR OF PHILOSOPHY

We accept this thesis as conforming to the required standard.

1. _____

Dr. Asif Ali
(Supervisor)

2. _____

Prof. Dr. Muhammad Yousaf Malik
(Chairman)

3. _____

Dr. Shahzad Mahmood
(External Examiner)
Principal Scientist
PINTECH, NILORE, Islamabad

4. _____

Prof. Dr. Nazir Ahmed Mir
(External Examiner)
Department of Basic Sciences
Riphah International University,
I-14 Hajj Complex Islamabad

Department of Mathematics
Quaid-I-Azam University,
Islamabad, PAKISTAN
2017

Certificate of Approval

This is to certify that the research work presented in this thesis entitled **Entropy Generation Effects During Flow and Heat Transfer Processes** was conducted by Mr. **Adnan Saeed Butt** under the supervision of **Dr. Asif Ali**. No part of this thesis has been submitted anywhere else for any other degree. This thesis is submitted to the Department of Mathematics, Quaid-i-Azam University, Islamabad in partial fulfillment of the requirements for the degree of Doctor of Philosophy in Field of Mathematics from Department of Mathematics, Quaid-i-Azam University Islamabad, Pakistan.

Student Name: **Adnan Saeed Butt** Signature: _____

External committee:

a) **External Examiner 1**: Signature: _____
Name: **Dr. Nazir Ahmad Mir**
Designation: Professor
Office Address: Department of Basic Sciences
Riphah International University,
I-14 Hajj Complex Islamabad

b) **External Examiner 2**: Signature: _____
Name**: Dr. Shahzad Mahmood**
Designation: Principal Scientist
Office Address: PINSTECH, Nilore, Islamabad

c) **Internal Examiner** : Signature: _____
Name: **Dr. Asif Ali**
Designation: Associate Professor
Office Address: Department of Mathematics, QAU Islamabad.

Supervisor Name: Signature: _____
Name: **Dr. Asif Ali**
Designation: Associate Professor
Office Address: Department of Mathematics, QAU Islamabad.

Name of Dean/ HOD Signature: _____

Name: **Dr. Muhammad Yousaf Malik**
Designation: Professor
Office Address: Department of Mathematics, QAU Islamabad.

Contents

List of Figures

List of tables

Nomenclature

Latin Symbols

$a,\ b,\ c$	Constants having dimension $1/T$
$\mathbf{B}$	Magnetic flux
$\mathbf{B_0}$	Applied magnetic field
$\mathbf{b_0}$	Induced magnetic field
(b_x, b_y, b_z)	body force components in (x, y, z)
(b_r, b_φ, b_z)	body force components in (r, φ, z)
Br	Brinkman number
Bi	Biot number
Be	Bejan number
c_p	Specific heat
C_f	Skin friction coefficient
C_i	Constants of integration
D	Domain
E_m	Squared residual error
Ec	Eckert number
Ec_x	Local Eckert number
$\mathbf{E}$	Electric field

f	Dimensionless stream function
f', g'	Dimensionless velocities
$f_0,\ g_0,\ v_0$	Initial guess for HAM solutions
$f_m,\ g_m,\ v_m$	mth order HAM solutions
f_m^*, g_m^*	Special solutions
$\mathbf{J}$	Current density
h'	Heat transfer coefficient
K	Permeability parameter
k	Thermal conductivity
k'	Permeability of the medium
L	Characteristic length
m	Order of approximation
M	Hartmann number
n	Temperature exponent
$p\ ,\ P$	Pressure
P^*	Dimensionless pressure
Nu	Nusselt number
$Nu_x,\ Nu_r$	Local Nusselt numbers
Ns	Local entropy generation number
N_H	Local entropy generation due to heat transfer
N_f	Local entropy generation due to fluid friction
N_m	Local entropy generation due to magnetic field

Ns_{tot}	Total entropy generation number
Pr	Prandtl number
q	Embedding parameter in HAM
q_w	Heat flux from the surface
Q	Electric charge density
$\mathbf{r}$	Position vector
R	Radius of cylinder
$\mathrm{Re}, \mathrm{Re}_L$	Reynolds number
$\mathrm{Re}_r, \mathrm{Re}_x$	Loal Reynolds number
S_G	Local entropy generation rate per unit volume
S_{G0}	Characteristic entropy generation rate
S_q	Squeezing parameter
T	Temperature of the fluid
T_{ref}	Reference temperature
T_f	Temperature of the hot fluid
T_w	Temperature of stretching surface
T_h	Temperature of upper stretching surface
T_∞	Temperature of the ambient fluid
ΔT	Temperature difference
U_0	Reference velocity
u_w, U_w	Velocity of stretching surface

$\mathbf{V}$	Velocity vector
V_0	Suction/injection velocity
V_h	Squeezing velocity
w_i	Transformation functions
w_0	Dimensionless suction/injection parameter
(u, v, w)	Velocity components
(x, y, z)	Cartesian coordinates
(r, φ, z)	Cylindrical coordinates
t	Time

Greek Symbols

α	Stretching ratio parameter
α'	Thermal diffusivity
β^*	Slip parameter
γ	Dimensionless slip parameter
$\delta = r/L$	Dimensionless parameter
ε_0	Permittivity of free space
η	Self similar space variable
$\Delta\eta$	Step size
$\eta_{\max}$	Numerical infinity
θ	Dimensionless temperature
κ	Curvature Parameter

μ_0	Magnetic permeability
μ	Dynamic viscosity of fluid
ν	Kinematic viscosity of fluid
$\xi = y/x$	Dimensionless parameter
τ_w	Local shear stress
ρ	Density of fluid
σ	Electrical conductivity of fluid
ψ	Stream function
$\Lambda,\ \Gamma,\ \Theta$	Deformation functions in HAM
Φ	Viscous dissipation
ω_0	Characteristic angular velocity
ω	Rotation parameter
$\boldsymbol{\omega}^*$	Angular velocity
Ω	Dimensionless temperature difference
$\hbar$ or $\hbar_i$	Convergence control parameter(s)
$\mathcal{L}$ or $\mathcal{L}_i$	Linear operator(s)
$\mathcal{N}$ or $\mathcal{N}_i$	Non-linear operator(s)
∇	Gradient operator

List of abbreviations

HAM	Homotopy Analysis Method

MHD	Magnetohydrodynamics

Chapter 1

Introduction

This chapter is concerned with the historical background of the entropy and literature review discussed in the subsequent chapters for the investigation of entropy generation in flow and heat transfer phenomena in different geometrical configurations under various physical assumptions.

1.1 Historical background and literature survey

Thermal fluid science includes numerous engineering and industrial processes involving: transport, heat transfer and conversion of energy from one state to the other. The transport phenomena are primarily based upon the conservation principles as well as the flux expressions. Momentum transport in fluid incorporates the study of fluids in motion and the interaction of forces during the course of motion. The branch of Science which deals with the moving fluids is known as fluid dynamics. The historical aspect of fluids shows the skillful knowledge that human beings have collected over the span of centuries through analytical or experimental work in the field of hydrodynamics. In ancient times, the main concern of human beings was the supply of water for cultivation and drinking purpose. Different technological processes were formulated for the completion of such purposes. *Archimedes* (287-212 B.C) played a significant role in this regard as he put forward the laws of buoyancy that were utilized to the floating and submerged objects. Later on, diverse important contributions were made by succeeding scientists in this field from theoretical and engineering point of view. Above all, the most noticeable contribution in this field was suggested by *Leonardo de Vinci* (1452-1519) who mathematically formulated mass conservation law for one dimensional steady state flow. *Newton* (1642-1727) also enriched the theory of fluid flow by formulating the laws of

motion which brought a revolution in *Fluid Dynamics*. In addition, he presented the law of viscosity of linear fluids which is acknowledged as Newton's law of viscosity. Moreover, *Leonhard Euler* (1707-1783) established the mathematical foundation of the fluid flow. By applying the Newton's second law and principle of conservation of mass, he obtained partial differential equations which include pressure and velocity fields. Later, the French mathematician *Claude-Louis Navie*r (1785-1836) and English mathematician *George Stokes* (1819-1903) individualistically contributed in developing the general equations for viscous fluid flow that are now commonly known as *Navier-Stokes* equations [1, 2]. German scientist Ludwig Prandtl [3] brought forward a revolution in the field of Fluid Dynamics by introducing the concept of boundary layer and hence provided a base for the theory of boundary layer. According to him, a boundary layer is a thin layer of fluid in theovicinity of a surface wherein the viscosity effects are dominant. Moreover, most of the heat transfer phenomena from a body to fluid also takes place within the boundary layer. Outside this layer, the effects of viscous force and heat transfer can be neglected. This allows the Navier-Stokes equations and the energy equation to be simplified significantly and closed-form solutions for the flow and thermal fields can be attained in some particular cases. After the introduction of this concept, the subject expanded at an exponential rate and contributions from mathematical and application points of view were made by different succeeding scientists.

The phenomenon of heat transfer takes place due to the temperature difference between two material bodies. This temperature difference in fluid is a driving force of flow that the fluid contains within itself. The larger the temperature difference is, the higher the rate of heat transfer occurs. Different engineering equipments such as heat exchangers, boilers, condensers, refrigerators are formulated on the theory of heat transfer. The physical understanding of the nature of heat dates back to ancient Greeks. Heraclitus (500 B.C) argued that there are three principal elements in nature: fire, earth and water. Of these, fire holds a central position and is regarded as an element that controls and modifies the other two. Around 1600 B.C, an English philosopher Francis Bacon stated [4] "*Heat itself, its essence and quiddity is motion and nothing else*". Till the middle of the nineteenth century, the basic understanding of the nature of heat transfer led to

the development of kinetic theory which treats molecules as tiny particles possessing kinetic energy. Later, French chemist *Antoine Lavoiser* (1743-1794) proposed the caloric theory [5] which asserts that heat is a fluid like substance called the caloric which can be dispensed from one body into another. The addition of the caloric to a body increases the temperature and its removal results in decrease in temperature. *Count Rumford (Benjamin Thompson)* overturned this idea in 1798 who concluded that heat was not a fluid released form a material but a result of the conversion of mechanical work into heat energy. *Sadi Carnot* in 1824 used the basic ideas of thermodynamics to discuss the efficiency of the idealized engine, which later came to be known as Carnot engine. In 1850, *James Joule* experimentally concluded that heat is a form of energy. The laws of thermodynamics were articulated by *Rudolf Clausius* and *William Thomson* (Lord Kelvin) around 1850. According to the first law, one form of energy can transformed in another form but the total amount of energy remains conserved. Thus, it provides a formal statement of the conservation of energy. However, it gives no information about the direction in which the process can spontaneously take place. This shows that the first law of thermodynamics becomes inadequate to picture the energy transfer process. Experiments indicate that once a change has occurred in a system, it is not always possible to bring the system back to its original state. This irreversible change in state is measured by a quantity known as entropy.

The concept of entropy was put forward by a German physicist *Rudolf Clausius* [6] which is the outcome of his research from 1850 to 1864 on the theory of heat and its applications related to engines. This inspiration for the idea came from the work of *Sadi Carnot* [7] that it is not possible to convert all the heat energy into mechanical work. Based on this study, Clausius formulated the second law of thermodynamics. It is based on the fact that the flow of heat is not from cold reservoir to the hot reservoir. Proceeding further on his work, Clausius introduced the new quantity which he termed as entropy. It is the ratio of heat to the temperature and is dependent only on the state of the system. In simple words, it is a quantity which measures the loss of energy in a system which cannot be reverted. In this manner, he explained the second law of thermodynamics in terms of increase of the entropy. Later on, Boltzman [8]

and Gibbs [9] contributed to explain the concepts of entropy and its connection with irreversibility. However, a revolution came in the field of the study of thermal and mechanical systems when Bejan [10, 11] used the idea of entropy to discuss the efficiency of the thermo-mechanical devices. He pointed out that different sources such as fluid friction, temperature difference, presence of magnetic field or thermal radiation are responsible for the entropy production. Later, Poulikakos and Bejan [12] theoretically discussed the entropy effects in different fin geometries and examined that the entropy generation can be minimized by selecting optimum dimensions. Thacher [13] used the concept of entropy production to analyze the efficiency of thermoelectrical generators and heat pumps. Mukherjee et al. [14] made a second law analysis of swirling flow in a cylindrical duct having constant wall temperature. Arpaci [15] theoretically discussed the entropy production in radiative flows and conversion of heat energy into entropy. Cheng and Huang [16] numerically investigated the influence of entropy production in force convective channel flows having pairs of transverse fins attached to the walls. Selamet and Arpaci [17] theoretically examined the entropy effects in boundary layer flows. Carrington and Sun [18] derived the expressions for entropy generation. They claimed that entropy is generated under the presence of both mass and heat transfer phenomenon. For the internal as well as external flows, the generation of entropy caused by transfer of heat and mass was investigated by the same authors [19] using control volume method. For heat regenerator, the analytical presentation for the entropy generation was given by Hajji [20].

Flow over flat or curved surfaces is subjected to energy losses due to entropy generation effects. This can affect the efficiency of the thermo-mechanical systems involving such flow processes. By carefully analyzing these processes, one can identify the factors that are responsible for the entropy production and can take measures to minimize the entropy effects. Budair [21] considered the unsteady flow of viscous fluid caused by the sudden motion of a flat plate and studied the entropy effects due to fluid frcition. He found that the entropy effects are more prominent at intial period of motion. Saouli and Saouli [22] inspected entropy effects in gravity driven liquid f*i*lm past an inclined porous surface with upper free surface. They considered the viscous dissipation effects and concluded that entropy generation effects

augment due to the presence of these effects. Gorla and Pratt [23] examined the entropy effects in fully developed hydromagnetic non-Newtonian liquid film falling under the action of gravity along an inclined heat plate. Esfahani and Jafarian [24] made use of different solution methodologies to study the entropy production in steady laminar flow over a flat plate. Makinde and Osalus [25] made a thermodynamical analysis of a thin liquid film developed along an inclined flat permeable surface and obtained analytical solutions of the problem. Later, Makinde [26] analyzed the irreversibility effects due to entropy generation in a non-Newtonian liquid film falling under the gravity influence along an inclined isothermal plate. Ozkol et al. [27] discussed the entropy effects natural convective viscous flow along an infinite vertical plate and concluded that the entropy production is significant at the flat surface and in the nearby region. Arikoglu [28] utilized the analytical technique known as *Differential Transform Method (DTM)* to discuss the impact of slip on entropy generation in hydromagnetic flow caused by rotation of a disk. Chen et al. [29] assumed the laminar forced convection flow along a wavy surface and the entropy effects were discussed during the flow and heat transfer phenomena. Reveillere and Baytas [30] studied entropy production in two-dimensional flow over a porous flat plate. They remarked that suction/blowing through the permeable surface has a dramatic effect on entropy production. In case of blowing, the entropy effects are strong within boundary layer. Tamayol [31] considered the boundary layer flow over a porous stretchable surface through a porous medium and performed a thermodynamical analysis. It was witnessed through the study that suction results in more entropy generation. Under the influence of Newtonian heating and thermal radiation, Makinde [32] analyzed the variable viscosity effects on entropy generation in flow over a flat surface. It was revealed that entropy effects are maximum within boundary layer and augment with increase in Newtonian heating effects. Malvandi et al. [33] employed homotopy perturbation method to analyze the entropy effects in viscous fluid flow past an isothermal flat plate. Makinde [34] examined the entropy effects in hydromagnetic flow of viscous fluid past a flat horizontal plate by considering the convective boundary condition at the ssurface and concluded that convective heat transfer at the surface of flat plate enhances the entropy generation rate. Das et al. [35] analyzed the entropy effects in free convective flow past an inclined flat surface inserted in a porous medium. They also considered the Hall

current effects and observed that entropy production augments due to the presence of Hall current. Rashidi and Freidoonimer [36] employed DTM to investigate the entropy effects in stagnation point flow over a flat surface through a porous medium. Khan et al. [37] investigated the entropy effects in nanofluid flow over a flat surface by considering prescribed heat surface and heat flux and remarked that entropy generation strongly depends upon the solid volume fraction of the nanoparticles.

Flow and heat transfer in channels is considered as one of the basic problems in engineering. Such flows are encountered in many engineering processes such as electronic cooling, heat pipes, heat exchangers, microchannels, insulation of buildings, flow inside human organs etc. It is worth mentioning that difference of temperature at the channel walls and viscous dissipation in fluid results in energy losses which can be enumerated by entropy analysis of the systems. This led the researchers to discuss entropy generation effects in channel under different physical circumstances. Yilbas et al. [38] numerically examined the entropy effects in a circular duct with restriction and rotation. He remarked that high swirling effects will result in the production of more entropy. Tasnim and Mahmud [39] obtained the closed form solutions of mixed convective flow in a vertical annular space and inpected the entropy generation effects. It was found that mixed convection causes entropy production rate to enhance. Mahmud and Fraser [40] thermodynamically analysed the flow and heat transfer inside a cylindrical annular space induced by relative motion of cylinders. A drop in entropy generation effects is observed as the ratio of velocities of both cylinder increases. Later on, Mahmud and Fraser [41] discussed the entropy effects in forced convective steady flow of viscous fluid inside circular channel and parallel plate channels. Makinde and Gbolagade [42] considered the viscous fluid flow through an inclined channel having isothermal walls and examined the local entropy generation rate. They found that the heat transfer entropy effects are dominant along the channel centerline whereas the fluid friction entropy is dominant near the channel walls. Hooman [43] analyzed the entropy generation in a fully developed forced convective laminar flow through a porous medium inside an elliptic duct including viscous dissipation effects. Andreozzi et al. [44] numerically inspected the local and global entropy generation rates in natural convectional flow in a symmetric vertical channel which is heated by a uniform heat flux. Hooman and Haji Sheikh [45] examined the entropy effects

in forced convective flow in a rectangular channel with pervious medium and isoflux wall conditions. Chen and Tian [46] used Lattice Boltzmann method to examine the slip effects on entropy generation in Couette flows in microchannels and found that presence of slip will reduce the entropy production. Chen et al. [47] assumed the laminar forced convection flow along a wavy surface and the entropy effects were discussed during the flow and heat transfer phenomena. Kobo and Makinde [48] analysed the influence of variable viscosity and Arrhenius kinetics on entropy effects in Couette flow. Chen et al. [49] examined viscous dissipation effects on entropy production in mixed convective channel flow via Differential Transform Method. Chinyoka and Makinde [50] assumed unsteady viscous flow in a porous channel and discussed the influence of variable viscosity, Navier Slip, convective cooling and suction/injection on the entropy generation rate. The effects of asymmetric Navier slip condition and variable electrical conductivity on steady viscous flow in a porous channel were numerically investigated by Eegunjobi and Makinde [51].

Magnetohydrodynamics deals with the flow of electrically conducting fluids under the influence of magnetic field. This is an established fact that the magnetic field affects the fluid motion and alters it. The magnetohydrodynamic fluid flow is described by featuring both the equations of fluid mechanics and that of electromagnetism. Such flows are found in plasma physics and various engineering problems such as nuclear reactors, geothermal energy extractions, magnetohydrodynamic (MHD) generators, oil exploration, control of the boundary layer aerodynamics etc. Several studies have been performed to investigate the impact of magnetic field on entropy effects in several physical situations as it has a key role in its production. The influence of magnetic field on entropy production under forced convective flow over a flat surface were discussed by Al-Odat et al. [52]. Mahmud and Fraser [53] assumed natural convection MHD flow in a saturated cavity and inspected the entropy effects. Saouli et al. [54] theoretically examined the impact of transverse magnetic field on generation of entropy in electrically conducting liquid film flow beside an inclined plate. The study revealed that the magnetic field has an increasing effect on entropy production. Damesh et al. [55] inspected the impact of magnetic field on entropy generation due to laminar incompressible flow in a channel. Butt and Ali [56] used the well-known Laplace transform method to

study hydromagnetic flow along an infinite vertical plate placed in a porous medium and studied the influence of magnetic field on entropy production. Liu and Lo [57] numerically analyzed the production of entropy in mixed convective MHD flow in a vertical channel. Rashidi et al. [58] considered the flow of an electrically conducting viscous fluid induced by a stretching rotating disk and made a thermodynamical analysis of the problem. Mahin et al. [59] studied the entropy effects in flow between two vertical cylinders with constant wall temperatures when the magnetic field is also present. Eegunjobi and Makinde [60] discussed the entropy effects in variable viscosity MHD flow of viscous fluid in a permeable channel having convective heating. Vyas and Srivastava [61] studied magnetic field effects on entropy generation in composite duct flow with asymmetric convective cooling at the walls and observed an enhancement in entropy generation due to magnetic field presence. Makinde [62] theoretically investigated the entropy effects in hydromagnetic rotating Cuotte flow with variable viscosity and Hall current effects. A rise in entropy production rate was observed due to fluid rotation and magnetic field presence increase the

Flow and heat transfer phenomena in porous media are investigated theoretically and experimentally due to numerous engineering applications such as solid matrix heat exchanger, coal and grain storage, filtration plants, electronics cooling system, geothermal system, nuclear waste disposal, microelectronic heat transfer equipment and catalytic converters. The analysis of entropy production in a porous medium has received the attention of researchers as it can significantly reduce the productivity of thermomechanical systems. Khan and Gorla [63] carried out a thermodynamical analysis of free convective non-Newtonian flow over horizontal plate entrenched in a porous medium under the action of prescribed heat flux. Dehsara et al. [64] numerically observed the entropy effects in nanofluid flow over a permeable plate in a porous medium. They assumed that the effects of solar radiation and variable magnetic field are also present and found that the entropy effects augment due to the presence of magnetic field and porous medium. Matin [65] studied the combined effects of flow, mass and heat transfer over a flat surface inserted in a porous medium by making use of the implicit finite difference scheme. Osalus and Makinde [66] analyzed the

entropy production due to laminar flow in a channel which is filled with saturated porous media. Hooman and Ejlali [67] numerically examined the second law of thermodynamics in a viscous flow through a porous medium confined between two parallel plates. Hooman [68] studied the entropy effects in a thermally developed forced convection flow through a circular tube with uniform temperature distribution filled with saturated porous medium. Later, Hooman [69] investigated the impact of temperature reliant viscosity on entropy generation in forced convective flow in a porous saturated circular tube using Darcy model. Silmi [70] analyzed the entropy generation in unsteady natural convectional flow in a radiative fluid through a titled saturated porous channel. Hooman et al. [71] inspected the entropy production in forced convection channel flow filled with a saturated porous medium by assuming two thermal boundary conditions. Heidary et al. [72] inspected the influence of free convection on entropy generation in an inclined square cavity that is filled with porous medium. Dhahri et al. [73] numerically studied the entropy effects in pulsating flow within a cylinder having a permeable medium.

Flow over stretching surfaces is frequently observed in manufacturing and industrial processes such as extrusion of a polymer sheet from a dye, wire drawing, cooling of metallic plates, paper production, hot rolling, aerodynamic extrusion of plastic sheets etc. Moreover, the final manufacturing product depends upon the rate of heating or cooling. Crane [74] was the first to initiate the study of viscous fluid flow over a linearly stretching surface by making use of boundary layer theory introduced by Prandtl [3]. Carragher and Crane [75] further carried the work to investigate the heat transfer phenomenon during flow over a stretching sheet. Afterwards, this topic gained tremendous attention of researchers and scientists and a lot of work has been done on it. Here, the major contributions are mentioned which are related to boundary layer viscous flow and transfer of heat above a stretching surface. Gupta and Gupta [76] discussed the impact of suction/blowing on flow, heat and mass transfer phenomena over a porous stretchable surface. Bank [77] attained the similarity solution of the boundary layer flow due to extending of a surface. Wang [78] contributed to the Crane's problem and analyzed 3D flow caused by two directional stretching of surface. He considered the stretching ratios in two directions to be different and numerically simulated the

problem. The heat transfer characteristics of viscous flow over a stretching surface with variable temperature were analytically studied by Grubka and Bobba [79]. Wang [80] investigated the flow of a liquid film over an unsteady stretching sheet. Ali [81] examined the same problem by assuming power law velocity and heat transfer distributions. Hadjinicolaou and Vajravelu [82] studied the convective heat transfer in hydromagnetic fluid over a stretchable surface with uniform free stream. Elbashbeshy [83] extended Gupta and Gupta [76] study by considering variable heat flux and suction/injection at the surface. Sriramalu et al. [84] examined the steady flow of a viscous fluid placed in a porous medium past a stretching surface. Anderrson [85] discussed the impact of partial slip at the stretching surface on flow characteristics and remarked that the presence of slip results in reduction of velocity of fluid. Wang [86] presented the exact solution of the flow phenomena due to the stretching surface with partial slip. Takhar et al. [87] analyzed the magnetohydrodynamic flow and heat transfer of a rotating viscous fluid over a linearly stretching surface. Liu [88] obtained analytical solutions of the problem of hydromagnetic flow, heat and mass transfer over a linearly stretching surface. Vajravelu and Cannon [89] numerically analyzed the viscous fluid flow over a nonlinearly stretching surface. Ariel [90] made use of analytical technique known as homotopy perturbation method to obtain the series solution of 3D flow over a bidirectional stretchable surface. Hayat and Javed [91] examined the generalized 3D flow of viscous fluid past a porous stretching sheet under the influence of magnetic field. Ahmer et al. [92-95] discussed the steady and unsteady flows over a stretching sheet from different physical point of views by making use of analytical technique commonly known as HAM. Hayat et al. [96] analyzed the three dimensional flow and heat transfer of viscous fluid over a bidirectional stretching surface by considering viscous and joule dissipation effects.

All the aforementioned studies are concerned with boundary layer flow over flat stretching surfaces. However, there are situations where boundary layer flow also occurs in other geometrical configurations such as radially stretching surfaces, stretching cylinder or flow in a channel with stretchable walls.

Ariel et al. [97] examined axisymmetric flow over a radially stretching surface and obtained the solution of the problem by means of homotopy perturbation method. Wang [98] discussed the natural convection

in flow past a vertical radially stretching surface. Shateyi and Makinde [99] studied the MHD stagnation point flow over a convectively heat radially stretching sheet. Khan et al. [100] analyzed the magnetodyrodynamic viscous flow over a permeable radially surface stretching with power law velocity. Fang and Zhang [101] obtained the exact similarity solution of the flow between two stretchable infinite disks. Hayat and Nawaz [102] inspected the magnetic field effects on heat transfer characteristics of Newtonian fluid between two radially stretching surfaces. Munawar et al. [103] considered the effects of slip at the surfaces of stretching disks and examined the flow and heat transfer phenomena by using Optimal Homotopy Analysis Method (OHAM). Wang [104] analyzed the flow due to stretching of a hollow cylinder and discussed asymptotic solutions for large Reynold number. He also presented the numerical solution of the problem. Ishak and Nazar [105] numerically investigated the heat transfer characteristics in viscous fluid flow over a stretching cylinder and found that the curvature of the cylinder has a significant impact on temperature distribution. Munawar et al. [106] examined the unsteady flow and transfer of heat induced by a stretching cylinder. Vajravelu et al. [107] analyzed the axisymmetric flow of Newtonian fluid induced by a stretching cylinder in the presence of heat generation/absorption. They considered the temperature dependent thermos-physical properties and numerically analyzed the problem. Shateyi and Marewo [108] employed Successive Relaxation Method (SRM) method to examine the axisymmetric flow past a stretching cylinder placed in absorbent medium. Bokakoti and Bharali [109] considered the hydromagnetic flow and heat transfer of viscous fluid confined between two horizontal plates with lower plate stretching in its own plane. Munawar et al. [110] studied the three dimensional squeezing flow of a viscous fluid in a rotating channel with the lower permeable stretching wall.

It is a well-known fact that the nature of the Navier-Stokes equations are highly nonlinear and there are no general exact solutions available for most of the time. One has to use analytical and numerical procedures to find the approximate solutions of these equations. Several methodologies are employed to obtain the solution of Navier Stokes equations. However, analytical method is preferable as it provides a clear insight of the interactions of the variables and their impact on the solutions. Perturbation techniques [111, 112, 113] are the most generally used methods used to solve Navier Stokes equations. However, it is

a fact that perturbation methods can be applied to those problems which involve a small parameter. In the absence of such parameters, it is not possible to employ perturbation techniques. The other approach is to look upon numerical schemes to solve such problems. Several numerical techniques have been devised for the solution of the Navier-Stokes equations by carefully examining the nature of the problem [114]. However, all these analytical and numerical methods have their advantages and limitations and are applicable to a limited number of problems. Liao [115] proposed an analytical technique known as Homotopy Analysis Method (HAM) in his doctoral thesis that is based on the idea of homotopy in the branch of topology [116]. The solutions obtained by Homotopy Analysis Method are in the form of infinite series. Liao [117] showed that unlike perturbation techniques, HAM offers a incredible liberty to manage and control the convergence and errors of the series solutions obtained by it. He applied his technique to various problems in fluid mechanics [117-131] to demonstrate that the method is quite valid and the results obtained by it are accurate. This method was later on adapted by different researchers to cope with different problems in fluid dynamics, heat and mass transfer, see for instance the work by Hayat et al. [132-138], Rashidi et al. [139-143], Xu et al. [144-146], Mehmood et al. [92-95]. The literature on Homotopy Analysis Method is so large that it is not possible to mention all of them in the document and only a few of them are cited here. Later, Liao [147] improved HAM by arguing that by choosing suitable value of the convergence control parameter that he introduced in HAM, the series solution convergence can be achieved earlier.

The organization of the thesis is made into nine chapters and a sketch of the layout is as follows:

Chapter 1 focuses on the historical background of the concept of entropy and discusses in detail the available literature regarding the investigation of entropy generation effects in different scenarios. Moreover, the literature regarding flow and heat transfer phenomena over a stretchable surface has also been mentioned. Some portion of this chapter is devoted to cite the literature on the analytical method known as Homotopy Analysis Method, which is the basic method used to solve the mathematical problems in this dissertation.

Chapter 2 deals with the basic concepts and the governing equations that are used in the present work. The boundary layer approximation of the equations that constitute the mathematical problem are

presented. The laws of thermodynamics and the mathematical expression for the entropy generation rate are briefly discussed. The dimensionless parameters involving in the problems are mentioned here. Furthermore, the general procedure of the methods used to solve the problems is given.

Chapter 3 deals with the theoretical study of entropy generation effects in flow and heat transfer phenomena of viscous fluid over a linearly stretching surface when the effects of slip and convective heat transfer are present at the surface. The effects of magnetic field and.viscous dissipation are also considered and the problem is solved with the help of Homotopy Analysis Method (HAM). The expression for entropy generation is calculated by using the expressions of the velocity and the temperature fields. The results are graphically presented for important parameters involving in the problem. Contents of this chapter are published in **International Journal of Physical Sciences 2 (4) (2014), 46-60**.

Chapter 4 numerically investigates the entropy effects in two dimensional hydromagnetic flow over a stretching cylinder embedded in a porous medium. A qualitative study has been carried out by comparing the effects of entropy generation in flow over a stretching cylinder having some curvature and in case of flat surface**.** The results are displayed with the help of tables and graphs and the impact of various physical parameters are discussed briefly. This work has been published in the journal **Energy 99 (2016), 237-249.**

Chapter 5 considers the problem of three dimensional flow and heatbtransfer over a bidirectional linearly stretching sheet when the effects of magneticifield are also there and the entropy generation effects are analyzed. The problem is mathematically formulated and is solved by Homotopy Method (HAM) and shooting technique. The obtained results are discussed briefly and the results areecompared with the existing literature. The contents discussed in this chapter are published in **Journal of the Brazilian Society of Mechanical Sciences and Engineering 37 (2015), 211-219.**

Chapter 6 is dedicated to examine the entropy effects in MHD flow and heat transfer of viscous fluid over a radially stretching sheet which is convectively heated from the bottom by passing a hot fluid. The physical problem is given a mathematical formulation and is solved by both analytical and numerical

methods. The impact of physical parameters on entropy production are presented graphically and are discussed in detail. The work presented in this chapter is published in **Journal of the Taiwan Institute of Chemical Engineers 45 (4) (2014), 1197-1203.**

Chapter 7 is devoted to analyze the effect of entropy generation in flow and heat transfer phenomena of Newtonian fluid through a porous medium between two surfaces stretching in radial directions with the same rate. A mathematical model has been developed for the problem and is solved with the help of analytical and numerical methods. A comprehensive study has been carried out and the influence of pertinent parameters on entropy production has been examined. This chapter has been published in the journal **International Journal of Exergy 18 (4) (2015), 501-519.**

Chapter 8 investigates the entropy generation effects in viscous fluid flow and heat transfer in a rotating channel whose lower wall is permeable and unsteadily stretching in its own plane and the upper wall is squeezing downwards. Analytical and numerical procedures have been employed to solve the mathematical modeled system and the results are presented with the aid of graphseand tables. The impact of physical parameters on entropy effects are discussed briefly. The contentsoof this chapter are published in **Journal of the Taiwan Institute of Chemical Engineers 48 (2015), 8-17.**

Chapter 9 gives the overall conclusion of the problems discussed in the thesis and important results are mentioned in this chapter.

Chapter 2

Preleminaries

This chapter discusses the basic concepts that are used in the problems studied in this thesis. The basic governing equations the problem as well as the definitions of the non-dimensional parameters are given. The concept of entropy and the description of expression of entropy generation rate is mentioned. The solution methodologies that are used for the solution of the governing equations have also been stated for the better understanding.

2.1 Governing laws

The basic governing equations in the field of fluid dynamics are based on the conservation laws specifically the law of conservation of mass, momentum and energy. The conservation law of linear momentum is also recognized as Newton's second law of motion and the law of conservation of energy is also known as the first law of thermodynamics. These laws discuss the momentum and thermo-dynamical characteristics of compressible/incompressible viscous fluids. The present study is, however limited to the incompressible fluids. Therefore, the above mentioned governing laws are stated for incompressible viscous fluids only which are read as

$$\nabla.\mathbf{V} = 0, \text{ (Law of conservation of mass)} \tag{2.1}$$

$$\rho\frac{D\mathbf{V}}{Dt} = -\nabla P + \mu\nabla^2\mathbf{V} + \rho\mathbf{b} + \mathbf{J}\times\mathbf{B}, \text{ (Law of conservation of momentum)} \tag{2.2}$$

$$\rho c_p\frac{DT}{Dt} = k\nabla^2 T + \Phi, \text{ (Law of conservation of energy)} \tag{2.3}$$

where

$$\underset{\text{total derivative}}{\frac{D}{Dt}} = \underset{\text{local derivative}}{\frac{\partial}{\partial t}} + \underset{\text{convective derivative}}{(\mathbf{V}.\nabla)} . \tag{2.4}$$

Here $\mathbf{V}$ denotes the velocity vector of fluid, T is the fluid temperature, ρ is the fluid density, P is the pressure, $\mathbf{b}$ is the body force, $\mathbf{J}$ is the current density, $\mathbf{B} = \mathbf{B}_0 + \mathbf{b}_0$ is the magnetic flux, $\mathbf{B}_0$ is the applied magnetic field and $\mathbf{b}_0$ is the induced magnetic field, c_p is the specific heat, k is the thermal conductivity of the fluid which is assumed to be constant and Φ is the viscous dissipation.

$$\rho\left(\frac{D\mathbf{V}}{Dt} + \boldsymbol{\omega}\times\boldsymbol{\omega}\times\mathbf{r} + 2\boldsymbol{\omega}\times\mathbf{V}\right) = -\nabla P + \mu\nabla^2\mathbf{V} + \rho\mathbf{b} + \mathbf{J}\times\mathbf{B}, \tag{2.5}$$

where $\boldsymbol{\omega}$ is the angular velocity and $\mathbf{r}$ denotes the position vector, $(\boldsymbol{\omega}\times\boldsymbol{\omega}\times\mathbf{r})$ represents the centripetal acceleration and $(2\boldsymbol{\omega}\times\mathbf{V})$ is the Coriolis acceleration.

In rotating flows, the momentum equation (2.2) takes the modified form as

In addition when the magnetic field is present, four more laws are considered in addition to (2.1-2.3) [148]:

$$\nabla.\mathbf{E} = \frac{\rho}{\varepsilon_0}, \text{ (Gauss's Law)} \tag{2.6}$$

$$\nabla\times\mathbf{E} = -\frac{\partial\mathbf{B}}{\partial t}, \text{ (Faraday's Law)} \tag{2.7}$$

$$\nabla\times\mathbf{B} = \mu_0\mathbf{J} + \mu_0\varepsilon_0\frac{\partial\mathbf{E}}{\partial t}, \text{ (Ampere's Law with Maxwell's correction)} \tag{2.8}$$

$$\nabla.\mathbf{B} = 0, \text{ (Gauss's Law for magnetism)} \tag{2.9}$$

where

$$\mathbf{J} = \sigma\left(\mathbf{E} + \mathbf{V}\times\mathbf{B}\right). \tag{2.10}$$

Here ε_0 is the permittivity of free space, μ_0 is the magnetic permeability, σ is the fluid electrical conductivity, $\mathbf{E}$ is the electric field and $\mathbf{B}$ is the magnetic field.

The energy equation (2.3) with Joule heating takes the form

$$\rho c_p \frac{DT}{Dt} = k\nabla^2 T + \Phi + \frac{\mathbf{J}^2}{\sigma}. \tag{2.11}$$

In components form, Eqs. (2.1-2.3) are read as:

$$\frac{\partial u}{\partial x} + \frac{\partial v}{\partial y} + \frac{\partial w}{\partial z} = 0, \tag{2.12}$$

$$\rho\left(\frac{\partial u}{\partial t} + u\frac{\partial u}{\partial x} + v\frac{\partial u}{\partial y} + w\frac{\partial u}{\partial z}\right) = -\frac{\partial P}{\partial x} + \mu\left(\frac{\partial^2 u}{\partial x^2} + \frac{\partial^2 u}{\partial y^2} + \frac{\partial^2 u}{\partial z^2}\right) + \rho b_x + \sigma B_0^2 u, \tag{2.13}$$

$$\rho\left(\frac{\partial v}{\partial t} + u\frac{\partial v}{\partial x} + v\frac{\partial v}{\partial y} + w\frac{\partial v}{\partial z}\right) = -\frac{\partial P}{\partial y} + \mu\left(\frac{\partial^2 v}{\partial x^2} + \frac{\partial^2 v}{\partial y^2} + \frac{\partial^2 v}{\partial z^2}\right) + \rho b_y + \sigma B_0^2 v, \tag{2.14}$$

$$\rho\left(\frac{\partial w}{\partial t} + u\frac{\partial w}{\partial x} + v\frac{\partial w}{\partial y} + w\frac{\partial w}{\partial z}\right) = -\frac{\partial P}{\partial z} + \mu\left(\frac{\partial^2 w}{\partial x^2} + \frac{\partial^2 w}{\partial y^2} + \frac{\partial^2 w}{\partial z^2}\right) + \rho b_z + \sigma B_0^2 w, \tag{2.15}$$

$$\begin{aligned}\rho c_p\left(\frac{\partial T}{\partial t} + u\frac{\partial T}{\partial x} + v\frac{\partial T}{\partial y} + w\frac{\partial T}{\partial z}\right) &= k\left(\frac{\partial^2 T}{\partial x^2} + \frac{\partial^2 T}{\partial y^2} + \frac{\partial^2 T}{\partial z^2}\right) \\ +2\mu\left\{\left(\frac{\partial u}{\partial x}\right)^2 + \left(\frac{\partial v}{\partial y}\right)^2 + \left(\frac{\partial w}{\partial z}\right)^2\right\} &+ \mu\left\{\left(\frac{\partial u}{\partial y} + \frac{\partial v}{\partial x}\right)^2 + \left(\frac{\partial u}{\partial z} + \frac{\partial w}{\partial x}\right)^2 + \left(\frac{\partial v}{\partial z} + \frac{\partial w}{\partial y}\right)^2\right\},\end{aligned} \tag{2.16}$$

where (u, v, w) are the velocity components in (x, y, z) directions.

In cylindrical coordinates, Eqs. (2.1-2.3) are given as

$$\frac{1}{r}\frac{\partial (ru)}{\partial r} + \frac{1}{r}\frac{\partial v}{\partial \varphi} + \frac{\partial w}{\partial z} = 0, \tag{2.17}$$

$$\rho\left(\frac{\partial u}{\partial t}+u\frac{\partial u}{\partial r}+\frac{v}{r}\frac{\partial u}{\partial \varphi}-\frac{v^2}{r}+w\frac{\partial u}{\partial z}\right)=-\frac{\partial P}{\partial r}+\mu\left[\begin{array}{l}\frac{1}{r}\frac{\partial}{\partial r}\left(r\frac{\partial u}{\partial r}\right)-\frac{u}{r^2}\\+\frac{1}{r^2}\frac{\partial^2 u}{\partial \varphi^2}-\frac{2}{r^2}\frac{\partial v}{\partial \varphi}+\frac{\partial^2 u}{\partial z^2}\end{array}\right]+\rho b_r+\sigma B_0^2 u, \tag{2.18}$$

$$\rho\left(\frac{\partial v}{\partial t}+u\frac{\partial v}{\partial r}+\frac{v}{r}\frac{\partial v}{\partial \varphi}+\frac{uv}{r}+w\frac{\partial v}{\partial z}\right)=-\frac{1}{r}\frac{\partial P}{\partial \varphi}+\mu\left[\begin{array}{l}\frac{1}{r}\frac{\partial}{\partial r}\left(r\frac{\partial v}{\partial r}\right)-\frac{v}{r^2}\\+\frac{1}{r^2}\frac{\partial^2 v}{\partial \varphi^2}+\frac{2}{r^2}\frac{\partial u}{\partial \varphi}+\frac{\partial^2 v}{\partial z^2}\end{array}\right]+\rho b_\varphi+\sigma B_0^2 v, \tag{2.19}$$

$$\rho\left(\frac{\partial w}{\partial t}+u\frac{\partial w}{\partial r}+\frac{v}{r}\frac{\partial w}{\partial \varphi}+w\frac{\partial w}{\partial z}\right)=-\frac{\partial P}{\partial z}+\mu\left[\begin{array}{l}\frac{1}{r}\frac{\partial}{\partial r}\left(r\frac{\partial w}{\partial r}\right)\\+\frac{1}{r^2}\frac{\partial^2 w}{\partial \varphi^2}+\frac{\partial^2 w}{\partial z^2}\end{array}\right]+\rho b_z+\sigma B_0^2 w, \tag{2.20}$$

$$\begin{aligned}&\rho c_p\left(\frac{\partial T}{\partial t}+u\frac{\partial T}{\partial r}+\frac{v}{r}\frac{\partial T}{\partial \varphi}+w\frac{\partial T}{\partial z}\right)=k\left[\frac{1}{r}\frac{\partial}{\partial r}\left(r\frac{\partial T}{\partial r}\right)+\frac{1}{r^2}\frac{\partial^2 T}{\partial \varphi^2}+\frac{\partial^2 T}{\partial z^2}\right]\\&+2\mu\left[\left(\frac{\partial u}{\partial r}\right)^2+\left(\frac{1}{r}\frac{\partial v}{\partial \varphi}+\frac{u}{r}\right)^2+\left(\frac{\partial w}{\partial z}\right)^2\right]\\&+\mu\left\{\left(r\frac{\partial}{\partial r}\left(\frac{v}{r}\right)+\frac{1}{r}\frac{\partial u}{\partial \varphi}\right)^2+\left(\frac{1}{r}\frac{\partial w}{\partial \varphi}+\frac{\partial v}{\partial z}\right)^2+\left(\frac{\partial u}{\partial z}+\frac{\partial w}{\partial r}\right)^2\right\},\end{aligned} \tag{2.21}$$

where (u,v,w) are velocity components in (r,φ,z) directions.

2.2 Boundary layer approximation

The concept of boundary layer was first introduced by Ludwig Prandtl [3] in 1904 which simplifies the flow equations by splitting the flow field into two regions. According to him, momentum boundary is a thin layer of fluid close to the solid surface in which the effects of viscous stresses are significant [149]. Outside this layer, the effects of viscosity are not that prominent and hence can be discarded.

2.2.1 In rectangular coordinates

Consider a two dimensional flow of an incompressible viscous fluid. The continuity equation and the momentum equations in the absence of body force are written as

$$\frac{\partial u}{\partial x}+\frac{\partial v}{\partial y}=0, \tag{2.22}$$

$$\frac{\partial u}{\partial t}+u\frac{\partial u}{\partial x}+v\frac{\partial u}{\partial y}=-\frac{1}{\rho}\frac{\partial P}{\partial x}+\nu\left(\frac{\partial^2 u}{\partial x^2}+\frac{\partial^2 u}{\partial y^2}\right), \tag{2.23}$$

$$\frac{\partial v}{\partial t}+u\frac{\partial v}{\partial x}+v\frac{\partial v}{\partial y}=-\frac{1}{\rho}\frac{\partial P}{\partial y}+\nu\left(\frac{\partial^2 v}{\partial x^2}+\frac{\partial^2 v}{\partial y^2}\right), \tag{2.24}$$

where $\nu=\frac{\mu}{\rho}$ is the kinematic viscosity. In order to non-dimensionalize Eqs. (2.22-2.24), the following transformations are introduced

$$t^*=\frac{tU_o}{L}, x^*=\frac{x}{L}, y^*=\frac{y}{L}, u^*=\frac{u}{U_o}, v^*=\frac{v}{U_o}, P^*=\frac{P}{\rho {U_o}^2} \tag{2.25}$$

where U_o is the reference velocity and L is the characteristic length of surface in *x*-direction. The utilization of transformation (2.25) in Eqs. (2.22-2.24) results in the following system:

$$\frac{\partial u^*}{\partial x^*}+\frac{\partial v^*}{\partial y^*}=0, \tag{2.26}$$

$$\frac{\partial u^*}{\partial t^*}+u^*\frac{\partial u^*}{\partial x^*}+v\frac{\partial u^*}{\partial y^*}=-\frac{\partial P^*}{\partial x^*}+\frac{1}{\mathrm{Re}}\left(\frac{\partial^2 u^*}{\partial x^{*2}}+\frac{\partial^2 u^*}{\partial y^{*2}}\right), \tag{2.27}$$

$$\frac{\partial v^*}{\partial t^*}+u^*\frac{\partial v^*}{\partial x^*}+v\frac{\partial v^*}{\partial y^*}=-\frac{\partial P^*}{\partial y^*}+\frac{1}{\mathrm{Re}}\left(\frac{\partial^2 v^*}{\partial x^{*2}}+\frac{\partial^2 v^*}{\partial y^{*2}}\right), \tag{2.28}$$

where $\mathrm{Re}=\frac{U_0 L}{\nu}$ is the Reynolds number.

For momentum boundary layer approximation, the order of magnitude analysis of Eqs. (2.26-2.28) is done as described in [149]. The order of magnitude of length x^* and velocity u^* is taken to be 1, i.e. $x^* = O(1),\ u^* = O(1)$ and the length y^* and velocity v^* have order of magnitude of the boundary layer thickness $O(\delta^*)$. Moreover, it is considered that the local accelerations (i.e. $\partial u^* / \partial t^*$) have the same order of magnitude as the convective acceleration (i.e. $u^* \partial u^* / \partial x^*$) and the factor $1/\mathrm{Re}$ has order of magnitude $O(\delta^{*2})$. Also $\frac{\partial P^*}{\partial x} = O(1)$ and $\frac{\partial P^*}{\partial y} = O\left(\frac{1}{\delta}\right)$. The continuity equation has the same order of magnitude. Then

$$\begin{array}{ccccccccc} \dfrac{\partial u^*}{\partial t^*} & + & u^* \dfrac{\partial u^*}{\partial x^*} & + & v^* \dfrac{\partial u^*}{\partial y^*} & = & -\dfrac{\partial P^*}{\partial x^*} & + & \dfrac{1}{\mathrm{Re}}\left(\dfrac{\partial^2 u^*}{\partial x^{*2}} + \dfrac{\partial^2 u^*}{\partial y^{*2}} \right), \\ \downarrow & & \downarrow & & \downarrow & & & & \downarrow \quad \downarrow \\ 1 & & 1.1 & & \delta^*.\dfrac{1}{\delta^*} & & & & \delta^{*2} \quad 1 \quad \dfrac{1}{\delta^{*2}} \end{array} \tag{2.29}$$

$$\begin{array}{ccccccccc} \dfrac{\partial v^*}{\partial t^*} & + & u^* \dfrac{\partial v^*}{\partial x^*} & + & v^* \dfrac{\partial v^*}{\partial y^*} & = & -\dfrac{\partial P^*}{\partial y^*} & + & \dfrac{1}{\mathrm{Re}}\left(\dfrac{\partial^2 v^*}{\partial x^{*2}} + \dfrac{\partial^2 v^*}{\partial y^{*2}} \right). \\ \downarrow & & \downarrow & & \downarrow & & & & \downarrow \quad \downarrow \\ \delta^* & & 1.\delta^* & & \delta^*.1 & & & & \delta^{*2} \quad \delta^* \quad \dfrac{1}{\delta^*} \end{array} \tag{2.30}$$

Ignoring the terms of δ^* and δ^{*2}, we have

$$\frac{\partial u^*}{\partial t^*} + u^* \frac{\partial u^*}{\partial x^*} + v \frac{\partial u^*}{\partial y^*} = -\frac{\partial P^*}{\partial x^*} + \frac{\partial^2 u^*}{\partial y^{*2}}, \tag{2.31}$$

$$\frac{\partial P^*}{\partial y^*} = 0. \tag{2.32}$$

The two dimensional energy equation with viscous dissipation reads as

$$\rho c_p\left(\frac{\partial T}{\partial t}+u\frac{\partial T}{\partial x}+v\frac{\partial T}{\partial y}\right)=k\left(\frac{\partial^2 T}{\partial x^2}+\frac{\partial^2 T}{\partial y^2}\right)$$
$$+2\mu\left\{\left(\frac{\partial u}{\partial x}\right)^2+\left(\frac{\partial v}{\partial y}\right)^2\right\}+\mu\left\{\left(\frac{\partial u}{\partial y}+\frac{\partial v}{\partial x}\right)^2+\left(\frac{\partial u}{\partial z}\right)^2+\left(\frac{\partial v}{\partial z}\right)^2\right\}. \quad (2.33)$$

The above equation can be normalized by using (2.25) and by introducing the dimensionless temperature

$$T^*=\frac{T-T_\infty}{T_w-T_\infty}, \quad (2.34)$$

as:

$$\frac{\partial T^*}{\partial x^*}+u^*\frac{\partial T^*}{\partial x^*}+v^*\frac{\partial T^*}{\partial y^*}=\frac{1}{\mathrm{Pr}\,\mathrm{Re}}\left(\frac{\partial^2 T^*}{\partial x^{*2}}+\frac{\partial^2 T^*}{\partial y^{*2}}\right)+\frac{Ec}{\mathrm{Re}}\left[\left(\frac{\partial u^*}{\partial x^*}\right)^2+\left(\frac{\partial v^*}{\partial y^*}\right)^2+\left(\frac{\partial u^*}{\partial y^*}+\frac{\partial v^*}{\partial x^*}\right)^2\right], \quad (2.35)$$

where $\mathrm{Pr}=\frac{\mu c_p}{k}$ is the Prandtl number and $Ec=\frac{U_0^2}{c_p\left(T_w-T_\infty\right)}$ is the Eckert number. Here $T=O(1)$, $y=O(\delta^*)$ and $\mathrm{Pr}\,\mathrm{Re}=O\left(\frac{1}{\delta_*^2}\right)$. It is also observed that $\frac{\partial^2 T^*}{\partial x^{*2}}\ll\frac{\partial^2 T^*}{\partial y^{*2}}$. On this basis, we have:

$$\frac{\partial T^*}{\partial x^*}+u^*\frac{\partial T^*}{\partial x^*}+v^*\frac{\partial T^*}{\partial y^*}=\frac{1}{\mathrm{Pr}\,\mathrm{Re}}\left(\frac{\partial^2 T^*}{\partial x^{*2}}+\frac{\partial^2 T^*}{\partial y^{*2}}\right)+\frac{Ec}{\mathrm{Re}}\left[\left(\frac{\partial u^*}{\partial x^*}\right)^2+\left(\frac{\partial v^*}{\partial y^*}\right)^2+\left(\frac{\partial u^*}{\partial y^*}+\frac{\partial v^*}{\partial x^*}\right)^2\right].$$
$$\downarrow\quad\downarrow\quad\downarrow\quad\downarrow\quad\downarrow\quad\downarrow\quad\downarrow\quad\downarrow\quad\downarrow\quad\downarrow\quad\downarrow \quad (2.36)$$
$$1\quad 1.1\quad \delta^*.\frac{1}{\delta^*}\quad \delta^{*2}\quad 1\quad \frac{1}{\delta^{*2}}\quad \delta^{*2}\quad 1\quad 1\quad \frac{1}{\delta^*}\quad \delta^*$$

Under these assumptions, the thermal boundary layer equation is given as

$$\frac{\partial T^*}{\partial x^*}+u^*\frac{\partial T^*}{\partial x^*}+v^*\frac{\partial T^*}{\partial y^*}=\frac{1}{\mathrm{Pr}}\frac{\partial^2 T^*}{\partial y^{*2}}+Ec\left(\frac{\partial u^*}{\partial y^*}\right)^2. \quad (2.37)$$

2.2.2 In cylindrical coordinates

For axisymmetric flow over a surface held at $z = 0$, the variation with respect to φ is neglected and the two dimensional continuity equation and the Navier-Stokes equations in the absence of body force can be written as

$$\frac{\partial^2 u}{\partial r^2} + \frac{1}{r}\frac{\partial u}{\partial r} + \frac{\partial w}{\partial z} = 0, \tag{2.38}$$

$$\frac{\partial u}{\partial t} + u\frac{\partial u}{\partial r} + w\frac{\partial u}{\partial z} = -\frac{1}{\rho}\frac{\partial P}{\partial r} + \nu\left(\frac{\partial^2 u}{\partial r^2} + \frac{1}{r}\frac{\partial u}{\partial r} - \frac{u}{r^2} + \frac{\partial^2 u}{\partial z^2}\right), \tag{2.39}$$

$$\frac{\partial w}{\partial t} + u\frac{\partial w}{\partial r} + w\frac{\partial w}{\partial z} = -\frac{1}{\rho}\frac{\partial P}{\partial z} + \nu\left(\frac{\partial^2 w}{\partial r^2} + \frac{1}{r}\frac{\partial w}{\partial r} + \frac{\partial^2 w}{\partial z^2}\right). \tag{2.40}$$

For boundary layer analysis, the procedure for the order of magnitude analysis given in [149] as practiced in the previous section is followed.

In order to make Eqs. (2.38-2.40) dimensionless, the transformations used are

$$t^* = \frac{tU_o}{L},\ r^* = \frac{r}{L},\ z^* = \frac{z}{L},\ u^* = \frac{u}{U_o},\ w^* = \frac{w}{U_o},\ P^* = \frac{P}{\rho U_o{}^2}, \tag{2.41}$$

In this case $r^* = O(1),\ u^* = O(1),\ z^* = O(\delta^*),\ w^* = O(\delta^*)$, $\frac{1}{\mathrm{Re}} = O(\delta^{*2})$, $\frac{\partial P^*}{\partial r} = O(1)$ and $\frac{\partial P^*}{\partial z} = O\left(\frac{1}{\delta}\right)$ due to which the Continuity equation (2.38) stays unchanged whereas the Eqs. (2.39) and (2.40) simplify as:

$$\frac{\partial u^*}{\partial t^*} + u^*\frac{\partial u^*}{\partial r^*} + w^*\frac{\partial u^*}{\partial z^*} = -\frac{\partial P^*}{\partial r^*} + \frac{\partial^2 u^*}{\partial z^{*2}}. \tag{2.42}$$

The two dimensional energy equation in cylindrical coordinates with viscous dissipation effects is

$$\rho c_p\left(\frac{\partial T}{\partial t}+u\frac{\partial T}{\partial r}+w\frac{\partial T}{\partial z}\right)=k\left[\frac{\partial^2 T}{\partial r^2}+\frac{1}{r}\frac{\partial T}{\partial r}+\frac{\partial^2 T}{\partial z^2}\right]$$
$$+2\mu\left[\left(\frac{\partial u}{\partial r}\right)^2+\left(\frac{u}{r}\right)^2+\left(\frac{\partial w}{\partial z}\right)^2\right]+\mu\left\{\left(\frac{\partial u}{\partial z}+\frac{\partial w}{\partial r}\right)^2\right\}. \quad (2.43)$$

Introducing $T^*=\frac{T-T_\infty}{T_w-T_\infty}$ and using (2.25), the above equation becomes

$$\frac{\partial T^*}{\partial t^*}+u^*\frac{\partial T^*}{\partial r^*}+w^*\frac{\partial T^*}{\partial z^*}=\frac{1}{\mathrm{Pr}\,\mathrm{Re}}\left[\frac{\partial^2 T^*}{\partial r^{*2}}+\frac{1}{r^*}\frac{\partial T^*}{\partial r^*}+\frac{\partial^2 T^*}{\partial z^{*2}}\right]$$
$$+\frac{Ec}{\mathrm{Re}}\left[2\left\{\left(\frac{\partial u^*}{\partial r^*}\right)^2+\left(\frac{u^*}{r^*}\right)^2+\left(\frac{\partial w^*}{\partial z^*}\right)^2\right\}+\left(\frac{\partial u^*}{\partial z^*}+\frac{\partial w^*}{\partial r^*}\right)^2\right]. \quad (2.44)$$

Taking $T=O(1)$ and using the orders defined above for velocities and lengths we have

$$\frac{\partial T^*}{\partial t^*}+u^*\frac{\partial T^*}{\partial r^*}+w^*\frac{\partial T^*}{\partial z^*}=\frac{1}{\mathrm{Pr}}\frac{\partial^2 T^*}{\partial z^{*2}}+Ec\left(\frac{\partial u^*}{\partial z^*}\right)^2. \quad (2.45)$$

2.3 Laws of thermodynamics

2.3.1 First law of thermodynamics

The first law of thermodynamics is simply the law of conservation of energy. It states that energy changes its form from one to another, but the total amount of energy remains conserved, i.e., the energy can neither be created nor be destroyed. The first law of thermodynamics indicates the equivalence of different forms of energy. If defines the internal energy of the system as a state function and gives the relationship between work and absorbed energy. However, it fails to predict whether the change of energy will occur or not and up to what extent will the change be. Moreover, it does not provide any information about the direction of the change during the spontaneous process, i.e., the reversibility aspect of thermodynamical processes.

2.3.2 Second law of thermodynamics

The first law of thermodynamics states about the conservation of energy, i.e., the quantity of energy remains the same. However, energy has qualitative aspect as well. Whenever there is a transaction of energy from one form to another, some part of it becomes useless which cannot be reversed. This useless energy is measured by using a standard metric known as entropy. In terms of entropy, the second law states that the entropy of the universe (system and its surroundings) either remains the same or increases. The second law of thermodynamics is utilized to determine the performance and efficiency of engineering systems.

2.4 Entropy generation

Entropy is associated with the thermodynamic irreversibility of the flow and heat transfer systems. It is a measure of randomness disorder in the system. As the entropy of the system increases, the energy that can be used by the system decreases. Thus, entropy destroys the available energy that can be used for work. The study of entropy generation effects is significant as it can be helpful to improve the efficiency and performance of the engineering systems. This can be achieved by minimizing the entropy generation effects in the system. Bejan [11] showed that there are several factors behind the generation of entropy, which destroys the useful work. The expression for the local entropy generation per unit volume is

$$S_G = \frac{k}{T_{ref}^{\,2}}\left(\nabla T\right)^2 + \frac{\mu}{T_{ref}}\Phi, \tag{2.46}$$

where the first term represents the entropy effects due to temperature gradient and second term represents the entropy generation due to viscous dissipation. When the effects of external forces such as magnetic or electric fields are present, then we have [28]

$$S_G = \frac{k}{T_{ref}^{\,2}}\left(\nabla T\right)^2 + \frac{\mu}{T_{ref}}\Phi + \frac{1}{T_{ref}}\left[\left(\mathbf{J} - Q\mathbf{V}\right).\left(\mathbf{E} + \mathbf{V}\times\mathbf{B}\right)\right], \tag{2.47}$$

where k is the thermal conductivity, μ is the viscosity, T_{ref} is the reference temperature, Φ is the viscous dissipation, Q is the electric charge density, $\mathbf{V}$ denotes the velocity vector, $\mathbf{E}$ represents the electric field, $\mathbf{B}$ is the magnetic field and J is the current density given by

$$\mathbf{J} = \sigma\left(\mathbf{E} + \mathbf{V} \times \mathbf{B}\right), \tag{2.48}$$

where σ denotes the electrical conductivity of the fluid.

The local entropy generation number can be made dimensionless by dividing the local entropy generation S_G by the characteristic entropy generation $S_{Go} = \dfrac{k\left(\Delta T\right)^2}{T_{ref}{}^2 L^2}$ and is called entropy generation number dentoed by Ns, i.e.

$$Ns = \frac{S_G}{S_{G0}}. \tag{2.49}$$

The total entropy generation number is given by integrating S_G over the entire domain

$$S_{G_{tot}} = \int S_G d\forall, \tag{2.50}$$

where $\forall$ represents the considered domain.

Another useful parameter used in entropy generation analysis is Bejan number which gives information whether entropy generation due to viscous dissipation is dominant over heat transfer entropy effects or vice versa. It is defined as

$$Be = \frac{Entropy\ due\ to\ heat\ transfer}{\text{Local } entropy\ generation}. \tag{2.51}$$

From (2.51), it is quite evident that the range of Bejan number is $0 \le Be \le 1$. For $Be > 0.5$, the entropy effects due to heat transfer dominate over fluid friction entropy effects. On the other hand, when $Be < 0.5$, the entropy effects due to fluid friction are prominent. The contribution of entropy due to heat transfer is equal to that of fluid friction when $Be = 0.5$. When $Be = 0$, the fluid friction effects are in fully

dominant and the value $Be = 1$ shows the dominance of heat transfer entropy effects. The expression for local entropy generation defined in Eq. (2.46) in terms of rectangular coordinates (x, y, z) can be written as

$$S_G = \frac{k}{{T_{ref}}^2}\left[\left(\frac{\partial T}{\partial x}\right)^2 + \left(\frac{\partial T}{\partial y}\right)^2 + \left(\frac{\partial T}{\partial z}\right)^2\right] + \frac{\mu}{T_{ref}}\left[\begin{array}{l} 2\left\{\left(\frac{\partial u}{\partial x}\right)^2 + \left(\frac{\partial v}{\partial y}\right)^2 + \left(\frac{\partial w}{\partial z}\right)^2\right\} \\ +\left\{\left(\frac{\partial u}{\partial y} + \frac{\partial v}{\partial x}\right)^2 + \left(\frac{\partial u}{\partial z} + \frac{\partial w}{\partial x}\right)^2 + \left(\frac{\partial v}{\partial z} + \frac{\partial w}{\partial y}\right)^2\right\} \end{array}\right]. \tag{2.52}$$

In cylindrical coordinates, it takes the form

$$S_G = \frac{k}{{T_{ref}}^2}\left[\left(\frac{\partial T}{\partial r}\right)^2 + \left(\frac{1}{r}\frac{\partial T}{\partial \theta}\right)^2 + \left(\frac{\partial T}{\partial z}\right)^2\right] + \frac{\mu}{T_{ref}}\left[\begin{array}{l} 2\left\{\left(\frac{\partial u}{\partial r}\right)^2 + \left(\frac{1}{r}\frac{\partial v}{\partial \varphi} + \frac{u}{r}\right)^2 + \left(\frac{\partial w}{\partial z}\right)^2\right\} \\ +\left\{\left(r\frac{\partial}{\partial r}\left(\frac{v}{r}\right) + \frac{1}{r}\frac{\partial u}{\partial \varphi}\right)^2 + \left(\frac{1}{r}\frac{\partial w}{\partial \varphi} + \frac{\partial v}{\partial z}\right)^2 + \left(\frac{\partial u}{\partial z} + \frac{\partial w}{\partial r}\right)^2\right\} \end{array}\right]. \tag{2.53}$$

2.5 Aims and objectives of the current study

The present study aims to theoretically investigate the effects of entropy generation in laminar flow and heat transfer phenomena of viscous fluid over stretching surfaces in some internal and external flows.

The objectives of the present theoretical study are:

(i) To calculate the entropy generation rate in internal and external flows past a stretching surface.

(ii) The impact of applied magnetic field, porous medium, convective heat transfer or squeezing of channel wall etc, on the entropy generation rate in various flow situations.

(iii) Dependence of the entropy generation rate and Bejan number upon the important physical parameters involved in a particular problem.

2.6 Solution methodologies

Both analytical and numerical techniques are employed to solve the nonlinear differential equations that rise from the mathematical modeling of physical problems. The analytical solutions of the problems are obtained in the form of series via Homotopy Analysis Method (HAM) and the numerical solutions are attained with the aid of shooting technique combined with fourth-fifth order Runge-Kutta-Felhberg method.

2.6.1 Homotopy Analysis Method (HAM)

Most problems of the physical world, when given mathematical formulation turn out to be highly nonlinear differential equations. It is not possible to obtain the exact solution of such equation by conventionally used techniques and one has to look towards approximate solutions. Several techniques are available in the literature which give approximate analytical solutions of such problems. Out of them, the Homotopy Analysis Method (HAM) is a powerful method that is employed to solve highly nonlinear equations. This method was proposed, modified and developed by Liao [115] which is based on the concept of homotopy from topology. This method gives an approximate analytical solution of the problem in the form of series solution.

Consider the nonlinear differential equation of the form:

$$\mathcal{N}\left[v(x)\right] = 0, \quad x \in D \tag{2.54}$$

where $\mathcal{N}$ denotes the non-linear operator and $v(x)$ is an unknown function. Let us denote the initial approximation of $v(x)$ by $v_0(x)$ and $\mathcal{L}$ represent the auxiliary linear operator having the property

$$\mathcal{L}\left[v_0(x)\right] = 0. \tag{2.55}$$

The choice of linear operator and initial approximation guess are made such that they satisfy the initial and boundary condition of the original problem. By the introduction of non-zero auxiliary parameter $\hbar$ and a non-zero auxiliary function $H(x)$, the so called zero order deformation equation can be defined as

$$(1-q)\mathcal{L}\left[\Lambda(x;q,\hbar,H)-v_0(x)\right]=q\hbar H(x)\mathcal{N}\left[\Lambda(x;q,\hbar,H)\right], \tag{2.56}$$

where $q\in[0,1]$ is an embedding parameter. It is quite evident from Eq. from Eq. (2.56) that we get the initial guess

$$\Lambda(x;q)=v_0(x) \text{ at } q=0, \tag{2.57}$$

and the final solution

$$\Lambda(x;q)=v(x) \text{ at } q=1. \tag{2.58}$$

Then, the solution $\Lambda(x;q)$ varies from the initial approximation $v_0(x)$ to final solution $v(x)$ as the value of q varies from 0 to 1. Here the auxiliary parameter $\hbar$ is significant as it helps us to handle the convergence of the solution. The solution $\Lambda(x;q)$ is expanded by in the form of Taylor's series with respect to q as follows:

$$\Lambda(x;q)=v_0(x)+\sum_{m=1}^{\infty}v_m(x)q^m, \tag{2.59}$$

where

$$v_m(x)=\frac{1}{m!}\frac{\partial^m\Lambda(x;q)}{\partial q^m}\bigg|_{q=0}. \tag{2.60}$$

Observe that if the series (2.59) converges as the value of q approaches to 1, then the function $\Lambda(x;q)$ represents the solution of the differential equation. The mth order deformation equation is attained by differentiating Eq. (2.56) m-times with respect to the embedding parameter q and then setting $q=0$ and finally dividing by $m!$. Thus we get

$$\mathcal{L}\left[v_m(x)-\chi_{m-1}v_{m-1}(x)\right]=\hbar H(x)\mathcal{R}_m(x), \tag{2.61}$$

where

$$\mathcal{R}_m(x)=\frac{1}{(m-1)!}\frac{\partial^{m-1}\mathcal{N}\left[\Lambda(x;q)\right]}{\partial q^{m-1}}\bigg|_{q=0}, \tag{2.62}$$

and

$$\chi_m=\begin{cases}0, & m\le 1,\\ 1, & m>1.\end{cases} \tag{2.63}$$

Here Eq. (2.61) indicates a system of linear differential equations whose solution can be solved for $m\ge 1$. Thus the solution of v_m can be obtained for $m\ge 1$ and the final solution can be attained in the form of infinite series as:

$$v(x)=v_0(x)+\sum_{m=1}^{\infty}v_m(x). \tag{2.64}$$

It is quite evident from Eq. (2.64) that the obtained Homotopy series solution not only depends on the variable but also on the auxiliary parameter $\hbar$ defined in Eq. (2.56). It was shown by Liao [117] that the auxiliary parameter $\hbar$ can be used to control and adjust the convergence rate of the series solution (2.64). By choosing admissible value of the $\hbar$, one can assure the convergence of the series solution (2.64). The values of auxiliary parameter $\hbar$ are obtained by plotting so called $\hbar$-curve which is an interval in which the series solution (2.64) is convergent. It is worth mentioning that (2.64) converges for all values of $\hbar$-curve but the convergence rate is different for different values. By choosing the optimal value of auxiliary parameter $\hbar$, the rate of convergence rate of $v(x)$ can be accelerated. This optimal value of $\hbar$ can be attained by using averaged square residual error [147]

$$E_{m,v} = \frac{1}{N+1}\sum_{j=0}^{N}\left[\mathcal{N}\left(\sum_{i=0}^{m} v_i(j\Delta\zeta)\right)\right]^2. \tag{2.65}$$

The averaged square residual error contains the unknown convergence control parameter $\hbar$ whose optimized values can be calculated by minimizing $E_{m,v}$ corresponding to nonlinear algebraic equation

$$\frac{\partial E_{m,v}}{\partial \hbar} = 0. \tag{2.66}$$

By utilizing this optimal value of convergence control parameter $\hbar$, the convergence of the series solution (2.64) can be made rapid.

2.6.2 Shooting method

Shooting method is a numerical technique which is used to solve a boundary value problem (BVP) by converting into an initial value problem (IVP). This is done by reducing the boundary value problem into system of first order differential equations and replacing the one boundary condition with an initial condition which is to be determined. The system is solved by using the fourth-fifth order Runge-Kutta-Fehlberg method by initially guessing the initial condition. This condition is adjusted until the boundary condition at the end is satisfied.

Let us consider the two point boundary value problem

$$y'' = f(x, y, y'), \quad y(a) = A, \quad y(b) = B, \tag{2.67}$$

where $a < b$ and $x \in [a, b]$.

Converting the BVP to IVP by replacing the boundary condition $y(b) = B$ by $y'(a) = \varepsilon$ and denoting it by $y(x;\varepsilon)$. Introducing the following notation

$$\left.\begin{aligned} w_1(x;\varepsilon) &= y(x;\varepsilon), \\ w_2(x;\varepsilon) &= \frac{\partial}{\partial x} y(x;\varepsilon) \end{aligned}\right\}. \tag{2.68}$$

Then Eq. (2.66) takes the form

$$\left.\begin{aligned} \frac{\partial}{\partial x} w_1(x;\varepsilon) &= w_2(x;\varepsilon), & w_1(a) &= A, \\ \frac{\partial}{\partial x} w_2(x;\varepsilon) &= f\left(x, w_1(x;\varepsilon), w_2(x;\varepsilon)\right), & w_2(a) &= \varepsilon. \end{aligned}\right\} \tag{2.69}$$

The solution $w_1(x;\varepsilon)$ of the initial value problem (2.69) will match the solution $y(x)$ of the boundary value problem (2.66) provided that the value of ε can be found such that

$$W(\varepsilon) \equiv w_1(b;\varepsilon) - B = 0. \tag{2.70}$$

The theme of the shooting method is to find the root of the equation (2.70). The fourth-fifth order Runge-Kutta-Fehlberg technique is utilized to find the solution of the system (2.69). This method adapts to the proper step size that is to be used for computation. Two different approximations for the solution are computed and compared at each step of the calculation. If both the answers are in close agreement, then the approximation is accepted. On the other hand, the step size is adjusted according to the situation if the two approximations do not meet the required accuracy. At each step of Runge–Kutta Fehlberg algorithm, following six values are calculated:

$$\left.\begin{aligned} k_1 &= hf(x_i, y_i), \\ k_2 &= hf\left(x_i + \frac{h}{4}, y_i + \frac{1}{4}k_1\right), \\ k_3 &= hf\left(x_i + \frac{3h}{8}, y_i + \frac{3}{32}k_1 + \frac{9}{32}k_2\right), \\ k_4 &= hf\left(x_i + \frac{12h}{13}, y_i + \frac{1932}{2197}k_1 - \frac{7200}{2197}k_2 + \frac{7296}{2197}k_3\right), \\ k_5 &= hf\left(x_i + h, y_i + \frac{439}{216}k_1 - 8k_2 + \frac{3680}{513}k_3 - \frac{845}{4104}k_4\right), \\ k_6 &= hf\left(x_i + \frac{h}{2}, y_i - \frac{8}{27}k_1 + 2k_2 - \frac{3544}{2565}k_3 + \frac{1859}{4104}k_4 - \frac{11}{40}k_5\right). \end{aligned}\right\} \tag{2.71}$$

A Runge-Kutta method of order four is used to find an approximation of the IVP as:

$$y_{i+1} = y_i + \frac{25}{216}k_1 + \frac{1408}{2565}k_3 + \frac{2197}{4101}k_4 - \frac{1}{5}k_5. \tag{2.72}$$

Here, the four function values k_1, k_3, k_4 and k_5 are utilized while the value of k_2 is not used. The improved value of the solution is attained by using a Runge-Kutta method of order fifth as:

$$\tilde{y}_{i+1} = y_i + \frac{16}{135}k_1 + \frac{6656}{12825}k_3 + \frac{28561}{56430}k_4 - \frac{9}{50}k_5 + \frac{2}{55}k_6. \tag{2.73}$$

The error is estimated by subtracting the two obtained values. If the error increases the specified threshold, the step size is reduced and the results are calculated again. The optimal step size is computed as:

$$h_{new} = \left(\frac{\in h_{old}}{2|\tilde{y}_{i+1} - y_{i+1}|} \right)^{1/4} \tag{2.74}$$

2.7 Significant dimensionless numbers

Dimensionless numbers are the quantities having no physical dimension. They have either no units or are the ratios of physical quantities whose dimensions cancel out to become a unity. These numbers play an important role in the study of flow and heat transfer characteristics. They provide a numerical scaling of the differential equations and present the solution in a compact form. Some of the important dimensionless numbers that appear in our thesis are mentioned below:

2.7.1 Reynolds number

The Reynolds number Re is named after the British physicist and engineer Osborne Reynolds and is the ratio of inertial force to viscous forces. Mathematically, we write:

$$\mathrm{Re} = \frac{U_0 L}{\nu}, \tag{2.75}$$

where U_0 is the characteristic velocity, L is the reference length and ν is the kinematic viscosity. It is used to predict whether the flow is laminar or turbulent. When the Reynolds number Re is small, the effects of viscous forces are strong as compared to inertial force and the flow is laminar. On the other hand, when the value of Re is large, the inertial forces are dominant over viscous forces and the flow develops to become turbulent.

2.7.2 Hartmann number

The Hartmann number M was first introduced by Hartmann during his experiments with the magnetohydrodynamic viscous channel flow and is the ratio of the electromagnetic force to the viscous force. It is defined as:

$$M = B_0 L \sqrt{\frac{\sigma}{\mu}}, \tag{2.76}$$

where B_0 is the magnetic field, L is the characteristic length, σ is the electrical conductivity and μ is the dynamic viscosity.

2.7.3 Prandtl number

Prandtl number is an important dimensionless parameter that shows the relation between fluid viscosity and heat conduction. It is simply the ratio of kinematic viscosity to thermal diffusivity. Mathematically, it is written as:

$$\mathrm{Pr} = \frac{\nu}{\alpha'}, \tag{2.77}$$

where α' denotes the thermal diffusivity and ν is the kinematic viscosity of the fluid.

2.7.4 Eckert number

Eckert number is a significant dimensionless parameter that appears in the energy equation due to viscous dissipation effects. It is described mathematically as:

$$Ec = \frac{U_0^{\,2}}{c_p \Delta T}, \tag{2.78}$$

where U_o is the reference velocity, c_p represents the specific heat capacity and ΔT shows the difference between wall and fluid ambient temperature.

2.7.5 Biot number

Biot number is a dimensionless number named *Jean Baptiste Biot* and is simply the ratio of the heat transfer resistance inside and at the surface of a body. It is defined as:

$$Bi = \frac{h'L}{k}, \tag{2.79}$$

where h' is the coefficient of heat transfer, L is the characteristic length and k is the thermal conductivity of the body. The Biot number appears while non-dimensionalizing the boundary conditions for the heat transfer problems. It decides whether the body heats up or cools down over time from the thermal gradient applied to the surface.

2.7.6 Skin friction

Skin friction is a drag force between the surface and the fluid due to the viscous stresses. It is defined as the viscous force per unit area acting at the surface and is denoted by τ_w. In Cartesian coordinate system, it is given by:

$$\tau_w = \mu \left.\frac{\partial u}{\partial y}\right|_{y=0}. \tag{2.80}$$

The local skin friction coefficient C_f on the wall is given by:

$$C_f = \frac{\tau_w}{\rho U_0^{\,2}}, \tag{2.81}$$

2.7.7 Nusselt number

The Nusselt number is a dimensionless quantity which is named after *Wilhelm Nusselt* due to his significant contributions in the field of convective heat transfer. It is simply the dimensionless form of heat transfer coefficient and is the ratio convective to conductive heat transfer across (normal) to the surface. It is defined as:

$$Nu = \frac{q_w x}{k\Delta T}, \tag{2.82}$$

Where x is the distance of flow from the surface edge, ΔT is the temperature difference between the wall and fluid ambient, q_w is the heat transfer rate at the surface and is given by:

$$q_w = -k \left. \frac{\partial T}{\partial y} \right|_{y=0}. \tag{2.83}$$

2.8 Darcy law

Darcy's Law was enunciated by Henry Darcy. It describes the flow of a fluid through a porous medium and states that the volumetric flux (commonly known as Darcy velocity) is proportional to the pressure gradient. It is defined as:

$$\mathbf{V} = \frac{k'}{\mu} \nabla p, \tag{2.84}$$

where $\mathbf{V}$ is the volumetric flux, k' denotes the permeability parameter, μ is the dynamic viscosity and ∇p is the pressure gradient.

2.9 Partial slip boundary condition

In fluid dynamics, one of the basic principles is that the fluid adheres to the solid boundary and there is usually zero relative velocity between the fluid and solid interface. However, this is not the case in many practical situations and there are situations where the fluid may slip on the surface of the solid. Generally, the slip is assumed to depend on the shear stress at the wall and is given as:

$$u - u_{wall} = \beta^* \frac{\partial u}{\partial n}, \tag{2.85}$$

where n is the coordinate normal to the wall and β^* represents the slip length.

Chapter 3

Entropy analysis of MHD viscous flow over a stretching surface with partial slip and convective boundary

3.1 Introduction

This chapter concerns with the study of entropy effects in magnetohydrodynamic flow of a viscous fluid over a stretching sheet with partial slip and convective boundary. The nonlinear partial differential equations governing the flow and heat transfer phenomena are reduced to a set of nonlinear ordinary differential equations with the help of suitable similarity transformations. The transformed equations are then solved analytically with the help of analytical technique known as Homotopy Analysis Method (HAM). The expressions for the velocity and the temperature fields are obtained and utilized in order to compute the entropy generation number and Bejan number. Both numerical and graphical results are presented and discussed for various parameters involved in the problem.

3.2 Mathematical description of the problem

3.2.1 Flow modelling

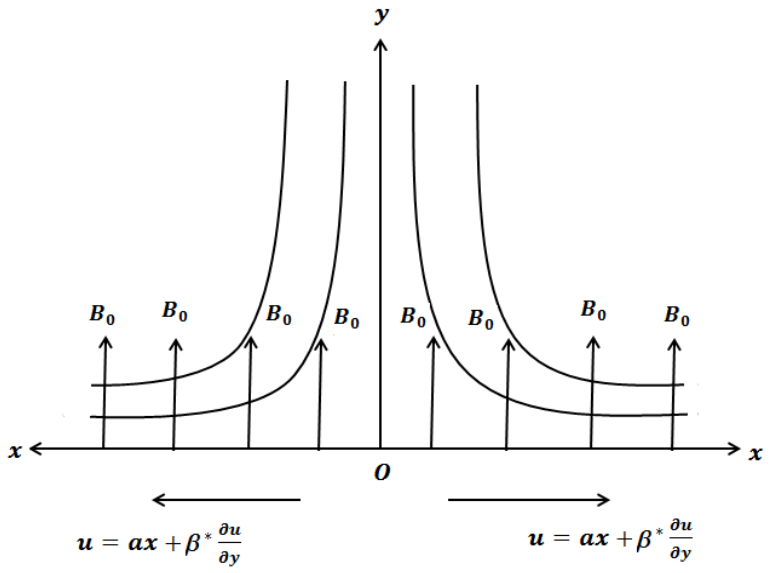

Figure 3.1: Schematic diagram of the considered problem

A steady 2D laminar, incompressible viscous fluid flow over a stretching sheet is considered. The sheet is placed in the plane $y = 0$ whereas the fluid lies above the sheet, i.e. in the region $y > 0$. The coordinate x is considered to be along the stretching sheet and y is normal to the surface. The sheet is being stretched by applying two equal and opposite forces along the x-axis, keeping the origin fixed. In the direction of y-axis, a uniform magnetic field of strength B_0 is applied. The presence of electric field and induced magnetic field is neglected which results in small magnetic Reynolds number. Thus, the equations governing the flow phenomenon are obtained by applying boundary layer approximation on Eqs. (2.1-2.2) and are written as

$$\frac{\partial u}{\partial x} + \frac{\partial v}{\partial y} = 0, \tag{3.1}$$

$$u\frac{\partial u}{\partial x} + v\frac{\partial u}{\partial y} = \nu\frac{\partial^2 u}{\partial y^2} - \frac{\sigma B_0^2 u}{\rho}. \tag{3.2}$$

The associated boundary conditions are

$$\left.\begin{aligned} u = u_w(x) + \beta^* \frac{\partial u}{\partial y}, \quad v = 0, \quad at \quad y = 0, \\ u \to 0, \qquad\qquad\qquad as \quad y \to \infty, \end{aligned}\right\} \tag{3.3}$$

where $u_w(x) = ax$, u and v are the x and y components of the velocity respectively, ν is the kinematic viscosity of the fluid, σ is the electrical conductivity of the fluid, B_0 is the applied magnetic field, ρ is the density of the fluid, β^* is the slip parameter and $a > 0$ is the dimensional constant.

The equations (3.1-3.2) can be made dimensionless by introducing the following set of similarity transformations

$$u = axf'(\eta), \quad v = -\sqrt{a\nu}\, f(\eta), \quad \eta = \sqrt{\frac{a}{\nu}}y. \tag{3.4}$$

By substituting (3.4) into Eqs. (3.1-3.2), the continuity equation (3.1) is identically satisfied and Eq. (3.2) takes the non-dimensional form

$$f''' + ff'' - f'^2 - Mf' = 0, \tag{3.5}$$

and the boundary conditions (3.3) take the form

$$f'(0) = 1 + \gamma f''(0), \quad f(0) = 0, \quad f(\infty) = 0. \tag{3.6}$$

The skin friction coefficient C_f is defined as

$$C_f = \frac{\tau_w}{\rho(ax)^2}, \tag{3.7}$$

where τ_w is the shear wall stress and is expressed as

$$\tau_w = \mu\left(\frac{\partial u}{\partial z}\right)_{z=0}. \tag{3.8}$$

Using (3.8) in (3.7) and utilizing (3.4), the dimensionless form of skin friction coefficient becomes

$$C_f \, \mathrm{Re}_x^{1/2} = f''(0), \tag{3.9}$$

where $\mathrm{Re}_x = \frac{u_w x}{\nu}$ is the local Reynolds number.

3.2.2 Heat transfer analysis

The stretching surface is convectively heated by passing a hot fluid having a temperature T_f from its bottom which provides a heat transfer coefficient h'. The ambient fluid temperature is assumed to be T_∞. It is also considered that the viscous dissipation and Joule dissipation effects are also present. Then the boundary layer equation that governs the heat transfer phenomena is obtained from Eq. (2.3) and is given by

$$u\frac{\partial T}{\partial x} + v\frac{\partial T}{\partial y} = \frac{k}{\rho c_p}\frac{\partial^2 T}{\partial y^2} + \frac{\nu}{c_p}\left(\frac{\partial u}{\partial y}\right)^2 + \frac{\sigma B_0^2}{\rho c_p}u^2, \tag{3.10}$$

where the boundary conditions are

$$-k\frac{\partial T}{\partial y} = h'(T_f - T) \quad \text{at} \quad y = 0, \quad T = T_\infty \quad \text{as} \quad z \to \infty. \tag{3.11}$$

Here k is the thermal diffusivity of the fluid and c_p is the specific heat at constant pressure. The following similarity transformation is used to non-dimensionlize the Eq. (3.10)

$$\theta = \frac{T - T_\infty}{T_w - T_\infty}. \tag{3.12}$$

By using (3.4) and (3.12), the Eq. (3.10) can be written in dimensionless form as

$$\theta'' + \mathrm{Pr}\, f\theta' + \mathrm{Pr}\, Ec\, f''^2 + M\, \mathrm{Pr}\, Ec\, f'^2 = 0, \tag{3.13}$$

and the boundary conditions (3.11) become

$$\theta'(0) = -Bi\left(1-\theta(0)\right), \qquad \theta(\infty) = 0. \tag{3.14}$$

Here $\Pr = \dfrac{\mu c_p}{k}$ is the Prandtl number, $Ec = \dfrac{u_w^{\,2}}{c_p(T_w - T_\infty)}$ is the Eckert number and $Bi = \dfrac{h'}{k}\sqrt{\dfrac{\nu}{a}}$ is the Biot number.

The local Nusselt number Nu_x is given by

$$Nu_x = \frac{q_w}{k(T_w - T_\infty)}, \tag{3.15}$$

where the heat flux from the surface q_w is given by

$$q_w = -k\left(\frac{\partial T}{\partial z}\right)_{z=0}. \tag{3.16}$$

After substituting (3.16) into (3.15) and utilizing (3.12), the local Nusselt number becomes

$$\mathrm{Re}_x^{\,-1/2}\, Nu_x = -\theta'(0). \tag{3.17}$$

3.2.3 Entropy analysis

The local entropy generation rate per unit volume S_G for a viscous fluid in the presence of magnetic field is defined in Eq. (2.47) and after applying boundary layer approximation can be written as

$$S_G = \frac{k}{T_f^{\,2}}\left(\frac{\partial T}{\partial y}\right)^2 + \frac{\mu}{T_f}\left(\frac{\partial u}{\partial y}\right)^2 + \frac{\sigma B_0^{\,2}}{T_f}u^2. \tag{3.18}$$

The first term in Eq. (3.18) is the local entropy generation due to heat transfer, the second term is the entropy generation due to viscous dissipation and the third term is the local entropy generation due to the effects of the magnetic field. In terms of dimensionless variables, the entropy generation has the form

$$Ns = \frac{S_G}{S_{Go}} = \mathrm{Re}_L\,\theta'^2 + \mathrm{Re}_L\frac{Br}{\Omega}f''^2 + \mathrm{Re}_L\frac{Br}{\Omega}M f'^2, \tag{3.19}$$

where $S_{Go} = \frac{k(T_f - T_\infty)^2}{T_f{}^2 L^2}$ is the characteristic entropy generation rate, $\Omega = \frac{T_f - T_\infty}{T_f}$ is the dimensionless temperature difference and $Br = \Pr Ec$ is the Brinkman number. Thus dimensionless form of local entropy generation in Eq. (3.19) can be expressed as

$$Ns = N_H + N_f + N_m = N_H + N_F, \tag{3.20}$$

Where N_H is the local entropy generation due to heat transfer, N_f is the local entropy generation due to fluid friction and N_m is the local entropy generation due to magnetic field.

An alternative irreversibility distribution parameter called the Bejan number is defined as follows

$$Be = \frac{N_H}{Ns}. \tag{3.21}$$

Clearly, the Bejan number ranges from 0 to 1. When the value of Be is greater than 0.5, the irreversibility due to heat transfer dominates whereas $Be < 0.5$ refers to irreversibility due to viscous dissipation and magnetic field. The contribution of entropy due to heat transfer is equal to that of fluid friction and magnetic field, when $Be = 0.5$.

3.3 Solution methodology

The solutions of nonlinear ordinary differential equation for flow (3.5) with boundary conditions (3.6) and the equation representing the heat transfer phenomenon (3.13) having boundary conditions (3.14) are obtained using the Homotopy Analysis Method (HAM) proposed.by Liao [115,117]. In view of the boundary data (3.6) and (3.14), the following set of initial guesses are chosen

$$\left.\begin{aligned} f_0(\eta) &= \frac{1}{1+\gamma}\left(1-e^{-\eta}\right), \\ \theta_0(\eta) &= \frac{Bi}{1+Bi}e^{-\eta}. \end{aligned}\right\} \tag{3.22}$$

The linear operators are given as

$$\left.\begin{aligned} \mathcal{L}_f(f) &= \frac{d^3 f}{d\eta^3} - \frac{df}{d\eta}, \\ \mathcal{L}_\theta(\theta) &= \frac{d^2\theta}{d\eta^2} + \frac{d\theta}{d\eta}, \end{aligned}\right\} \tag{3.23}$$

with

$$\left.\begin{aligned} \mathcal{L}_f\left(C_1 + C_2 e^{-\eta} + C_3 e^{\eta}\right) &= 0, \\ \mathcal{L}_\theta\left(C_4 + C_5 e^{-\eta}\right) &= 0, \end{aligned}\right\} \tag{3.24}$$

where $C_i's,\ (i=1,2,...5)$ are the arbitrary constants.

The zeroth-order deformations are

$$(1-q)\mathcal{L}_f\left[\ \Lambda(\eta;q) - f_0(\eta)\right] = \hbar_f q \mathcal{N}_f\left[\Lambda(\eta;q)\right], \tag{3.25}$$

$$(1-q)\mathcal{L}_\theta\left[\Theta(\eta;p) - \theta_0(\eta)\right] = \hbar_\theta q \mathcal{N}_\theta\left[\Lambda(\eta;q), \Theta(\eta;q)\right], \tag{3.26}$$

$$\begin{aligned} &\Lambda(0;q) = 0, \quad \Lambda'(0;q) = 1+\gamma\ \Lambda''(0;q), \quad \Lambda'(\infty;q) = 0, \\ &\Theta'(0;q) = -Bi(1-\Theta(0;q)), \quad \Theta(\infty;q) = 0. \end{aligned} \tag{3.27}$$

In Eqs. (3.25-3.26), $\hbar_f$ and $\hbar_\theta$ are the non-zero auxiliary parameters and $q \in [0,1]$ is the embedding parameter.

The nonlinear operators are given by

$$\mathcal{N}_f\left[\Lambda(\eta;p)\right]=\frac{\partial^3\Lambda(\eta;q)}{\partial\eta^3}+\Lambda(\eta;p)\frac{\partial^2\Lambda(\eta;q)}{\partial\eta^2}-\left(\frac{\partial\Lambda(\eta;q)}{\partial\eta}\right)^2-M\frac{\partial\Lambda(\eta;q)}{\partial\eta}, \tag{3.28}$$

$$\left.\begin{aligned}\mathcal{N}_\theta\left[\Theta(\eta;q),\Lambda(\eta;q)\right]=\frac{\partial^2\Theta(\eta;q)}{\partial\eta^2}+\Pr\Lambda(\eta;q)\frac{\partial\Theta(\eta;q)}{\partial\eta}+\Pr Ec\left(\frac{\partial^2\Lambda(\eta;q)}{\partial\eta^2}\right)^2\\ +M\Pr Ec\left(\frac{\partial\Lambda(\eta;q)}{\partial\eta}\right)^2.\end{aligned}\right\} \tag{3.29}$$

For $q=0$ and $q=1$, we have

$$\left.\begin{aligned}\Lambda(\eta;0)=f_0(\eta), \quad \Lambda(\eta;1)=f(\eta),\\ \Theta(\eta;0)=\theta_0(\eta), \quad \Theta(\eta;1)=\theta(\eta).\end{aligned}\right\} \tag{3.30}$$

By use of Taylor series expansion, one obtains

$$\Lambda(\eta;p)=f_0(\eta)+\sum_{m=1}^{\infty}f_m(\eta)q^m, \tag{3.31}$$

$$\Theta(\eta;p)=\theta_0(\eta)+\sum_{m=1}^{\infty}\theta_m(\eta)q^m, \tag{3.32}$$

with

$$f_m(\eta)=\frac{1}{m}\frac{\partial^m\Lambda(\eta;q)}{\partial q^m}\bigg|_{q=0}, \tag{3.33}$$

$$\theta_m(\eta)=\frac{1}{m}\frac{\partial^m\Theta(\eta;q)}{\partial q^m}\bigg|_{q=0}. \tag{3.34}$$

It is quite clear from (3.31-3.32) that the convergence of series depend upon the auxiliary parameters $\hbar_f$ and $\hbar_\theta$. The values of $\hbar_f$ and $\hbar_\theta$ are selected in such a way that when $q=1$, the series solutions (3.31-3.32) converge. Hence

$$f(\eta)=f_0(\eta)+\sum_{m=1}^{\infty}f_m(\eta), \tag{3.35}$$

$$\theta(\eta) = \theta_0(\eta) + \sum_{m=1}^{\infty} \theta_m(\eta). \tag{3.36}$$

The mth-order deformation equations are given as

$$\mathcal{L}_f \left[f_m(\eta) - \chi_m f_{m-1}(\eta) \right] = \hbar_f \mathcal{R}_m^f(\eta), \tag{3.37}$$

$$\mathcal{L}_\theta \left[\theta_m(\eta) - \chi_m \theta_{m-1}(\eta) \right] = \hbar_\theta \mathcal{R}_m^\theta(\eta), \tag{3.38}$$

$$\left.\begin{aligned} f_m(0) = f'_m(0) - \gamma f''_m(0) = f_m(\infty) = 0, \\ \theta'_m(0) - Bi\,\theta_m(0) = \theta_m(\infty) = 0. \end{aligned}\right\} \tag{3.39}$$

Here

$$\mathcal{R}_m^f(\eta) = \frac{\partial^3 f_{m-1}}{\partial \eta^3} + \sum_{k=0}^{m-1} \left(f_{m-1-k} \frac{\partial^2 f_k}{\partial \eta^2} - \frac{\partial f_{m-1-k}}{\partial \eta} \frac{\partial f_k}{\partial \eta} \right) - M \frac{\partial f_{m-1}}{\partial \eta}, \tag{3.40}$$

$$\mathcal{R}_m^\theta(\eta) = \frac{\partial^2 \theta_{m-1}}{\partial \eta^2} + \Pr \sum_{k=0}^{m-1} f_{m-1-k} \frac{\partial \theta_k}{\partial \eta}, + \Pr Ec \sum_{k=0}^{m-1} \frac{\partial^2 f_{m-1-k}}{\partial \eta^2} \frac{\partial^2 f_k}{\partial \eta^2} + M \Pr Ec \sum_{k=0}^{m-1} \frac{\partial f_{m-1-k}}{\partial \eta} \frac{\partial f_k}{\partial \eta}, \tag{3.41}$$

$$\chi_m = \begin{cases} 0, & m \le 1, \\ 1, & m > 1. \end{cases} \tag{3.42}$$

The general form of solution of deformation equations (3.36-3.37) can be expressed as

$$f_m(\eta) = f_m^*(\eta) + C_1 + C_2 e^{-\eta} + C_3 e^{\eta}, \tag{3.43}$$

$$\theta_m(\eta) = \theta_m^*(\eta) + C_4 + C_5 e^{-\eta}, \tag{3.44}$$

where $f_m^*(\eta)$, $g_m^*(\eta)$, $\theta_m^*(\eta)$ are the solution functions.

From (3.35-3.36), it is quite evident that the convergence of the series solutions has strong dependence upon the auxiliary parameters $\hbar_f$ and $\hbar_\theta$. In order to determine the favorable ranges of $\hbar_f$ and $\hbar_\theta$ for which the series solutions converge, the so called $\hbar$-curves are drawn in Figure 3.2 at the 20th order of

approximation. On carefully observing the Figure, it is noticed that the admissible ranges of $\hbar_f$ and $\hbar_\theta$ are $-0.2 \le \hbar_f \le -1.0$ and $-0.3 \le \hbar_\theta \le -0.9$. Also, the averaged square residual errors are calculated by using the formulas

$$E_{m,f} = \frac{1}{N+1}\sum_{j=0}^{N}\left[\mathcal{N}_f\left(\sum_{i=0}^{m} f_i(j\Delta\zeta)\right)\right]^2, \tag{3.45}$$

$$E_{m,\theta} = \frac{1}{N+1}\sum_{j=0}^{N}\left[\mathcal{N}_\theta\left(\sum_{i=0}^{m} \theta_i(j\Delta\zeta)\right)\right]^2, \tag{3.46}$$

where $N = 20$, $\Delta\zeta = 0.05$. Table 3.1 presents the optimal values of $\hbar_f$ and $\hbar_\theta$ and the corresponding squared residual errors $E_{m,f}$ and $E_{m,\theta}$ at different orders of approximations. It is observed that the values of $E_{m,f}$ and $E_{m,\theta}$ decrease with an increase in the order of approximation. Furthermore, Table 3.2 is drawn to show the convergence of series solutions. It is observed that the series solutions (3.35-3.36) converge up to 6 decimal places at the 20th-order of approximation which shows that the use of the optimal values of $\hbar_f$ and $\hbar_\theta$ accelerate the convergence. In order to further ensure that the results obtained by Homotopy Analysis Method (HAM) are correct, the obtained numerical values of dimensionless skin friction and local Nusselt number are compared with those of Andersson [85] in the absence of Hartmann number in Table 3.3. A good agreement is observed between the studies that show the accuracy and validity of the Homotopy Analysis Method.

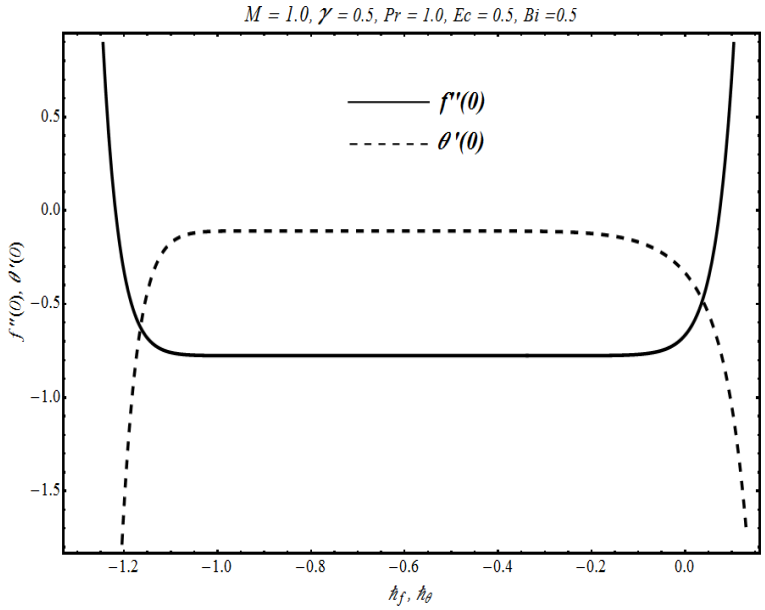

Figure 3.2: $\hbar-curves$ for 20th order of approximation

Table 3.1: Optimal values of $\hbar_f$ and $\hbar_\theta$ and their corresponding averaged squared residual errors $E_{m,f}$ and $E_{m,\theta}$ at different orders of approximations when $M=1.0,\ \gamma=0.5,\ \Pr=1.0,\ Ec=0.5,\ Bi=0.5$

Order of approximations m	$\hbar_f$	$\hbar_\theta$	$E_{m,f}$	$E_{m,\theta}$
3	-0.985649	-0.899213	2.32985×10^{-4}	1.79345×10^{-3}
6	-0.977189	-0.898804	3.49766×10^{-7}	1.82732×10^{-4}
9	-0.960928	-0.822989	5.51831×10^{-8}	1.83884×10^{-4}
12	-0.951473	-0.810794	1.90157×10^{-10}	2.48039×10^{-6}
15	-0.945454	-0.784919	3.95679×10^{-10}	9.98650×10^{-7}

Table 3.2: Convergence of HAM solutions for different orders of approximations when $M = 1.0$, $\gamma = 0.5$, $Bi = 0.5$, $\Pr = 1.0$, $Ec = 0.5$ and $\hbar_f = -0.945454$ and $\hbar_\theta = -0.784919$

Order of Convergence	$-f''(0)$	$-\theta'(0)$
5	0.776411	0.116428
10	0.776582	0.109267
15	0.776583	0.109036
20	0.776583	0.109028
25	0.776583	0.109028
30	0.776583	0.109028
35	0.776583	0.109028

Table 3.3: Comparison of numerical values of $f'(0)$ and $-f''(0)$ with Andersson [85] when $M = 0.0$

γ	$f'(0)$ *Andersson* [85]	$f'(0)$ *Present*	$-f''(0)$ *Andersson* [85]	$-f''(0)$ *Present*
0	1.0000	1.0000	1.0000	1.0000
0.1	0.9128	0.9128	0.8721	0.8721
0.2	0.8447	0.8447	0.7764	0.7764
0.5	0.7044	0.7044	0.5912	0.5912
1.0	0.5698	0.5698	0.4302	0.4302
2.0	0.4320	0.4320	0.2840	0.2840
5.0	0.2758	0.2759	0.1448	0.1448
10.0	0.1876	0.1876	0.0812	0.0812
20.0	0.1242	0.1242	0.0438	0.0438
50.0	0.0702	0.0702	0.0186	0.0186
100	0.0450	0.0449	0.0095	0.0095

3.4 Results and discussion

The effects of pertinent parameters on flow and heat transfer characteristics as well as on entropy generation effects are presented in this section with the aid of graphs and tables. Figure 3.3 shows the variation in velocity profiles against η when the values of Hartmann number M are varied. It is noticed that an increase in Hartmann number M causes the resistive force known as Lorentz force to become strong, which as a result retards the fluid motion. Due to this reason, a decrease in fluid velocity and hence the momentum boundary layer thickness is observed as the value of M increases. Figure 3.4 depicts the effects of slip parameter γ on velocity $f'(\eta)$. With increase in the value of slip parameter γ, the frictional force between the stretching surface and the fluid reduces which decreases the momentum transport. Thus, a decrease in fluid velocity $f'(\eta)$ is noticed at the surface of the stretching sheet.

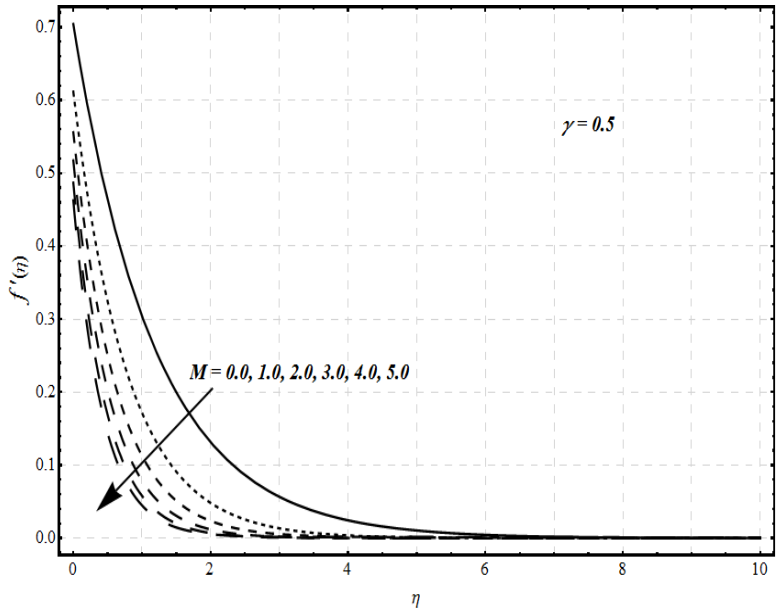

Figure 3.3: Influence of Hartmann number M on velocity profile $f'(\eta)$

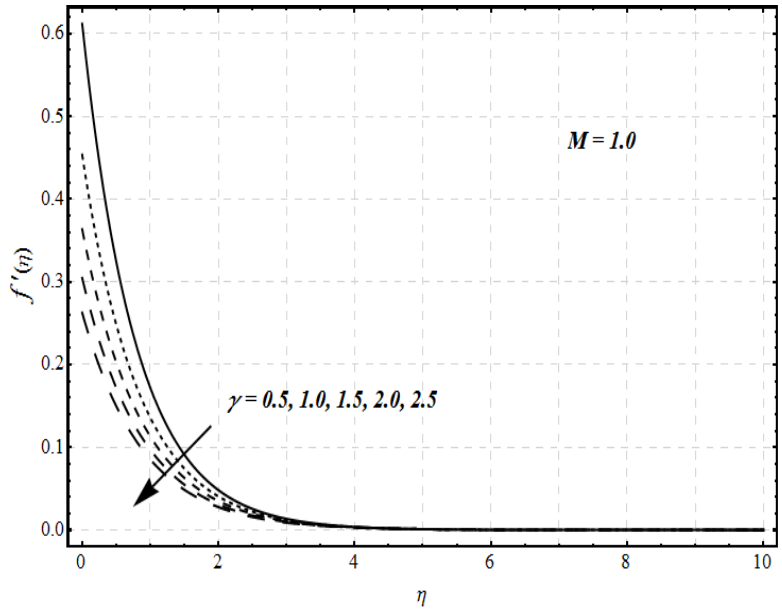

Figure 3.4: Influence of slip parameter γ on velocity profile $f'(\eta)$

Table 3.4: Numerical values of $f'(0)$ and $-f''(0)$ for different values of Hartmann number M and slip parameter γ

γ	M	$-f''(0)$	$f'(0)$
0.0	1.0	1.414210	1.000000
0.1		1.205640	0.879436
0.5		0.776583	0.611709
1.0		0.546602	0.453398
3.0		0.256325	0.231024
5.0		0.168641	0.156796
10.0		0.091250	0.087502
0.5	0.0	0.591195	0.704402
	0.5	0.698251	0.650875
	1.0	0.776583	0.611709
	1.5	0.838072	0.580964
	2.0	0.888480	0.555760

Table 3.4 presents the effects of different values of the slip parameter γ and the Hartmann number M on $f'(0)$ and $-f''(0)$. It is observed that an increase in the slip parameter γ causes the values of $-f''(0)$ and $f'(0)$ to decrease. However, opposite behavior is noticed in case of Hartmann number M.

Figure 3.5 shows that the influence of Hartmann number M on temperature profile $\theta(\eta)$. Due to increase in resistive force with increase in the value of Hartmann number M, a rise in temperature is observed. Figure 3.6 presents the effects of Prandtl number $\Pr$ on temperature $\theta(\eta)$. A decrease in the temperature profile is noticed with an increase in the values of the Prandtl number. The impact of increase in the value of the Eckert number Ec on temperature profile has been illustrated in Figure 3.7. The viscous dissipation effects augment with an increase in the value of Ec which results in an increase in thermal boundary layer thickness. Figure 3.8 displays the impact of variation in Biot number Bi on temperature distribution. It is noteworthy that an increase in thevvalue of the Biot number Bi causes the thermal boundary layer thickness to increase.

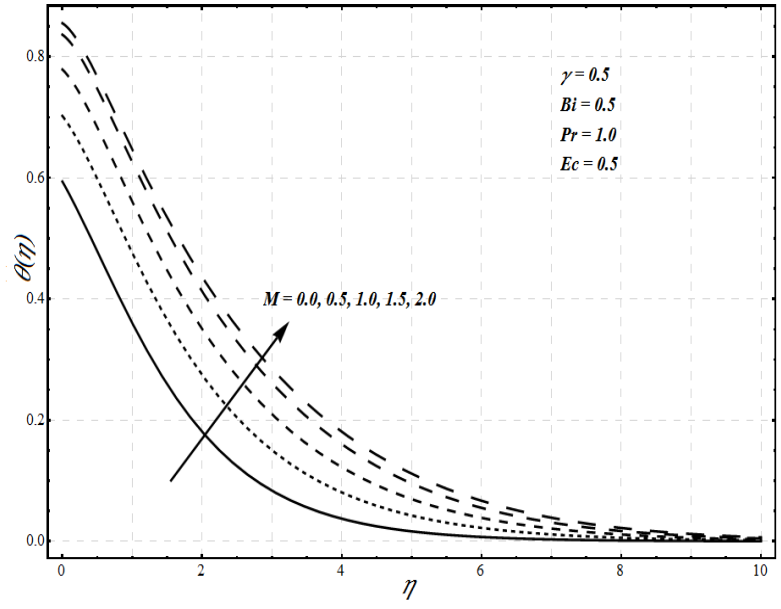

Figure 3.5: Influence of Hartmann number M on temperature profile $\theta(\eta)$

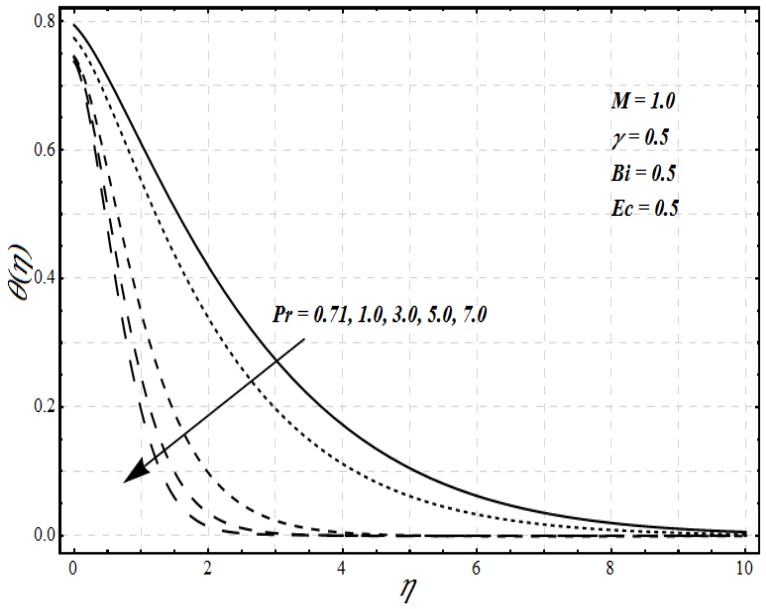

Figure 3.6: Influence of Prandtl number Pr on temperature profile $\theta(\eta)$

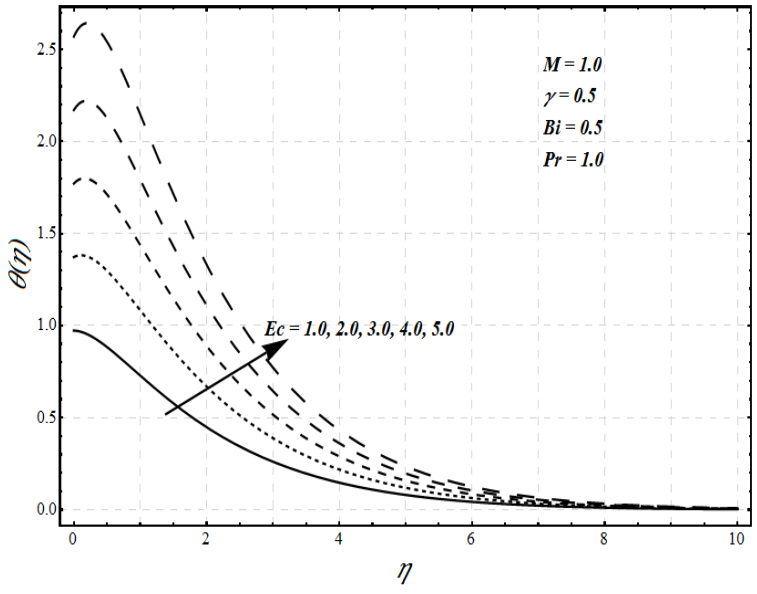

Figure 3.7: Influence of Eckert number Ec on temperature profile $\theta(\eta)$

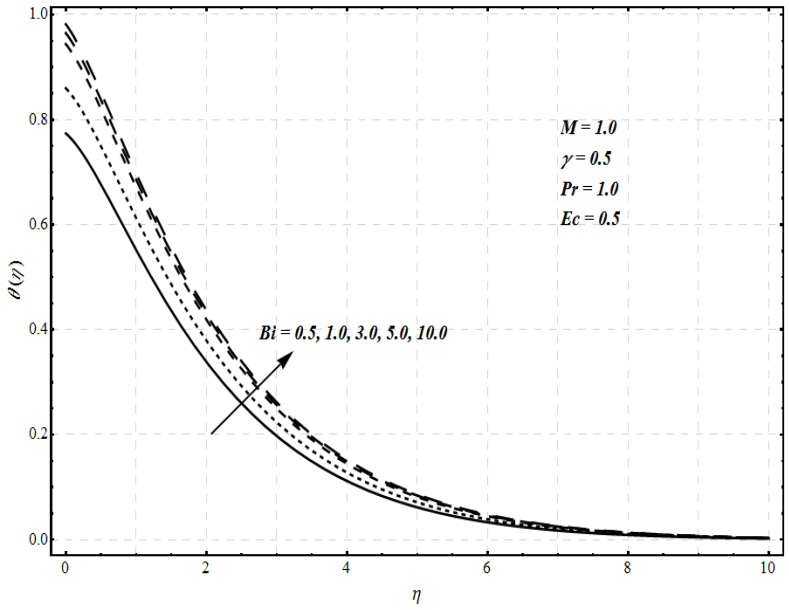

Figure 3.8: Influence of Biot number Bi on temperature profile $\theta(\eta)$

Table 3.5 depicts the variation of heat transfer at the surface $-\theta'(0)$ for different values of Hartmann number M, slip parameter γ, Biot number Bi, Prandtl number $\Pr$ and Eckert number Ec. It is observed that the heat transfer rate at the surface drops with an increase in the values of Hartmann number M, slip parameter γ and Eckert number Ec and enhances as the values of Prandtl number $\Pr$ and Biot number Bi augments.

Figures 3.9-3.12 depict the influence of different parameters involved in the problem on local entropy generation number Ns. Figure 3.9 shows the effects of the Hartmann number M on theolocal entropy generation number. It is noteworthy that in the absence of the magnetic field, the entropy generation rate is low. However, the presence of the magnetic field causes more entropy generation in the fluid. Also, it is noticed that for a fixed value of the entropy generation is maximum near the stretching surface and decreases with η.

Table 3.5: Numerical values of $-\theta'(0)$ for different values of Hartmann number M, slip parameter γ, Biot number Bi, Prandtl number Pr and Eckert number Ec

γ	M	Bi	Pr	Ec	$-\theta'(0)$
0.3	1.0	0.5	1.0	0.2	0.170283
0.5					0.169964
1.0					0.161406
3.0					0.123537
5.0					0.098983
0.5	0				0.229466
	0.5				0.195924
	1.0				0.169964
	1.5				0.148843
	2.0				0.131204
0.5	1.0	0.1	1.0	0.2	0.063308
		0.5			0.169964
		1.0			0.215304
		3.0			0.261877
		5.0			0.273719
0.5	1.0	0.5	0.7	0.2	0.143966
			1.0		0.169964
			2.0		0.215231
			3.0		0.235761
			5.0		0.253850
0.5	1.0	0.5	1.0	0.1	0.190276
				0.2	0.169964
				0.5	0.109028
				0.8	0.048092
				1.0	0.085241

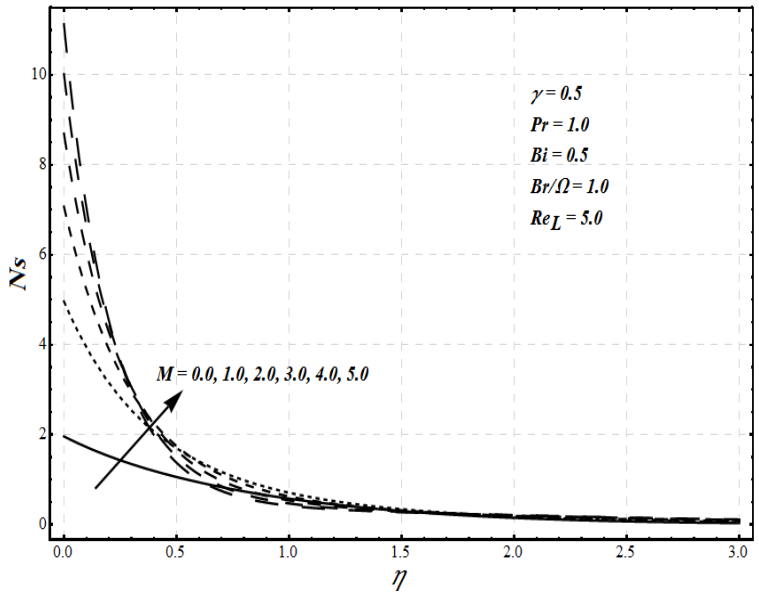

Figure 3.9: Influence of Hartmann number M on local entropy generation number Ns

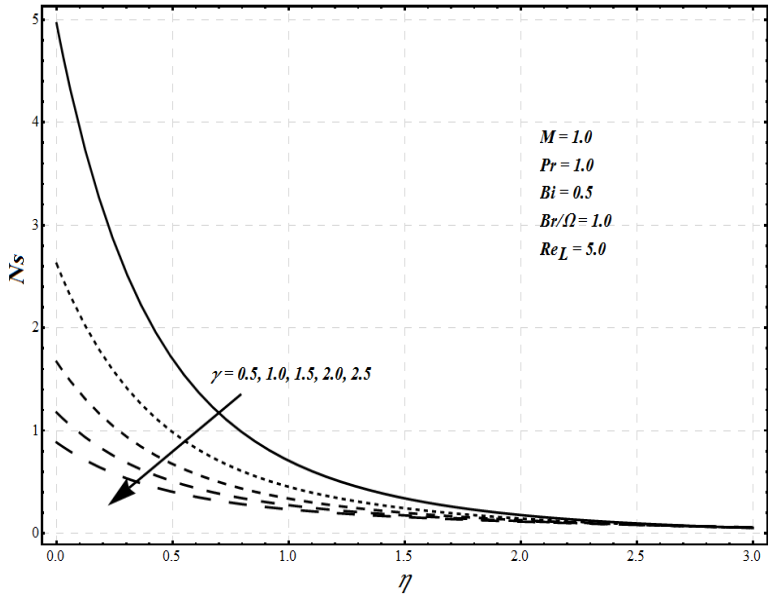

Figure 3.10: Influence of slip parameter γ on local entropy generation number Ns

Figure 3.10 illustrates that increase in the value of slip parameter γ reduces the friction between the stretching surface and the fluid which depreciates the entropy generation effects. The variation in the local entropy generation number Ns for various values of Biot number Bi has been presented in Figure 3.11. It is seen that the convective heat transfer from the stretching surface increases with an increase in the value of Biot which ultimately augments the local entropy generation number Ns. However, for large values of Bi, these effects are not so prominent. The effects of the group parameter Br/Ω on Ns are significant as it determines the relative importance of viscous effects. It is observed in Figure 3.12 that the entropy production increases with Br/Ω.

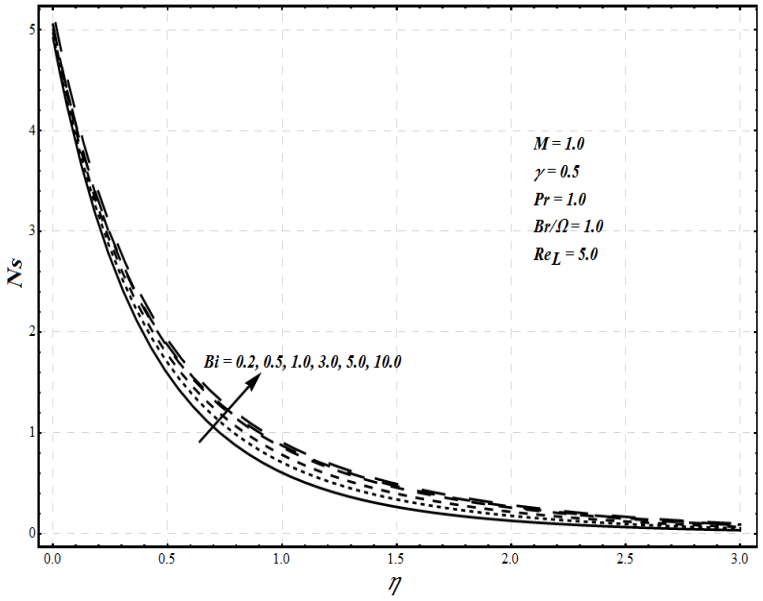

Figure 3.11: Influence of Biot number Bi on local entropy generation number Ns

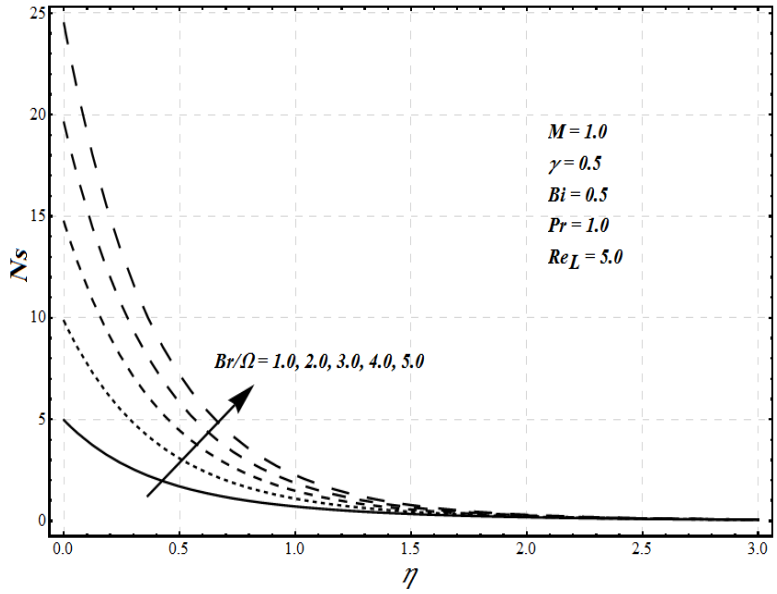

Figure 3.12: Influence of group parameter Br/Ω on local entropy generation number Ns

To get an idea of whether the fluid friction and magnetic field entropy effects dominate over the heat transfer entropy effects or vice versa, the Bejan number Be is introduced. Figure 3.13 depicts that the entropy effects due to fluid friction and magnetic field become dominant near the stretching surface with increase in the Hartmann number M. The situation is reversed in the boundary layer region and the heat transfer irreversibility dominates fully in the mainstream regime. Figure 3.14 shows that with an increase in slip parameter γ, the frictional force between the stretching surface and fluid becomes less which causes the entropy generation effects due to fluid friction and magnetic field to decrease at the surface of stretching sheet. However, in the main stream region, the heat transfer irreversibility effects are dominant. Figure 3.15 illustrates that for a particular value of Biot number, the influence of the fluid friction and magnetic field entropy is significant near the surface and in the free stream regime, the entropy effects due to heat transfer are prominent. However, with an increase in the value of Biot number, the fluid friction and magnetic field entropy effects become slightly less near the surface. In case of the group parameter, the fluid friction and magnetic field entropy effects become dominant near

the surface with an increase in Br/Ω as presented in Figure 3.16. In the mainstream regime, the entropy effects due to heat transfer dominate.

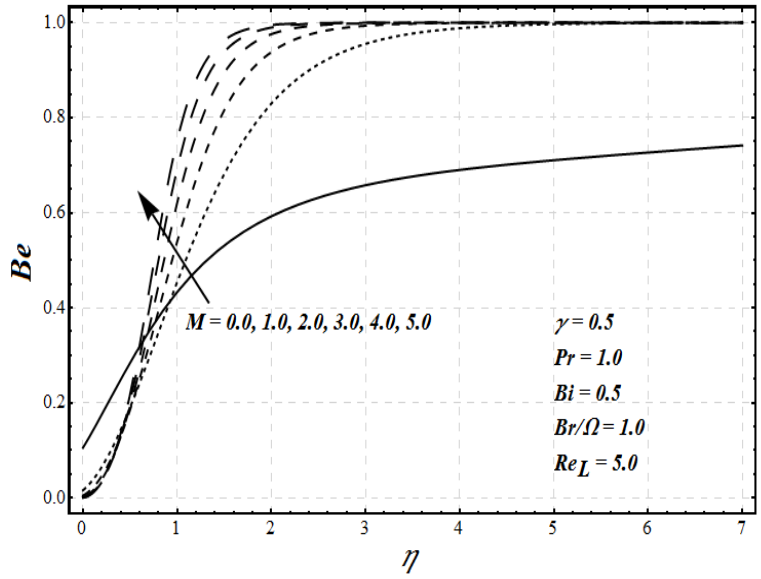

Figure 3.13: Influence of Hartmann number M on Bejan number Be

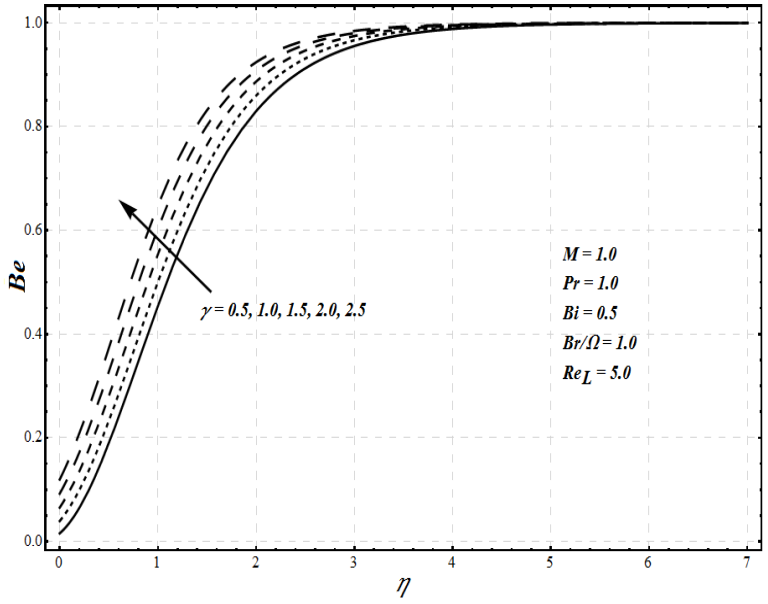

Figure 3.14: Influence of slip parameter γ on Bejan number Be

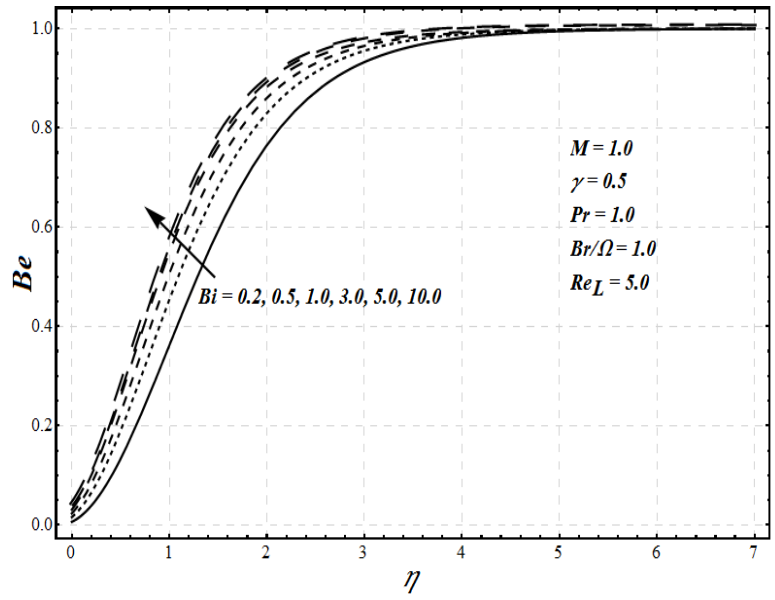

Figure 3.15: Influence of Biot number Bi on Bejan number Be

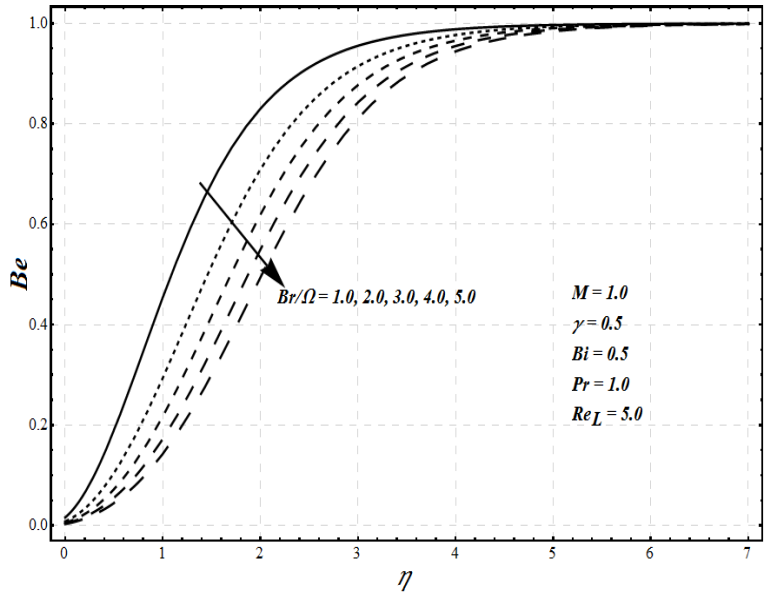

Figure 3.16: Influence of group parameter Br/Ω on Bejan number Be

3.5 Conclusions

In this chapter, the entropy generation effects are studied in magnetohydrodynamic flow over a stretching surface with partial slip and convective boundary condition. The solution is obtained using the Homotopy Analysis Method and the graphs are presented for different physical parameters. It is observed that the resistive force known as the Lorentz force strengthens with an increase in Hartmann number M which reduces the fluid velocity and enhances the temperature. Consequently, the skin friction increases and the heat transfer rate from the surface decreases as M increases. On the other hand, as the value of slip parameter γ increases, the fluid motion due to the stretching of the sheet diminishes. Furthermore, the skin friction also reduces as the value of γ increases. The thermal boundary layer thickness enhances with Eckert number and decreases with Prandtl number. The stretching surface is a strong agent of entropy production. Also the effects of increasing Hartmann number M, the Biot number Bi and the group parameter Br/Ω on local entropy generation number are increasing and a rise in entropy production is noticed. Moreover, it is noteworthy that the fluid friction and magnetic field entropy effects are dominant on the stretching surface and in the neighboring region and the heat transfer entropy effects are dominant in the mainstream region.

Chapter 4

Entropy generation in MHD viscous flow over a stretching cylinder embedded in porous medium

4.1 Introduction

In this chapter, a study has been carried out to investigate the effects of entropy generation in hydromagnetic viscous fluid flow and heat transfer over a horizontal stretching cylinder embedded in a porous medium. The problem is mathematically modeled and is solved numerically. The effects of physical parameters on the velocity profiles, temperature distribution, local entropy generation number and Bejan number are examined through graphs and tables. Moreover, a comparison has been made for the results of the stretching cylinder having some curvature and those in the case of flat stretching surface. It is seen that the thickness of momentum and thermal boundary layers are more for the case of stretching cylinder having curvature parameter $\kappa = 1.0$ as compared to flat stretching surface $\kappa = 0.0$.

4.2 Mathematical modelling

4.2.1 Flow and heat transfer phenomena

Consider a steady, axisymmetric laminar flow of an incompressible viscous fluid due to continuous stretching of a horizontal cylinder having radius R embedded in a porous medium. As presented in Figure

4.1, the direction of the x-axis is taken along the axis of the cylinder and the r-axis is considered to be in the radial direction. A uniform magnetic field of strength B_o is applied in the radial direction, i.e., normal to the stretching cylinder. The stretching velocity $U_w(x)$ of the cylinder is assumed to be of the form $u_w(x) = U_0\left(\frac{x}{L}\right)$, where $U_0 > 0$ is a constant and L is the characteristic length. The surface of the stretching cylinder is subjected to a variable temperature $T_w(x) = T_\infty + T_0\left(\frac{x}{L}\right)^n$ and the ambient fluid temperature is T_∞. The induced magnetic field effects are considered negligible due to which magnetic Reynolds number is not taken. Moreover, it is supposed that the viscous dissipation and Joule dissipation effects are present.

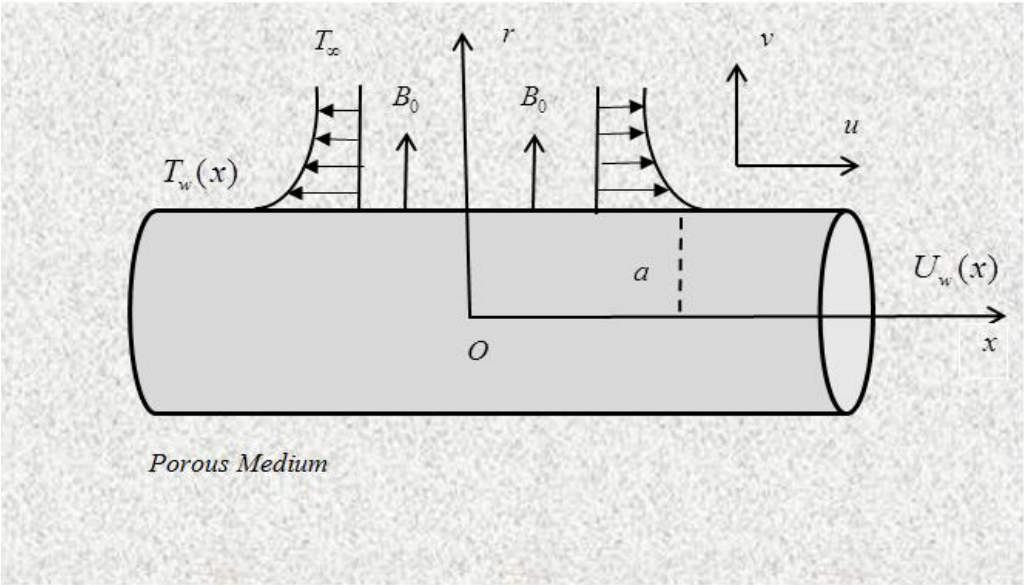

Figure 4.1: Schematic diagram of the considered problem

Under all these assumptions, the Eqs. (2.1-2.3) that represent the flow and heat transfer phenomena can be written after applying boundary layer approximation as

$$\frac{\partial}{\partial x}(ru) + \frac{\partial}{\partial r}(rv) = 0, \tag{4.1}$$

$$u\frac{\partial u}{\partial x} + v\frac{\partial u}{\partial r} = \frac{\nu}{r}\frac{\partial}{\partial r}\left(r\frac{\partial u}{\partial r}\right) - \frac{\nu}{k'}u - \frac{\sigma B_0^2}{\rho}u,$$

(4.2)

$$u\frac{\partial T}{\partial x}+v\frac{\partial T}{\partial r}=\frac{k}{r}\frac{\partial}{\partial r}\left(r\frac{\partial T}{\partial r}\right)+\frac{\nu}{c_p}\left(\frac{\partial u}{\partial r}\right)^2+\frac{\sigma B_0^2}{\rho c_p}u^2+\frac{\nu}{c_p k'}u^2, \tag{4.3}$$

and the associated boundary conditions are:

$$\left.\begin{aligned} &u=u_w(x),\quad v=0,\quad T=T_w(x)\ \ at\ \ r=R,\\ &u\to 0,\quad T\to T_\infty\ \ ar\ \ r\to\infty, \end{aligned}\right\} \tag{4.4}$$

where (u,v) are the velocity components in the (x,r) directions, k' is the permeability of the medium, n is the temperature exponent and T is the temperature of the fluid. Introducing the following similarity variables:

$$\left.\begin{aligned} &\eta=\frac{r^2-R^2}{2R}\left(\frac{U_w}{\nu x}\right)^{\frac{1}{2}},\quad \psi=\left(U_w\nu x\right)^{\frac{1}{2}}Rf(\eta),\\ &\theta=\frac{T-T_\infty}{T_w-T_\infty}. \end{aligned}\right\} \tag{4.5}$$

Here η denotes the similarity variable, ψ is the stream function, f and θ are the dimensionless stream function and temperature respectively. The stream function is defined as:

$$u=\frac{1}{r}\frac{\partial\psi}{\partial r}\quad\text{and}\quad v=-\frac{1}{r}\frac{\partial\psi}{\partial x}. \tag{4.6}$$

By substitution of (4.5) and (4.6), the Eq. (4.1) is automatically satisfied and Eqs. (4.2-4.3) are converted into following nonlinear ordinary differential equations:

$$(1+2\kappa\eta)f'''+2\kappa f''+ff''-f'^2-(M+K)f'=0, \tag{4.7}$$

$$(1+2\kappa\eta)\theta''+2\kappa\theta'+\Pr\left(f\theta'-nf'\theta\right)+\Pr Ec(1+2\kappa\eta)f''^2+\Pr Ec(M+K)f'^2=0, \tag{4.8}$$

and the boundary conditions (4.4) upon introducing (4.5) becomes

$$\left.\begin{aligned} &f(0)=0,\quad f'(0)=1,\quad \theta(0)=1,\\ &f'\to 0,\quad \theta\to 0,\quad \text{as}\quad \eta\to\infty. \end{aligned}\right\} \tag{4.9}$$

Here $\kappa = \frac{1}{R}\left(\frac{\nu L}{U_0}\right)^{\frac{1}{2}}$ is the curvature parameter, $M = \frac{\sigma B_0^2 L}{\rho U_0}$ is the Hartmann number, $K = \frac{\nu L}{U_0 k'}$ is the permeability parameter of the porous medium, $\Pr = \frac{\mu c_p}{k}$ is the Prandtl number and $Ec = \frac{u_w^2}{c_p\left(T_w - T_\infty\right)}$ is the Eckert number.

It is noticeable that when $\kappa = 0$ (flat surface) and $M = 0,\ K = 0$, the Eq. (4.7) reduces to that of Crane's problem [74] which has the solution $f(\eta) = 1 - e^{-\eta}$. Moreover, also when $Ec = 0$, the considered problem is reduced to that of Grubka and Bobba [79].

4.2.2 Quantities of physical interest

The quantities that are of significant physical importance are skin friction coefficient and local Nusselt number defined as:

$$C_f = \frac{\tau_w}{\frac{1}{2}\rho u_w^2}, \tag{4.10}$$

$$Nu_r = \frac{rq_w}{k(T_w - T_\infty)}. \tag{4.11}$$

Here $\tau_w = \mu\left(\frac{\partial u}{\partial r}\right)_{r=R}$ is the shear stress at the cylinder surface and $q_w = -k\left(\frac{\partial T}{\partial r}\right)_{r=R}$ is the surface heat flux.

On plugging values of τ_w and q_w into (4.10) and (4.11) and making use of dimensionless variables (4.5), we get the non-dimensional form of skin friction coefficient and local Nusselt number as:

$$\frac{1}{2}\mathrm{Re}_x^{1/2} C_f = f''(0), \tag{4.12}$$

$$\mathrm{Re}_x^{-1/2} Nu_x = -\theta'(0), \tag{4.13}$$

where $\mathrm{Re}_x = \frac{u_w x}{\nu}$ is the local Reynolds number.

4.2.3 Entropy generation

Using the boundary layer approximations, the local entropy generation rate per unit volume S_G given in Eq. (2.47) in the presence of magnetic field and porous medium is given by:

$$S_G = \underbrace{\frac{k}{T_\infty^{\,2}}\left[\left(\frac{\partial T}{\partial r}\right)^2\right]}_{\substack{\text{entropy effects}\\ \text{due to}\\ \text{heat transfer}}} + \underbrace{\frac{\mu}{T_\infty}\left(\frac{\partial u}{\partial r}\right)^2 + \frac{\mu}{T_\infty k'}\mathrm{u}^2}_{\substack{\text{entropy effects}\\ \text{due to}\\ \text{fluid friction}}} + \underbrace{\frac{\sigma B_0^{\,2}}{T_\infty}\mathrm{u}^2}_{\substack{\text{entropy effects}\\ \text{due to}\\ \text{magnetic field}}} . \tag{4.14}$$

Making use of (4.5), Eq. (4.14) becomes

$$Ns = \frac{S_G}{S_{G0}} = \frac{\mathrm{Re}_L}{X}(1+2\kappa\eta)\theta'^2 + \frac{\mathrm{Re}_L}{X}\frac{Br}{\Omega}(1+2\kappa\eta) f''^2 + \frac{\mathrm{Re}_L}{X}\frac{Br}{\Omega} M f'^2 + \frac{\mathrm{Re}_L}{X}\frac{Br}{\Omega} K f'^2, \tag{4.15}$$

where $S_{G0} = \frac{k(T_w - T_\infty)^2}{T_\infty^{\,2} L^2}$ is the characteristic entropy generation rate, $\Omega = \frac{(T_w - T_\infty)}{T_\infty}$ is the dimensionless temperature difference and $X = \frac{x}{L}$ is the dimensionless number. Eq. (4.15) can be expressed as:

$$Ns = N_H + N_f + N_m = N_H + N_F. \tag{4.16}$$

The Bejan number which is used to determine whether heat transfer entropy effects dominate over fluid friction and magnetic field entropy effects or vice versa is defined as:

$$Be = \frac{N_H}{Ns}. \tag{4.17}$$

4.3 Numerical solution and its validation

The system of nonlinear ordinary differential equations (4.7-4.8) along with the boundary conditions (4.9) are solved numerically by shooting technique with fourth-fifth order Runge-Kutta-Fehlberg algorithm. This method is employed by converting the two point boundary value problem defined in system

(4.7-4.9) into a system of initial value problem. This is achieved by making the following substitution $f = w_1,\ f' = w_2,\ f'' = w_3,\ \theta = w_4,\ \theta' = w_5$. Thus, we attain a system of first order ordinary differential equations:

$$\left.\begin{aligned} w_1' &= w_2, \\ w_2' &= w_3, \\ w_3' &= \frac{1}{(1+2\kappa\eta)}\left(-2\kappa w_3 - w_1 w_3 + w_2^{\,2} + (M+K)w_2\right), \\ w_4' &= w_5, \\ w_5' &= \frac{1}{(1+2\kappa\eta)}\left(-2\kappa w_5 - \Pr\left(w_1 w_5 - n w_2 w_4\right) - \Pr Ec(1+2\kappa\eta)w_3^{\,2} - \Pr Ec(M+K)w_2^{\,2}\right), \end{aligned}\right\} \tag{4.18}$$

and the boundary conditions (4.9) associated with the system are converted to initial conditions as:

$$\left.\begin{aligned} w_1(0) &= 0, \\ w_2(0) &= 1, \\ w_3(0) &= s_1, \\ w_4(0) &= 1, \\ w_5(0) &= s_2. \end{aligned}\right\} \tag{4.19}$$

where the values of s_1 and s_2 are unknowns required to solve the system (4.18) together with the initial conditions (4.19). The values of s_1 and s_2 are initially guessed and the fourth-fifth order Runge-Kutta Fehlberg scheme is applied. The procedure is repeated iteratively until the boundary conditions at infinity (given in Eq. (4.9)) are asymptotically satisfied. The whole procedure is done by replacing the semi-infinite domain $[0,\infty[$ with a finite domain $[0,\eta_\infty]$ where η_∞ is taken to be 20 for all values of parameters. A step size of 0.001 is chosen and the convergence criterion is set up to 10^{-6}.

To validate the results obtained by this routine, the computed numerical values of $-f''(0)$ and $-\theta'(0)$ are compared with some previous studies under some limiting cases. Table 4.1 presents the value of $-f''(0)$ compared with that of Vajravelu et al. [107] for no suction/injection case by taking $\kappa = M = K = 0.0$. An excellent agreement between the values is detected. Moreover, the values of

$-f''(0)$ are compared with those of Shateyi and Marewo [108] for variation in curvature parameter by keeping $M = 0.0,\ K = 0.0$ and are presented in Table 4.2. The values of both the studies excellently match up to 6 decimal places. This validates the accuracy and authenticity of our numerical scheme.

Table 4.1: Comparison of numerical value of $-f''(0)$ with that of Vajravelu [107] when $\kappa = 0.0,\ M = 0.0,\ K = 0.0$

$-f''(0)$ Vajravelu et al. [107]		$-f''(0)$ Present
Analytical	Numerical	
1.000180	1.000000	1.000000

Table 4.2: Comparison of numerical values of $-f''(0)$ for variation in curvature parameter κ with those of Shateyi and Marewo [108] when $M = 0.0,\ K = 1.0$

κ	$-f''(0)$ Shateyi and Marewo [108]	$-f''(0)$ Present
0.0	1.41421356	1.41421356
0.25	1.52316810	1.52316832
0.50	1.62648794	1.62648779

Table 4.3: Comparison of numerical values of $-\theta'(0)$ for variation in Prandtl number $\Pr$ and temperature exponent n with those of Ishak and Nazar [105] and Grubka and Bobba [79] for flat surface (i.e. $\kappa = 0.0$) when $M = 0.0,\ K = 0.0,\ Ec = 0.0$

$\Pr$	n	$-\theta'(0)$ Ishak and Nazar [105]	$-\theta'(0)$ Grubka and Bobba [79]	$-\theta'(0)$ Present
1.0	−2.0	−1.0000	−1.0000	−1.0000
	−1.0	0.0000	0.0000	0.0000
	0.0	0.5820	0.5820	0.5820
	1.0	1.0000	1.0000	1.0000
	2.0	1.3333	1.3333	1.3333
10.0	−2.0	−10.0000	−10.000	−10.000
	−1.0	0.0000	0.0000	0.0000
	0.0	2.3080	2.3080	2.3080
	1.0	3.7207	3.7207	3.7207
	2.0	4.7969	4.7969	4.7969

Table 4.3 is constructed to make a comparison of the values of $-\theta'(0)$ with those of Grubka and Bobba [79] and Ishak and Nazar [105] for flat surface case ($\kappa = 0.0$) for several values of temperature exponent n and Prandtl number $\Pr$, when $M = 0.0,\ K = 0.0,\ Ec = 0.0$. It is witnessed that there is an excellent matching between the values.

4.4 Results and discussion

The nonlinear differential equations (4.7-4.8) having the boundary condition (4.9) are solved numerically and the problem is being discussed from the first and the second law of thermodynamics points of view. The effects of involved physical parameters on flow and heat transfer characteristics are described through graphs and tables.

Figure 4.2 illustrates the effects of curvature parameter κ and Hartmann number M on velocity profile $f'(\eta)$. The solid line represents the case when there is no curvature and the stretching surface is

flat whereas the dashed line represents the problem of stretching cylinder in which the value of curvature parameter is equal to 1.

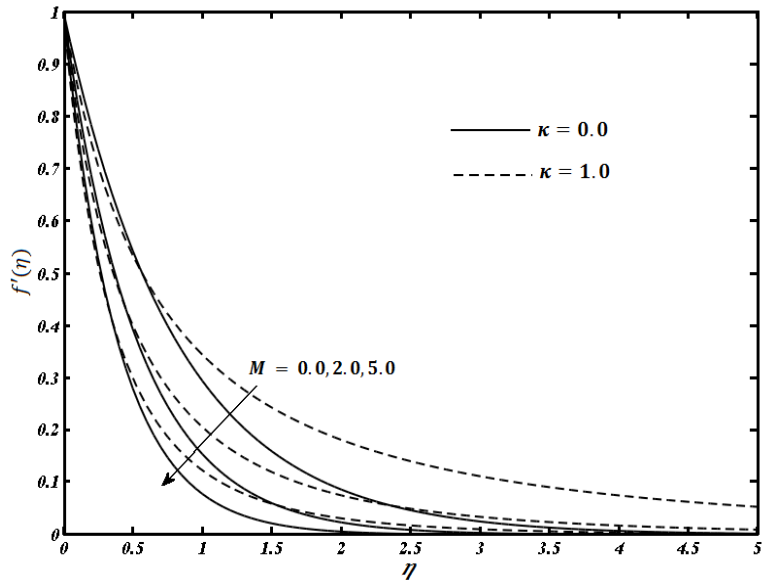

Figure 4.2: Effects of Hartmann number M on velocity profile $f'(\eta)$ when $K = 0.5$

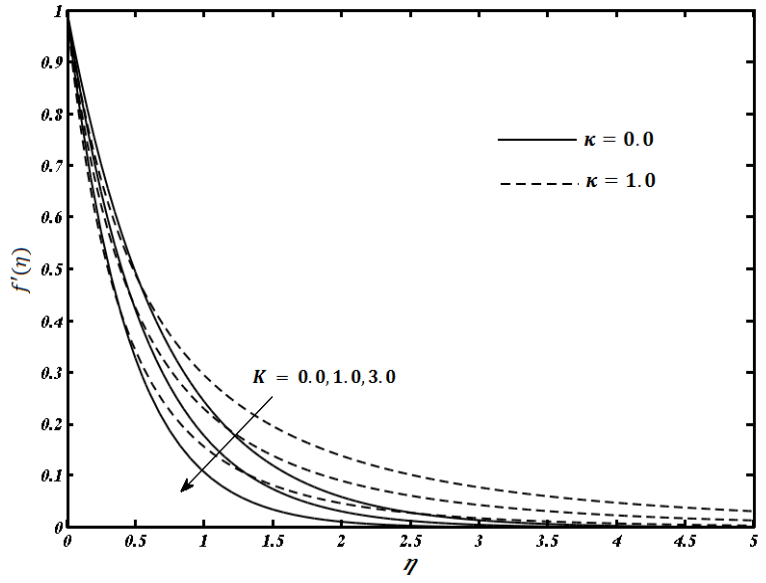

Figure 4.3: Effects of permeability parameter K on velocity profile $f'(\eta)$ when $M = 1.0$

From the Figure, it is quite evident that the boundary layer effects last for longer distance in case of stretching cylinder as compared to flat stretching surface. The thickness of the boundary layer is more for curved cylinder as compared to flat stretching sheet. Furthermore, it is noticed that increase in the value of Hartmann number M results in reduction of fluid velocity in both the cases. This is quite compatible with the physics of the problem as increase in M causes the Lorentz force to become strong which resists the fluid motion and slows it down. Figure 4.3 demonstrates the effects of permeability parameter K on velocity profiles for flat stretching surface ($\kappa = 0.0$) and stretching cylinder having the value of curvature parameter equal to 1, i.e. $\kappa = 1.0$. In both the cases, increase in the value of permeability parameter enlarges the resistance caused by the porous medium to fluid flow that depreciates the fluid velocity. Table 4.4 is constructed to numerically present the values of dimensionless skin friction coefficient $-f''(0)$ for different values of curvature parameter κ, Hartmann number M and permeability parameter K. An increase in skin friction is noticed with increase in the values of all the afore-mentioned parameters.

Table 4.4: Numerical values of $-f''(0)$ for variation in curvature parameter κ, Hartmann number M and permeability parameter K

κ	M	K	$-f''(0)$
1.0	1.0	0.5	1.999783
		1.0	2.158903
		2.0	2.437763
1.0	0.0	0.5	1.612136
	1.0		1.999783
	3.0		2.562964
0.0	1.0	0.5	1.581139
0.5			1.799322
1.0			1.999782

The influence of the physical parameters such as Hartmann number M, permeability parameter K, Eckert number Ec and temperature exponent n on temperature profiles are shown in Figures 4.4-4.7. In all the graphs, the value of Prandtl number is fixed at 6.2 which corresponds to pure water. The effects of Hartmann number M on temperature distribution $\theta(\eta)$ are displayed in Figure 4.4. Increasing the value of M strengthens the Lorentz force that resists the fluid motion. As a result, the temperature of the fluid rises within the boundary layer thickness. The thermal boundary layer thickness is more in case of stretching cylinder as compared to the flat stretching surface. Figure 4.5 exhibits the impact of permeability parameter K on temperature profile. An enlargement in the value of K leads to more opposition to the fluid flow that ultimately results the fluid temperature to augment.

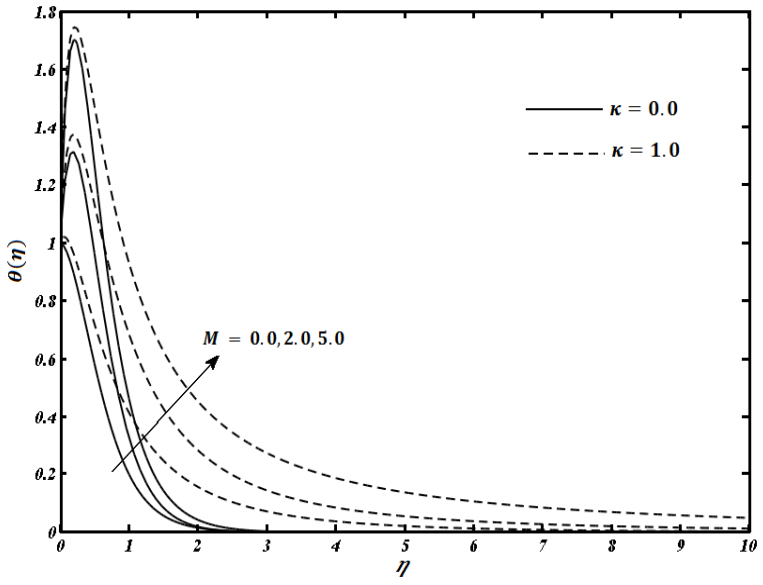

Figure 4.4: Effects of Hartmann number M on temperature profile $\theta(\eta)$ when $K = 0.5,\ \Pr = 6.2,\ Ec = 0.5,\ n = 1.0$

The impact of increasing the Eckert number Ec on temperature $\theta(\eta)$ is illustrated in Figure 4.6. An augmentation in the temperature and hence in the thermal boundary layer thickness is noticed for both the values of curvature parameter i.e., for $\kappa = 0.0$ which corresponds to flat stretching surface and for $\kappa = 1.0$ which represents a particular case of stretching cylinder. This increase in temperature is prominent near the

stretching surface cylinder. As the distance from the surface increases, the temperature starts to drop and asymptotically approaches to zero in the far away region. Moreover, thickness of thermal boundary layer is more prominent in the case of stretching flat surface ($\kappa = 0.0$). However, the temperature effects last for longer distance in case of stretching cylinder. Figure 4.7 indicates that an increase in the value of temperature exponent n results in decrease in fluid temperature $\theta(\eta)$. The values of local Nusselt number $-\theta'(0)$ for various physical parameters are presented in Table 4.5. It depicts that the heat transfer rate from the surface of stretching cylinder augments with increase in the value of temperature exponent. On the other hand, a decrease in Nusselt number is noticed as the values of Hartmann number M, permeability parameter K, Eckert number Ec and curvature parameter κ increase.

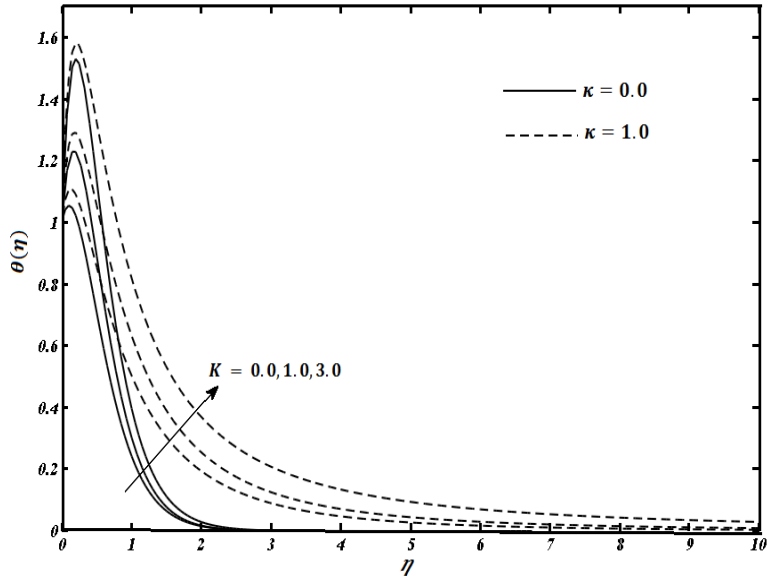

Figure 4.5: Effects of permeability parameter K on temperature profile $\theta(\eta)$ when $M = 1.0,\ \Pr = 6.2,\ Ec = 0.5,\ n = 1.0$

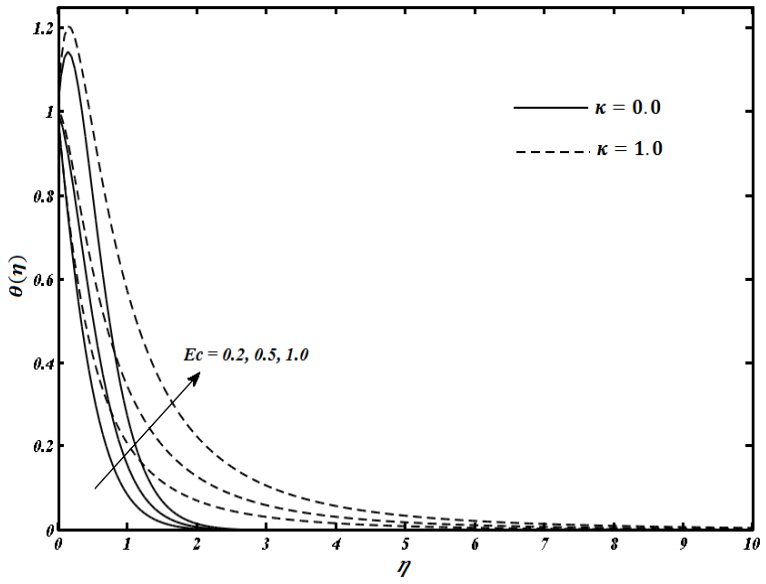

Figure 4.6: Effects of Eckert number Ec on temperature profile $\theta(\eta)$ when $M = 1.0,\ K = 0.5,\ \Pr = 6.2,\ n = 1.0$

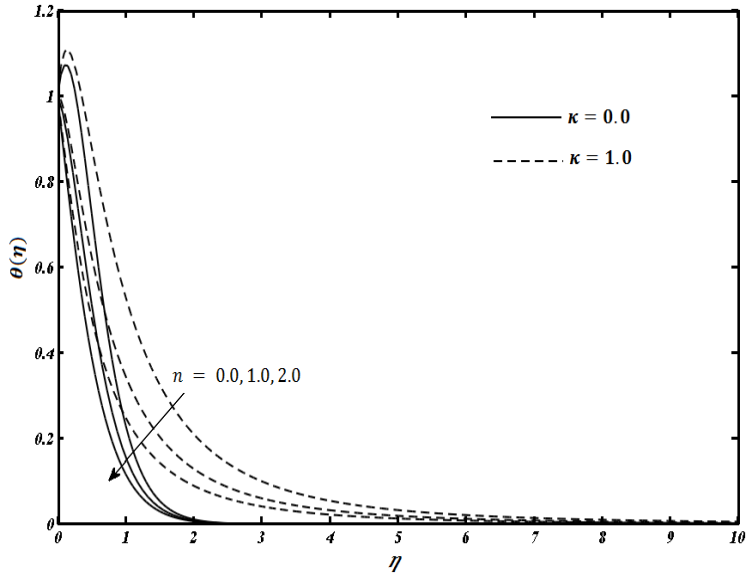

Figure 4.7: Effects of temperature exponent n on temperature profile $\theta(\eta)$ when $M = 1.0,\ K = 0.5,\ \Pr = 6.2,\ Ec = 0.5$

Table 4.5: Numerical values of $-\theta'(0)$ for variation in curvature parameter κ, Hartmann number M, permeability parameter K, temperature exponent n and Eckert number Ec

κ	M	K	Ec	n	$-\theta'(0)$
1.0	1.0	0.5	0.5	0.0	−1.834351
				1.0	−0.031329
				2.0	1.219121
1.0	1.0	0.5	0.3	1.0	1.205831
			1.0		−3.123907
			2.0		−9.309443
0.0	1.0	0.5	0.5	1.0	−0.031329
0.5		1.0			−0.572305
1.0		2.0			−1.538964
1.0	0.0	0.5	0.5	1.0	1.244339
	1.0				−0.031329
	3.0				−1.979819
0.0	1.0	0.5	0.5	1.0	0.313998
0.5					0.125993
1.0					−0.031166

The effects of various physical parameters on local entropy generation number Ns are depicted in Figures 4.8-4.11. The values of curvature parameters are chosen to be $\kappa = 0.0$ and $\kappa = 1.0$ which correspond to flat stretching surface and a stretching cylinder having some curvature respectively. In all the Figures 4.8-4.11, it is worth mentioning that the entropy generation number is higher for curved stretching cylinder as compared to flat stretching surface. Thus, entropy production is more in case of curved surface and enhances with increase in curvature parameter κ. Figure 4.8 indicates that increase in the Hartmann number M results in the enhancement of entropy production near the stretching surface. This is quite compatible with the physical laws as increasing the value of Hartmann number results in more drag force that augments the entropy effects. Also, it can be seen that for a fixed value of M, the entropy generation number is high near the stretching surface cylinder and decreases as the distance increases. In the far away region, the entropy effects are negligible.

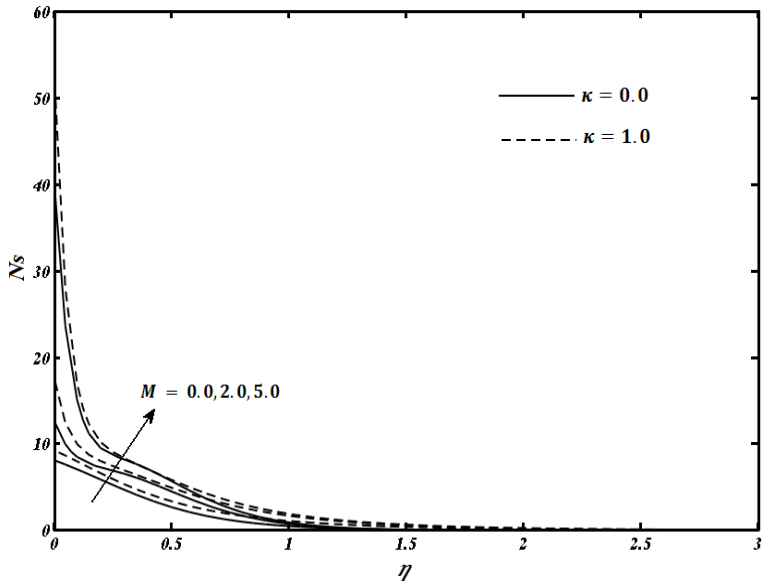

Figure 4.8: Effects of Hartmann number M on local entropy generation number Ns when

$K = 0.5,\ \Pr = 6.2,\ Ec = 0.5,\ n = 1.0,\ \mathrm{Re}_L = 2.0,\ X = 1.0,\ Br/\Omega = 1.0$

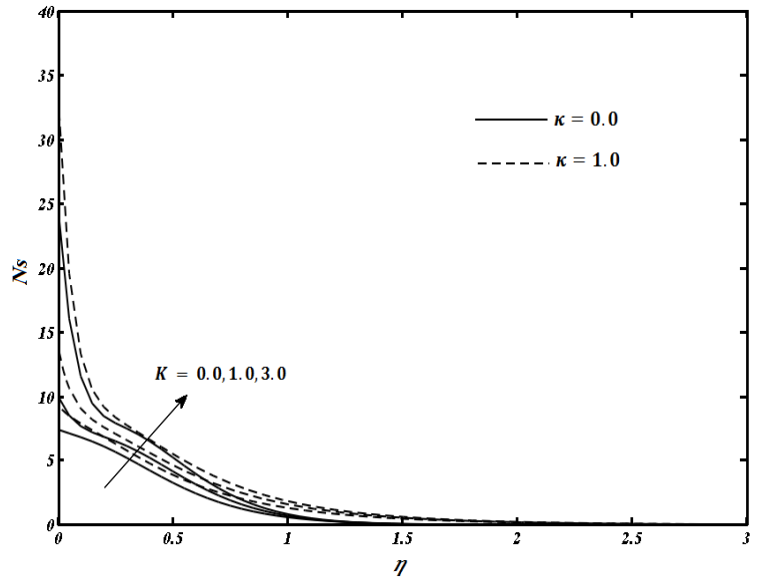

Figure 4.9: Effects of permeability parameter K on local entropy generation number Ns when

$M = 1.0,\ \Pr = 6.2,\ Ec = 0.5,\ n = 1.0,\ \mathrm{Re}_L = 2.0,\ X = 1.0,\ Br/\Omega = 1.0$

The effects of permeability parameter K on local entropy generation number Ns are shown in Figure 4.9. The entropy effects are higher near the stretching cylinder surface and start to decrease as the distance from the surface increases. In the case of stretching cylinder, these entropy effects can be observed for large distance. As the value of permeability parameter increases, the resistance of the porous medium to flow increases which results in more entropy generation. Figure 4.10 shows that increase in the value of temperature exponent n results in increase in entropy production in the vicinity of the stretching cylinder surface. However, as the distance from the surface increases, the situation is reversed and a decreasing behavior is noticed. The variation of group parameter Br/Ω on local entropy generation number is presented in Figure 4.11. An augmentation in entropy generation is detected as the value of Br/Ω augments.

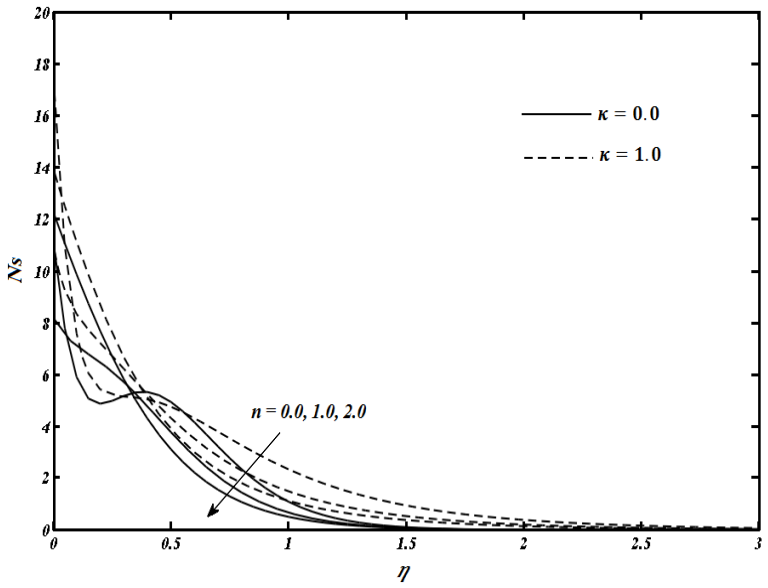

Figure 4.10: Effects of temperature exponent n on local entropy generation number Ns when

$$M = 1.0,\ K = 0.5, \Pr = 6.2,\ Ec = 0.5,\ \mathrm{Re}_L = 2.0,\ X = 1.0,\ Br/\Omega = 1.0$$

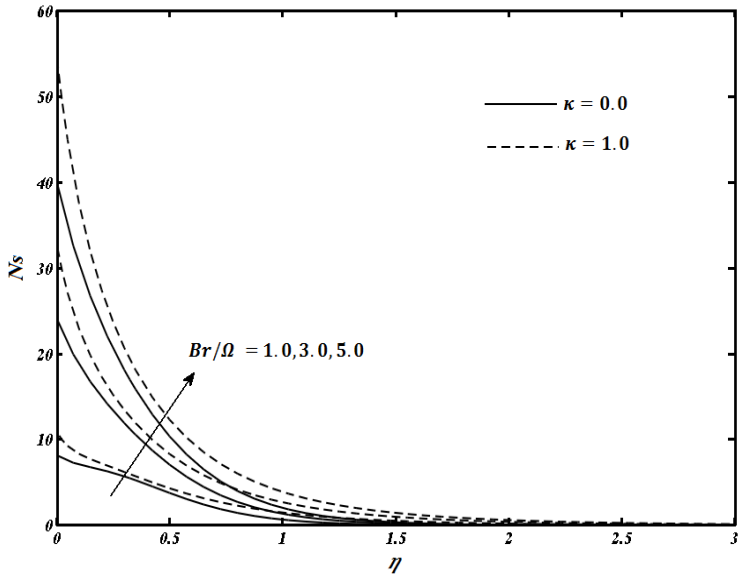

Figure 4.11: Effects of group parameter Br/Ω on local entropy generation number Ns when

$$M = 1.0,\ K = 0.5, \Pr = 6.2,\ Ec = 0.5,\ \mathrm{Re}_L = 2.0,\ X = 1.0,\ n = 1.0$$

The variation in Bejan number with curvature parameter κ and Hartmann number M is illustrated in Figure 4.12. In case of flat stretching surface ($\kappa = 0.0$), the Bejan number Be decreases with the increase in M at the surface which indicates the dominance of fluid friction and magnetic field entropy effects. For small values of Hartmann number, it is observed that the value of Be increases and reaches a maximum value within the boundary layer region. It then starts to decrease and asymptotically approaches to zero. However, for higher values of Hartmann number, the effects of heat transfer entropy become fully dominant by within the boundary layer region and in the far away region. On the other hand, it is observed that in case of stretching cylinder, the heat transfer entropy effects start to dominate over fluid friction and magnetic field entropy effects in the far away region, as the value of Hartmann number is increased. Similar effects are also observed for the permeability parameter K as displayed in Figure 4.13. For flat stretching surface, the dominance of fluid friction and magnetic field entropy effects can be clearly seen at the surface and in the far away region. For stretching cylinder, the entropy effects due to fluid friction and magnetic field are significant at the stretching surface and heat transfer entropy effects become dominant

in the far away region with the increase in the value of K. Figure 4.14 illustrates that heat transfer entropy effects become strong with increase in temperature exponent n at the surface of flat stretching sheet and stretching cylinder. Nevertheless, in case of flat surface ($\kappa = 0.0$), the fluid friction and magnetic field entropy effects are fully dominant in the far away region. In case of stretching cylinder, the fluid friction and magnetic field entropy effects start to take over heat transfer entropy effects with increase in temperature exponent n. However, these effects are not fully dominant even at a large distance from the surface. Figure 4.15 shows that the increase in the value of group parameter causes the fluid friction and magnetic field entropy effects to become dominant over heat transfer entropy effects for both flat stretching surface and stretching cylinder. However, these effects are not in full dominance in case of stretching cylinder.

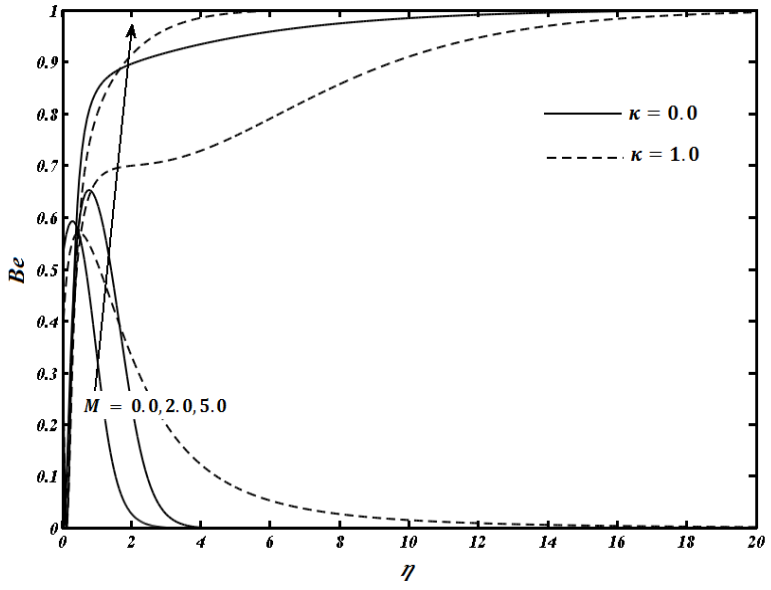

Figure 4.12: Effects of Hartmann number M on Bejan number Be when $K = 0.5,\ \Pr = 6.2,\ Ec = 0.5,\ n = 1.0,\ \mathrm{Re}_L = 2.0,\ X = 1.0,\ Br/\Omega = 1.0$

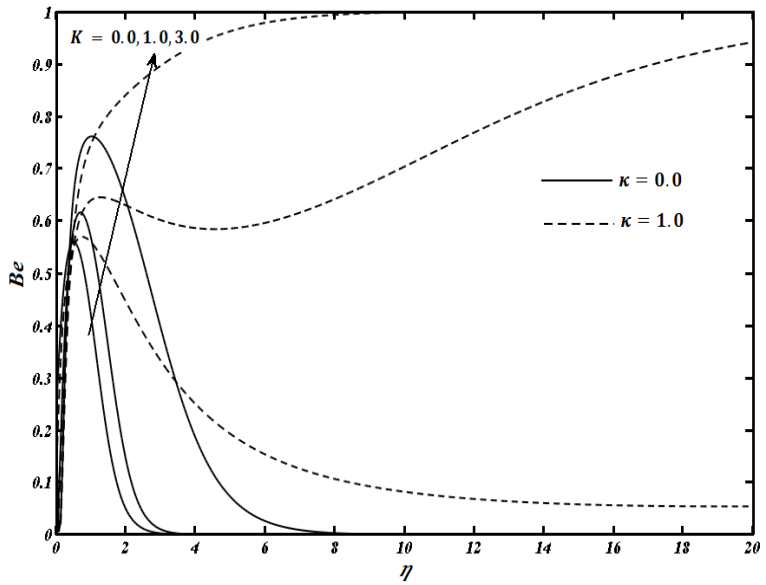

Figure 4.13: Effects of permeability parameter K on Bejan number Be when $M = 1.0,\ \Pr = 6.2,\ Ec = 0.5,\ n = 1.0,\ \mathrm{Re}_L = 2.0,\ X = 1.0,\ Br/\Omega = 1.0$

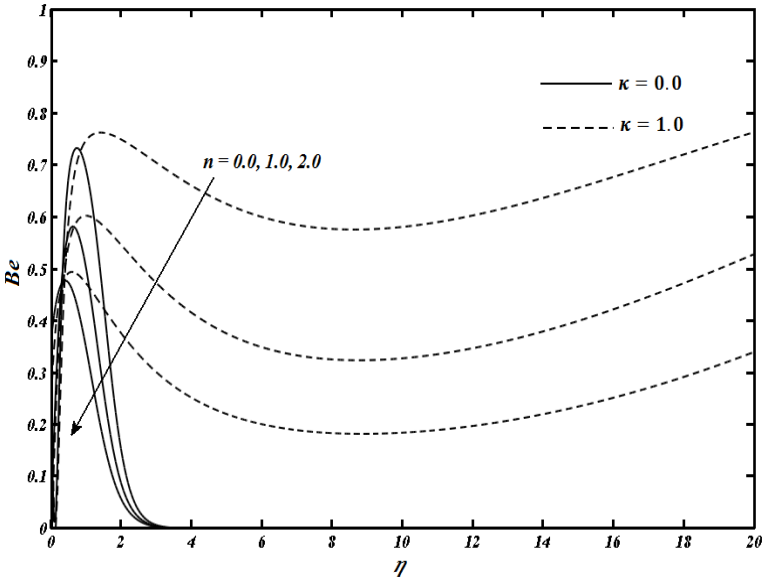

Figure 4.14: Effects of temperature exponent n on Bejan number Be when $M = 1.0,\ K = 0.5, \Pr = 6.2,\ Ec = 0.5,\ \mathrm{Re}_L = 2.0, X = 1.0,\ Br/\Omega = 1.0$

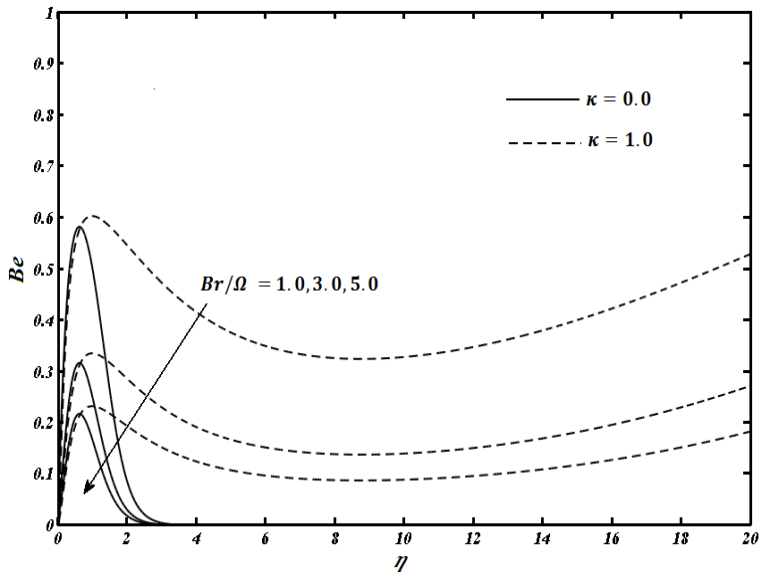

Figure 4.15: Effects of group parameter Br/Ω on Bejan numbe Be when $M=1.0,\ K=0.5, \Pr=6.2,\ Ec=0.5,\ \mathrm{Re}_L=2.0,\ n=1.0,\ X=1.0$

4.5 Concluding remarks

The hydromagnetic boundary layer flow and heat transfer phenomena of viscous fluid over a stretching cylinder embedded in a porous medium has been considered and the entropy generation effects have been investigated. It is observed that the presence of magnetic field and porous medium resists the fluid motion, which decreases the momentum boundary layer thickness and increases the thermal boundary layer thickness. Due to this resistance in flow, the skin friction increases and the heat transfer rate at the surface of stretching cylinder decreases with increase in Hartmann number M and permeability parameter K. Thus, a drop in heat transfer rate is noticed with the increase in curvature parameter κ. The entropy generation number Ns which characterizes the entropy generation rate increases with increase in Hartmann number M and permeability parameter K. Thus, the presence of magnetic field, porous medium and viscous dissipation effects augment the entropy effects. The presence of curvature also causes the entropy production to increase, i.e., the entropy effects are more in case of stretching cylinder as compared to the flat stretching surface. Furthermore, it is quite evident that as the

value of Hartmann number increases, the fluid friction and magnetic field entropy effects are dominant at the surface and in the far away region and heat transfer entropy effects are prominent within the boundary layer region for flat surface case. However, for stretching cylinder, heat transfer entropy effects become dominant with an increase in M in the far away region. By increasing the values of permeability parameter K, it is noticed that the fluid friction and magnetic field entropy effects are dominant at the surface of flat stretching sheet and in the far away region. Nonetheless, for stretching cylinder, heat transfer entropy effects become dominant with an increase in K in the far away region.

Chapter 5

Entropy analysis of MHD three dimensional viscous flow and heat transfer over a stretching sheet

5.1 Introduction

In the last two chapters, entropy generation effects in two dimensional flow of viscous fluid over a flat stretching surface and stretching cylinder have been investigated. This chapter focuses on examining the entropy generation effects in three dimensional flow and heat transfer of an electrically conducting fluid over a bidirectional stretching sheet. The effects of viscous dissipation and Joule dissipation have also been taken into consideration. The partial differential equations that govern the flow and thermal fields are transformed into non linear ordinary differential equations by using suitable similarity transformations. The converted equations are then solved analytically with the help of Homotopy Analysis Method (HAM) and numerically by using shooting technique with Runge-Kutta-Fehlberg method. The values computed by both the methods are compared to a previous study under limiting case. The influence of pertinent parameters involved in the considered problems on flow and heat transfer characteristics is shown with the aid of tables and graphs. Moreover, the effects of these parameters on entropy generation are also illustrated.

5.2 Mathematical formulation

5.2.1 Flow equation

The steady, three dimensional laminar boundary layer flow of an electrically conducting incompressible viscous fluid induced by the linear stretching of a sheet in two lateral directions has been assumed. The stretching surface is situated in the plane $z = 0$ whereas the fluid is confined in the region $z \geq 0$. The sheet is stretching in the x and y directions with the velocities $u = u_w$ and $v = v_w$ where a, b are constants. A uniform magnetic field of strength is applied perpendicular to the sheet lying in the plane $z = 0$ as shown in Figure 5.1. It is considered that there is no electric field present and the magnetic Reynolds number can be neglected, as the induced magnetic field is very small.

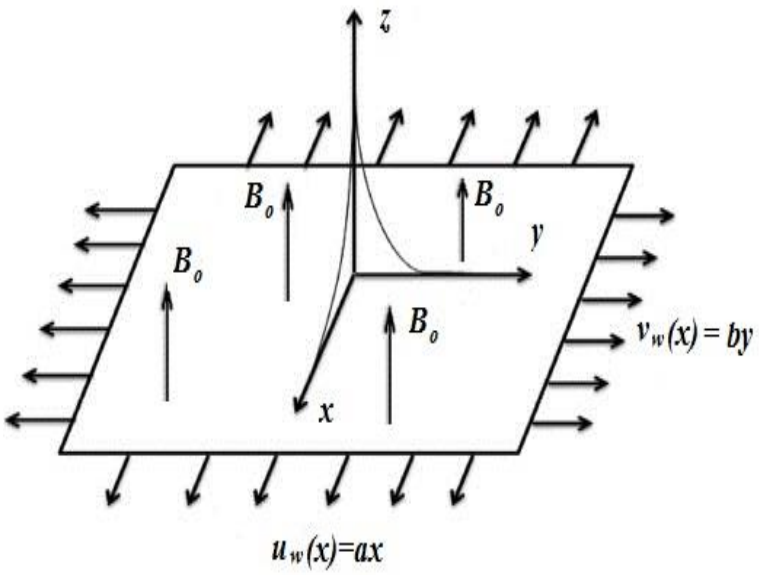

Figure 5.1: Geometry of the considered problem

Then, after applying boundary layer approximation, Eqs. (2.1-2.2) that govern the flow phenomenon can be expressed as

$$\frac{\partial u}{\partial x} + \frac{\partial v}{\partial y} + \frac{\partial w}{\partial z} = 0, \tag{5.1}$$

$$u\frac{\partial u}{\partial x}+v\frac{\partial u}{\partial y}+w\frac{\partial u}{\partial z}=\nu\frac{\partial^2 u}{\partial z^2}-\frac{\sigma B_o{}^2}{\rho}u, \tag{5.2}$$

$$u\frac{\partial v}{\partial x}+v\frac{\partial v}{\partial y}+w\frac{\partial v}{\partial z}=\nu\frac{\partial^2 v}{\partial z^2}-\frac{\sigma B_o{}^2}{\rho}v. \tag{5.3}$$

The boundary conditions related to flow problem are:

$$\begin{aligned} &u=u_w, \quad v=v_w, \quad w=0, \quad \text{at} \quad z=0,\\ &u\to 0, \quad v\to 0, \qquad\qquad \text{as} \quad z\to\infty, \end{aligned} \tag{5.4}$$

where (u,v,w) are the velocity components in (x,y,z) directions respectively, σ is the electrical conductivity, ρ is the density of fluid, μ is the fluid velocity and ν is the kinematic viscosity.

Following set of similarity transformation is introduced to transform the Eqs. (5.1-5.3) in dimensionless nonlinear ordinary differential equations

$$u=axf'(\eta), \quad v=ayg'(\eta), \quad w=-\sqrt{a\nu}\{f(\eta)+g(\eta)\}, \quad \eta=\sqrt{\frac{a}{\nu}}z. \tag{5.5}$$

Using (5.5) in Eqs. (5.1-5.3), the continuity equation (5.1) is identically satisfied and Eqs. (5.2-5.3) take the non-dimensional form:

$$f'''+(f+g)f''-f'^2-Mf'=0, \tag{5.6}$$

$$g'''+(f+g)g''-g'^2-Mg'=0, \tag{5.7}$$

having boundary conditions

$$\begin{aligned} &f'(0)=1, \quad g'(0)=b/a=\alpha, \quad f(0)+g(0)=0,\\ &f'(\infty)=g'(\infty)=0. \end{aligned} \tag{5.8}$$

Without the loss of generality, we assume

$$f(0)=g(0)=0. \tag{5.9}$$

Here $M = \frac{\sigma B_o^2}{\rho a}$ is the Hartman number, $\alpha = \frac{b}{a}$ is the stretching ratio parameter and $\xi = \frac{y}{x}$ is the dimensionless parameter. In case when $\alpha = 0,$ our problem reduces to two dimensional flow. When $\alpha = 1$, we get $f = g$ and the flow is axi-symmetric.

The expressions of the skin friction coefficients C_{fx} and C_{fy} in x and y directions are

$$C_{fx} = \frac{\mu\left(\frac{\partial u}{\partial z}\right)_{z=0}}{\rho(ax)^2}, \quad C_{fy} = \frac{\mu\left(\frac{\partial v}{\partial z}\right)_{z=0}}{\rho(ax)^2}. \tag{5.10}$$

By substituting (5.5) in (5.10), we obtain

$$\mathrm{Re}_x^{1/2} C_{fx} = f''(0), \quad \xi^{-1} \mathrm{Re}_x^{1/2} C_{fy} = g''(0). \tag{5.11}$$

5.2.2 Heat transfer modelling

For heat transfer analysis of the considered problem, it is assumed that the stretching surface has a constant temperature $T = T_w$ and the temperature of the ambient fluid is T_∞. In addition, it is presumed that the effects of viscous dissipation and Joule dissipation are also present. Then, the equation governing the heat transfer phenomenon can be attained as:

$$u\frac{\partial T}{\partial x} + v\frac{\partial T}{\partial y} + w\frac{\partial T}{\partial z} = \frac{k}{\rho c_p}\frac{\partial^2 T}{\partial z^2} + \frac{\nu}{c_p}\left[\left(\frac{\partial u}{\partial z}\right)^2 + \left(\frac{\partial v}{\partial z}\right)^2\right] + \frac{\sigma {B_0}^2}{\rho c_p}\left(u^2 + v^2\right). \tag{5.12}$$

The corresponding thermal boundary conditions are:

$$T = T_w \quad \text{at} \quad z = 0, \quad T = T_\infty \quad \text{as} \quad z \to \infty. \tag{5.13}$$

The Eq. (5.12) is normalized by considering the following similarity transformation:

$$\theta = \frac{T - T_\infty}{T_w - T_\infty}. \tag{5.14}$$

By using (5.14) and (5.5), the Eq. (5.12) takes the form:

$$\theta'' + \Pr(f+g)\theta' + \Pr Ec\left(f''^2 + \xi^2 g''^2\right) + M \Pr Ec\left(f'^2 + \xi^2 g'^2\right) = 0, \tag{5.15}$$

and the boundary conditions become

$$\theta(0) = 1, \qquad \theta(\infty) = 0. \tag{5.16}$$

In Eq. (5.15), $\Pr = \dfrac{\mu c_p}{k}$ is the Prandtl number and $Ec = \dfrac{u_w^{\,2}}{c_p(T_w - T_\infty)}$ is the Eckert number.

The local Nusselt number Nu_x is given by

$$Nu_x = \frac{x\left(\dfrac{\partial T}{\partial z}\right)_{z=0}}{k(T_w - T_\infty)}. \tag{5.17}$$

Using (5.14), the dimensionless form of (5.17) is

$$\mathrm{Re}_x^{-1/2} Nu_x = -\theta'(0). \tag{5.18}$$

5.2.3 Entropy analysis

By using Eq. (2.47), the local entropy generation rate per unit volume S_G for a viscous fluid in the presence of magnetic field, after applying boundary layer approximation is defined as

$$S_G = \frac{k}{T_\infty^{\,2}}\left[\left(\frac{\partial T}{\partial z}\right)^2\right] + \frac{\mu}{T_\infty}\left[\left(\frac{\partial u}{\partial z}\right)^2 + \left(\frac{\partial v}{\partial z}\right)^2\right] + \frac{\sigma B_0^{\,2}}{T_\infty}\left(u^2 + v^2\right). \tag{5.19}$$

From (5.19), it is quite evident that the factors causing the entropy production are heat transfer, fluid friction and magnetic field. In order to obtain the non-dimensional form of the entropy generation, we define the characteristic entropy generation rate as:

$$S_{Go} = \frac{k\Delta T^2}{T_w{}^2 L^2} \tag{5.20}$$

and the dimensionless entropy generation number is given as

$$Ns = \frac{S_G}{S_{Go}} = \mathrm{Re}_L\,\theta'^2 + \mathrm{Re}_L\,\frac{Br}{\Omega}\left(f''^2 + \xi^2 g''^2\right) + \mathrm{Re}_L\,\frac{Br}{\Omega} M\left(f'^2 + \xi^2 g'^2\right), \tag{5.21}$$

where $\Omega = \dfrac{T_w - T_\infty}{T_\infty}$ is the dimensionless temperature difference. The Eq. (5.21) can be expressed in the form

$$Ns = N_H + N_f + N_m = N_H + N_F. \tag{5.22}$$

and the Bejan number is defined as follows

$$Be = \frac{N_H}{Ns}. \tag{5.23}$$

5.3 Solution of the problem

5.3.1 Analytical method

The dimensionless nonlinear ordinary differential equations (5.6-5.7), together with the boundary conditions (5.8-5.9) for flow field and the non dimensional energy equation (5.15) with boundary condition (5.16) are solved analytically with the help of the Homotopy Analysis Method (HAM). The following set of initial guesses has been selected by observing the problem

$$\left.\begin{aligned} f_0(\eta) &= 1 - e^{-\eta}, \\ \mathrm{g}_0(\eta) &= \alpha\left(1 - e^{-\eta}\right), \\ \theta_0(\eta) &= e^{-\eta}. \end{aligned}\right\} \tag{5.24}$$

The auxiliary linear operators are chosen as:

$$\left.\begin{aligned}\mathcal{L}_f(f)&=\frac{d^3f}{d\eta^3}-\frac{df}{d\eta},\\ \mathcal{L}_g(g)&=\frac{d^3g}{d\eta^3}-\frac{dg}{d\eta},\\ \mathcal{L}_\theta(\theta)&=\frac{d^2\theta}{d\eta^2}-\theta.\end{aligned}\right\} \tag{5.25}$$

The zeroth-order deformations are constructed as:

$$(1-q)\mathcal{L}_f\left[\Lambda(\eta;q)-f_0(\eta)\right]=\hbar_f q\mathcal{N}_f\left[\Lambda(\eta;q),\Gamma(\eta;q)\right], \tag{5.26}$$

$$(1-q)\mathcal{L}_g\left[\Gamma(\eta;q)-g_0(\eta)\right]=\hbar_g q\mathcal{N}_g\left[\Lambda(\eta;q),\Gamma(\eta;q)\right], \tag{5.27}$$

$$(1-q)\mathcal{L}_\theta\left[\Theta(\eta;q)-\theta_0(\eta)\right]=\hbar_\theta q\mathcal{N}_\theta\left[\Lambda(\eta;q),\Gamma(\eta;q),\Theta(\eta;q)\right], \tag{5.28}$$

where non-linear operators are defined by

$$\left.\begin{aligned}\mathcal{N}_f\left[\Lambda(\eta;q),\Gamma(\eta;q)\right]&=\frac{\partial^3\Lambda(\eta;q)}{\partial\eta^3}+\left(\Lambda(\eta;q)+\hat{g}(\eta;q)\right)\frac{\partial^2\Lambda(\eta;q)}{\partial\eta^2}\\ &-\left(\frac{\partial\Lambda(\eta;q)}{\partial\eta}\right)^2-M\frac{\partial\Lambda(\eta;q)}{\partial\eta},\end{aligned}\right\} \tag{5.29}$$

$$\left.\begin{aligned}\mathcal{N}_g\left[\Lambda(\eta;q),\Gamma(\eta;q)\right]&=\frac{\partial^3\Gamma(\eta;q)}{\partial\eta^3}+\left(\Lambda(\eta;q)+\Gamma(\eta;q)\right)\frac{\partial^2\Gamma(\eta;q)}{\partial\eta^2}\\ &-\left(\frac{\partial\Gamma(\eta;q)}{\partial\eta}\right)^2-M\frac{\partial\Gamma(\eta;q)}{\partial\eta},\end{aligned}\right\} \tag{5.30}$$

$$\left.\begin{aligned}\mathcal{N}_\theta\left[\Theta(\eta;q),\Lambda(\eta;q),\Gamma(\eta;q),\right]&=\frac{\partial^2\Theta(\eta;q)}{\partial\eta^2}+\Pr\left(\Lambda(\eta;q)+\Gamma(\eta;q)\right)\frac{\partial\Theta(\eta;q)}{\partial\eta}\\ &+\Pr Ec\left[\left(\frac{\partial^2\Lambda(\eta;q)}{\partial\eta^2}\right)^2+\xi^2\left(\frac{\partial^2\Gamma(\eta;q)}{\partial\eta^2}\right)^2\right].\end{aligned}\right\} \tag{5.31}$$

The m-th order deformation equations in the final form are

$$\mathcal{L}_f\left[f_m(\eta)-\chi_m f_{m-1}(\eta)\right]=\hbar_f \mathcal{R}_m^f(\eta), \tag{5.32}$$

$$\mathcal{L}_g\left[g_m(\eta)-\chi_m g_{m-1}(\eta)\right]=\hbar_g \mathcal{R}_m^g(\eta), \tag{5.33}$$

$$\mathcal{L}_\theta\left[\theta_m(\eta)-\chi_m \theta_{m-1}(\eta)\right]=\hbar_\theta \mathcal{R}_m^\theta(\eta), \tag{5.34}$$

with the corresponding boundary conditions

$$\left.\begin{aligned} &f_m(0)=f'_m(0)=g_m(0)=g'_m(0)=\theta_m(0)=0,\\ &f'_m(\infty)=g'_m(\infty)=\theta_m(\infty)=0. \end{aligned}\right\} \tag{5.35}$$

Here

$$\mathcal{R}_m^f(\eta)=\frac{\partial^3 f_{m-1}}{\partial\eta^3}+\sum_{k=0}^{m-1}\left(f_{m-1-k}\frac{\partial^2 f_k}{\partial\eta^2}+g_{m-1-k}\frac{\partial^2 f_k}{\partial\eta^2}-\frac{\partial f_{m-1-k}}{\partial\eta}\frac{\partial f_k}{\partial\eta}\right)-M\frac{\partial f_{m-1}}{\partial\eta}, \tag{5.36}$$

$$\mathcal{R}_m^g(\eta)=\frac{\partial^3 g_{m-1}}{\partial\eta^3}+\sum_{k=0}^{m-1}\left(f_{m-1-k}\frac{\partial^2 g_k}{\partial\eta^2}+g_{m-1-k}\frac{\partial^2 g_k}{\partial\eta^2}-\frac{\partial g_{m-1-k}}{\partial\eta}\frac{\partial g_k}{\partial\eta}\right)-M\frac{\partial g_{m-1}}{\partial\eta}, \tag{5.37}$$

$$\left.\begin{aligned} \mathcal{R}_m^\theta(\eta)=&\frac{\partial^2\theta_{m-1}}{\partial\eta^2}+\Pr\sum_{k=0}^{m-1}\left(f_{m-1-k}\frac{\partial\theta_k}{\partial\eta}+g_{m-1-k}\frac{\partial\theta_k}{\partial\eta}\right)\\ &+\Pr\sum_{k=0}^{m-1}\left[Ec\left(\frac{\partial^2 f_{m-1-k}}{\partial\eta^2}\frac{\partial^2 f_k}{\partial\eta^2}+\xi^2\frac{\partial^2 g_{m-1-k}}{\partial\eta^2}\frac{\partial^2 g_k}{\partial\eta^2}\right)+M\,Ec\left(\frac{\partial f_{m-1-k}}{\partial\eta}\frac{\partial f_k}{\partial\eta}+\xi^2\frac{\partial g_{m-1-k}}{\partial\eta}\frac{\partial g_k}{\partial\eta}\right)\right], \end{aligned}\right\} \tag{5.38}$$

where

$$\chi_m=\begin{cases}0, & m\le 1,\\ 1, & m>1.\end{cases} \tag{5.39}$$

The final solutions obtained by HAM in the forms of the series are given by

$$f(\eta) = f_0(\eta) + \sum_{m=1}^{\infty} f_m(\eta), \tag{5.40}$$

$$g(\eta) = g_0(\eta) + \sum_{m=1}^{\infty} g_m(\eta), \tag{5.41}$$

$$\theta(\eta) = \theta_0(\eta) + \sum_{m=1}^{\infty} \theta_m(\eta). \tag{5.42}$$

From (5.40-5.42), it can be seen that the convergence of series solutions $f(\eta)$, $g(\eta)$ and $\theta(\eta)$ obtained by Homotopy Analysis Method (HAM) strongly depend upon the unknown parameters h_f, h_g and h_θ. These parameters enable us to control and adjust the convergence of the series solutions. In Figure 5.2, the so called $\hbar$-curves are drawn at the 15th order of approximation.

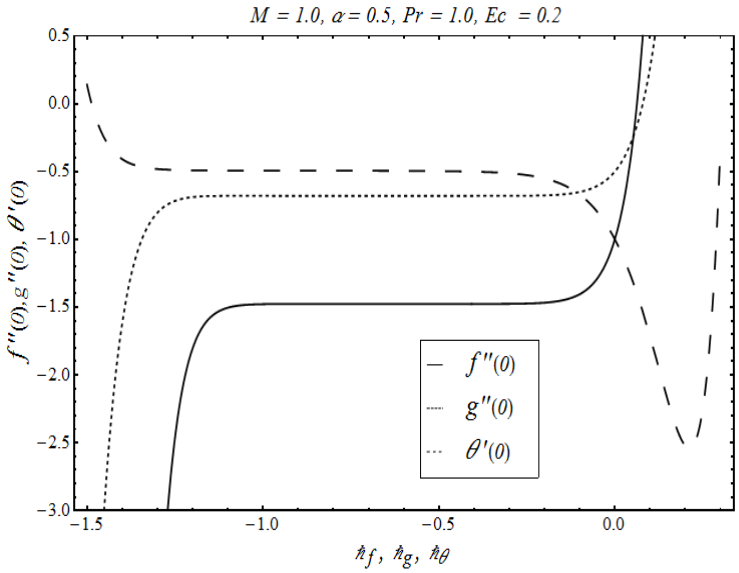

Figure 5.2: $\hbar - curves$ plotted at 20th order of approximation

It can be observed the suitable ranges of $\hbar_f$, $\hbar_g$ and $\hbar_\theta$ for which the series solutions converge are $-0.2 \le \hbar_f \le -1.0$, $-0.1 \le \hbar_g \le -1.1$ and $-0.3 \le \hbar_\theta \le -1.2$. In Table 5.1, the optimal values of $\hbar_f$, $\hbar_g$ and $\hbar_\theta$ and their corresponding square residual errors $E_{m,f}$, $E_{m,g}$ and $E_{m,\theta}$ at different orders of approximations are displayed. It is quite obvious that the squared residual errors $E_{m,f}$, $E_{m,g}$ and $E_{m,\theta}$ reduce as the order of approximation m increases. Moreover, the convergence of series solutions is also presented in tabular form in Table 5.2 while using the optimal values of $\hbar_f$, $\hbar_g$ and $\hbar_\theta$ at the 15th order of approximation. It is noticed that the series solutions converge at the 40th-order of approximation up to 6 decimal places.

Table 5.1: Numerical values of averaged squared residual errors $E_{m,f}$, $E_{m,g}$ and $E_{m,\theta}$ at different orders of approximations corresponding to the optimal values of $\hbar_f$, $\hbar_g$ and $\hbar_\theta$ when

$$\alpha = 0.5,\ M = 1.0,\ \Pr = 1.0,\ Ec = 0.2$$

Order of approximations m	$\hbar_f$	$\hbar_g$	$\hbar_\theta$	$E_{m,f}$	$E_{m,g}$	$E_{m,\theta}$
3	-0.686151	-0.790754	-1.268020	3.14461×10^{-4}	1.78030×10^{-5}	4.22755×10^{-4}
6	-0.697394	-0.769361	-0.984778	1.03438×10^{-6}	7.61713×10^{-8}	1.47908×10^{-5}
9	-0.681669	-0.738828	-0.896382	6.42345×10^{-8}	1.84838×10^{-9}	9.35736×10^{-5}
12	-0.687220	-0.730241	-0.943446	6.47934×10^{-10}	5.73610×10^{-11}	1.14621×10^{-6}
15	-0.681179	-0.719999	-0.886904	1.72482×10^{-11}	3.03064×10^{-11}	8.14315×10^{-6}

Table 5.2: Convergence of HAM solutions for different order of approximations when $M = 1.0$, $\alpha = 0.5, \Pr = 1.0, Ec = 0.2$ *and* $\hbar_f = -0.681179, \hbar_g = -0.719999, \hbar_\theta = -0.886904$

Order of Convergence	$-f''(0)$	$-g''(0)$	$-\theta'(0)$
5	1.476220	0.679727	0.444287
10	1.476770	0.679809	0.422877
15	1.476770	0.679809	0.421615
20	1.476770	0.679809	0.421413
25	1.476770	0.679809	0.421376
30	1.476770	0.679809	0.421369
35	1.476770	0.679809	0.421367
40	1.476770	0.679809	0.421366
45	1.476770	0.679809	0.421366
50	1.476770	0.679809	0.421366

5.3.2 Numerical method

In order to countercheck the results obtained by Homotopy Analysis Method (HAM), the nonlinear ordinary differential equations (5.6-5.7) having the boundary conditions (5.8-5.9) and the non-dimensional energy equation (5.15) with boundary condition (5.16) are again solved numerically using shooting technique with fourth-fifth order Runge-Kutta-Fehlberg method. The step size $\Delta\eta = 0.001$ is used with $\eta_{\max} = 18$. The choice of $\eta_{\max}$ ensured the convergence of the numerical solution. The accuracy up to 6 decimal places is chosen as the criterion of convergence. The procedure is employed by making the following substitution $f = w_1,\ f' = w_2,\ f'' = w_3,\ g = w_4,\ g' = w_5,\ g'' = w_6,$ $\theta = w_7,\ \theta' = w_8.$ Thus, we have the system of first order differential equations as

$$
\left.
\begin{aligned}
w_1' &= w_2, \\
w_2' &= w_3, \\
w_3' &= -(w_1 + w_4)w_3 + {w_2}^2 + Mw_2, \\
w_4' &= w_5, \\
w_5' &= w_6, \\
w_6' &= (w_1 + w_4)w_6 + {w_5}^2 + Mw_5, \\
w_7' &= w_8, \\
w_8' &= -\Pr(w_1 + w_4)w_8' - \Pr Ec({w_3}^2 + \xi^2 {w_6}^2) - \Pr Ec({w_2}^2 + \xi^2 {w_5}^2).
\end{aligned}
\right\} \tag{5.43}
$$

The boundary conditions associated with the system are converted to initial conditions as

$$
\left.
\begin{aligned}
w_1(0) &= 0, \\
w_2(0) &= 1, \\
w_3(0) &= s_1, \\
w_4(0) &= 0, \\
w_5(0) &= \alpha, \\
w_6(0) &= s_2, \\
w_7(0) &= 1, \\
w_8(0) &= s_3.
\end{aligned}
\right\} \tag{5.44}
$$

The values of unknown initial conditions s_1, s_2, and s_3 are guessed and the integration is carried out repeatedly until the boundary conditions are asymptotically satisfied.

5.4 Validation of the obtained results

In order to further ensure the accuracy and validity of the results obtained by Homotopy Analysis Method and shooting technique, the values of $-f''(0)$ and $-g''(0)$ are compared to those presented by Ariel [90] in Table 5.3 for different values of α by keeping Hartmann number equal to zero, i.e., $M = 0.0$. It is found that there is an excellent agreement between the values of both the studies.

Table 5.3: Comparison of values of $-f''(0)$ and $-g''(0)$ with those reported by Ariel [90] when $M = 0.0$

	$-f''(0)$				$-g''(0)$			
α	HPM [90]	$Exact$ [90]	HAM	$Numerical$	HPM [90]	$Exact$ [90]	HAM	$Numerical$
0.0	-1	-1	-1	-1	0	0	0	0
0.1	1.017027	1.020260	1.020260	1.020260	0.073099	0.066847	0.066847	0.066847
0.2	1.034587	1.039495	1.039495	1.039495	0.158231	0.148737	0.148737	0.148737
0.3	1.052470	1.057955	1.057955	1.057955	0.254347	0.243360	0.243360	0.243360
0.4	1.070529	1.075788	1.075788	1.075788	0.254347	0.243360	0.243360	0.243360
0.5	1.088662	1.093095	1.093095	1.093095	0.476290	0.465205	0.465205	0.465205
0.6	1.106797	1.109947	1.109947	1.109947	0.600833	0.590529	0.590529	0.590529
0.7	1.124882	1.126398	1.126398	1.126398	0.733730	0.724532	0.724532	0.724532
0.8	1.142879	1.142489	1.142489	1.142489	0.874551	0.866683	0.866683	0.866683
0.9	1.160762	1.158254	1.158254	1.158254	1.022922	1.016539	1.016539	1.016539
1.0	1.178511	1.173721	1.173721	1.173721	1.178511	1.173721	1.173721	1.173721

5.5 Results and discussion

This section is devoted to show the influence of different physical parameters on velocity components, temperature, skin friction coefficient, Nusselt number, entropy generation number and Bejan number, and the results are presented with the help of graphs and tables.

The influence of Hartmann number M and stretching ratio parameter α on velocity components $f'(\eta)$ and $g'(\eta)$ are presented in Figures 5.3 and 5.4. Figure 5.3 is drawn to see the effects of Hartmann number on fluid velocity profiles $f'(\eta)$ and $g'(\eta)$. A decrease in boundary layer thickness is observed with increase in the Hartmann number. This reduction in velocity profiles is due to increase in the Lorentz force with increase in M which retards the fluid motion.

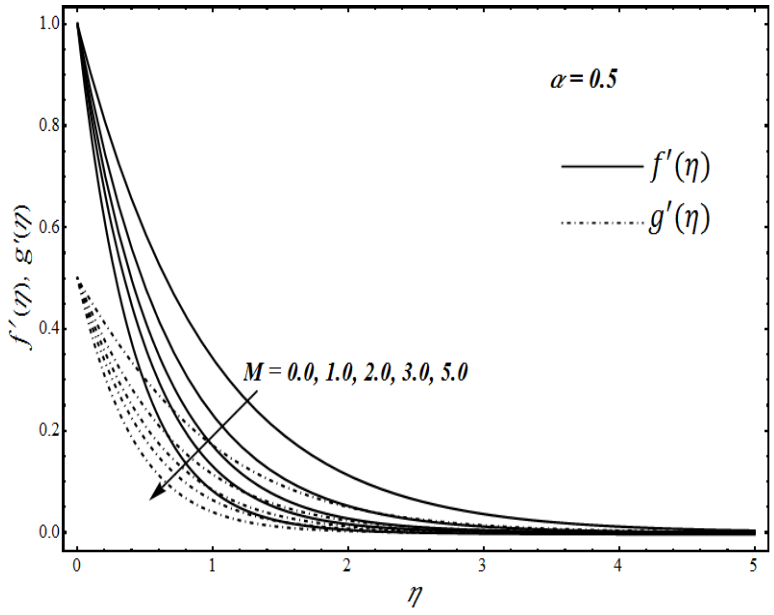

Figure 5.3: Velocity profiles $f'(\eta)$ and $g'(\eta)$ for variation in Hartmann number M

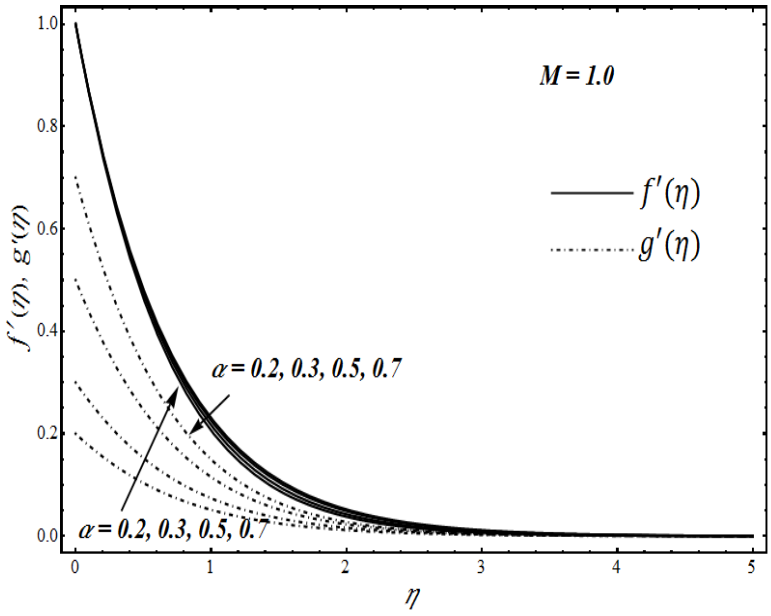

Figure 5.4: Velocity profiles $f'(\eta)$ and $g'(\eta)$ for variation in stretching ratio parameter α

In Figure 5.4, the influence of stretching ratio parameter α on velocities $f'(\eta)$ and $g'(\eta)$ are illustrated. It is detected that the velocity profile $f'(\eta)$ decreases as the stretching ratio parameter α rises. On the other hand, an increase in velocity $g'(\eta)$ is noticed with increase in α. The values of dimensionless skin friction coefficients $-f''(0)$ and $-g''(0)$ for different values of Hartmann number M and stretching ratio parameter α are tabulated in Table 5.4. Both the Hartmann number and stretching ratio parameter have increasing effects on $-f''(0)$ and $-g''(0)$.

Figure 5.5 depicts the consequence of variation in Hartmann number M on temperature profile $\theta(\eta)$. This resistance caused by Lorentz force results in rise in the temperature of fluid. Figure 5.6 illustrates that the temperature distribution $\theta(\eta)$ diminishes with increase in the stretching ratio parameter α. The influence of Eckert number Ec on temperature profile is shown in Figure 5.7. Increase in Eckert number augments the frictional forces within the fluid which causes the fluid temperature to rise.

Table 5.4: Numerical values of dimensionless skin friction coefficients $-f''(0)$ and $-g''(0)$ for variation in the values of Hartmann number M and stretching ratio parameter α

M	α	$-f''(0)$ *HAM*	$-f''(0)$ *Numerical*	$-g''(0)$ *HAM*	$-g''(0)$ *Numerical*
0	0.5	1.09309	1.09309	0.465205	0.465205
0.5		1.29831	1.29831	0.581835	0.581835
1.0		1.47677	1.47677	0.679809	0.679809
2.0		1.78216	1.78216	0.843091	0.843091
1.0	0.1	1.42707	1.42707	0.119896	0.119896
	0.3	1.45225	1.45225	0.384597	0.384597
	0.5	1.47677	1.47677	0.679809	0.679809
	0.7	1.50072	1.50072	1.002960	1.002960

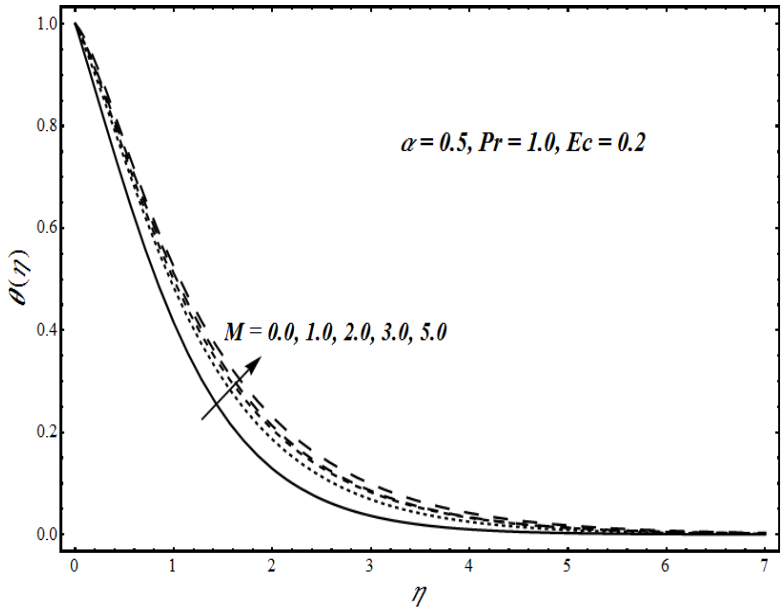

Figure 5.5: Temperature profile $\theta(\eta)$ for variation in Hartmann number M

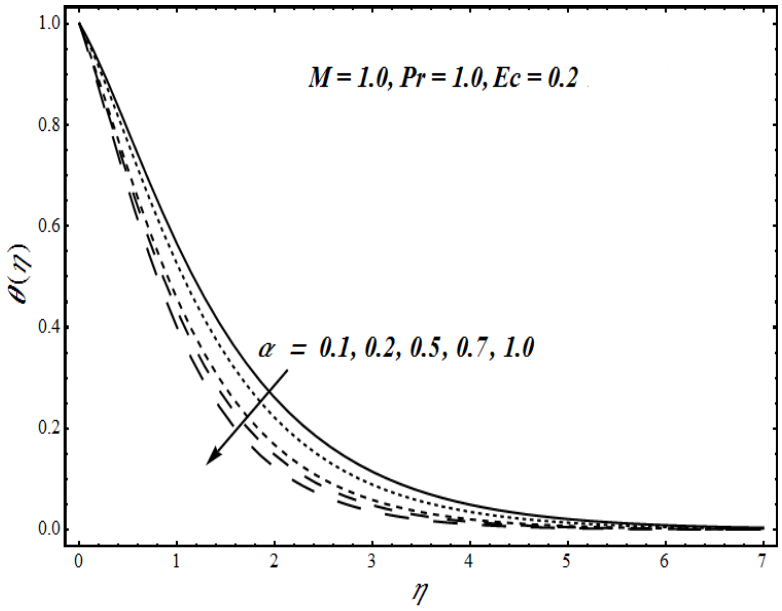

Figure 5.6: Temperature profile $\theta(\eta)$ for variation in stretching ratio parameter α

Table 5.5 is constructed to see the effects of various parameters on the local Nusselt number when $\Pr = 1.0$. It is noted that the rate of heat transfer reduces with increase in the value of Hartmann number M and Eckert number Ec and enhances with an increase in stretching parameter α .

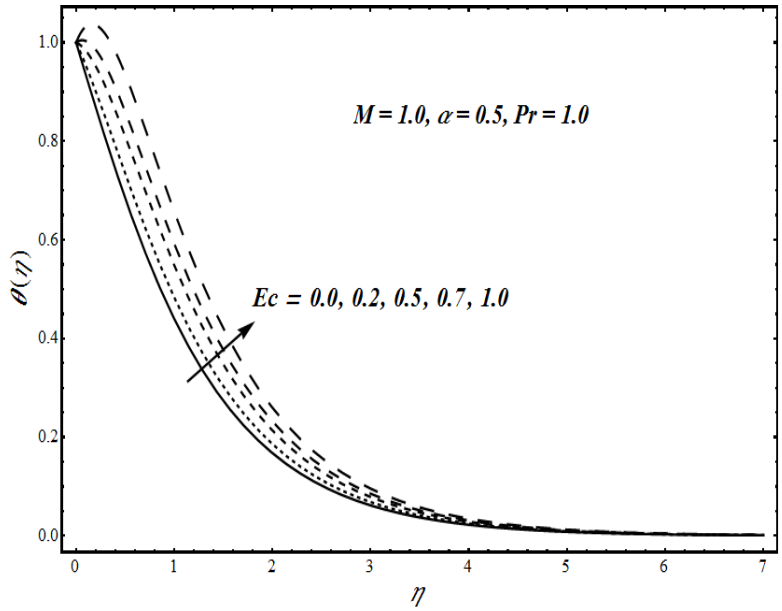

Figure 5.7: Temperature profile $\theta(\eta)$ for variation in Eckert number Ec

Table 5.5: Numerical values of dimensionless Nusselt number $-\theta'(0)$ for different values of Hartmann number M, stretching ratio parameter α and Eckert number Ec

M	α	Ec	$-\theta'(0)$ HAM	$-\theta'(0)$ $Numerical$
0.0	0.5	0.2	0.619645	0.619645
0.5			0.551836	0.551836
1.0			0.493990	0.493990
2.0			0.398667	0.398667
1.0	0.1	0.2	0.407857	0.407857
	0.3		0.459702	0.459702
	0.5		0.493990	0.493990
	0.7		0.511139	0.511139
1.0	0.5	0.2	0.493990	0.493990
		0.3	0.412301	0.412301
		0.5	0.248923	0.248923
		0.7	0.085547	0.085547

The effects of Hartmann number M, stretching ratio parameter α and group parameter Br/Ω on local entropy generation number Ns are presented in Figures 5.8-5.10. Figure 5.8 shows that Hartmann number has increasing effects on Ns which is due to the fact that increase in M results in more friction which causes the entropy production rate to augment. In Figure 5.9, the influence of stretching ratio parameter α on local entropy generation number is illustrated. As observed in Tables 5.3 and 5.4, increase in stretching ratio parameter α augments the heat transfer rate and friction at the surface of stretching sheet which ultimately results in enhancement of entropy generation. The influence of group parameter Br/Ω on Ns is shown in Figure 5.10. The group parameter has importance as it gives information about the viscous effects. It is recorded that the viscous effects become strong with increase in Br/Ω which cause the entropy generation number to rise.

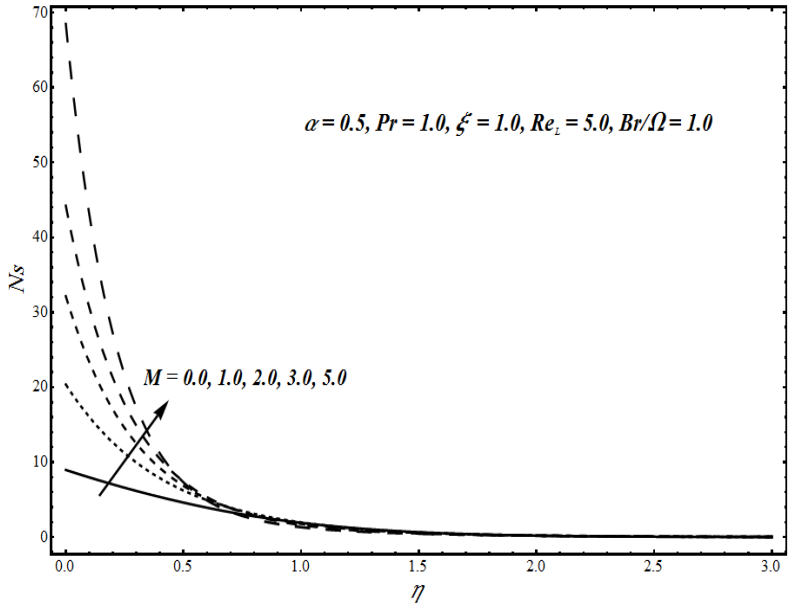

Figure 5.8: Local entropy generation number Ns plotted against η for variation in Hartmann number M

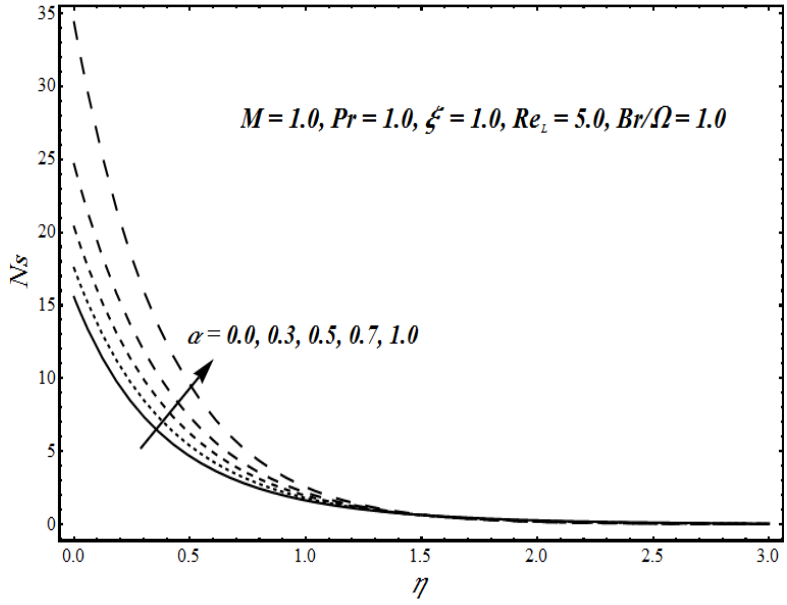

Figure 5.9: Local entropy generation number Ns plotted against η for variation in stretching ratio parameter α

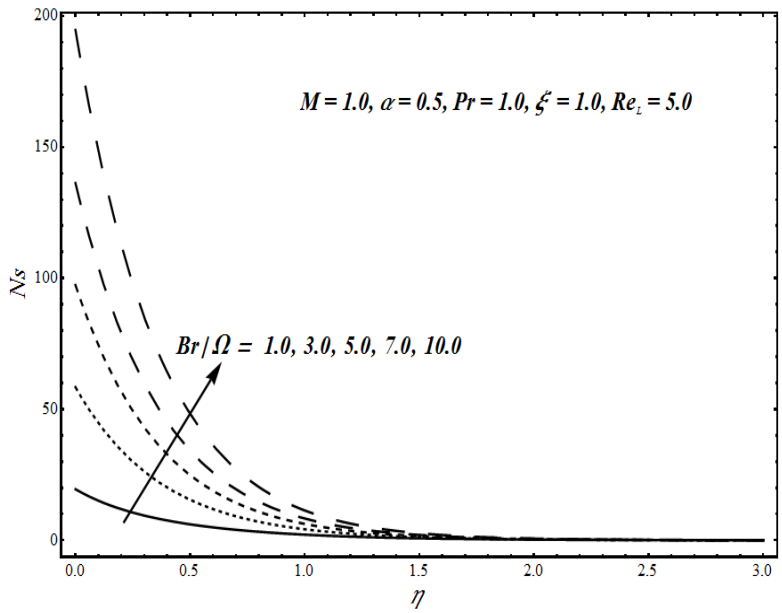

Figure 5.10: Local entropy generation number Ns plotted against η for variation in group parameter Br/Ω

The variation of Bejan number Be with Hartmann number M, stretching ratio parameter α and group parameter Br/Ω are depicted in Figures 5.11-5.13 respectively against η. Figure 5.11 illustrates that the entropy effects due to fluid friction and magnetic field prevail near the stretching surface. As the distance from the surface increases, these effects reduce and the heat transfer entropy effects become strong. In the far away region, the entropy effects due to heat transfer are in full dominance. Moreover, it is found that heat transfer entropy effects become influential earlier for large values of M. Figure 5.12 shows the effects of stretching ratio parameter α on Be. The entropy effects due to fluid friction and magnetic field are prominent near the stretching surface and the heat transfer entropy effects are dominant in the far away region.

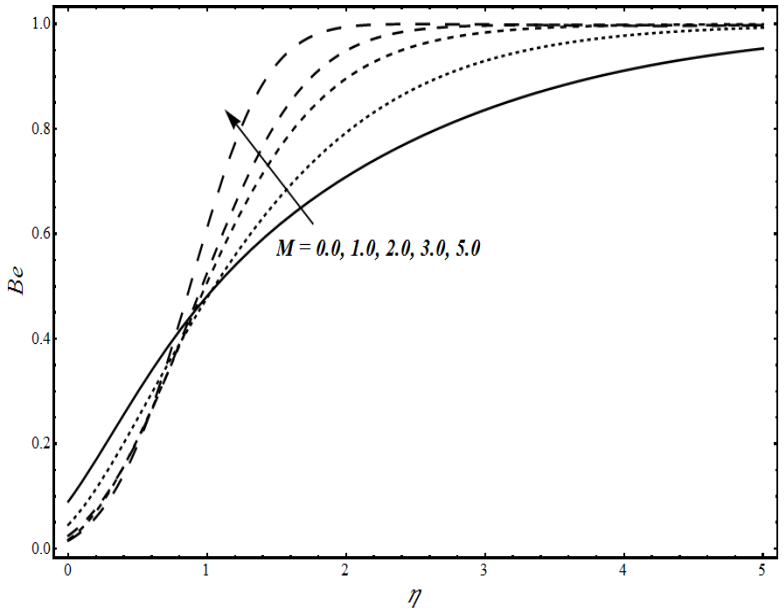

Figure 5.11: Bejan number Be plotted against η for variation in Hartmann number M

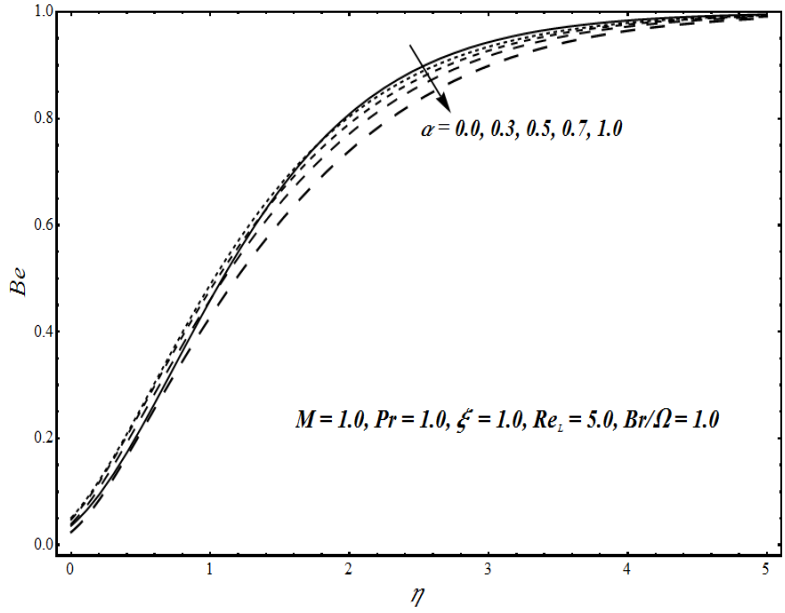

Figure 5.12: Bejan number Be plotted against η for variation in stretching ratio parameter α

The influence of group parameter Br/Ω on Bejan number Be is shown in Figure 5.13. It can be seen that the fluid friction and magnetic field effects are prominent near the stretching surface. In the far away region, the entropy due to heat transfer dominates.

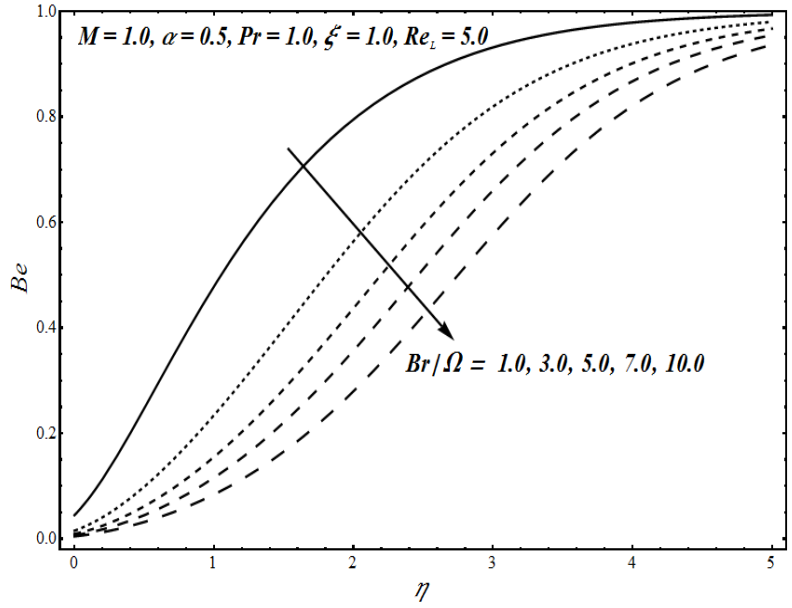

Figure 5.13: Bejan number Be plotted against η for variation in group parameter Br/Ω

5.6 Concluding remarks

The entropy effects in three dimensional magnetohydrodynamic flow and heat transfer over a surface stretching in two directions are examined. It is observed that there is a decrease in velocity profiles $f'(\eta)$ and $g'(\eta)$ as the value of Hartmann number M increases. This decrease in fluid velocities is due to the resistive force which ultimately increases the fluid temperature $\theta(\eta)$. On the other hand, the stretching parameter α has decreasing effect on velocity profile $f'(\eta)$ whereas an increase in the velocity $g'(\eta)$ is noted with increase in α. Furthermore, a decrease in thermal boundary layer thickness is noticed with increase in stretching ratio parameter α. The local entropy generation number Ns which is a measure of entropy generation tends to increase with increase in the values of Hartmann number M and the stretching ratio parameter α. Also, the present study reveals that the fluid friction and magnetic field entropy effects dominate near the three dimensional stretching surface and the heat transfer entropy effects are dominant in the far away region.

Chapter 6

Entropy analysis of MHD viscous fluid flow over a convectively heated radially stretching surface

6.1 Introduction

In the previous chapters, entropy generation effects are examined in flow and heat transfer over a linearly stretching surface. This chapter extends the previous work to examine the entropy generation effects in magnetohydrodynamic flow and heat transfer of a viscous fluid over a radially stretching surface which is convectively heated by crossing a hot fluid from below. The partial differential equations that govern the flow and heat transfer phenomena are transformed to non-linear differential equations by using similarity variables. The transformed system is then, solved by using analytical and numerical techniques and the obtained results are compared to each other. The effects of various thermophysical parameters on velocity, temperature, local skin friction, Nusselt number, the local entropy generation number and Bejan number are discussed in detail with the help of graphs and tables.

6.2 Mathematical analysis

6.2.1 Flow phenomenon

Assume a steady two dimensional boundary layer flow of an electrically conducting incompressible viscous fluid due to the stretching of a convectively heated disk in the radial direction. The disk is stretching

with velocity proportional to the distance from the origin i.e., $u = ar$, where a is a constant. The sheet is located in the plane $z = 0$ and the fluid is confined to the region $z > 0$. A uniform transverse magnetic field of strength B_0 is applied parallel to z-axis as shown in Figure 6.1. It is considered that the magnetic Reynolds number is small so that the induced magnetic field is neglected. In addition, there is no existence of electric field. Then the Eqs. (2.1-2.2) governing the fluid flow after applying boundary layer approximation take the form

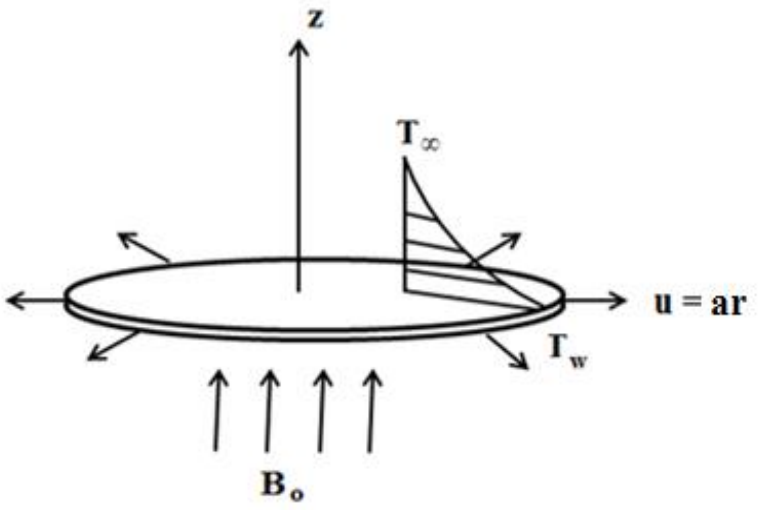

Figure 6.1: Schematic diagram and coordinate system

$$\frac{\partial}{\partial r}(ru) + \frac{\partial}{\partial z}(rw) = 0, \tag{6.1}$$

$$u\frac{\partial u}{\partial r} + w\frac{\partial u}{\partial z} = \nu\frac{\partial^2 u}{\partial z^2} - \frac{\sigma B_0^2}{\rho}u, \tag{6.2}$$

and the boundary conditions for the flow are

$$\begin{aligned} &u = u_w(r) = ar, \quad w = 0, \quad \text{at } z = 0, \\ &u \to 0, \quad \text{at } z \to \infty. \end{aligned} \tag{6.3}$$

Here u and v are the velocity components in the radial and axial directions respectively.

In order to non-dimensionalize the Eqs. (6.1-6.2), following similarity transformations are introduced:

$$u = arf'(\eta), \qquad v = -\sqrt{av}\, f(\eta), \quad \eta = \sqrt{\frac{a}{\nu}}z. \tag{6.4}$$

By substituting (6.4) into Eqs. (6.1-6.2), the Eq. (6.1) is automatically satisfied and the Eq. (6.2) takes the form

$$f''' + 2ff'' - f'^2 - Mf' = 0. \tag{6.5}$$

Making use of (6.4), the boundary conditions (6.3) become

$$f(0) = 0, \quad f'(0) = 1, \quad f'(\infty) = 0. \tag{6.6}$$

The expressions of local skin friction coefficient C_f is given by

$$C_f = \frac{\tau_w}{\frac{1}{2}\rho u_w^{\,2}}, \tag{6.7}$$

where τ_w is the shear wall stress and is expressed as

$$\tau_w = \mu\left(\frac{\partial u}{\partial z}\right)_{z=0}. \tag{6.8}$$

Substituting (6.8) in (6.7) and after using (6.4), the non-dimensional form of local skin friction coefficient is

$$\frac{1}{2}C_f\, \mathrm{Re}_r^{1/2} = -f''(0). \tag{6.9}$$

6.2.2 Heat transfer phenomenon

The heat transfer from the surface stretching in the radial direction is due to the fact that its bottom surface is convectively heated by a hot fluid of temperature T_f which provides a heat transfer coefficient h'. The temperature of the ambient fluid is considered to be T_∞. The viscous dissipation and the Joule

dissipation effects are also assumed to be present. Then the energy equation (2.3) after the application of boundary layer approximation becomes

$$u\frac{\partial T}{\partial r}+w\frac{\partial T}{\partial z}=\frac{k}{\rho c_p}\frac{\partial^2 T}{\partial z^2}+\frac{\mu}{\rho c_p}\left(\frac{\partial u}{\partial z}\right)^2+\frac{\sigma B_0^2}{\rho c_p}u^2, \tag{6.10}$$

where the corresponding thermal boundary conditions are

$$-k\frac{\partial T}{\partial z}=h'(T_f-T) \quad \text{at } z=0, \quad \text{and} \quad T=T_\infty \quad \text{at } z\to\infty. \tag{6.11}$$

To following similarity transformation is considered to non-dimensionalize the Eq. (6.10)

$$\theta(\eta)=\frac{T-T_\infty}{T_f-T_\infty}. \tag{6.12}$$

After utilizing (6.4) and (6.12), the Eq. (6.10) becomes

$$\theta''+2\,\mathrm{Pr}\, f\theta'+\mathrm{Pr}\, Ecf''^2+M\,\mathrm{Pr}\, Ecf'^2=0, \tag{6.13}$$

and the thermal boundary conditions (6.11) take the form

$$\theta'(0)=-Bi(1-\theta(0)), \qquad \theta(\infty)=0. \tag{6.14}$$

The local Nusselt number Nu_r is expressed as

$$Nu_r=\frac{rq_w}{k\left(T_f-T_\infty\right)}, \tag{6.15}$$

where the heat flux from the surface q_w is given by

$$q_w=-k\left(\frac{\partial T}{\partial z}\right)_{z=0}. \tag{6.16}$$

The dimensionless form of local Nusselt number after substitution of (6.16) in (6.15) and using (6.12) is

$$\mathrm{Re}_r^{-1/2}\,Nu_r=-\theta'(0). \tag{6.17}$$

6.2.3 Entropy generation effects

By applying the boundary layer approximation, the local volumetric rate of entropy generation S_G defined in (2.46) for a viscous fluid in the presence of magnetic field can be expressed by:

$$S_G = \underbrace{\frac{k}{T_f^{\,2}}\left(\frac{\partial T}{\partial z}\right)^2}_{\substack{\text{entropy effects}\\ \text{due to}\\ \text{heat transfer}}} + \underbrace{\frac{\mu}{T_f}\left(\frac{\partial u}{\partial z}\right)^2}_{\substack{\text{entropy effects}\\ \text{due to}\\ \text{fluid friction}}} + \underbrace{\frac{\sigma B_0^{\,2}}{T_f}u^2}_{\substack{\text{entropy effects}\\ \text{due to}\\ \text{magnetic field}}} . \tag{6.18}$$

The normalized form of local entropy generation after using (6.4) and (6.12) is expressed as:

$$Ns = \frac{S_G}{S_{Go}} = \mathrm{Re}_L\,\theta'^2 + \mathrm{Re}_L\,\frac{Br}{\Omega}\,f''^2 + \mathrm{Re}_L\,\frac{Br}{\Omega}M\,f'^2, \tag{6.19}$$

where $S_{Go} = \dfrac{k(T_f - T_\infty)^2}{T_f^{\,2}L^2}$ is the characteristic entropy generation rate, $\Omega = \dfrac{T_f - T_\infty}{T_f}$ is the dimensionless temperature difference. Thus local entropy generation in Eq. (6.19) can be written as:

$$Ns = N_H + N_f + N_m = N_H + N_F. \tag{6.20}$$

Another important irreversibility distribution parameter is known as Bejan number and is defined as follows:

$$Be = \frac{N_H}{Ns}. \tag{6.21}$$

6.3 Solution of the problem

The nonlinear differential equation (6.5) along with the boundary conditions (6.6) and the equation (6.13) with boundary conditions (6.14) are solved analytically by using a method known as Homotopy Analysis Method (HAM) and numerically by shooting procedure with fourth-fifth order Runge-Kutta-Fehlberg method.

6.3.1 Homotopy solution

By keeping in view the nature of the considered physical problem, we choose the following set of initial guesses

$$\left.\begin{aligned} f_0(\eta) &= 1 - e^{-\eta}, \\ \theta_0(\eta) &= \frac{Bi}{1+Bi} e^{-\eta}. \end{aligned}\right\} \tag{6.22}$$

The linear operators are given as:

$$\left.\begin{aligned} \mathcal{L}_f(f) &= \frac{d^3 f}{d\eta^3} - \frac{df}{d\eta}, \\ \mathcal{L}_\theta(\theta) &= \frac{d^2\theta}{d\eta^2} + \frac{d\theta}{d\eta}. \end{aligned}\right\} \tag{6.23}$$

In order to obtain the analytical series solution of the problem, the procedure elaborated in section 3.3 and 5.3.1 is followed. To avoid repetition, the details of rest of the method are concealed and the mth order-deformation equations are given as:

$$\mathcal{L}_f\left[f_m(\eta) - \chi_m f_{m-1}(\eta)\right] = \hbar_f \mathcal{R}_m^f(\eta), \tag{6.24}$$

$$\mathcal{L}_\theta\left[\theta_m(\eta) - \chi_m \theta_{m-1}(\eta)\right] = \hbar_\theta \mathcal{R}_m^\theta(\eta), \tag{6.25}$$

$$\left.\begin{aligned} f_m(0) = f'_m(0) = f_m(\infty) = 0, \\ \theta'_m(0) - Bi\theta_m(0) = \theta_m(\infty) = 0. \end{aligned}\right\} \tag{6.26}$$

Here

$$\mathcal{R}_m^f(\eta) = \frac{\partial^3 f_{m-1}}{\partial \eta^3} + 2\sum_{k=0}^{m-1}\left(f_{m-1-k}\frac{\partial^2 f_k}{\partial \eta^2} - \frac{\partial f_{m-1-k}}{\partial \eta}\frac{\partial f_k}{\partial \eta}\right) - M\frac{\partial f_{m-1}}{\partial \eta}, \tag{6.27}$$

$$\mathcal{R}_m^\theta(\eta) = \frac{\partial^2 \theta_{m-1}}{\partial \eta^2} + 2\Pr\sum_{k=0}^{m-1} f_{m-1-k}\frac{\partial \theta_k}{\partial \eta}, + \Pr Ec\sum_{k=0}^{m-1}\frac{\partial^2 f_{m-1-k}}{\partial \eta^2}\frac{\partial^2 f_k}{\partial \eta^2} + M\Pr Ec\sum_{k=0}^{m-1}\frac{\partial f_{m-1-k}}{\partial \eta}\frac{\partial f_k}{\partial \eta}, \tag{6.28}$$

$$\chi_m = \begin{cases} 0, & m \le 1, \\ 1, & m > 1. \end{cases} \tag{6.29}$$

The series solution of the problem is given by:

$$f(\eta) = f_0(\eta) + \sum_{m=1}^{\infty} f_m(\eta), \tag{6.30}$$

$$\theta(\eta) = \theta_0(\eta) + \sum_{m=1}^{\infty} \theta_m(\eta). \tag{6.31}$$

The equations (6.24-6.25) have been solved one after the other in the order $m = 1, 2, 3\ldots$ by using the symbolic software MATHEMATICA.

6.3.1.1 Convergence of series solution

The convergence of the series solutions (6.30-6.31) strongly depends upon the auxiliary parameters $\hbar_f$ and $\hbar_\theta$. The so-called $\hbar$-curves are drawn in Figure 6.2 at the 20th order-of approximation to determine the admissible ranges of $\hbar_f$ and $\hbar_\theta$ for which the series solutions converge. It is observed that the suitable ranges of $\hbar_f$ and $\hbar_\theta$ are $-0.2 \le \hbar_f \le -0.9$ and $-0.1 \le \hbar_\theta \le -0.6$. By using the formulae defined in (3.45-3.46) for averaged square residual errors, table 6.1 is constructed which displays the values of the optimal

values of $\hbar_f$ and $\hbar_\theta$ and their corresponding square residual errors $E_{m,f}$ and $E_{\theta,m}$ at different orders of approximation m. A considerable decrease in the value of $E_{m,f}$ and $E_{\theta,m}$ is observed as the orders of approximation increase which shows the validity of HAM solution. Moreover, Table 6.2 is constructed to present the convergence of series solutions which shows that the seriess olutions converge at the 35th-order of approximation up to 6 decimal places.

Table 6.1: Optimal values of $\hbar_f$ and $\hbar_\theta$ and their corresponding averaged squared residual errors $E_{m,f}$ and $E_{m,\theta}$ at different orders of approximations when $M = 1.0,\ \Pr = 1.0,\ Ec = 0.5,\ Bi = 0.5$

$Order\ of\ approximations\ m$	$\hbar_f$	$\hbar_\theta$	$E_{m,f}$	$E_{m,\theta}$
3	-0.675595	-0.598645	2.64271×10^{-4}	2.73415×10^{-3}
6	-0.649974	-0.588295	4.48313×10^{-6}	3.71436×10^{-4}
9	-0.644763	-0.516601	8.23592×10^{-8}	8.13267×10^{-4}
12	-0.645664	-0.532724	2.34264×10^{-9}	6.27438×10^{-6}
15	-0.642311	-0.504139	8.01812×10^{-11}	4.61691×10^{-5}

Table 6.2: Convergence of HAM solutions for different order of approximations when $M = 1.0,\ Bi = 0.5,\ \Pr = 1.0,\ Ec = 0.5$

$Order\ of\ Convergence$	$-f''(0)$	$-\theta'(0)$
5	1.521959	0.145426
10	1.535181	0.120805
15	1.535688	0.118073
20	1.535710	0.117794
25	1.535710	0.117766
30	1.535711	0.117764
35	1.535711	0.117763
40	1.535711	0.117763

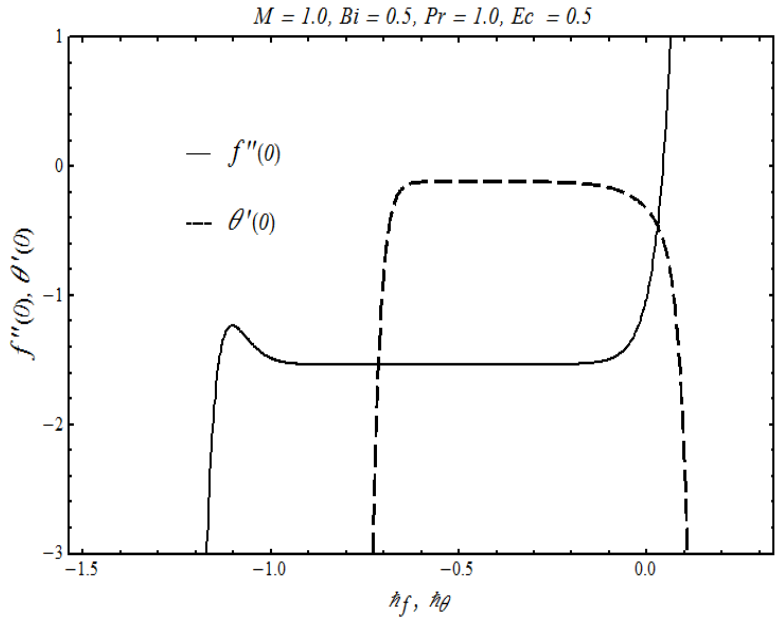

Figure 6.2: $\hbar-curves$ for 20th order of approximation

6.3.2 Numerical method

To verify the results obtained by Homotopy Analysis Method (HAM), the nonlinear differential equations (6.5) along with the boundary conditions (6.6) and (6.13) with boundary conditions (6.14) are also solved numerically by reducing them into a system of first order differential equations and employing the fourth-fifth order Runge-Kutta-Fehlberg method. The first order system of differential equations are formed by following substitutions $f = w_1, f' = w_2, f'' = w_3, \theta = w_4, \theta = w_5$ .Thus, we have:

$$\left.\begin{aligned} w_1' &= w_2, \\ w_2' &= w_3, \\ w_3' &= -2w_1w_3 + w_2^{\,2} + Mw_2, \\ w_4' &= w_5, \\ w_5' &= -2\,\mathrm{Pr}\, w_1w_5' - \mathrm{Pr}\, Ecw_3^{\,2} - M\,\mathrm{Pr}\, Ecw_2^{\,2}, \end{aligned}\right\} \tag{6.32}$$

having the associated initial conditions

$$\left.\begin{aligned} w_1(0) &= 0, \\ w_2(0) &= 1, \\ w_3(0) &= s_1, \\ w_4(0) &= s_2, \\ w_5(0) &= -Bi(1-s_2). \end{aligned}\right\} \tag{6.32}$$

The values of s_1 and s_2 are initially being guessed and the integration is iteratively performed till the boundary conditions are asymptotically satisfied. For the purpose of computation, the infinity is taken to be 20 and a step size of 0.001 is chosen. The convergence criterion is set up to 10^{-6}.

6.4 Results and discussion

Figure 6.3 illustrates the effects of variation in Hartmann number M on velocity profile. It is noticed that with an increase in the value of M, a drag force known as Lorentz force becomes strong which causes the fluid velocity $f'(\eta)$ to decrease.

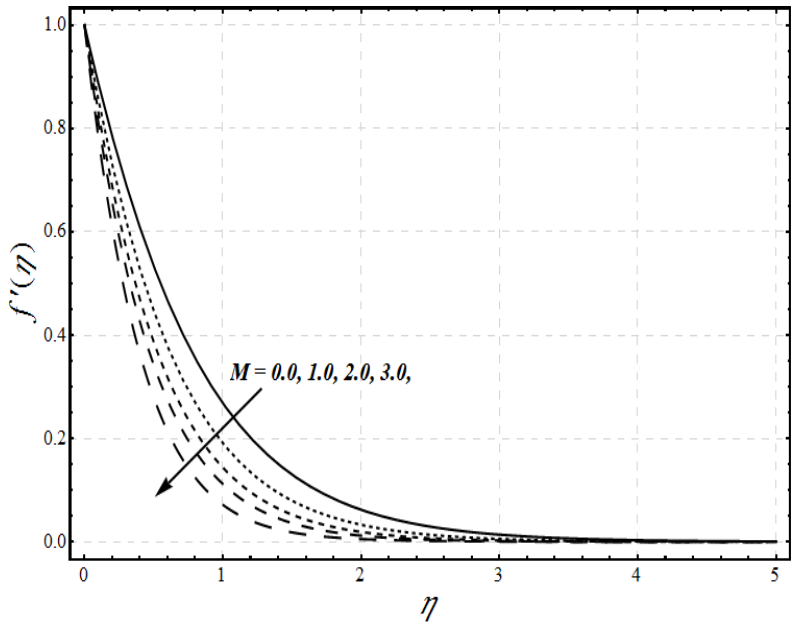

Figure 6.3: Effects of variation in Hartmann number M on velocity profile $f'(\eta)$

Numerical values of dimensionless local skin friction coefficient $-f''(0)$ are recorded in Table 6.3 by both analytical and numerical methods for different values of Hartmann number M. It is quite clear from the table that there is an excellent agreement between the values found by both techniques. Moreover, it is observed that as the value of Hartmann number M increases, the resistance offered to the flow by Lorentz force augments the skin friction at the radially stretching surface.

The influence of Hartmann number M on temperature profile is presented in Figure 6.4. As the value of Hartmann number increases, the resistance to the motion of flow increases which ultimately results in a rise in temperature of the fluid. The effects of Eckert number Ec on temperature profile $\theta(\eta)$ are shown in Figure 6.5. By increasing the value of Ec, the frictional heating generates within the fluid which results in an increase in fluid temperature. In Figure 6.6, the effects of variation in Biot number Bi on $\theta(\eta)$ are presented. An increase in temperature is observed with increase in Biot number. This is due to the fact that increasing the values of Bi increase the rate of heat transfer from the radially stretching surface which leads to an increase in temperature of fluid.

Table 6.3: Numerical values of dimensionless local skin friction coefficient $-f''(0)$ for different values of Hartmann number M

M	$-f''(0)$ HAM	$-f''(0)$ $Numerical$
0.0	1.17372	1.17372
0.5	1.36581	1.36581
1.0	1.53571	1.53571
2.0	1.83049	1.83049
3.0	2.08484	2.08484

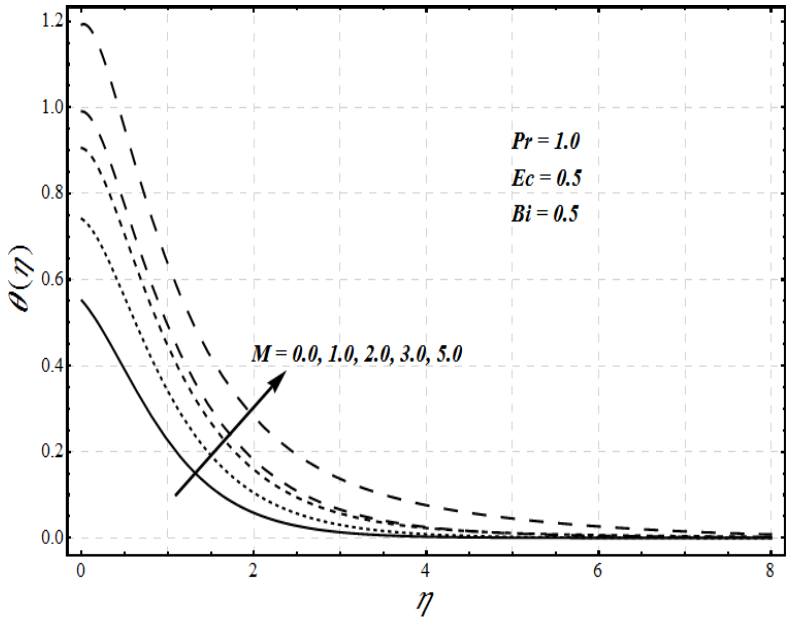

Figure 6.4: Effects of variation in Hartmann number M on temperature profile $\theta(\eta)$

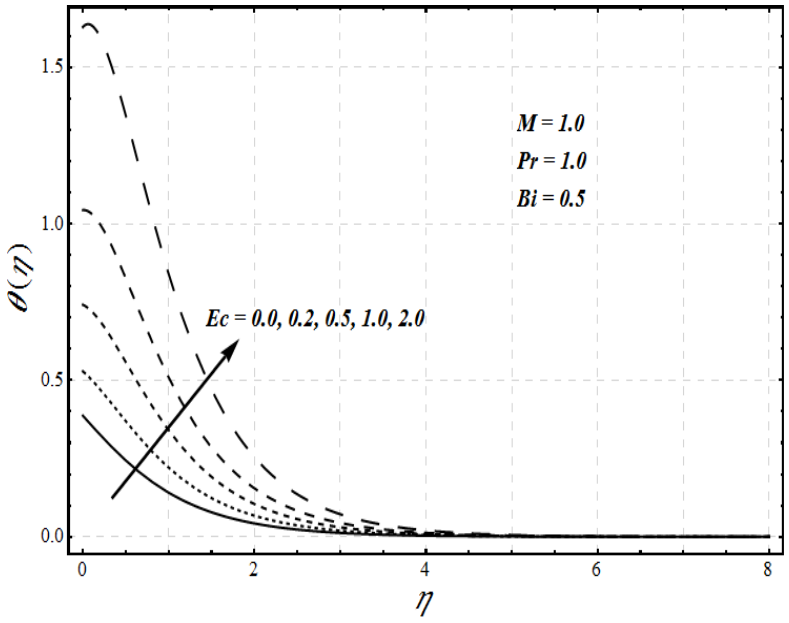

Figure 6.5: Effects of variation in Eckert number Ec on temperature profile $\theta(\eta)$

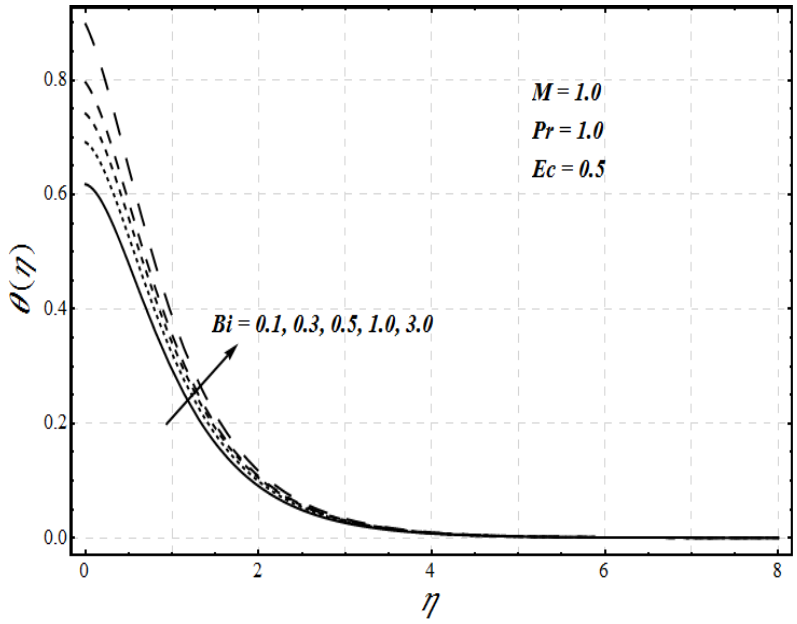

Figure 6.6: Effects of variation in Biot number Bi on temperature profile $\theta(\eta)$

Table 6.4: Numerical values of dimensionless local Nussselt number $-\theta'(0)$ for different values of Hartmann number M, Biot number Bi and Eckert number Ec with $\Pr = 1.0$

M	Bi	Ec	$-\theta'(0)$ HAM	$-\theta'(0)$ $Numerical$
0.0	0.5	0.5	0.21914	0.21914
0.5			0.16621	0.16621
1.0			0.11776	0.11776
2.0			0.02992	0.02992
3.0			0.04974	0.04974
1.0	0.1	0.5	0.03425	0.03425
	0.2		0.06151	0.06151
	0.5		0.11776	0.11776
	1.0		0.16940	0.16940
	2.0		0.21697	0.21697
1.0	0.5	0.1	0.30483	0.30483
		0.3	0.19259	0.19259
		0.5	0.11776	0.11776
		0.7	0.04294	0.04294
		0.8	0.00552	0.00552

Table 6.4 is drawn to show the variation in the values of Hartmann number M, Eckert number Ec and Biot number Bi on dimensionless local Nusselt number $-\theta'(0)$ by keeping Prandtl number fixed at $Pr = 1.0$. By observing it, it is noticed that rate of heat transfer from the radially stretching surface reduces as the values of M and Ec increases whereas increase in Bi enhances the $-\theta'(0)$.

Figures 6.7-6.9 illustrate the influence of physical parameters involved in the problem on local entropy generation number Ns. Figure 6.7 presents the effects of Hartmann number M on local entropy generation number. In the absence of magnetic field, entropy generation effects are low. However, when magnetic field is present, the entropy generation rate increases as the value of Hartmann number increases. This is in accordance with the physical fact, because the drag force becomes stronger with an increase in the value of M which causes more resistance to flow and ultimately results in more entropy production. Also, it can be noticed the entropy generation effects are more prominent near the radially stretching disk. These effects decrease as the distance from the surface increases.

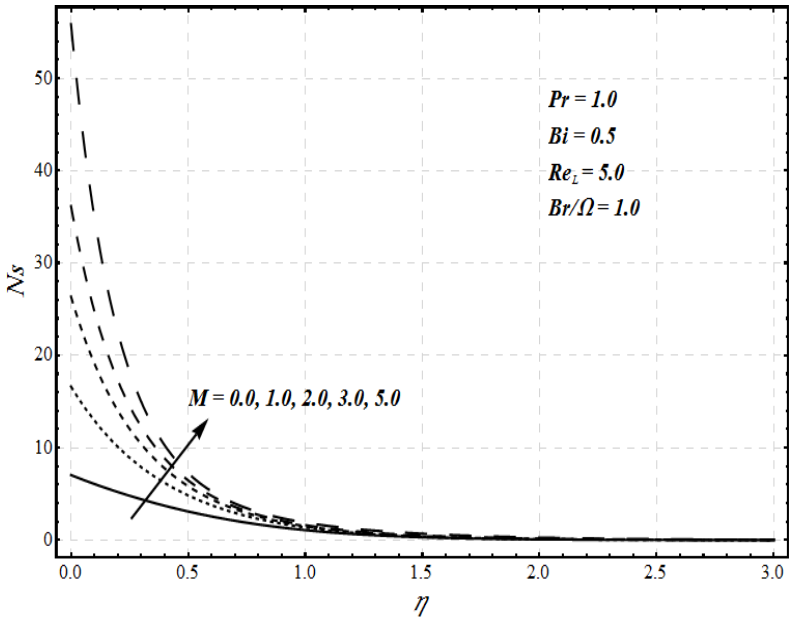

Figure 6.7: Effects of variation in Hartmann number M on local entropy generation number Ns

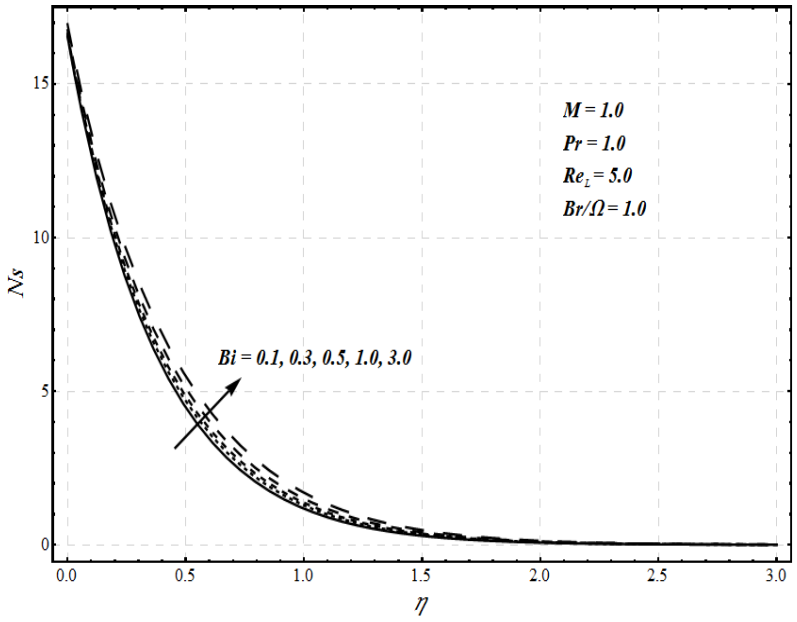

Figure 6.8: Effects of variation in Biot number Bi on local entropy generation number Ns

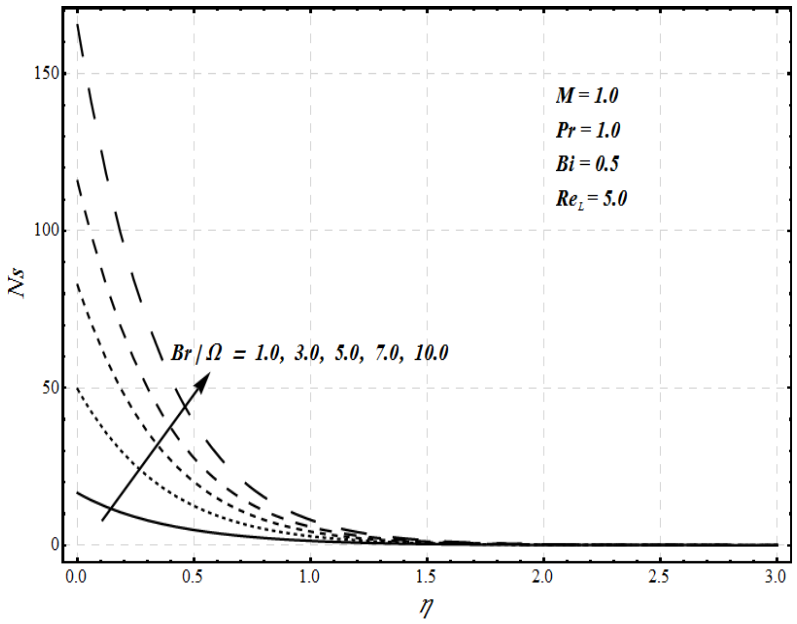

Figure 6.9: Effects of variation in group parameter Br/Ω on local entropy generation number Ns

The effect of the Biot number Bi on the local entropy generation number Ns is illustrated in Figure 6.8. Near the stretching disk, the effects of Bi on Ns are not so prominent. However, the value of Ns increases within the boundary layer region with an increase in the value of the Biot number. In the far away region, entropy effects are negligible. Figure 6.9 shows that entropy generation rate increase with an increase in the value of group parameter Br/Ω. These effects are more prominent near the radially stretching disk and in the far away region, these effects are insignificant.

In Figures 6.10-6.12, Bejan number Be is plotted to get an idea whether fluid friction and magnetic field irreversibility dominates over heat transfer irreversibility or vice versa. In Figure 6.10, the effects of Hartmann number M on Bejan number are presented. The entropy effects due to fluid friction and magnetic field are fully dominant near the stretching disk and in the far away region, heat transfer entropy effects are dominant. Moreover, for large values of M, the fluid friction and magnetic field entropy effects are observed for large distance before the heat transfer entropy effects become dominant.

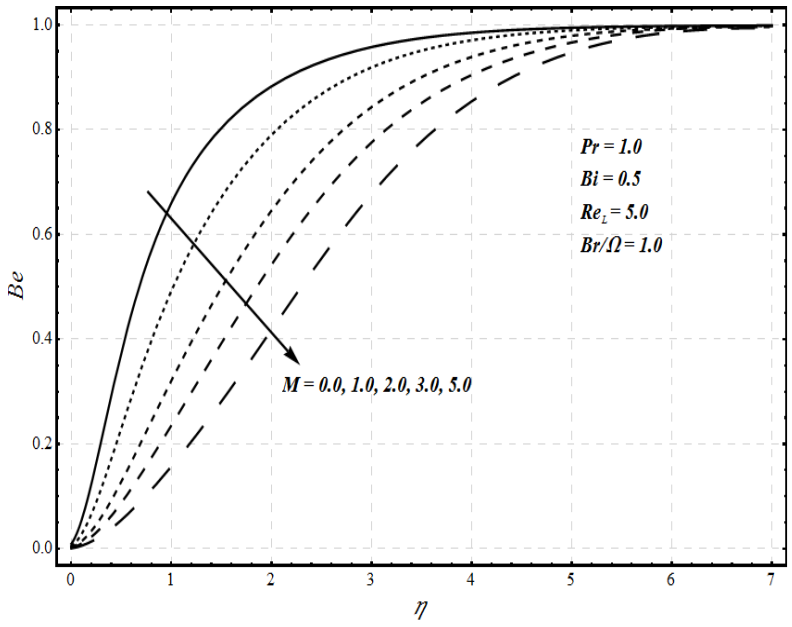

Figure 6.10: Effects of variation in Hartmann number M on Bejan number Be

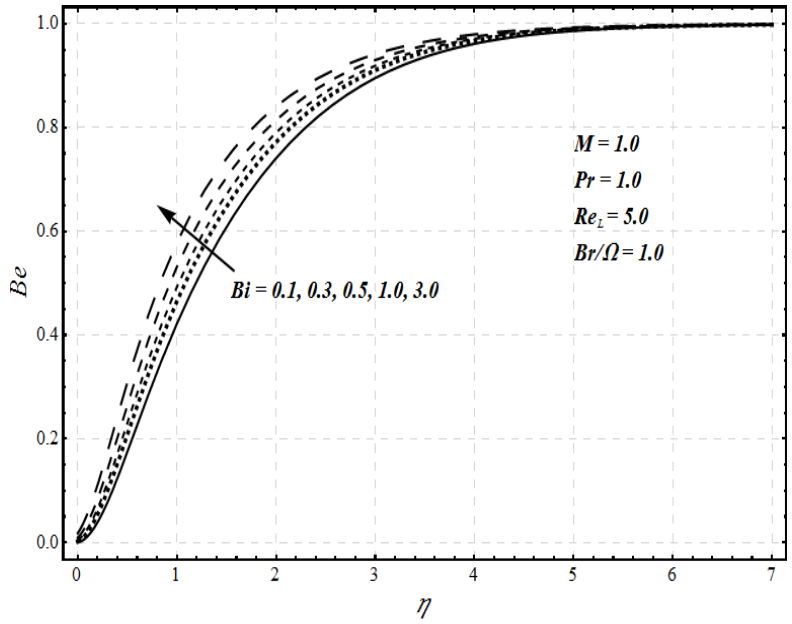

Figure 6.11: Effects of variation in Biot number Bi on Bejan number Be

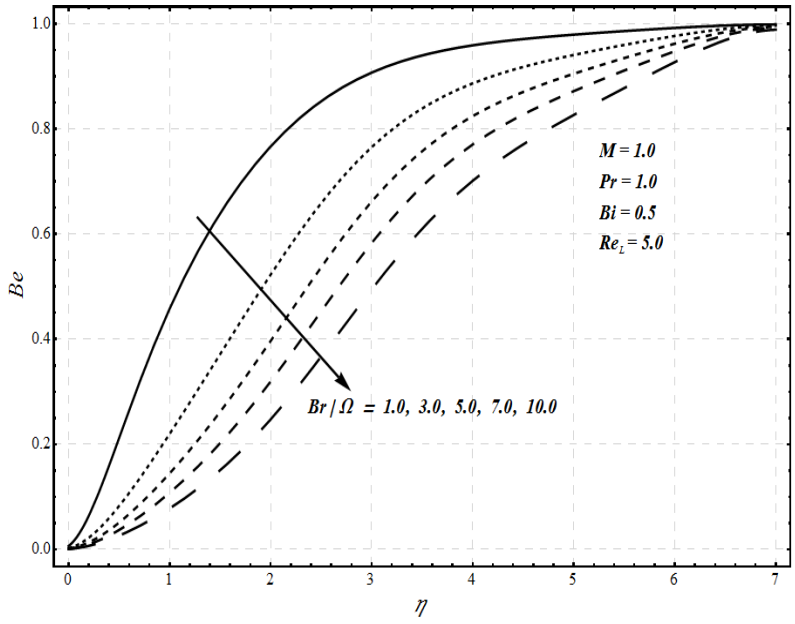

Figure 6.12: Effects of variation in group parameter Br/Ω on Bejan number Be

Figure 6.11 depicts the effects of the Biot number Bi on Bejan number. For a particular value of Bi, the fluid friction and magnetic field entropy effects are significant near the radially stretching disk and in the far away, the heat transfer entropy effects are dominant. Moreover, increasing the value of Bi results in a slight decrease in fluid friction and magnetic field entropy near the stretching disk surface. Figure 6.12 shows that with an increase in group parameter Br/Ω, the fluid friction and magnetic field entropy effects become dominant near the surface of stretching disk. In the far away region, entropy due to heat transfer dominates.

6.5 Conclusions

The magnetohydrodynamic flow and heat transfer over a convectively heated radially stretching surface has been considered and the entropy effects have also been examined during the process. The presence of magnetic field causes the velocity profile $f'(\eta)$ to decrease and the temperature $\theta(\eta)$ of the fluid to augment. As a result, the local skin friction coefficient $-f''(0)$ increases whereas the local Nusselt number $-\theta'(0)$ decreases as the value of Hartmann number M increases. On the other hand, increase in Biot number Bi enhances the rate of heat transfer from the radially stretching sheet which consequently has an increasing impact on temperature. Moreover, an increase in local entropy generation number Ns is observed with increase in the values of magnetic field parameter M, the Biot number Bi and the group parameter Br/Ω. This indicates that all these parameters are the main causes of entropy production. It is further noticed that the fluid friction and magnetic field entropy effects dominate near the radially stretching disk and the entropy effects due to heat transfer irreversibility are dominant in the far away region.

Chapter 7

Entropy generation effects in viscous flow through porous medium between two radially stretching surfaces

7.1 Introduction

In continuation to the last chapter, the study is extended, in this chapter, to investigate the entropy generation effects in viscous fluid flow and heat transfer through a porous medium between two radially stretching surfaces. The problem is mathematically modelled and the solutions are obtained by analytical and numerical procedures. The effects of various dimensionless parameters on flow and heat transfer characteristics as well as on entropy generation are discussed in detail through graphs and tables.

7.2 Mathematical formulation

7.2.1 Governing equations

Consider a steady, axi-symmetric flow of a viscous fluid through a porous medium bounded between two infinite sheets stretching in the radial direction at the same rate. The two stretching surfaces are placed at $z = \pm L$ and the fluid fills the porous space in between. The schematic diagram of the considered problem is shown in Figure 7.1. The lower radially stretching surface has a constant temperature T_w and upper stretching sheet is kept at a temperature T_h. Moreover, it is assumed that the temperature of the

lower radially stretching surface is greater than the temperature of upper surface stretching in its plane in radial direction, i.e., $T_w > T_h$. The effects of viscous dissipation are also taken into account.

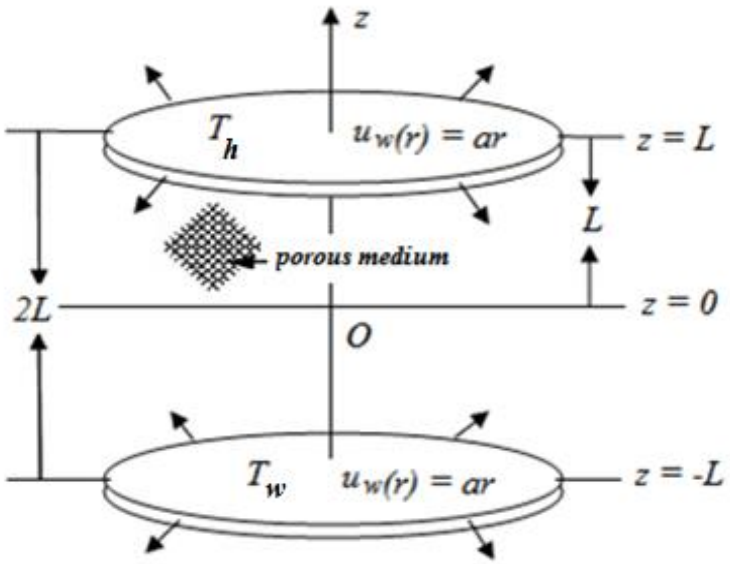

Figure 7.1: Geometrical configuration and coordinate system of the considered problem

With all these assumptions, the boundary layer equations for the flow and thermal fields in cylindrical coordinates can be written as follows

$$\frac{\partial u}{\partial r}+\frac{u}{r}+\frac{\partial w}{\partial z}=0, \tag{7.1}$$

$$u\frac{\partial u}{\partial r}+w\frac{\partial u}{\partial z}=-\frac{1}{\rho}\frac{\partial p}{\partial r}+\nu\left(\frac{\partial^2 u}{\partial r^2}+\frac{1}{r}\frac{\partial u}{\partial r}+\frac{\partial^2 u}{\partial z^2}-\frac{u}{r^2}\right)-\frac{\nu}{k'}u, \tag{7.2}$$

$$u\frac{\partial w}{\partial r}+w\frac{\partial w}{\partial z}=-\frac{1}{\rho}\frac{\partial p}{\partial z}+\nu\left(\frac{\partial^2 w}{\partial r^2}+\frac{1}{r}\frac{\partial w}{\partial r}+\frac{\partial^2 w}{\partial z^2}\right)-\frac{\nu}{k'}w, \tag{7.3}$$

$$u\frac{\partial T}{\partial r}+w\frac{\partial T}{\partial z}=\frac{k}{\rho c_p}\left(\frac{\partial^2 T}{\partial r^2}+\frac{1}{r}\frac{\partial T}{\partial r}+\frac{\partial^2 T}{\partial z^2}\right)$$
$$+\frac{\mu}{\rho c_p}\left(2\left(\frac{\partial u}{\partial r}\right)^2+2\frac{u^2}{r^2}+2\left(\frac{\partial w}{\partial z}\right)^2+\left(\frac{\partial w}{\partial r}\right)^2+\left(\frac{\partial u}{\partial z}\right)^2+2\frac{\partial u}{\partial z}\frac{\partial w}{\partial r}\right)+\frac{\mu}{\rho c_p k' T_1}u^2, \tag{7.4}$$

where (u,w) are the velocity components in (r,z) directions respectively and T denotes the temperature of the fluid. The corresponding boundary conditions are given as:

$$\left.\begin{aligned} &u=u_w(r)=ar, \quad w=0, \quad T=T_w \quad \text{at} \quad z=-L\\ &u=u_w(r)=ar, \quad w=0, \quad T=T_h \quad \text{at} \quad z=L. \end{aligned}\right\} \tag{7.5}$$

In order to convert the Eqs. (7.1-7.4) in dimensionless form, we define:

$$u=arf'(\eta), \quad w=-2aLf(\eta), \quad \theta(\eta)=\frac{T-T_h}{T_w-T_h}, \quad \eta=\frac{z}{L}. \tag{7.6}$$

Utilizing the following transformations, the Eq. (7.1) is satisfied identically and the Eqs. (7.2-7.5) after elimination of pressure reduce to:

$$f^{IV}+2\,\mathrm{Re}\,ff'''-K\,\mathrm{Re}\,f''=0, \tag{7.7}$$

$$\theta''+2\,\mathrm{Pr}\,\mathrm{Re}\,f\theta'+Br\left(\frac{12}{\delta^2}f'^2+f''^2\right)+K\,\mathrm{Re}\,Brf'^2=0. \tag{7.8}$$

The boundary conditions (7.5) after utilizing (7.6) take the form:

$$\left.\begin{aligned} &f'(-1)=1, \quad f(-1)=0, \quad f'(1)=1, \quad f(1)=0,\\ &\theta(-1)=0, \quad \theta(1)=1. \end{aligned}\right\} \tag{7.9}$$

Here $\mathrm{Re}=\frac{aL^2}{\nu}$ is the Reynolds number, $K=\frac{\nu}{k'a}$ is the permeability parameter, $\mathrm{Pr}=\frac{\mu c_p}{k}$ is the Prandtl number, $Ec=\frac{u_w^2}{c_p(T_h-T_w)}$ is the Eckert number, $\delta=\frac{r}{L}$ is the dimensionless parameter and $Br=\mathrm{Pr}\,Ec$ is the Brinkman number.

7.2.1.1 Significant physical quantities

The skin friction coefficient C_f at the upper radially stretching surface is defined as:

$$C_f = \frac{\tau_{rz}\big|_{z=L}}{\rho u_w^{\,2}} = \frac{\mu\left(\frac{\partial u}{\partial z} + \frac{\partial w}{\partial r}\right)\Big|_{z=L}}{\rho u_w^{\,2}}. \tag{7.10}$$

Using (7.6), the skin friction coefficient in non-dimensional form can be written as:

$$\mathrm{Re}_r\, C_f = f''(1). \tag{7.11}$$

Here $\mathrm{Re} = \frac{u_w r}{\nu}$ is the local Reynolds number.

The Nusselt number Nu at the upper radially stretching surface is given as:

$$Nu = \frac{L q_w}{k(T_h - T_w)} = -\frac{L\left(\frac{\partial T}{\partial z}\right)\Big|_{z=L}}{k(T_h - T_w)}. \tag{7.12}$$

By utilizing (7.6), the dimensionless form of Nu is:

$$Nu = -\theta'(1). \tag{7.13}$$

7.2.2 Entropy analysis

The local entropy generation rate per unit volume S_G defined in Eq. (2.45) in the presence of porous medium after using boundary layer approximation is given as:

$$\left.\begin{aligned} S_G &= \frac{k}{T_h^{\,2}}\left[\left(\frac{\partial T}{\partial r}\right)^2+\left(\frac{\partial T}{\partial z}\right)^2\right] \\ &+\frac{\mu}{T_h}\left[2\left(\frac{\partial u}{\partial r}\right)^2+2\frac{u^2}{r^2}+2\left(\frac{\partial w}{\partial z}\right)^2+\left(\frac{\partial w}{\partial r}\right)^2+\left(\frac{\partial u}{\partial z}\right)^2+2\frac{\partial u}{\partial z}\frac{\partial w}{\partial r}\right]+\frac{\mu}{k'T_h}u^2. \end{aligned}\right\} \tag{7.14}$$

Clearly, it is evident from (7.14) that the factors responsible for entropy generation are heat transfer and fluid friction. In terms of dimensionless variables, Eq. (7.14) after making use of (7.6) becomes:

$$Ns=\frac{S_G}{S_{Go}}=\theta'^2+\frac{12}{\delta^2}\frac{Br}{\Omega}f'^2+\frac{Br}{\Omega}f''^2+\mathrm{Re}\frac{Br}{\Omega}K f'^2, \tag{7.15}$$

where $S_{Go}=\dfrac{k\left(T_w-T_h\right)^2}{T_h^{\,2}L^2}$ is the characteristic entropy generation rate and $\Omega=\dfrac{\left(T_w-T_h\right)}{T_h}$ is the dimensionless temperature difference. Eq. (7.15) can be written in the form:

$$Ns=N_H+N_F, \tag{7.16}$$

where N_H represents the entropy generation due to heat transfer and N_F is the entropy generation due to fluid friction. The total entropy generation rate is given by integrating S_G over the domain $-L\le z\le L$, i.e.,

$$S_{tot}=\int_{-L}^{L}S_G dz. \tag{7.17}$$

The dimensionless form of total entropy generation rate is:

$$Ns_{tot} = \int_{-1}^{1} Ns \, d\eta = \int_{-1}^{1} \left[\theta'^2 + \frac{12}{\delta^2} \frac{Br}{\Omega} f'^2 + \frac{Br}{\Omega} f''^2 + \mathrm{Re} \frac{Br}{\Omega} K f'^2 \right] d\eta. \tag{7.18}$$

The Bejan number is defined as follows:

$$Be = \frac{N_H}{Ns}. \tag{7.19}$$

7.3 Solution procedure

The dimensionless nonlinear ordinary differential equations (7.7-7.8) representing the flow and heat transfer phenomena with the boundary conditions (7.9), are solved analytically by using Homotopy Analysis Method (HAM). By keeping in mind that the considered problem has bounded domain, the following set of base functions is taken:

$$\{\eta^{2n+1}, n \geq 0\}. \tag{7.20}$$

By using these base function, $f(\eta)$ and $\theta(\eta)$ can be expressed as:

$$f(\eta) = \sum_{n=0}^{\infty} a_n \eta^{2n+1}, \tag{7.21}$$

$$\theta(\eta) = \sum_{n=0}^{\infty} b_n \eta^{2n+1}, \tag{7.22}$$

where a_n and b_n are the coefficients.

The initial guesses for the considered problem are:

$$\left.\begin{aligned} f_0(\eta) &= \frac{1}{2}\left(\eta^3 - \eta\right), \\ \theta_0(\eta) &= \frac{1}{2}\left(1 + \eta\right). \end{aligned}\right\} \tag{7.23}$$

The linear operators are given as:

$$\left.\begin{aligned}\mathcal{L}_f(f)&=\frac{d^4 f}{d\eta^4},\\ \mathcal{L}_\theta(\theta)&=\frac{d^2\theta}{d\eta^2},\end{aligned}\right\} \tag{7.24}$$

with

$$\left.\begin{aligned}\mathcal{L}_f\left(C_1\eta^3+C_2\eta^2+C_3\eta+C_4\right)&=0,\\ \mathcal{L}_\theta\left(C_5\eta+C_6\right)&=0,\end{aligned}\right\} \tag{7.25}$$

where $C_i's,\ (i=1,2,...6)$ are the arbitrary constants.

The m-th order deformation equations are:

$$\mathcal{L}_f\left[f_m(\eta)-\chi_m f_{m-1}(\eta)\right]=\hbar_f\mathcal{R}_m^f(\eta), \tag{7.26}$$

$$\mathcal{L}_\theta\left[\theta_m(\eta)-\chi_m\theta_{m-1}(\eta)\right]=\hbar_\theta\mathcal{R}_m^\theta(\eta), \tag{7.27}$$

$$\left.\begin{aligned}f_m(0)=f'_m(0)=\theta_m(0)=0,\\ f_m(1)=0=f'_m(1)=\theta_m(1)=0.\end{aligned}\right\} \tag{7.28}$$

Here

$$\mathcal{R}_m^f(\eta)=\frac{\partial^4 f_{m-1}}{\partial\eta^4}+2\,\mathrm{Re}\sum_{k=0}^{m-1}f_{m-1-k}\frac{\partial^3 f_k}{\partial\eta^3}-K\,\mathrm{Re}\frac{\partial^2 f_{m-1}}{\partial\eta^2}, \tag{7.29}$$

$$\mathcal{R}_m^\theta(\eta)=\frac{\partial^2\theta_{m-1}}{\partial\eta^2}+2\,\mathrm{PrRe}\sum_{k=0}^{m-1}f_{m-1-k}\frac{\partial\theta_k}{\partial\eta}+B\mathrm{r}\sum_{k=0}^{m-1}\left[\frac{12}{\delta^2}\frac{\partial f_{m-1-k}}{\partial\eta}\frac{\partial f_k}{\partial\eta}+\frac{\partial^2 f_{m-1-k}}{\partial\eta^2}\frac{\partial^2 f_k}{\partial\eta^2}\right], \tag{7.30}$$

and

$$\chi_m = \begin{cases} 0, & m \le 1, \\ 1, & m > 1. \end{cases} \tag{7.31}$$

The final solutions in the form of infinite series can be written as:

$$f(\eta) = f_0(\eta) + \sum_{m=1}^{\infty} f_m(\eta), \tag{7.32}$$

$$\theta(\eta) = \theta_0(\eta) + \sum_{m=1}^{\infty} \theta_m(\eta), \tag{7.33}$$

where $f_m(\eta)$ and $\theta_m(\eta)$ are the solutions of mth-order deformation equations corresponding to velocity and temperature functions. The rest of the details of the methods are similar as defined in the previous chapters and are concealed for simplicity.

It is quite evident from (7.32-7.33) that the convergence of the series solutions $f(\eta)$ and $\theta(\eta)$ can be controlled with the help of unknown parameters $\hbar_f$ and $\hbar_\theta$ as they strongly depend on them. Figures 7.2 and 7.3 are drawn at the 15th order of approximation to show the $\hbar$ -curves which gives information about the region in which the series solutions (7.32-7.33) are convergent. It is found that the suitable ranges of $\hbar_f$ and $\hbar_\theta$ are $-0.4 \le h_f \le -1.35$ and $-0.7 \le h_\theta \le -1.25$. Also, Table 7.1 is constructed to show the convergence of the series solution in tabular form. It is noticed that the series solutions converge at the 12th order of approximation up to 6 decimal places.

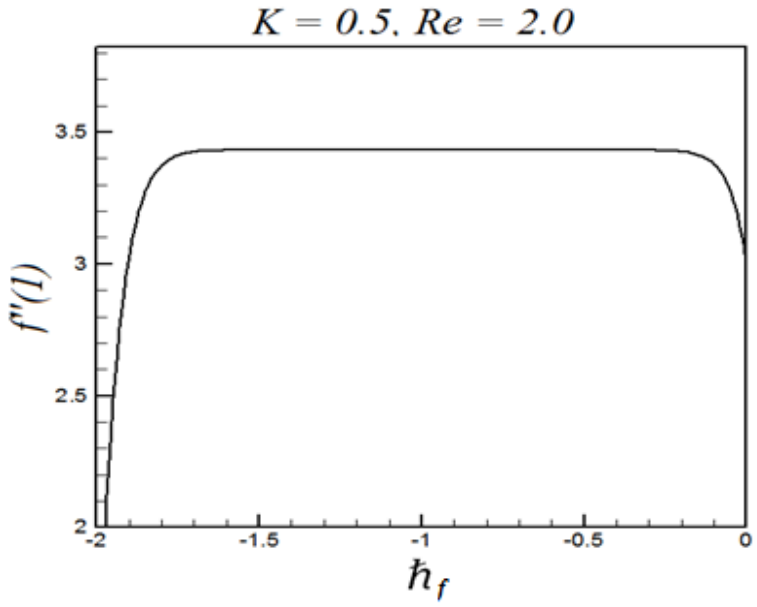

Figure 7.2: $\hbar_f$ -curve for $f''(1)$ at 15th order of approximation.

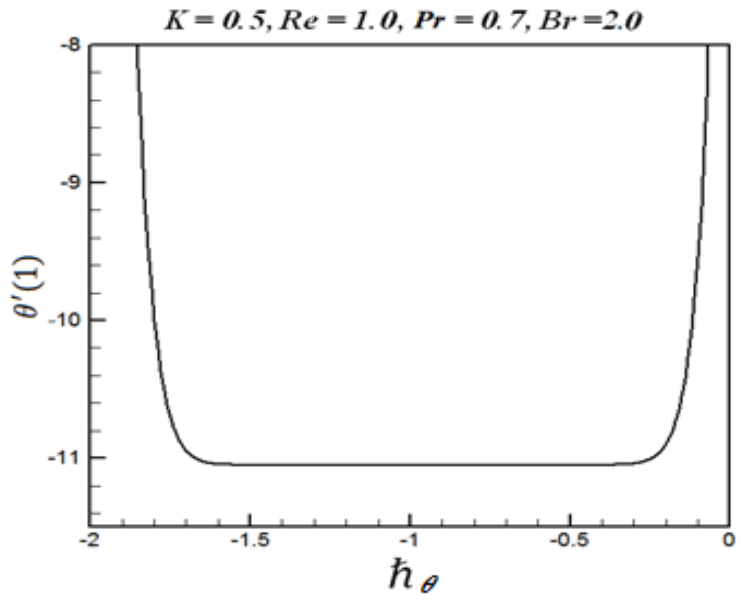

Figure 7.3: $\hbar_\theta$ -curve for $\theta'(1)$ at 15th order of approximation

Also, Table 7.1 is constructed in which the optimal values of $\hbar_f$ and $\hbar_\theta$ with their corresponding averaged squared residual errors $E_{m,f}$ and $E_{m,\theta}$ at different orders of approximations are presented. From the table, it is clear that there is a drop in the values of $E_{m,f}$ and $E_{m,\theta}$ with increase in the order of approximation m. Moreover, Table 7.2 is drawn to show the convergence of the series solutions by using the optimal values of $\hbar_f$ and $\hbar_\theta$ as given in Table 7.1 at the 15th order of approximation. It is noticed that the series solutions defined in (7.32-7.33) converge at the 12th order of approximation up to 6 decimal places.

Table 7.1: Optimal values of convergence control parameters $\hbar_f$ and $\hbar_\theta$ and the corresponding averaged squared residual errors $E_{m,f}$ and $E_{m,\theta}$ at different orders of approximations when $K = 0.5,\ \mathrm{Re} = 1.0,\ \mathrm{Pr} = 0.7,\ Br = 2.0$

Order of approximations m	$\hbar_f$	$\hbar_\theta$	$E_{m,f}$	$E_{m,\theta}$
3	-0.935468	−0.946291	7.14821×10^{-7}	3.63337×10^{-4}
6	−0.919992	−0.959699	7.81426×10^{-11}	6.89139×10^{-8}
9	−0.943521	−0.938200	3.20120×10^{-14}	2.69047×10^{-11}
12	−0.929500	−0.938570	1.24334×10^{-16}	3.27536×10^{-13}
15	−0.931201	−0.923101	7.80834×10^{-17}	1.92974×10^{-13}

Table 7.2: Convergence of HAM solutions for different order of approximations when

$K = 0.5,\ \mathrm{Re} = 1.0,\ \mathrm{Pr} = 0.7,\ Br = 2.0$ and $\hbar_f = -0.931201,\ \hbar_\theta = -0.923101$

Order of Convergence	$f''(1)$	$\theta'(1)$
3	3.215526	− 10.675398
6	3.215551	−10.683369
9	3.215551	−10.683374
12	3.215551	−10.683374
15	3.215551	−10.683374
18	3.215551	−10.683374
21	3.215551	−10.683374

The results obtained by Homotopy Analysis Method (HAM) are further validated by employing shooting technique with fourth-fifth order Runge-Kutta-Fehlberg method on system (7.7-7.9). For this, the boundary value problem is transformed into a set of initial value problem according to the procedure as mentioned in the previous chapters. The transformed system will contain some unknown initial values that are to be determined. By guessing these unknown, the set of initial value problem is integrated by employing a fourth-fifth order Runge-Kutta-Fehlberg method until the given boundary conditions are satisfied. The computations are carried out on symbolic software MATHEMATICA. A step size $\Delta\eta = 0.001$ and accuracy up to 6 decimal places is chosen as the criterion of convergence.

7.4 Results and discussion

In this section, our findings have been presented through graphs and tables and the effects of various physical parameters on radial and axial velocities, temperature profiles, skin friction coefficient, Nusselt number, the entropy generation number and Bejan number are analyzed and discussed.

The effect of permeability parameter K on radial velocity $f'(\eta)$ is presented in Figure 7.4. Due to stretching of sheets, a slight increase in magnitude of velocity $f'(\eta)$ is observed near both the stretching surfaces. However, in the center of the channel, an increase in the permeability parameter enhances the resistance by the porous medium that causes the magnitude of $f'(\eta)$ to decrease. Figure 7.5 depicts the effects of K on axial velocity $f(\eta)$. The magnitude of $f(\eta)$ decreases with increase in the permeability parameter.

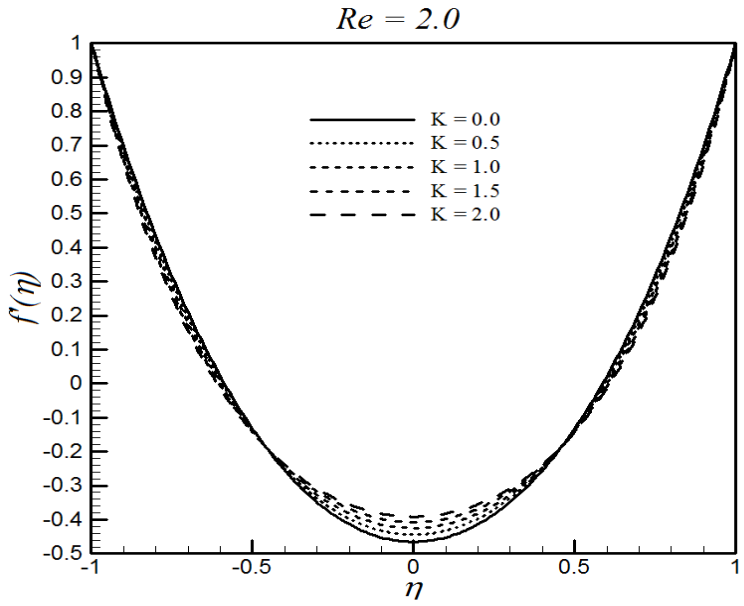

Figure 7.4: Effects of permeability parameter K on radial velocity $f'(\eta)$

The influence of Reynolds number Re on radial and axial velocities is shown in figures 7.6 and 7.7. Figure 7.6 depicts that the profiles of radial velocity are parabolic for all values of Re. Furthermore, it can be noticed that with an increase in the value of Re, the magnitude of $f'(\eta)$ increases near the stretching

surfaces and in the center of the channel, a decrease in magnitude of the velocity is detected. Figure 7.7 illustrates that the magnitude of axial velocity $f(\eta)$ decreases with increase in Reynolds number Re.

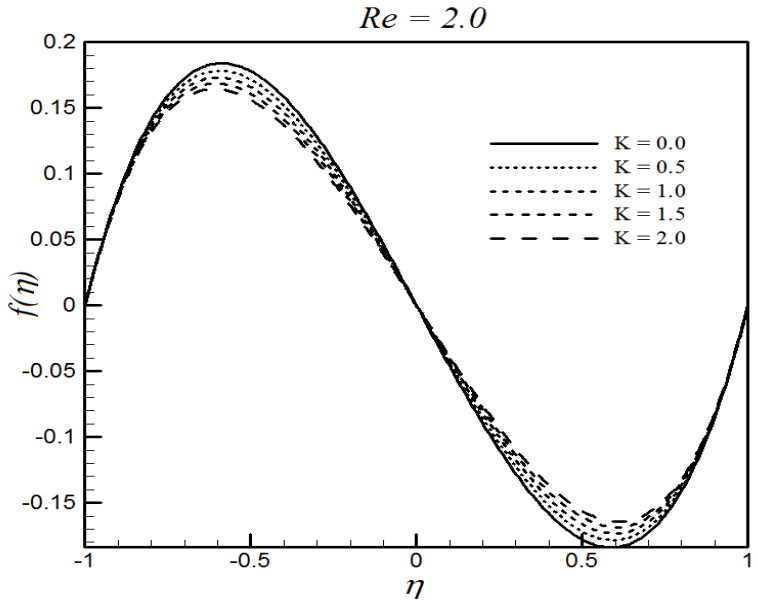

Figure 7.5: Effects of permeability parameter K on axial velocity $f(\eta)$

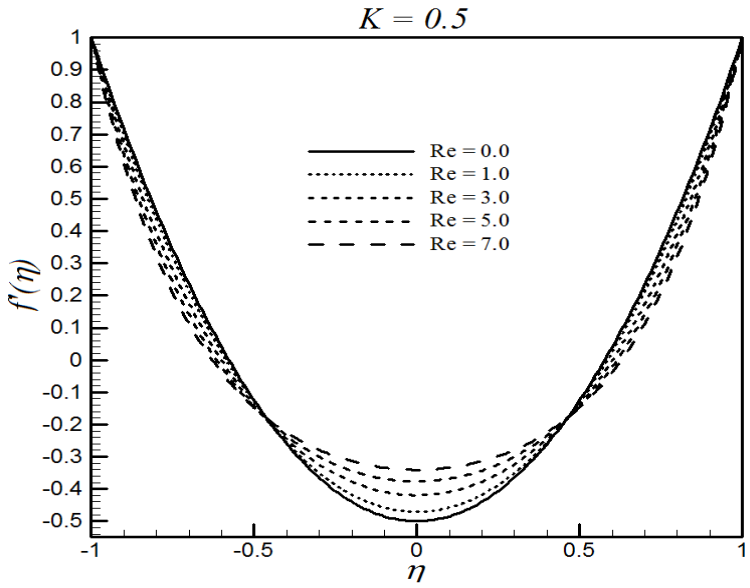

Figure 7.6: Effects of Reynolds number Re on radial velocity $f'(\eta)$

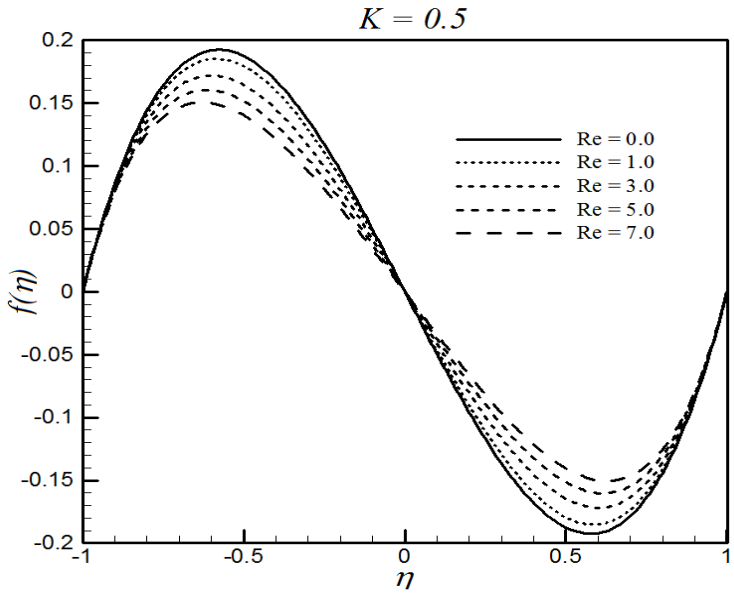

Figure 7.7: Effects of Reynolds number Re on axial velocity $f(\eta)$

Table 7.3 is drawn to see the influence of permeability parameter K and Reynolds number Re on skin friction coefficient $\mathrm{Re}_r C_f$. It is noticed that there is an increase in skin friction with increase in the values of K and Re.

Table 7.3: Numerical values of skin friction coefficient $\mathrm{Re}_r C_f$ for different values of permeability parameter K and Reynolds number Re

K	Re	$\mathrm{Re}_r C_f$ *HAM*	$\mathrm{Re}_r C_f$ *Numerical*
0.0	1.0	3.11728	3.11728
0.5		3.21555	3.21555
1.0		3.31107	3.31107
1.5		3.40403	3.40403
2.0		3.49457	3.49457
0.5	0.0	3.00000	3.00000
	1.0	3.21555	3.21555
	3.0	3.64719	3.64719
	5.0	4.06875	4.06875
	7.0	4.47356	4.47356

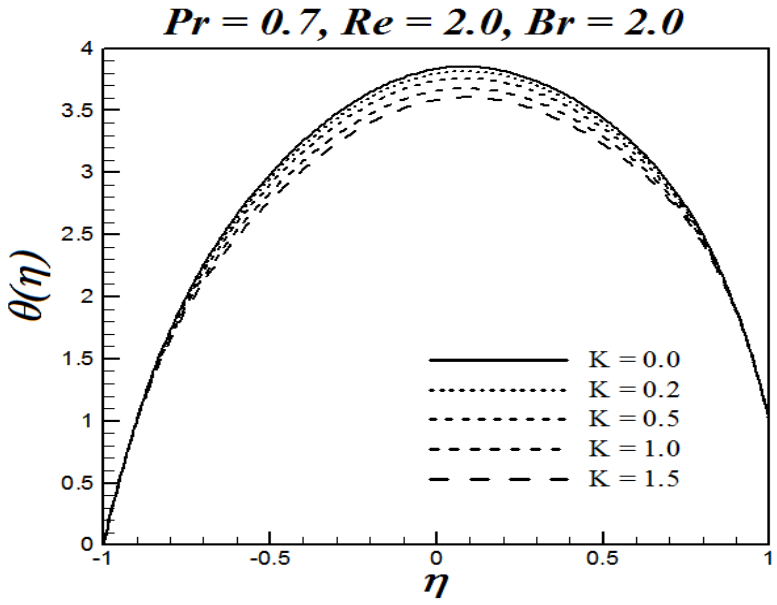

Figure 7.8: Effects of permeability parameter K on temperature profile $\theta(\eta)$

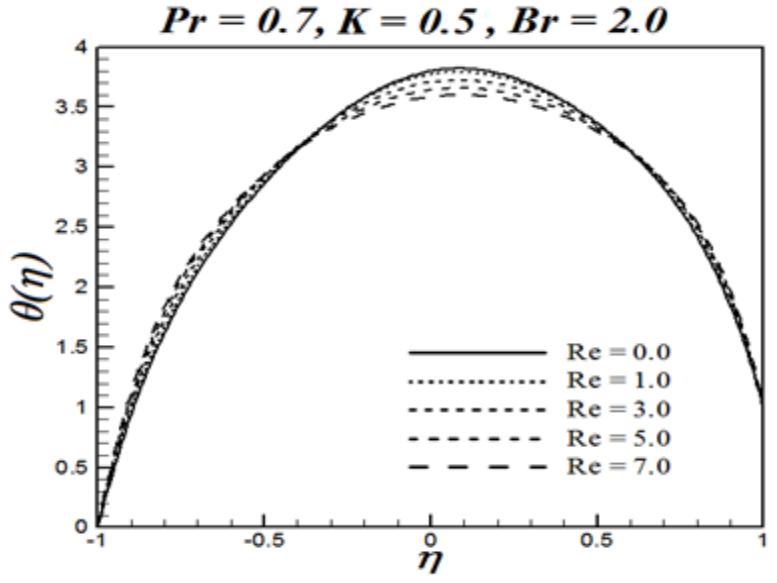

Figure 7.9: Effects of Reynolds number Re on temperature profile $\theta(\eta)$

The effects of physical parameters on dimensionless temperature $\theta(\eta)$ are presented in Figures 7.8-7.11. The temperature profile decreases with an increase in the permeability parameter K as shown in Figure 7.8. Figure 7.9 represents the influence of Reynolds number Re on temperature $\theta(\eta)$. An increase in temperature is noticed near the stretching surfaces and in the central region, the temperature decreases. The impact of Prandtl number Pr on temperature profiles is indicated in Figure 7.10. It is observed that the Prandtl number has increasing effects on $\theta(\eta)$. In Figure 7.11, the influence of Brinkman number Br on temperature profiles is depicted. The value $Br = 0$ corresponds to the case when viscous dissipation effects are not present and higher values of Br indicates the presence of viscous dissipation effects. It is observed that there is a rise in temperature with increase in the value of Brinkman number.

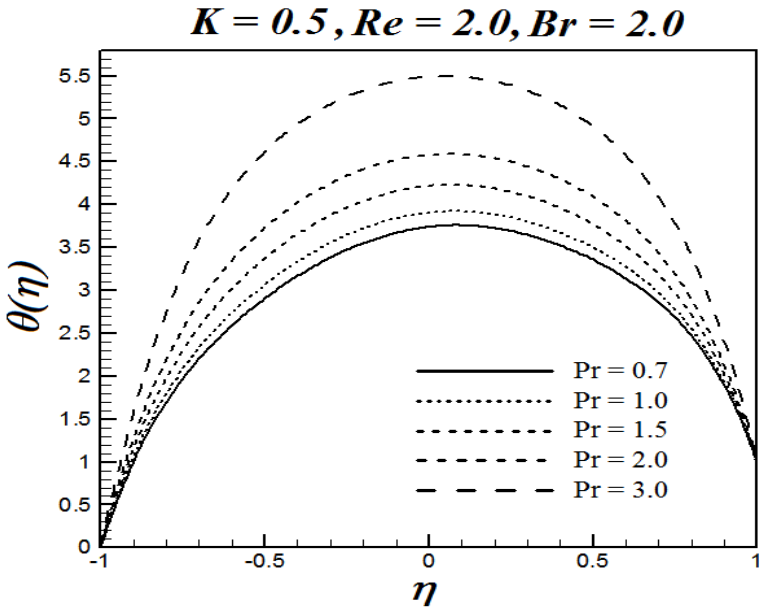

Figure 7.10: Effects of Prandtl number Pr on temperature profile $\theta(\eta)$

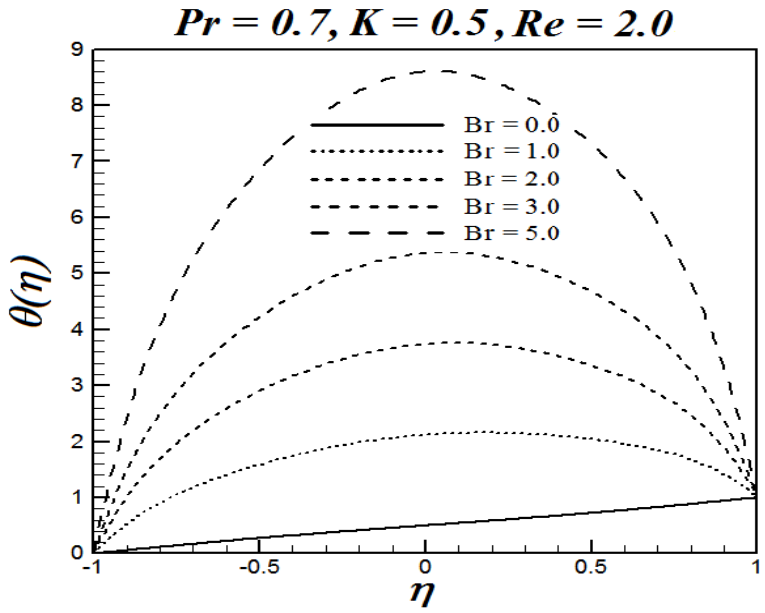

Figure 7.11: Effects of Brinkman number Br on temperature profile $\theta(\eta)$

Table 7.4 shows the numerical values of Nusselt number Nu for different values of permeability parameter K, Reynolds number Re, Prandtl number Pr and Brinkman number Br. Nusselt number Nu is a measure of heat transfer from the stretching surface to the fluid. The permeability parameter K has declining effect on heat transfer rate whereas the Reynolds number Re, the Prandtl number Pr and the Brinkman number Br enhance the heat transfer rate.

Figures 7.12-7.14 are plotted to see the impact of permeability parameter K, Reynolds number Re and group parameter Br/Ω on local entropy generation number Ns. Figure 7.12 illustrates the influence of permeability parameter K on Ns. The radially stretching surfaces act as a strong source of entropy generation. This is because friction between the fluid and stretching sheets and heat transfer rate is high at the surfaces. At the center and in the nearby region, the entropy effects are negligible. Moreover, it is detected that with an increase in the value of K, the heat transfer rate through the surfaces becomes less which causes the local entropy generation number Ns to decrease.

Table 7.4: Numerical values of Nusselt number Nu for different values of permeability parameter K, Reynolds number Re, Prandtl number Pr and Brinkman number Br

K	Re	Pr	Br	$-Nu$ *HAM*	$-Nu$ *Numerical*
0.0	1.0	0.7	2.0	10.62738	10.62738
0.5				10.68337	10.68337
1.0				10.74300	10.74300
1.5				10.80576	10.80576
2.0				10.87126	10.87126
0.5	0.0	0.7	2.0	10.30000	10.30000
	1.0			10.68337	10.68337
	3.0			11.39915	11.39915
	5.0			12.06513	12.06513
	7.0			12.69839	12.69839
0.5	1.0	0.7	2.0	10.68337	10.68337
		1.0		10.91124	10.91124
		1.5		11.31973	11.31973
		2.0		11.76754	11.76754
		3.0		12.79924	12.79924
0.5	1.0	0.7	0.5	2.26112	2.26112
			1.0	5.06854	5.06854
			2.0	10.68337	10.68337
			3.0	16.29821	16.29821
			5.0	27.52788	27.52788

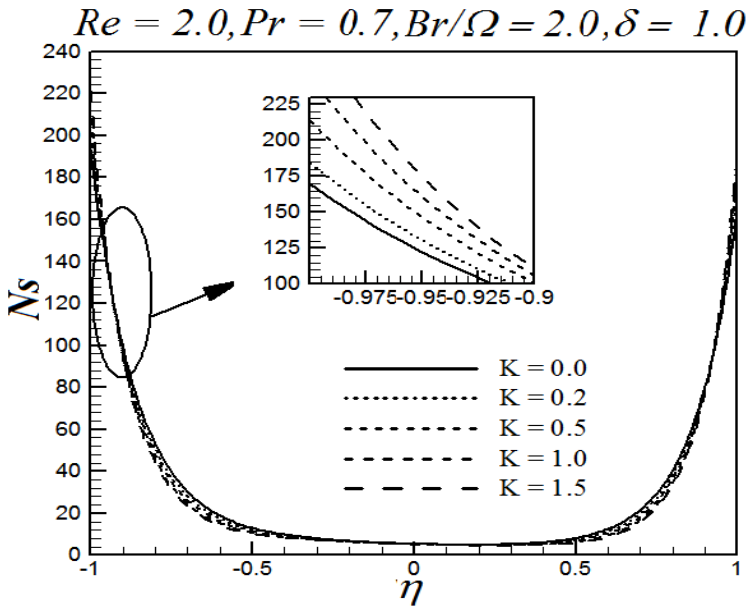

Figure 7.12: Effects of permeability parameter K on local entropy generation number Ns

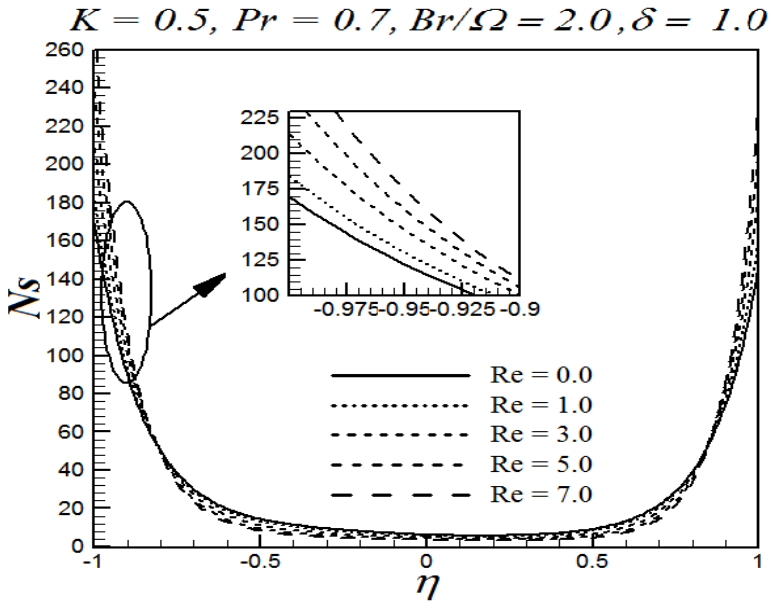

Figure 7.13: Effects of Reynolds number Re on local entropy generation number Ns

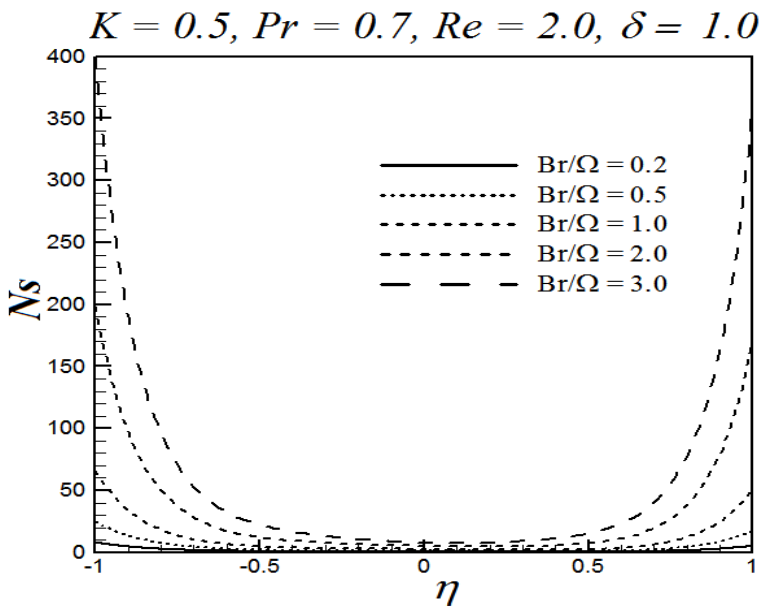

Figure 7.14: Effects of group parameter Br/Ω on local entropy generation number Ns

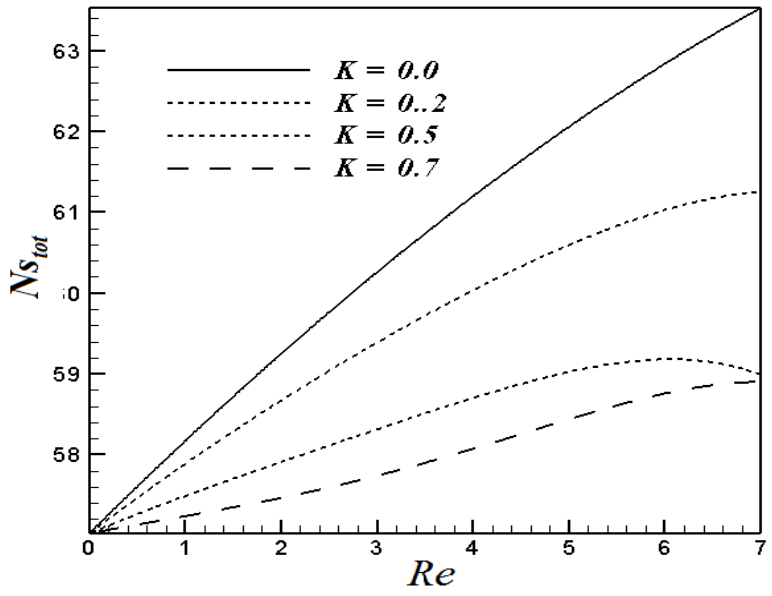

Figure 7.15: Effects of permeability parameter K on total entropy generation number Ns_{tot} plotted against Reynolds number Re

The total entropy generation number Ns_{tot} is plotted against Reynolds number Re for different values of permeability parameter K and group parameter Br/Ω in Figures 7.15 and 7.16. It is quite obvious from the Figure 7.15 that the total entropy generation number Ns_{tot} increases with increase in Reynolds number Re. Moreover, there is a decrease in total entropy production with an increase in permeability parameter. Figure 7.16 depicts that increase in group parameter Br/Ω results in increase in Ns_{tot}. However, for a particular value of Br/Ω, the effects of Reynolds number Re on Ns_{tot} are almost constant.

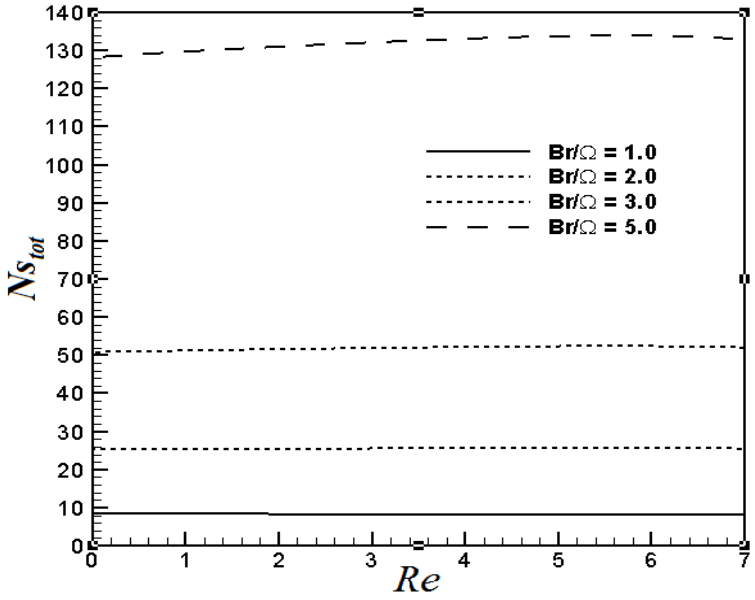

Figure 7.16: Effects of group parameter Br/Ω on total entropy generation number Ns_{tot} plotted against Reynolds number Re

Bejan number is plotted in Figures 7.17-7.19 which gives an idea whether heat transfer entropy effects dominate over fluid friction entropy effects or vice versa. Figure 7.17 shows the behavior of Bejan number for different values of permeability parameter K. It is noticed that the heat transfer entropy effects are prominent at both the radially stretching surfaces and near the center, the fluid friction entropy effects are dominant. Moreover, Bejan number Be decreases with increase in the values of K. Figure 7.18 illustrates

that the effects of Reynolds number Re on Be are similar as that of permeability parameter K, i.e. Bejan number decreases as the value of Reynolds number increases.

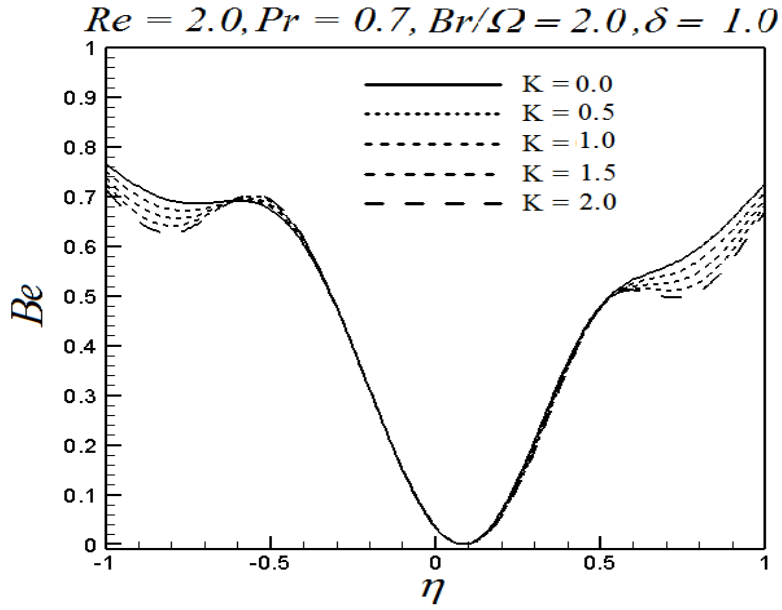

Figure 7.17: Effects of permeability parameter K on Bejan number Be

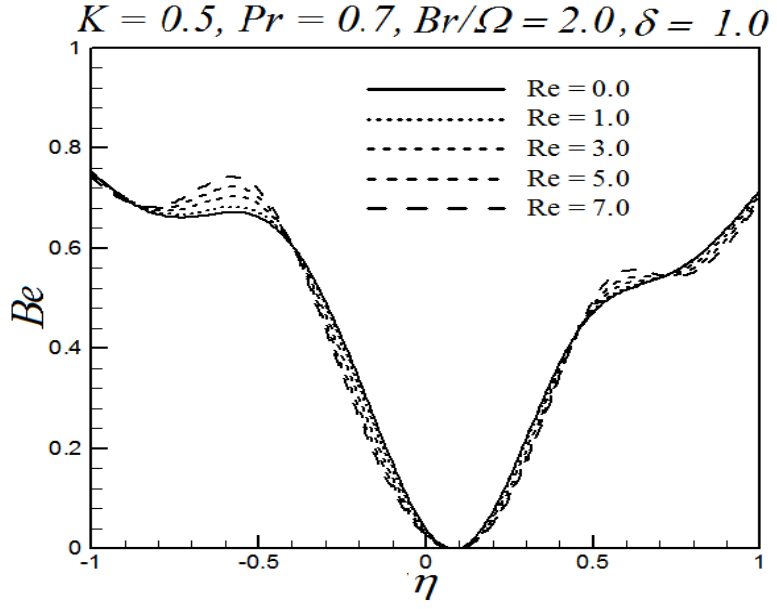

Figure 7.18: Effects of Reynolds number Re on Bejan number Be

The influence of group parameter Br/Ω on Bejan number is shown in Figure 7.19. With an increase in the value of group parameter Br/Ω, the heat transfer entropy effects become dominant at both the

stretching surfaces and entropy effects due to fluid friction are strong in the vicinity of upper stretching surface. Furthermore, for large values of Br/Ω the fluid friction entropy effects are dominant near the center of both radially stretching surfaces.

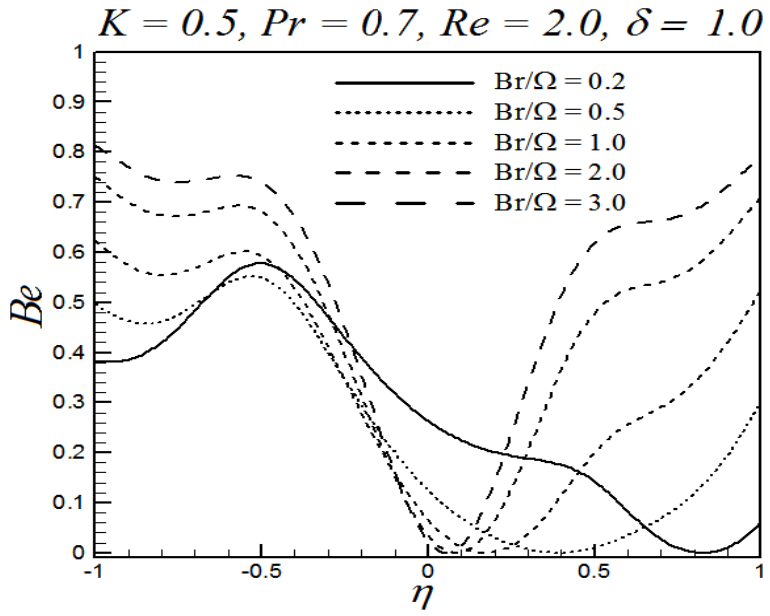

Figure 7.19: Effects of group parameter Br/Ω on Bejan number Be

7.5 Concluding remarks

The chapter examines the entropy effects in viscous fluid flow through a porous medium bounded by two radially stretching surfaces. It is noticed that the radial velocity profiles $f'(\eta)$ are parabolic in nature generally. Furthermore, increase in permeability parameter K and Reynolds number Re increase the magnitude of velocity near the radially stretching surfaces and in the center, an opposite behavior is observed. The magnitude of axial velocity $f(\eta)$ decreases with increase in the values of permeability parameter K and Reynolds number Re. In addition to that, increasing the value of permeability parameter K and Reynolds number Re results in a drop in the fluid temperature. As far as the entropy effects are concerned, it is seen that the entropy generation number that quantifies the entropy production is high at both the radially stretching surfaces and is zero at the center and in the nearby region. Also, increase in

permeability parameter K causes the entropy number number Ns to decrease. In case of Reynolds number Re, the entropy generation number increases with increase in Reynolds number Re near the radially stretching surfaces and in the central region, a decreasing effect is noticed. The total entropy generation number Ns_{tot} increases with increase in Reynolds number and group parameter Br/Ω and decrease with increase in permeability parameter. It is also noteworthy that heat transfer entropy effects are dominant near the radially stretching surfaces and fluid friction entropy effects are prominent near the central region.

Chapter 8

Entropy generation in unsteady squeezing flow in a rotating channel with lower stretching permeable wall

8.1 Introduction

This chapter aims to examine the entropy effects due to the flow of a viscous fluid in a rotating channel having a lower porous wall which is stretching in its own plane and upper wall squeezing downwards. The considered problem is modeled by using Navier-Stokes equations and similarity solutions are obtained by using analytical and numerical methods. The effects of various physical parameters on flow and heat transfer characteristics as well as on entropy production are displayed through tables and graphs and the results are discussed in detail.

8.2 Mathematical modeling

8.2.2 Flow phenomenon

Assume a three dimensional rotating flow of an incompressible viscous fluid in a parallel plate channel. The lower wall is placed at $y = 0$ and is stretching along the x-direction with a velocity $U_w = \frac{ax}{1-ct}$. The upper wall of the channel is situated at a distance $h(t) = \sqrt{\frac{\nu(1-ct)}{a}}$ and is squeezing downwards with a time dependent velocity $V_h = \frac{dh}{dt}$. Further, it is considered that there is a suction of fluid from the lower wall of

the channel with a velocity $\frac{-V_0}{1-ct}$. The walls of the channel and the fluid confined between them are rotating about the y-axis with an angular velocity $\boldsymbol{\omega} = \frac{\omega_0}{1-ct}$ as shown in Figure 8.1. Here c is the parameter having dimensions of $(time)^{-1}$ and $ct < 1$. Then by using Eq. (2.5) and applying boundary layer approximation, the governing equations are given as:

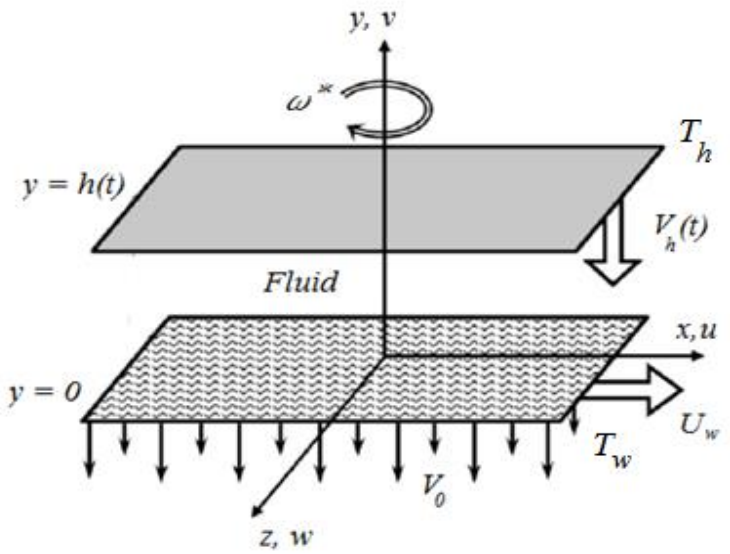

Figure 8.1: Geometrical configuration and coordinate system

$$\frac{\partial u}{\partial x} + \frac{\partial v}{\partial y} = 0, \tag{8.1}$$

$$\frac{\partial u}{\partial t} + u\frac{\partial u}{\partial x} + v\frac{\partial u}{\partial y} + 2\frac{\omega_0}{1-ct}w = -\frac{1}{\rho}\frac{\partial P}{\partial x} + \nu\left(\frac{\partial^2 u}{\partial x^2} + \frac{\partial^2 u}{\partial y^2}\right), \tag{8.2}$$

$$\frac{\partial v}{\partial t} + u\frac{\partial v}{\partial x} + v\frac{\partial v}{\partial y} = -\frac{1}{\rho}\frac{\partial P}{\partial y} + \nu\left(\frac{\partial^2 v}{\partial x^2} + \frac{\partial^2 v}{\partial y^2}\right), \tag{8.3}$$

$$\frac{\partial w}{\partial t} + u\frac{\partial w}{\partial x} + v\frac{\partial w}{\partial y} - 2\frac{\omega_0}{1-ct}u = \nu\left(\frac{\partial^2 w}{\partial x^2} + \frac{\partial^2 w}{\partial y^2}\right), \tag{8.4}$$

subject to the boundary conditions:

$$\left.\begin{aligned} &u(x,y,t)=U_w=\frac{ax}{1-ct},\ v(x,y,t)=\frac{-V_0}{1-ct},\ w(x,y,t)=0, \qquad \text{at } y=0,\\ &u(x,y,t)=0,\ v(x,y,t)=V_h=-\frac{c}{2}\sqrt{\frac{\nu}{a(1-ct)}},\ w(x,y,t)=0,\ \text{at } y=h(t). \end{aligned}\right\} \tag{8.5}$$

Here $a>0$ is the constant representing the stretching rate of the lower wall of the channel and (u,v,w) are the components of velocities in (x,y,z) directions.

In order to convert the Eqs. (8.1-8.4) with boundary conditions (8.5) in non-dimensional form, following similarity variables are taken:

$$\eta=\frac{y}{h(t)},\ u=U_w f'(\eta),\ v=-\sqrt{\frac{a\nu}{1-ct}}f(\eta),\ w=U_w g(\eta). \tag{8.6}$$

By utilizing (8.6) in Eqs. (8.1-8.5), the continuity equation is satisfied identically and the Eqs. (8.2-8.4) after elimination of pressure take the shape:

$$f^{IV}-f'f''+ff'''-\frac{S_q}{2}(3f''+\eta f''')-2\omega g'=0, \tag{8.7}$$

$$g''+fg'-f'g-S_q\left(g+\frac{\eta}{2}g'\right)+2\omega f'=0, \tag{8.8}$$

and the boundary conditions (8.5) in dimensionless form are:

$$\left.\begin{aligned} &f(0)=w_0,\ f'(0)=1,\ g(0)=0,\\ &f(1)=\frac{S_q}{2},\ f'(1)=0,\ g(1)=0. \end{aligned}\right\} \tag{8.9}$$

Here $\omega=\frac{\omega_0}{a}$ is the rotation parameter, $w_0=\frac{V_0}{ah}$ is the suction parameter and $S_q=\frac{c}{a}$ is the squeezing parameter. It is important to note that when $S_q>0$, the upper plate is moving in a downward direction with a velocity $V_h<0$ which creates a squeezing effect on fluid. When $S_q<0$, the upper plate moves

away from the lower plate at $y = 0$. When $S_q = 0$, we arrive at the case where upper plate is stationary and there is no squeezing effect or there is a steady state.

8.2.2 Heat transfer phenomenon

In order to analyze the heat transfer phenomenon, it is supposed that the lower stretching wall of the channel has the temperature T_w and the upper squeezing wall has temperature T_h such that $T_w > T_h$. Also the viscous dissipation effects are also considered in the considered problem. Then the energy equation is given by:

$$\frac{\partial T}{\partial t} + u\frac{\partial T}{\partial x} + v\frac{\partial T}{\partial y} = \frac{k}{\rho c_p}\left(\frac{\partial^2 T}{\partial y^2} + \frac{\partial^2 T}{\partial y^2}\right) + \frac{\mu}{\rho c_p}\left[4\left(\frac{\partial u}{\partial x}\right)^2 + \left(\frac{\partial u}{\partial y} + \frac{\partial v}{\partial x}\right)^2 + \left(\frac{\partial w}{\partial x}\right)^2 + \left(\frac{\partial w}{\partial y}\right)^2\right]. \quad (8.10)$$

The boundary conditions corresponding to Eq. (8.10) are:

$$T(x, y, t) = T_w \quad at \quad y = 0 \quad \text{and } T(x, y, t) = T_h \quad at \quad y = h. \quad (8.11)$$

To non-dimensionlize Eq. (8.10), following similarity transformed is considered

$$\theta(\eta) = \frac{T - T_h}{T_w - T_h}. \quad (8.12)$$

By using (8.6) and (8.12), the dimensionless form of Eq. (8.10) is

$$\theta'' + \Pr f\theta' - \Pr\frac{S_q}{2}\eta\theta' + Pr\left[Ec\left(4f'^2 + g^2\right) + Ec_x\left(f''^2 + g'^2\right)\right] = 0, \quad (8.13)$$

and the boundary conditions take the form:

$$\left.\begin{aligned}\theta = 1 \quad at \quad \eta = 0\\ \theta = 0 \quad at \quad \eta = 1.\end{aligned}\right\} \quad (8.14)$$

The Nusselt number at the lower wall is

$$Nu_x = \frac{q_w x}{k(T_w - T_h)}, \quad (8.15)$$

where the heat transfer rate is

$$q_w = -k\left(\frac{\partial T}{\partial y}\right)_{y=0}, \tag{8.16}$$

The dimensionless form of (8.15) using (8.12) is

$$Nu_x = -\frac{x}{h(\mathrm{t})}\theta'(0). \tag{8.17}$$

8.2.3 Entropy formulation

The local entropy generation rate for a viscous incompressible fluid after the application of boundary layer approximation is defined by:

$$S_G = \frac{k}{T_h^2}\left[\left(\frac{\partial T}{\partial x}\right)^2 + \left(\frac{\partial T}{\partial y}\right)^2\right] + \frac{\mu}{T_h}\left[4\left(\frac{\partial u}{\partial x}\right)^2 + \left(\frac{\partial u}{\partial y} + \frac{\partial v}{\partial x}\right)^2 + \left(\frac{\partial w}{\partial x}\right)^2 + \left(\frac{\partial w}{\partial y}\right)^2\right]. \tag{8.18}$$

From (8.18), it can be seen that the first two terms represent the entropy generation due to heat transfer and the other four terms represent the entropy effects due to fluid friction.

By utilizing (8.6) and (8.12), the non-dimensional form of local entropy generation rate is given as:

$$Ns = \frac{S_G}{S_{Go}} = \theta'^2 + \frac{\mathrm{Pr}}{\Omega}\left[Ec\left(4f'^2 + g^2\right) + Ec_x\left(f''^2 + g'^2\right)\right], \tag{8.19}$$

where $S_{Go} = \dfrac{k\left(T_w - T_h\right)^2}{T_h{}^2 h^2}$ denotes the characteristic entropy generation rate and $\Omega = \dfrac{\left(T_w - T_h\right)}{T_h}$ is the dimensionless temperature difference. The dimensionless form of entropy generation number Ns can be expressed as:

$$Ns = N_H + N_F. \tag{8.20}$$

The total entropy generation rate is given

$$S_{tot} = \int_0^h S_G dy. \tag{8.21}$$

In normalized form, the total entropy generation rate is obtained by integrating Ns over the region $0 \le \eta \le 1$, i.e.,

$$Ns_{tot} = \int_0^1 Ns \, d\eta = \int_0^1 \left[\theta'^2 + \frac{\Pr}{\Omega} \left[Ec\left(4 f'^2 + g^2\right) + Ec_x \left(f''^2 + g'^2 \right) \right] \right] d\eta. \tag{8.22}$$

The Bejan number is defined as:

$$Be = \frac{N_H}{Ns}. \tag{8.23}$$

8.3 Solution of the problem

8.3.1 Analytical solution

The HAM procedure is employed to evaluate the solution of Eqs. (8.7-8.8) having boundary conditions (8.9) and the Eq. (8.13) together with boundary condition (8.14). The initial guesses and linear operators chosen by keeping in mind the nature of the considered problem are:

$$\left.\begin{aligned} f_0(\eta) &= \eta - 2\eta^2 + \eta^3 + w_0(1 - 3\eta^2 + 2\eta^3) + S_q\left(\frac{3}{2} - \eta\right)\eta^2, \\ g_0(\eta) &= 0, \\ \theta_0(\eta) &= 1 - \eta. \end{aligned}\right\} \tag{8.24}$$

$$\left.\begin{aligned} \mathcal{L}_f(f) &= \frac{d^4 f}{d\eta^4}, \\ \mathcal{L}_g(g) &= \frac{d^2 g}{d\eta^2}, \\ \mathcal{L}_\theta(\theta) &= \frac{d^2 \theta}{d\eta^2}. \end{aligned}\right\} \tag{8.25}$$

The m-th order deformation equations are:

$$\mathcal{L}_f\left[f_m(\eta)-\chi_m f_{m-1}(\eta)\right]=\hbar_f\mathcal{R}_m^f(\eta), \tag{8.26}$$

$$\mathcal{L}_g\left[g_m(\eta)-\chi_m g_{m-1}(\eta)\right]=\hbar_g\mathcal{R}_m^g(\eta), \tag{8.27}$$

$$\mathcal{L}_\theta\left[\theta_m(\eta)-\chi_m \theta_{m-1}(\eta)\right]=\hbar_\theta\mathcal{R}_m^\theta(\eta), \tag{8.28}$$

$$\left.\begin{aligned} f_m(0)=f'_m(0)=\ g_m(0)=\theta_m(0)=0,\\ f_m(1)=0=f'_m(1)=\ g_m(1)=\theta_m(1)=0. \end{aligned}\right\} \tag{8.29}$$

where

$$\mathcal{R}_m^f(\eta)=\frac{\partial^4 f_{m-1}}{\partial\eta^4}-\sum_{k=0}^{m-1}\left(\frac{\partial f_{m-1-k}}{\partial\eta}\frac{\partial^2 f_k}{\partial\eta^2}-f_{m-1-k}\frac{\partial^3 f_k}{\partial\eta^3}\right)-\frac{S_q}{2}\left(3\frac{\partial^2 f_{m-1}}{\partial\eta^2}+\eta\frac{\partial^3 f_{m-1}}{\partial\eta^3}\right)-2\omega\frac{\partial g_{m-1}}{\partial\eta}, \tag{8.30}$$

$$\mathcal{R}_m^g(\eta)=\frac{\partial^2 g_{m-1}}{\partial\eta^2}-\sum_{k=0}^{m-1}\left(\frac{\partial f_{m-1-k}}{\partial\eta}g_k-f_{m-1-k}\frac{\partial g_k}{\partial\eta}\right)-S_q\left(g_{m-1}+\frac{\eta}{2}\frac{\partial g_{m-1}}{\partial\eta}\right)+2\omega\frac{\partial f_{m-1}}{\partial\eta}, \tag{8.31}$$

$$\left.\begin{aligned} \mathcal{R}_m^\theta(\eta)=\frac{\partial^2\theta_{m-1}}{\partial\eta^2}+\Pr\sum_{k=0}^{m-1}f_{m-1-k}\frac{\partial\theta_k}{\partial\eta}-\Pr\frac{S_q}{2}\eta\frac{\partial\theta_{m-1}}{\partial\eta}\\ +\Pr\sum_{k=0}^{m-1}\left[Ec\left(4\frac{\partial f_{m-1-k}}{\partial\eta}\frac{\partial f_k}{\partial\eta}+g_{m-1-k}g_k\right)+Ec_x\left(\frac{\partial^2 f_{m-1-k}}{\partial\eta^2}\frac{\partial^2 f_k}{\partial\eta^2}+\frac{\partial g_{m-1-k}}{\partial\eta}\frac{\partial g_k}{\partial\eta}\right)\right], \end{aligned}\right\} \tag{8.32}$$

Thus, the final solution are given in the form of infinite series are given as:

$$f(\eta)=f_0(\eta)\ +\sum_{m=1}^{\infty}f_m(\eta), \tag{8.33}$$

$$\mathrm{g}(\eta)=g_0(\eta)+\sum_{m=1}^{\infty}g_m(\eta), \tag{8.34}$$

$$\theta(\eta)=\theta_0(\eta)\ +\sum_{m=1}^{\infty}\theta_m(\eta). \tag{8.35}$$

where $f_m(\eta)$, $g_m(\eta)$, $\theta_m(\eta)$ are the solution functions obtained from the mth-order Eqs. (8.26-8.28) which are solved in the order $m = 1, 2, 3...$ by using the symbolic software MATHEMATICA.

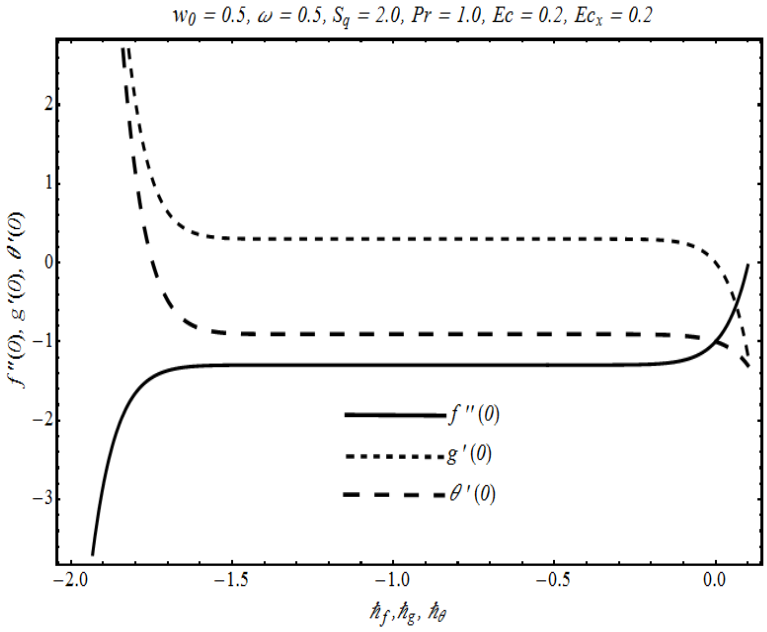

Figure 8.2: $\hbar-curves$ for 15th order of approximation

In order to make sure that the series (8.33-8.35) obtained by HAM are the approximate solutions of the considered problem, it is important to prove their convergence. The series solutions $f(\eta)$, $g(\eta)$ and $\theta(\eta)$ has strong dependence on the auxiliary parameters $\hbar_f$, $\hbar_g$ and $\hbar_\theta$ and a rough estimate of the convergence region can be obtained by plotting the so-called $\hbar$-curves. From Figure 8.2, it is seen that the admissible regions of $\hbar_f$, $\hbar_g$ and $\hbar_\theta$ are $-0.2 \le h_f \le -1.5$, $-0.3 \le h_g \le -1.3$ and $-0.7 \le h_\theta \le -1.25$.

Table 8.1 displays the optimal values of $\hbar_f$, $\hbar_g$ and $\hbar_\theta$ and the corresponding averaged squared residual errors $E_{m,f}$, $E_{m,g}$ and $E_{m,\theta}$ as defined in (5.43-5.45) at different orders of approximations m. A

considerable decrease in the values of $E_{m,f}$, $E_{m,g}$ and $E_{m,\theta}$ is seen as the order of approximation increases which shows that the values of $\hbar_f$, $\hbar_g$ and $\hbar_\theta$ are well chosen.

Table 8.1: Numerical optimal values of auxiliary parameters $\hbar_f$, $\hbar_g$ and $\hbar_\theta$ and the corresponding averaged squared residual errors $E_{m,f}$, $E_{m,g}$ and $E_{m,\theta}$ at different orders of approximations when

$$S_q = 2.0,\ w_0 = 0.5,\ \omega = 0.5,\ \mathrm{Pr} = 1.0,\ Ec_x = 0.2,\ Ec = 0.2$$

Order of approximations m	$\hbar_f$	$\hbar_g$	$\hbar_\theta$	$E_{m,f}$	$E_{m,g}$	$E_{m,\theta}$
3	-0.959559	-0.844437	-0.840864	6.74554×10^{-7}	1.13652×10^{-5}	2.48902×10^{-5}
6	-0.901444	-0.872493	-0.894657	7.96866×10^{-10}	8.05443×10^{-9}	1.24958×10^{-8}
9	-0.901341	-0.881210	-0.894367	5.52680×10^{-13}	2.42042×10^{-12}	1.71064×10^{-10}
12	-0.902321	-0.889100	-0.899430	1.84524×10^{-16}	2.83921×10^{-15}	9.95077×10^{-14}
15	-0.900141	-0.88459	-0.89332	1.68792×10^{-16}	3.37603×10^{-16}	2.23706×10^{-15}

Table 8.2: Convergence of HAM solutions for different order of approximations when

$$S_q = 2.0,\ w_0 = 0.5,\ \omega = 0.5,\ \mathrm{Pr} = 1.0,\ Ec_x = 0.2,\ Ec = 0.2$$

Order of approximations m	$f''(0)$	$g'(0)$	$\theta'(0)$
3	-1.296804	0.300143	-0.906701
6	-1.297045	0.3003125	-0.906246
9	-1.297045	0.3003129	-0.906244
12	-1.297045	0.3003129	-0.906244
15	-1.297045	0.3003129	-0.906244
18	-1.297045	0.3003129	-0.906244

The numerical values of $f''(0)$, $g'(0)$ and $\theta'(0)$ at different orders of approximations are presented in Table 8.2 while utilizing the optimal values of $\hbar_f, \hbar_g$ and $\hbar_\theta$. It is quite clear that the use of optimal values $\hbar_f, \hbar_g$ and $\hbar_\theta$ increases the convergence rate rather than randomly choosing them from the convergence region in the $\hbar$ -curves.

8.3.2 Numerical solution

The system of non-linear differential equations (8.7-8.8) having boundary conditions (8.9) and the Eq. (8.13) together with boundary condition (8.14) are also solved numerically by using shooting technique with fourth-fifth order Runge-Kutta-Fehlberg method by fixing the values of all other physical parameters in the considered problem. The procedure defined in the previous chapters is employed to convert the boundary value problem into a system of the initial value problem and the system is solved. The step size is taken $\Delta\eta = 0.001$ and the convergence criterion is selected as 10^{-6}.

8.4 Results and discussion

This section of the chapter discusses the effects of pertinent parameters involving in the considered problem on the velocity and temperature profiles, shear stresses, heat transfer rate and entropy generation effects. Figure 8.3 presents the effects of squeezing parameter S_q on velocity component $f'(\eta)$. As the value of S_q increases, there is an increase in the velocity $f'(\eta)$. Moreover, for the negative values of squeezing parameter, flow reversal is observed which depreciates with increase in S_q.

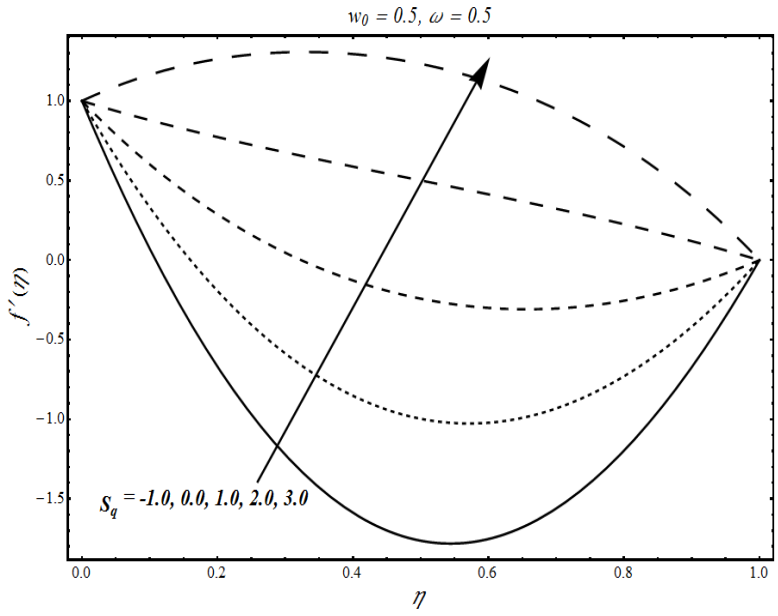

Figure 8.3: Influence of squeezing parameter S_q on velocity profile $f'(\eta)$

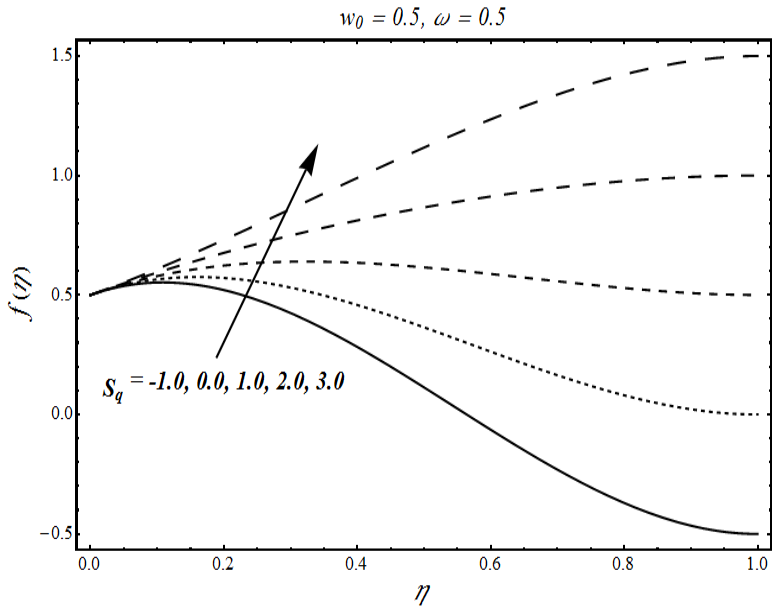

Figure 8.4: Influence of squeezing parameter S_q on velocity profile $f(\eta)$

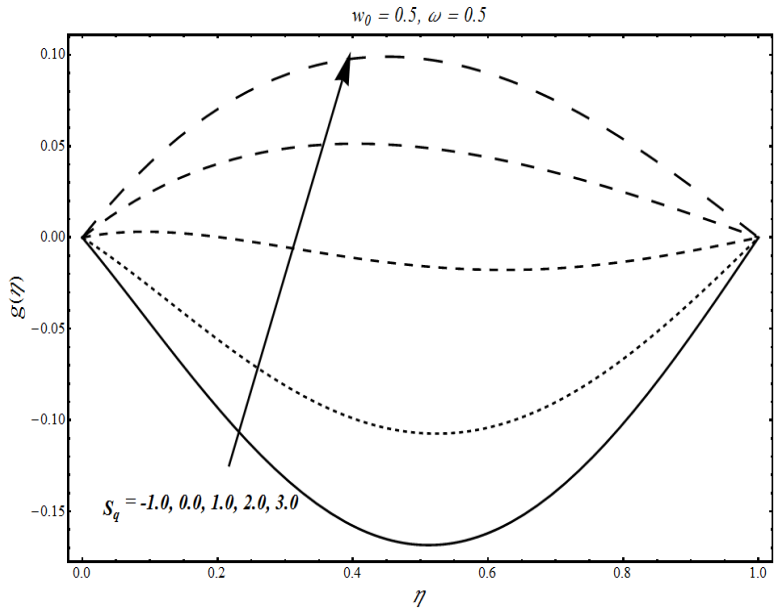

Figure 8.5: Influence of squeezing parameter S_q on velocity profile $g(\eta)$

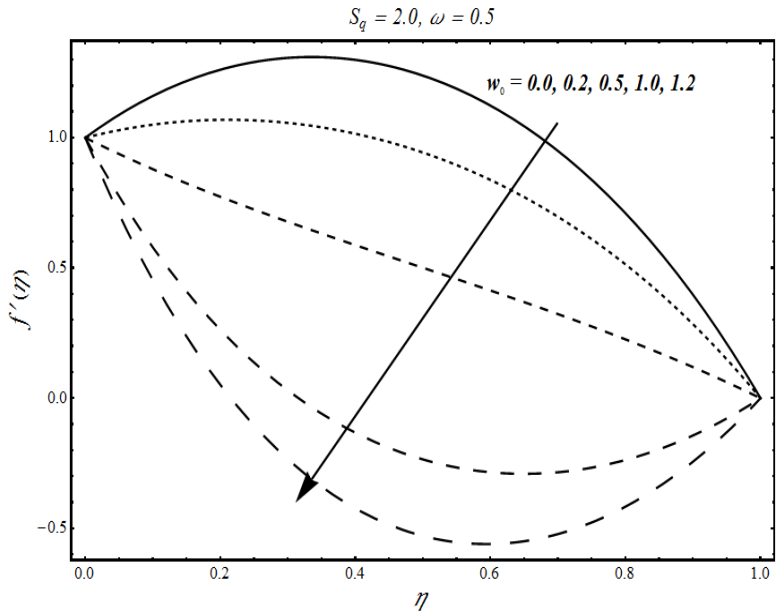

Figure 8.6: Influence of suction parameter W_0 on velocity profile $f'(\eta)$

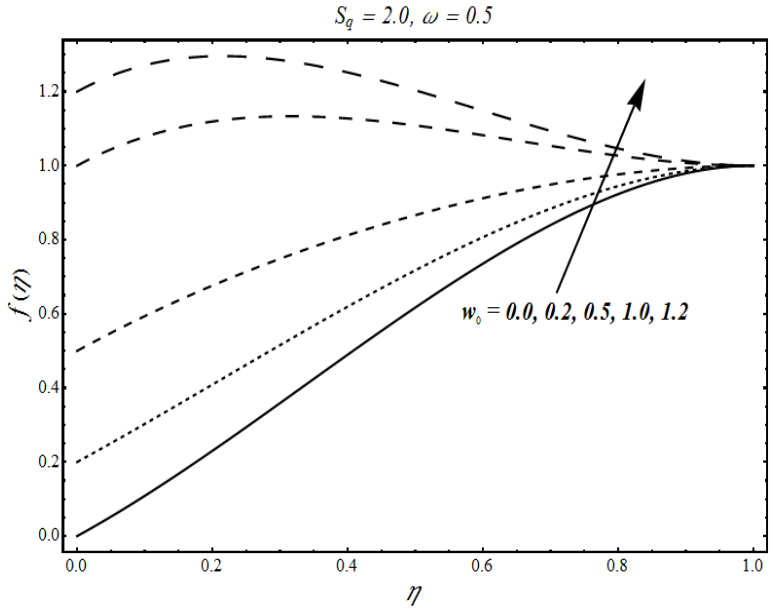

Figure 8.7: Influence of suction parameter W_0 on velocity profile $f(\eta)$

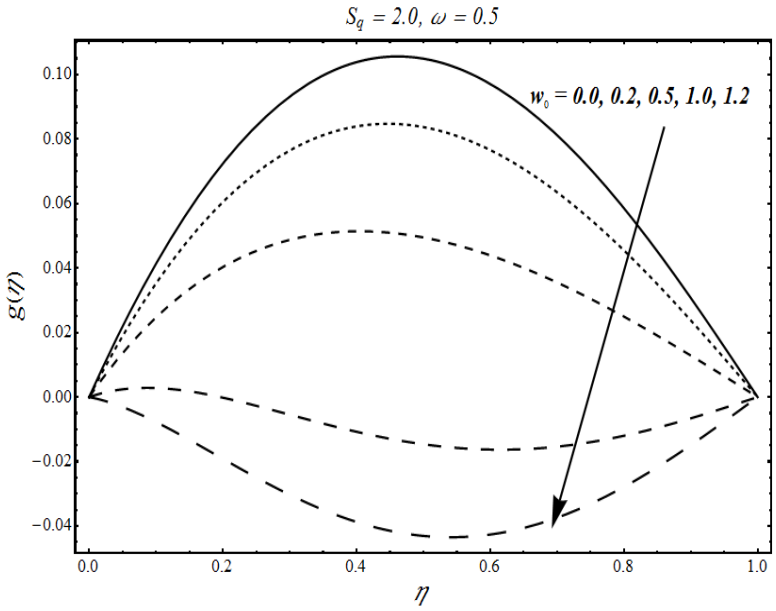

Figure 8.8: Influence of suction parameter W_0 on velocity profile $g(\eta)$

The influence of squeezing parameter on $f(\eta)$ is indicated in Figure 8.4. It is detected that the velocity component $f(\eta)$ increases near the upper plate as S_q increases which shows the squeezing effects of upper plate on fluid flow. Moreover, the velocity component $g(\eta)$ also augments with increase in S_q and these increasing effects are prominent in the central region of the channel as depicted in Figure 8.5. Figure 8.6 demonstrates the effects of suction parameter W_0 on velocity profile $f'(\eta)$. It can be seen that increase in suction parameter causes the velocity component $f'(\eta)$ to lessen. Furthermore, it is remarked that large suction from the lower permeable wall of the channel results in flow reversal. On the other hand, the consequence of variation in W_0 has significant increasing effects on the velocity component $f(\eta)$ near the lower stretching permeable wall of the channel as shown in Figure 8.7. Figure 8.8 demonstrates that the velocity component $g(\eta)$ decreases as the suction rate from the lower wall augments and for large suction, reverse flow develops.

Table 8.3 is constructed to display the numerical values of shear stresses $f''(0)$ and $g'(0)$ for variation in rotation parameter ω, suction parameter W_0 and squeezing parameter S_q. It is noteworthy that values obtained by both analytical and numerical techniques are in excellent accord with each other which is a clear validation of accuracy and cogency of our outcomes. Moreover, it is observed that $f''(0)$ and $g'(0)$ increase with an increase in the squeezing parameter S_q and rotation parameter ω and decreases as the value of suction parameter W_0 increases.

Table 8.3: Numerical values of $f''(0)$ and $g'(0)$ obtained by HAM and numerical procedure for variation in rotation parameter ω, suction parameter w_0 and squeezing parameter S_q

ω	w_0	S_q	$f''(0)$ *HAM*	$f''(0)$ *Numerical*	$g'(0)$ *HAM*	$g'(0)$ *Numerical*
0.5	0.5	−1.0	−10.214133	−10.214133	−0.707731	−0.707731
		0.0	−7.419696	−7.419696	−0.237555	−0.237555
		1.0	−4.445146	−4.445146	0.075782	0.075782
		2.0	−1.297045	−1.297045	0.300313	0.300313
		3.0	2.018006	2.018006	0.469820	0.469820
0.5	0.3	2.0	0.025724	0.025724	0.372682	0.372682
	0.5		−1.297045	−1.297045	0.300313	0.300313
	0.8		−3.369658	−3.369658	0.172282	0.172282
	1.0		−4.814071	−4.814071	0.072293	0.072293
	1.2		−6.311701	−6.311701	−0.040879	−0.040879
1.0	0.5	2.0	−1.291472	−1.291472	0.600474	0.600474
3.0			−1.231657	−1.231657	1.796681	1.796681
5.0			−1.110254	−1.110254	2.979537	2.979537
7.0			−0.924676	−0.924676	4.142754	4.142754
10.0			−0.522086	−0.522086	5.844396	5.844396

The effects of squeezing parameter S_q on temperature $\theta(\eta)$ are depicted in Figure 8.9. It can be seen that for $S_q < 0$, i.e., when the upper plate is moving apart, the temperature reduces. On the other hand, when the upper plate is moving in downwards direction, the fluid molecules come closer which generates heat energy which consequently results in a rise in the temperature. Figure 8.10 illustrates that the temperature profile decreases as the value of suction parameter w_0 increases. The effects of rotation parameter ω on

temperature are presented in Figure 8.11. It is discovered that the temperature climbs up with increase in ω which is due to high convection rate as a consequence of large rotation of fluid and channel.

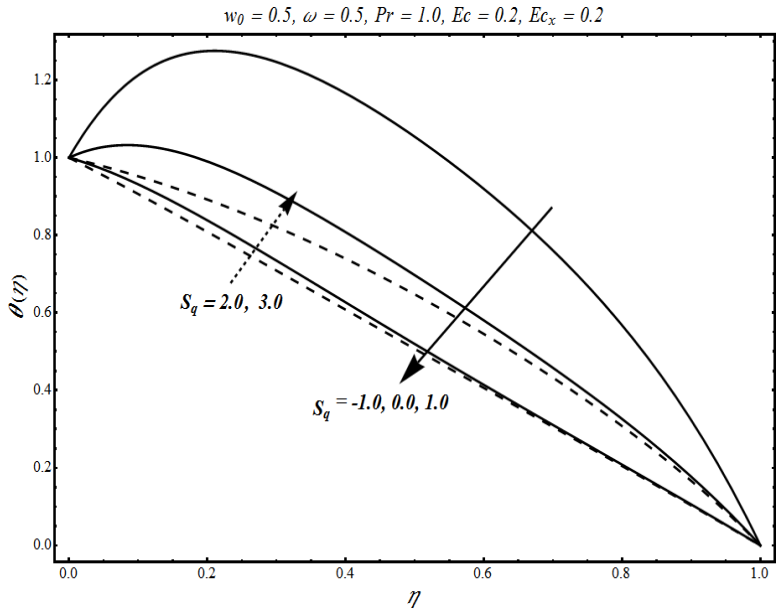

Figure 8.9: Influence of squeezing parameter S_q on temperature profile $\theta(\eta)$

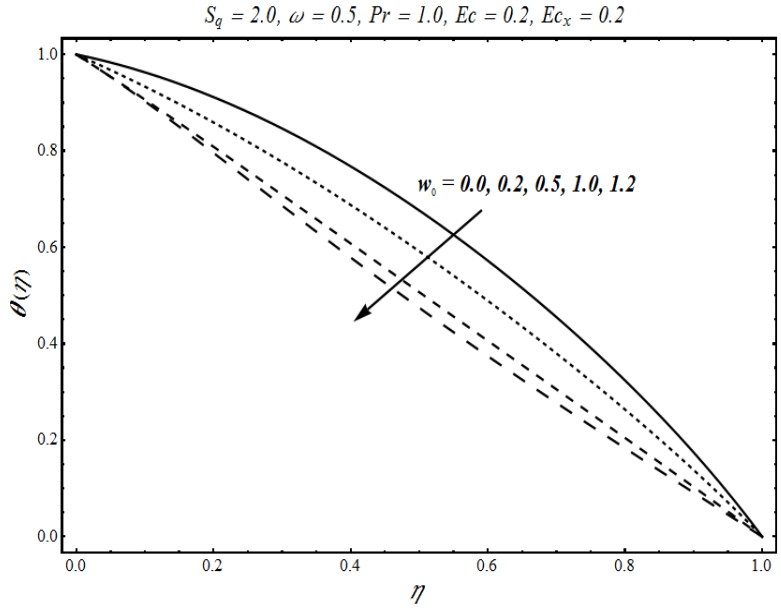

Figure 8.10: Influence of suction parameter W_0 on temperature profile $\theta(\eta)$

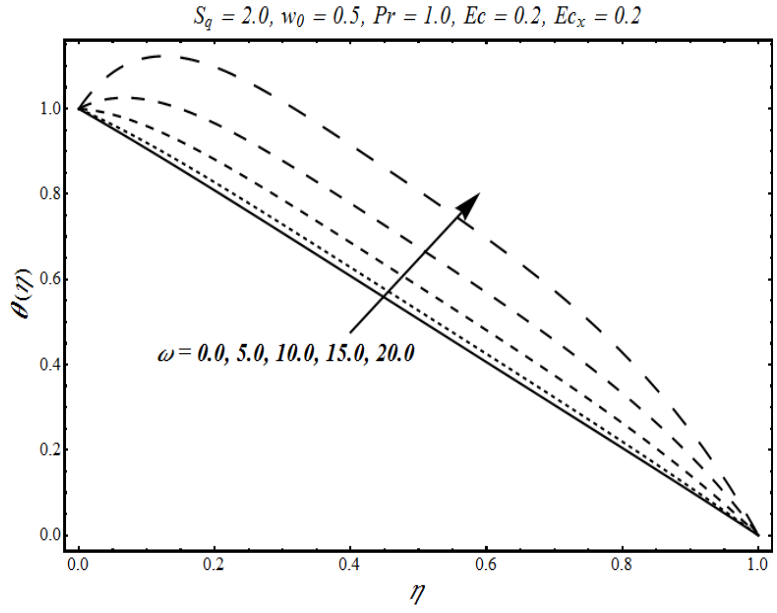

Figure 8.11: Influence of rotation parameter ω on temperature profile $\theta(\eta)$

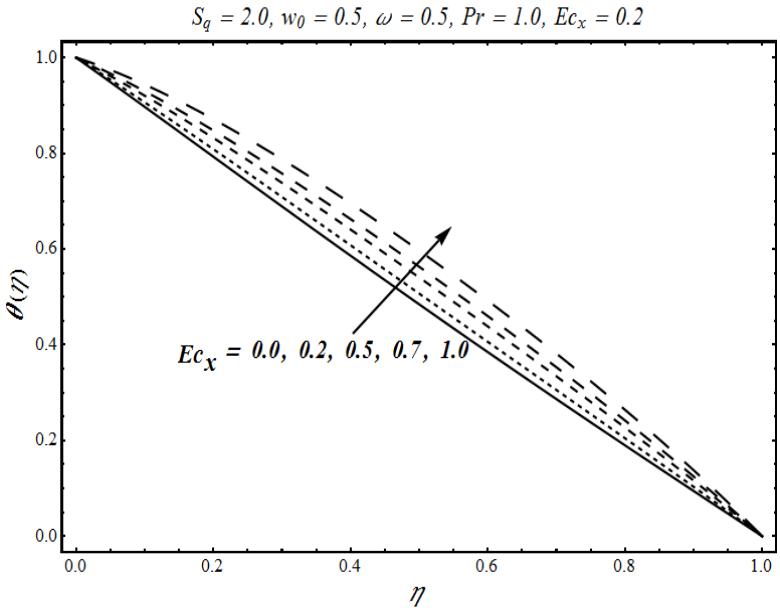

Figure 8.12: Influence of local Eckert number Ec_x on temperature profile $\theta(\eta)$

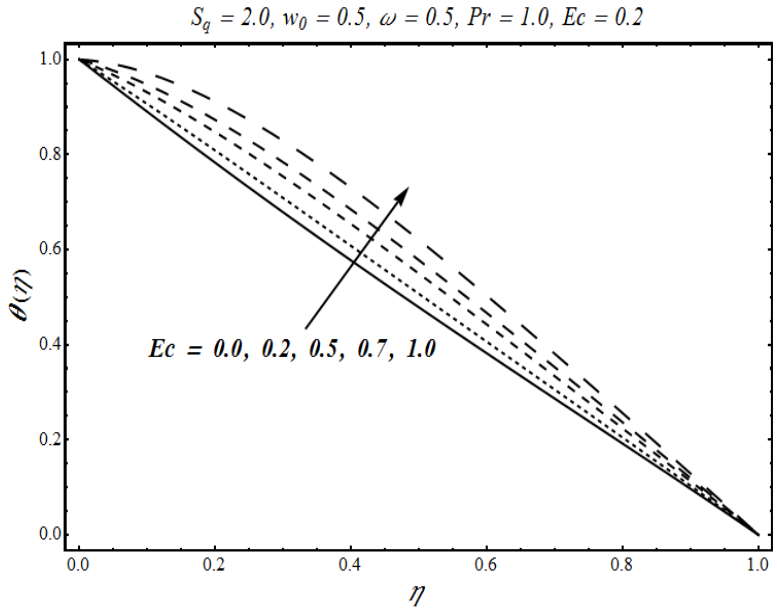

Figure 8.13: Influence of Eckert number Ec on temperature profile $\theta(\eta)$

Figures 8.12 and 8.13 are plotted to illustrate the consequence of varying the values of local Eckert number Ec_x and Eckert number Ec on temperature $\theta(\eta)$. Increasing the values of Ec_x and Ec augments the viscous dissipation effects within the fluid which consequently raises the temperature of the fluid and reduces the heat transfer rate from the lower stretching channel wall.

Table 8.4 shows the effects of various parameters on dimensionless Nusselt number. It can be seen that the heat transfer rate $-\theta'(0)$ reduces as the values of rotation parameter $\omega,$, Prandtl number $\Pr$, local Eckert number Ec_x and Eckert number Ec increase. In case of squeezing parameter S_q, it is detected that as S_q increases, the heat transfer rate first drops and then enhances for higher values of squeezing parameter. Furthermore, an increase in suction parameter w_o initially enhances $-\theta'(0)$ and then causes it to reduce.

Table 8.4: Numerical values of $-\theta'(0)$ obtained by HAM and numerical procedure for variation in rotation parameter ω, suction parameter w_o and squeezing parameter S_q

ω	w_0	S_q	Pr	Ec	Ec_x	$-\theta'(0)$ HAM	$-\theta'(0)$ $Numerical$
0.5	0.5	2.0	1.0	0.2	0.0	1.018241	1.018241
					0.2	0.906244	0.906244
					0.5	0.738249	0.738249
					1.0	0.458256	0.458256
0.5	0.5	2.0	1.0	0.0	0.2	1.110433	1.110433
				0.2		0.906244	0.906244
				0.5		0.599962	0.599962
				1.0		0.089492	0.089492
0.5	0.5	2.0	1.0	0.2	0.2	0.906244	0.906244
			2.0			0.805892	0.805892
			3.0			0.699222	0.699222
			5.0			0.468654	0.468654
0.5	0.5	−1.0	1.0	0.2	0.2	3.138926	3.138926
		0.0				0.833320	0.833320
		1.0				0.500581	0.500581
		2.0				0.906244	0.906244
0.5	0.5	2.0	1.0	0.2	0.2	0.906244	0.906244
	0.7					0.925122	0.925122
	1.0					0.660729	0.660729
	1.2					0.263867	0.263867
1.0	0.5	2.0	1.0	0.2	0.2	0.899782	0.899782
3.0						0.831333	0.831333
5.0						0.697004	0.697004
10.0						0.105967	0.105967

The effects of different physical parameters on local entropy generation number Ns are illustrated in Figures 8.14-8.17. Figure 8.14 depicts the influence of squeezing parameter S_q on Ns. A decrease in entropy production is noticed with an increase in squeezing parameter. The effects of entropy production are high at the walls of the channel, whereas, in the center, these effects are minimum. Figure 8.15 illustrates that the entropy generation number increases with increase in suction parameter w_0 near the lower permeable stretching wall. Nevertheless, in the vicinity of the upper squeezing plate, the entropy effects are not so prominent. The consequence of variation in rotation parameter ω on local entropy generation number is shown in Figure 8.16. There is an increase in entropy production as the value of ω augments and these effects are significant near the channel walls. Figure 8.17 shows the impact of variation in local Eckert number Ec_x on Ns. It is observed that the local entropy generation number increases with increase in Ec_x and these effects are more prominent near upper squeezing wall.

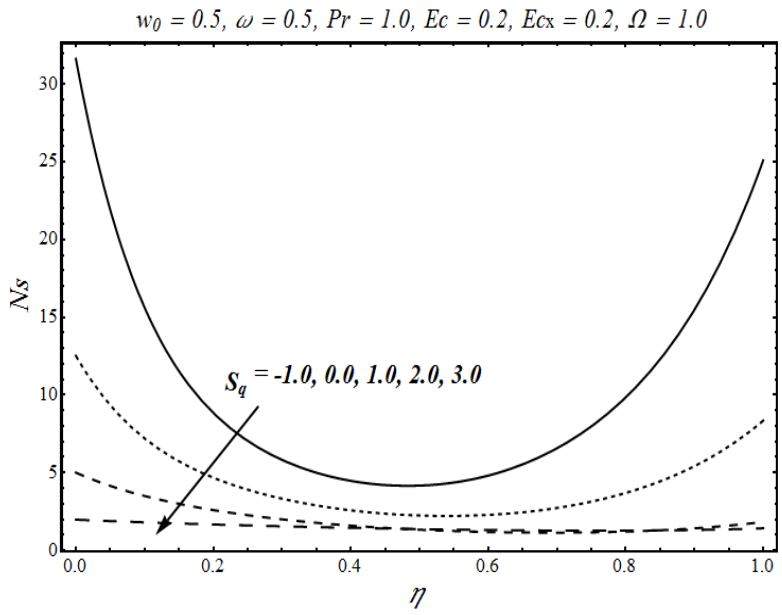

Figure 8.14: Influence of sequeezing parameter S_q on local entropy generation number Ns

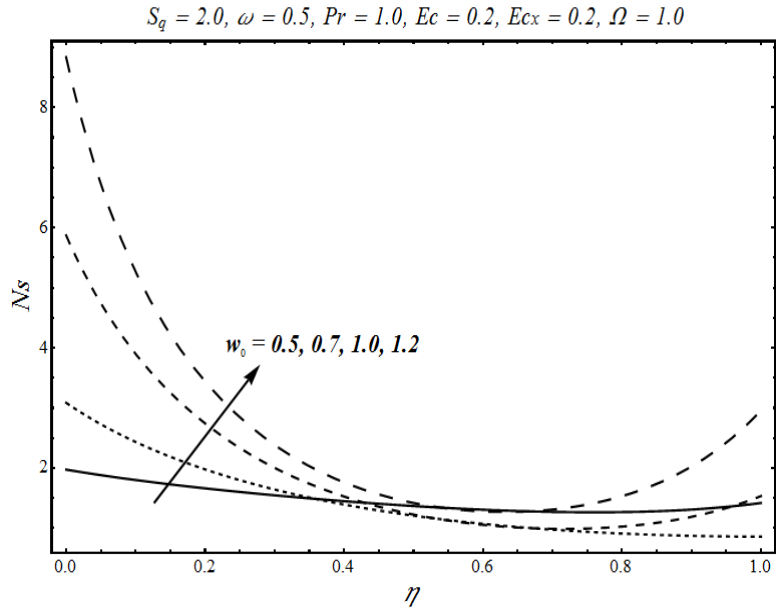

Figure 8.15: Influence of suction parameter W_0 on local entropy generation number Ns

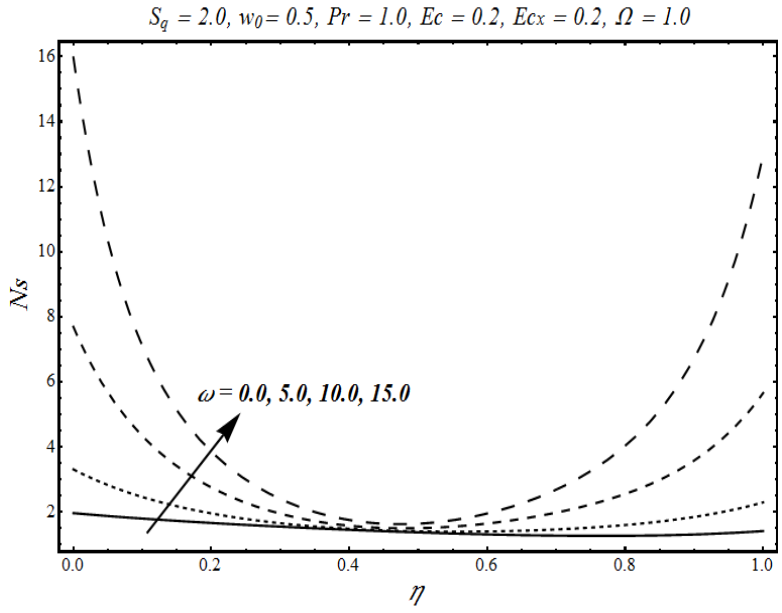

Figure 8.16: Influence of rotation parameter ω on local entropy generation number Ns

Furthermore, the local entropy generation number Ns augments with an increase in Eckert number Ec as illustrated in Figure 8.18. Furthermore, it is noteworthy that the effects of entropy production are significant near the lower permeable stretching wall of the channel.

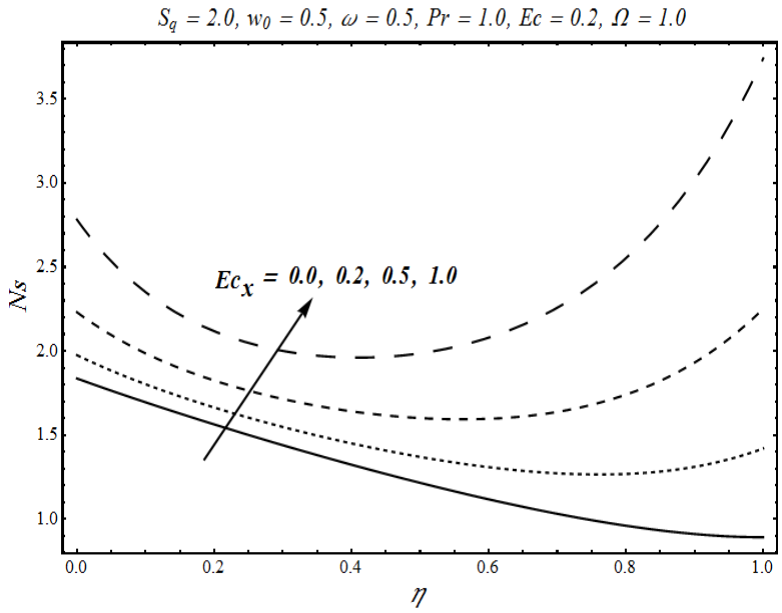

Figure 8.17: Influence of local Eckert number Ec_x on local entropy generation number Ns

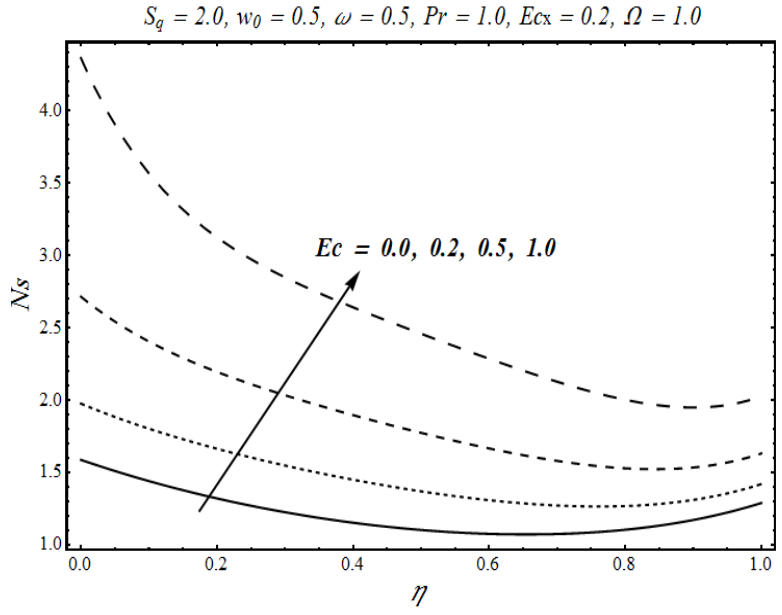

Figure 8.18: Influence of Eckert number Ec on local entropy generation number Ns

The total entropy generation number Ns_{tot} is plotted against the squeezing number S_q in Figures 8.19-8.21 and the variations of other parameters are examined. Figure 8.19 depicts that there is an increase in total entropy generation number Ns_{tot} as the value of suction parameter w_0 increases. Moreover, for a particular value of w_0, the total entropy generation number is high for small values of S_q, then it decreases as the value of S_q increases and again increasing effects are observed for large values of squeezing parameter. Figure 8.20 shows that Ns_{tot} augments with increase in local Eckert number Ec_x . Also, by fixing value of Ec_x, it is detected that a decreasing behavior in Ns_{tot} is first sighted as the squeezing parameter increases and then an increase in total entropy generation is observed at high squeezing rate. Similar effects are noticed in case of Eckert number Ec in Figure 8.21 which are more significant for larger values of S_q.

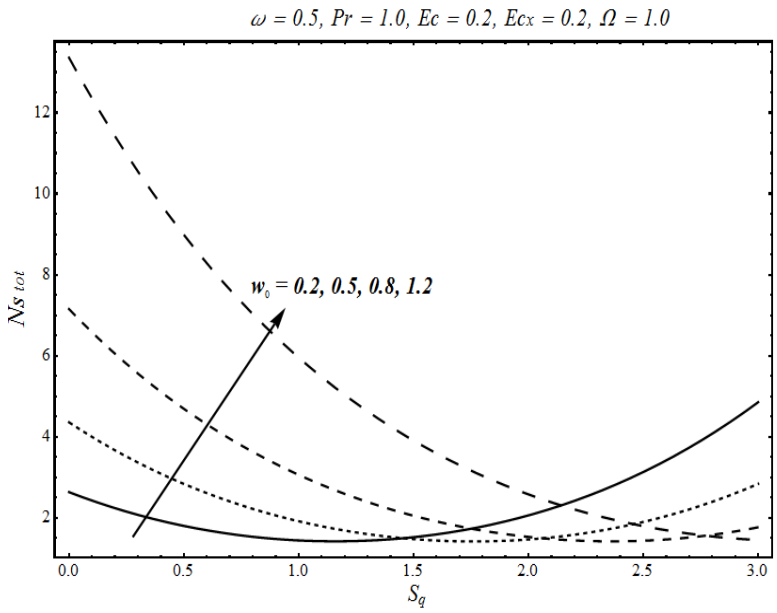

Figure 8.19: Influence of suction parameter w_0 on total entropy generation number Ns_{tot} plotted against squeezing parameter S_q

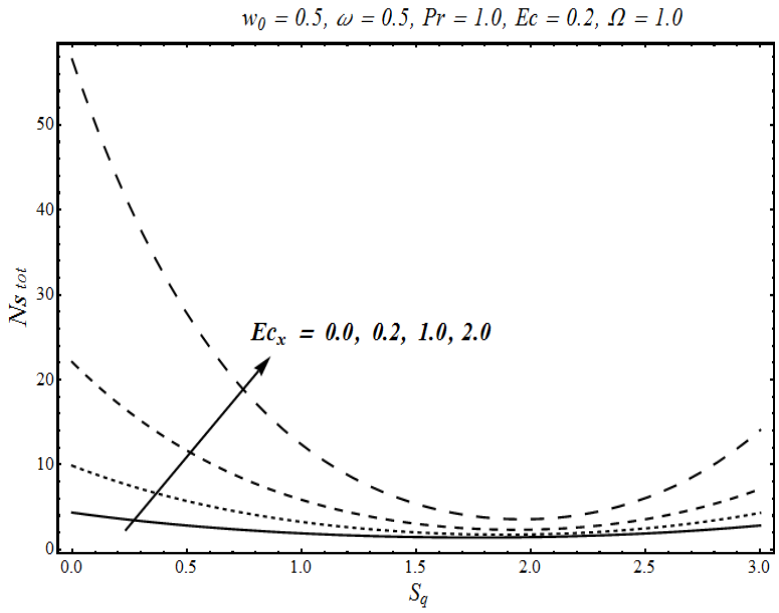

Figure 8.20: Influence of local Eckert number Ec_x on total entropy generation number Ns_{tot} plotted against squeezing parameter S_q

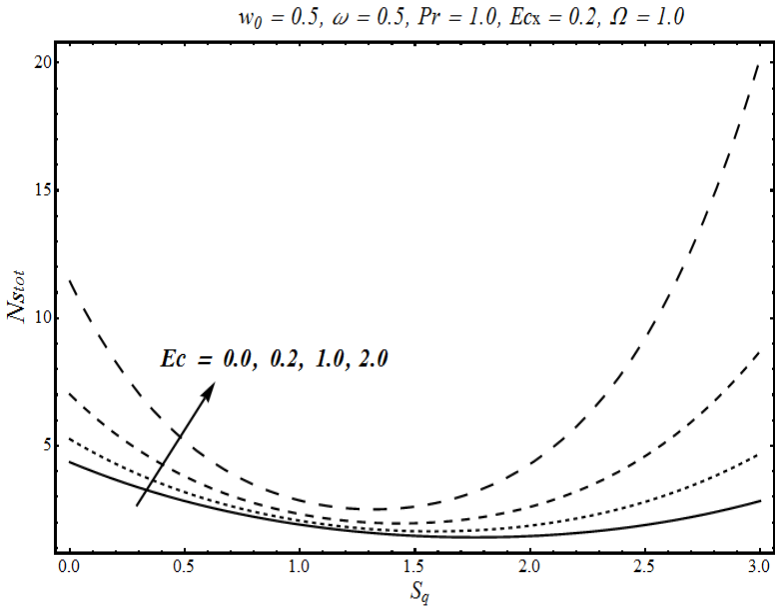

Figure 8.21: Influence of Eckert number Ec on total entropy generation number Ns_{tot} plotted against squeezing parameter S_q

Bejan number Be is plotted against η in Figures 8.22-8.25 to observe the effects of dominance of fluid friction entropy effects on the heat transfer entropy or vice versa. Figure 8.22 demonstrates the impact of squeezing parameter S_q on Bejan number. It can be seen that near the permeable stretching lower wall of the channel, the profiles are confined in the region $0 \le Be < 0.5$ which shows the fluid friction entropy dominance. On the other hand, entropy due to heat transfer is dominant near the upper squeezing wall of the channel. By observing Figure 8.23, it can be seen that with an increase in suction parameter w_0, the entropy effects due to fluid friction become dominant near the lower stretching wall of the channel. In the neighborhood of the upper plate, heat transfer entropy effects are dominant for small values of w_0 and as this value increase, fluid friction entropy effects start to become strong. The consequence of increasing local Eckert number Ec on Be is displayed in Figure 8.24. An increment in the value of Ec results in dominance of fluid friction entropy effects near both the walls of the channel. On the other hand, Figure 8.25 depicts that with an increase in Eckert number Ec, the effects of fluid friction entropy become dominant.

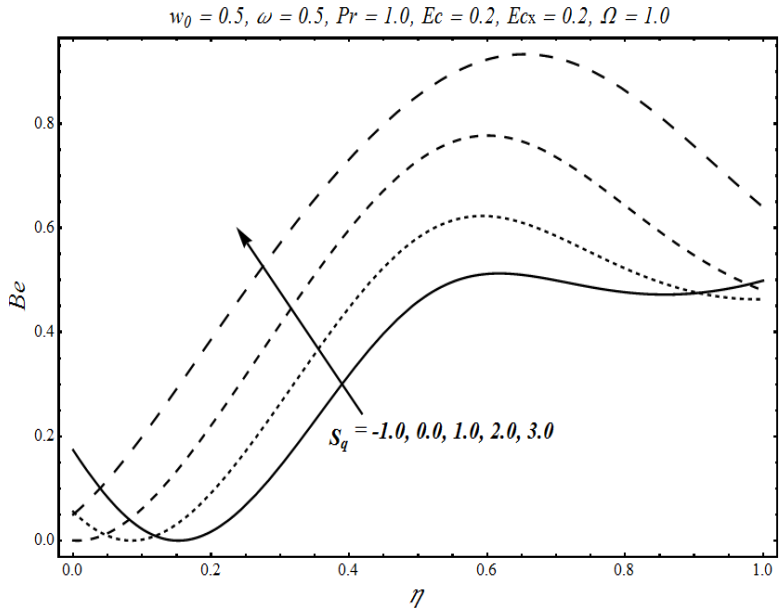

Figure 8.22: Influence of squeezing parameter S_q on Bejan number Be

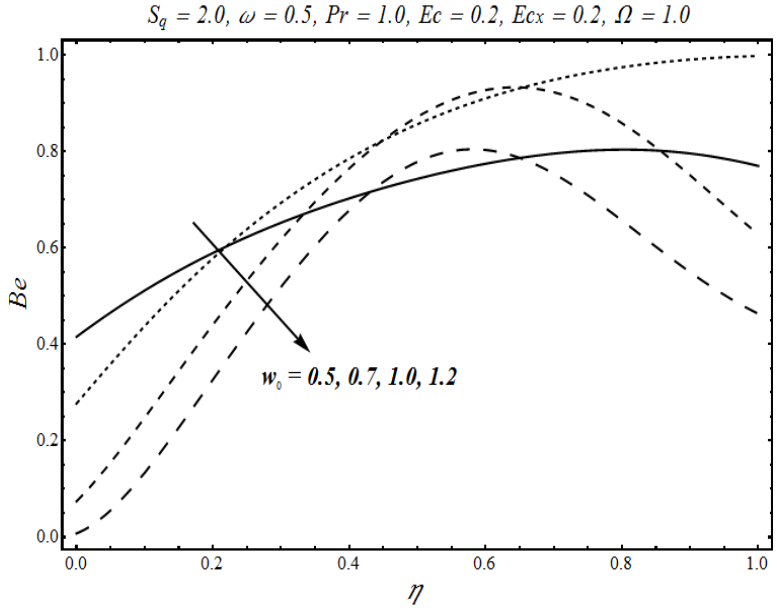

Figure 8.23: Influence of suction parameter W_0 on Bejan number Be

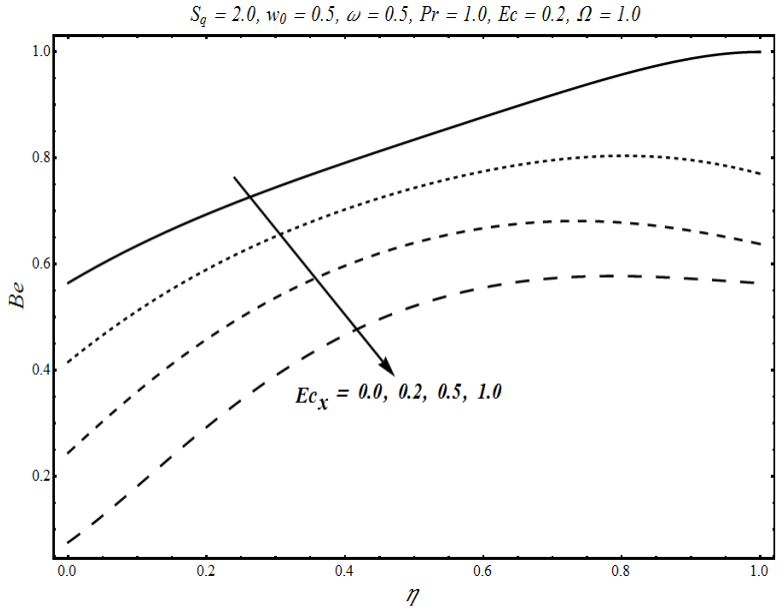

Figure 8.24: Influence of local Eckert number Ec_x on Bejan number Be

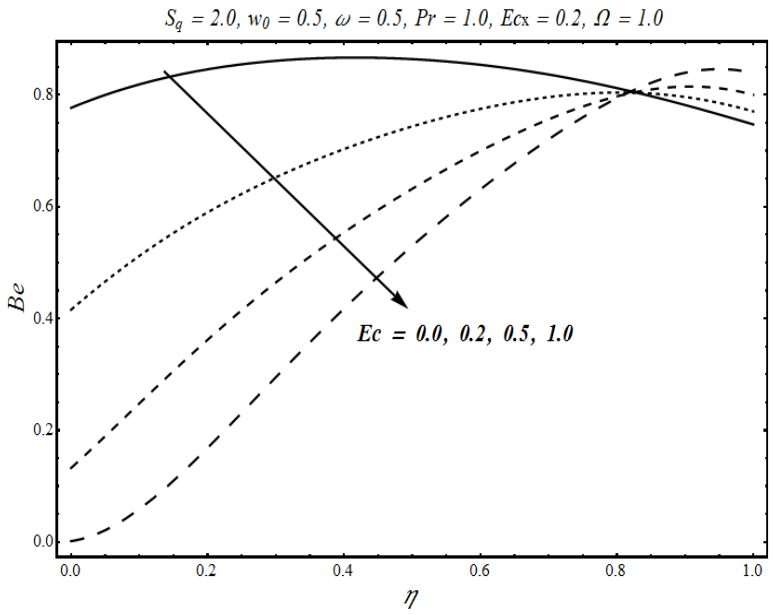

Figure 8.25: Influence of Eckert number Ec on Bejan number Be

8.5 Conclusions

Three dimensional unsteady flow and heat transfer of viscous fluid in a rotating channel with lower permeable wall is considered and the entropy effects are investigated. Furthermore, it is assumed that the lower wall is stretched in its plane and the upper wall is moving vertically downward which creates squeezing effects on flow. It is found that increase in squeezing parameter S_q causes the downward motion of upper wall to expedite which results in increase in velocities $f'(\eta)$, $f(\eta)$ and $g(\eta)$. However, increase in the value of suction parameter w_0 results in the development of reverse flow in x and z directions. Moreover, it is noticed that increase in suction through the lower stretching wall results in an increase in the velocity in y direction. The shear stresses coefficients $f''(0)$ and $g'(0)$ rise with increase in squeezing parameter S_q and rotation parameter ω and decreases with suction parameter w_0. Also, it is revealed that there is a rise in temperature as the value of rotation. Due to this increase, the heat transfer rate $-\theta'(0)$ from the lower stretching wall reduces. On the other hand, it is detected that

the temperature is a decreasing function of suction parameter w_0. An increase in local entropy generation number Ns is perceived with increase in suction parameter w_0 and rotation parameter ω whereas the squeezing parameter has decreasing effects on Ns. In case of total entropy generation number Ns_{tot}, it is noticed that increasing the value of suction parameter w_0 augments Ns_{tot}. For the squeezing parameter S_q, a decrease in total entropy generation number Ns_{tot} is first noticed with increase in S_q and then the entropy effects again start to build up as squeezing parameter S_q increases. The fluid friction entropy effects are strongest near the lower stretching surface of the channel and the heat transfer entropy effects are prominent in the neighboring region of the upper wall. The fluid friction entropy effects become strong with increase in suction parameter w_0.

Chapter 9

Conclusion

9.1 Concluding remarks

Investigation of entropy generation effects gives a physical insight of the factors that are the major cause of entropy production. It is a well established fact that the heat transfer through the surface and viscous dissipation effects are two major factors that contribute to entropy generation. During the studies carried out in the thesis, it is noticed that at the surface of linear, bidirectional and radially stretching sheets, the friction between the surface and fluid gives rise to more entropy generation. Moreover, there is a frictional force within the fluid that augments the entropy effects. Therefore, entropy generation effects are more prominent near the stretching surfaces. With an increase in the distance from the stretching surface, the value of local entropy generation number, that characterizes the entropy generation, starts to decrease and in the far away region, the effects of entropy generation are almost negligible. Thus, the entropy effects due to fluid friction are prominent near the stretching surface and heat transfer entropy effects are significant in far regime. In case of flow between radially stretching surfaces or channel having a stretching surface, the entropy effects are strongly noticeable in the vicinity of stretching surfaces and minimal at the centre. For the flow between radially stretching surfaces, it is observed that fluid friction entropy effects are prominent near the central region whereas heat transfer entropy effects are dominant near the walls. For the channel with lower wall stretching and upper wall squeezing, the fluid friction entropy effects are

prevailing at the lower stretching wall, whereas the effects of heat transfer entropy are noteworthy in the neighboring region of the upper squeezing wall.

The presence of magnetic field is another factor responsible for the generation of entropy. It has been witnessed that a retarding force develops, due to the presence of a magnetic field applied in the transverse direction to the stretching surface, which deaccelerates the fluid motion and augments the temperature. As a result, a significant increase in entropy effects is noticed with an increase in Hartmann number. This increase in the value of Hartmann number makes the entropy effects due to fluid friction more dominant over heat transfer entropy effects. In the similar manner, if the fluid flow is confined through the porous medium, the presence of porous medium causes a resistance to the flow which ultimately augments the local entropy generation number. For the viscous fluid flow between two radially stretching surfaces, the effects of entropy enhance close by the stretching surfaces but the situation reverses in the central region. Also, the Biot number Bi which measures the rate of heat transfer from the stretching sheet cause an increase in temperature and in the local entropy generation number. However, this increasing behavior is not as prominent as in the case of magnetic field and porous medium. The presence of slip condition at the stretching surface reduces the skin friction which reduces the entropy effects near the stretching sheet. The group parameter which signifies the viscous dissipation effects is also a major factor that is responsible for entropy generation. Other parameters that contribute in the enhancement of entropy effects are suction parameter, Reynolds number, local Eckert number, Eckert number and rotation parameter. On the otherhand, a decrease in entropy production is observed for squeezing parameter.

9.2 Further work

The studies that are performed in this dissertation are very useful to identify the major causes of entropy generation during flow over stretching surfaces. However, the work done in this thesis is limited to the investigation of viscous fluid flow. By taking into consideration the non-Newtonian behavior of the fluids, further information can be gathered about the factors that can affect the production of entropy. Also, all the

problems discussed are related to steady flow phenomenon. One can incorporate the effects of time and can examine its impact on the entropy generation as the flow develops. There is still a great potential to investigate the entropy effects in flow induced by stretching sheet from different physical and geometrical aspects.

9.3 List of publications

1. Adnan Saeed Butt, Asif Ali, Ahmer Mehmood, Irreversibility analysis of magnetohydrodynamic flow over a stretching sheet with partial slip and convective boundary, *International Journal of Physical Sciences*, 2(4) (2014), 46-60.
2. Adnan Saeed Butt, Asif Ali, Ahmer Mehmood, Numerical investigation of magnetic field effects on entropy generation in viscous flow over a stretching cylinder embedded in a porous medium, *Energy*, 99 (2016), 237-249.
3. Adnan Saeed Butt, Asif Ali, Investigation of entropy generation effects in magnetohydrodynamic three-dimensional flow and heat transfer of viscous fluid over a stretching surface, *Journal of the Brazilian Society of Mechanical Sciences and Engineering*, 37 (1) (2015), 211-219.
4. Adnan Saeed Butt, Asif Ali, Entropy analysis of magnetohydrodynamic flow and heat transfer over a convectively heated radially stretching surface, *Journal of the Taiwan Institute of Chemical Engineers*, 45 (4) (2014), 1197-1203.
5. Adnan Saeed Butt, Asif Ali, Analysis of entropy generation effects in flow and heat transfer of viscous fluid through a porous medium between two radially stretching surfaces, *International Journal of Exergy*, 18 (4) (2015), 501-520.
6. Adnan Saeed Butt, Asif Ali, Analysis of entropy generation effects in unsteady squeezing flow in a rotating channel with lower stretching permeable wall, *Journal of the Taiwan Institute of Chemical Engineers*, 48 (2015), 8-17.

Bibliography

[1] C.L.M.H. Navier, Mémoire sur les lois du mouvement des fluides, Mem. Acad. Sci. Inst. Fr., 6 (1823), 389-416.

[2] G.G. Stokes, On the theories of the internal friction of fluids in motion, and of the equilibrium and motion of elastic solids, Trans. Camb. Phil. Soc., 8 (1845), 287-305.

[3] L. Prandtl, Über Flüssigkeitsbewegung bei sehr kleiner Reibung, Verhandl. III. Intern. Math. Kongr. Heidelberg, (1904).

[4] J. Tyndall, Heat considered as a mode of motion (Appendix to Chapter II, pg. 52), D. Appleton and Co., (1875).

[5] A.L. Lavoisier, Elements of Chemistry in new systematic order, containing all modern discoveries. Illustrated with thirteen copper plates, translated from the French by Rober Kerr, Ist Ed., Edinburgh: William Creech, (1790).

[6] R. Clausius, The mechanical theory of heat - with its application to the steam engine and to physical properties of body, John Van Voorst, London, (1872).

[7] S. Carnot, Réflexions sur la puissance du feu et sur les machines propres à développer cette puissance, Bachelier, Paris, (1824).

[8] J. Uffink, Boltzmann's Work in Statistical Physics, Stanford Encyclopedia of Philosophy, (2004).

[9] J. W. Gibbs, Elementary Principles in Statistical Mechanics, Dover Publication, New York, (1960).

[10] A. Bejan, A study of entropy generation in fundamental convective heat transfer, J. Heat Transf., 101 (1979), 718-725.

[11] A. Bejan, Entropy generation through heat and fluid flow, John Wiley & Sons, New York, (1982).

[12] D. Poulikakos, A. Bejan, Fin geometry for minimum entropy generation in forced convection, J. Heat Transf., 10 (4) (1982), 616-623.

[13] E.F. Thacher, Entropy production and thermoelectric device performance, J. Heat Transfer, 106 (4) (1984), 881-885.

[14] P. Mukherjee, G. Biswas, P.K. Nag, Second-law analysis of heat transfer in swirling flow through a cylindrical duct, J. Heat Transf., 109 (2) (1987), 308-313.

[15] V.S. Arpaci, Radiative entropy production-cost heat into entropy, Int. J. Heat Transf., 30 (10) (1987), 2115-2123.

[16] C.H. Cheng, W.H. Huang, Entropy generation and heat transfers via laminar forced-convection channel flows over transverse fins in entrance regions, Appl. Energy, 32 (1989), 241 267.

[17] A. Selamet, V.S. Arpaci, Entropy production in boundary layers, J. Thermophys. Heat Transf., 4 (3) (1990), 404–407.

[18] C.G. Carrington, Z.F. Sun, Second law analysis of combined heat and mass transfer phenomena, Int. J. Hear Mass Transf., 34 (11) (1991), 2767-2113.

[19] C.G. Carrington, Z.F. Sun, Second law analysis of combined heat and mass transfer in internal and external flows, Int. J. Heat Fluid Flow, 13 (1) (1992), 65-70.

[20] A. Hajji, Analysis of entropy production in a heat regenerator, Int. Commun. Heat Mass Transf., 21 (1994), 9-16.

[21] M.O. Budair, Entropy analysis of unsteady flow on flat plate, Int. J. Energy Res., 25 (2001), 519-524.

[22] S. Saouli, S.A. Saouli, Second law analysis of laminar falling liquid film along an inclined heated plate, Int. Commun. Heat Mass Transf., 31 (6) (2004), 879-886.

[23] R.S.R. Gorla, D.M. Pratt, Second law analysis of a non-Newtonian laminar falling liquid film along an inclined heated plate, Entropy, 9 (1) 2007, 30-41.

[24] J.A. Esfahani, M.M. Jafarian, Entropy generation analysis of a flat plate boundary layer with various solution methods, Sci. Iranica, 12 (2) (2005), 233-240.

[25] O.D. Makinde, E. Osausi, Entropy generation in a liquid film falling along an inclined porous heated plate, Mech.Research Commun., 33 (5) (2006), 692-698.

[26] O.D. Makinde, Irreversibility analysis for a gravity driven non-Newtonian liquid film along an inclined isothermal plate, Phys. Scr., 74 (2006), 642-645.

[27] I. Ozkol, G. Komurgoz, A. Arikoglu, Entropy generation in laminar natural convection from a constant temperature vertical plate in an infinite fluid, Proc. IMechE, Part A: J. Power and Energy, 221 (2007), 609-616.

[28] A. Arikoglu, I. Ozkol, G. Komurgoz, Effect of slip on entropy generation in a single rotating disk in MHD flow, Appl. Energy, 85 (2008), 1225-1236.

[29] C.K. Chen, Y.T. Yang, K.H. Chang, Entropy generation of laminar-forced convection along the wavy surface, Int. J. Exergy, 7 (5) (2010), 564-578.

[30] A. Reveillere, A.C. Baytas, Minimum entropy generation for laminar boundary layer flow over a permeable plate, Int. J. Exergy, 7 (2) (2010),164-177.

[31] A. Tamayol, K. Hooman, M. Bahrami, Thermal analysis of flow in a porous medium over a permeable stretching wall, Transp. Porous Med., 85 (2010), 661–676.

[32] O.D. Makinde, Second law analysis for variable viscosity hydromagnetic boundary layer flow with thermal radiation and Newtonian heating, Entropy, 13 (8) (2011), 1446-1464.

[33] A. Malvandi, D.D. Ganji, F. Hedayati, M.H. Kaffash, M. Jamshidi, Series solution of entropy generation towards an isothermal flat plate, Therm. Sci., 16 (5) (2012), 1289-1295.

[34] O.D. Makinde, Entropy analysis for MHD boundary layer flow and heat transfer over a flat plate with a convective surface boundary condition, Int. J. Exergy, 10 (2) (2012), 142-154.

[35] S. Das, B.C. Sarkar, R.N. Jana, Entropy generation in MHD free convective boundary layer flow past an inclined flat plate embedded in a porous medium with Hall currents, Int. J. Comput. Appl., 84 (9) (2013), 36-46.

[36] M. M. Rashidi, N. Freidoonimehr, Analysis of entropy generation in MHD stagnation point flow in porous media with heat transfer, Int. J. Comput. Methods Eng. Sci. Mech., 15 (2014), 345–355.

[37] W.A. Khan, R. Culham, A. Aziz, Second law analysis of heat and mass transfer of nanofluids along a plate with prescribed surface heat flux, J. Heat Transf., 137 (8) (2015), 081701-081709.

[38] B.S. Yilbas, S.Z. Shuja, M.O. Budair, Second law analysis of a swirling flow in a circular duct with restriction, International J. Heat Mass Transf., 42 (1999), 4027-4041.

[39] S.H. Tasnim, S. Mahmud, Mixed convection and entropy generation in a vertical annular space, Int. J. Exergy, 2 (2002), 373-379.

[40] S. Mahmud, R.A. Fraser, Second law analysis of heat transfer and fluid flow inside a cylindrical annular space, Int. J. Exergy, 2 (4) (2002), 322-329.

[41] S. Mahmud, R.A. Fraser, The second law analysis in fundamental convective heat transfer problems, Int. J. Therm. Sci., 42 (2) (2003), 177-186.

[42] O.D. Makinde, A.W. Gbolagade, Second law analysis of incompressible viscous flow through an inclined channel with isothermal walls, Rom. J. Phys., 50 (9) (2005), 923–930.

[43] K. Hooman, Fully developed temperature distribution in a porous saturated duct of elliptical cross section with viscous dissipation effects and entropy generation analysis, Heat Transf. Res., 36 (3) (2005), 237-245.

[44] A. Andreozzi, A. Auletta, O. Manca, Entropy generation in natural convection in a symmetrically and uniformly heated vertical channel, Int. J. Heat Mass Transf., 49 (17) (2006), 3221-3228.

[45] K. Hooman, A. Haji-Sheikh, Analysis of heat transfer and entropy generation for a thermally developing Brinkman-Brinkman forced convection problem in a rectangular duct with isoflux walls, Int. J. Heat Mass Transf., 50 (21) (2007), 4180-4194.

[46] S. Chen, Z.Tian, Entropy generation analysis of thermal micro-Couette flow in slip regime, Int. J. Therm. Sci., 49 (11) (2010), 2211-2221.

[47] C.K. Chen, Y.T. Yang, K.H. Chang, Entropy generation of laminar-forced convection along the wavy surface, Int. J. Exergy, 7 (5) (2010), 564-578.

[48] N.S. Kobo, O.D. Makinde, Second law analysis for a variable viscosity reactive Couette flow under Arrhenius kinetics, Math. Probl. Eng. (2010), 278104.

[49] C.K. Chen, H.Y. Lai, C.C. Liu, Numerical analysis of entropy generation in mixed convection flow with viscous dissipation effects in vertical channel, Int. J. Heat Mass Transf., 38 (3) (2011), 285-290.

[50] T. Chinyoka, O.D. Makinde, Analysis of entropy generation rate in an unsteady porous channel flow with Navier slip and convective cooling, Entropy, 15 (6) (2013), 2081-2099.

[51] A.S. Eegunjobi, O.D. Makinde, Second law analysis for MHD permeable channel flow with variable electrical conductivity and asymmetric Navier slips, Open Phys., 13 (2015),100–110.

[52] M.Q.A Odat, R.A. Damseh, M.A.A. Nimr, Effect of magnetic field on entropy generation due to laminar forced convection past a horizontal flat plate, Entropy, 4 (2004), 293-303.

[53] S. Mahmud, R.A. Fraser, Magnetohydrodynamic free convection and entropy generation in a square cavity, Int. J. Heat Mass Transfer, 47 (2004), 3245-3256.

[54] S.A. Saouli, S. Saouli, N. Settou, N. Meza, Thermodynamic analysis of gravity-driven liquid film along an inclined heated plate with hydromagnetic and viscous dissipation effects, Entropy, *8* (4) 2006, 188-199.

[55] R.A. Damesh, M.Q.A. Odat, M.A.A. Nimr, Entropy generation during fluid flow in a channel under the effect of transverse magnetic field, Heat Mass Transf., 44 (2008), 897-904.

[56] A.S. Butt, A. Ali, Entropy effects in hydromagnetic free convection flow past a vertical plate embedded in a porous medium in the presence of thermal radiation, Eur. Phys. J. Plus, 51 (2013), 128-143.

[57] C.C. Liu, C.Y.Lo, Numerical analysis of entropy generation in mixed-convection MHD flow in vertical channel, Int. Commun. Heat Mass Transf., 39 (9) (2012), 1354-1359.

[58] M.M. Rashidi, O.A. Bég, N. Freidoonmehr, B. Rostami, Second law analysis of hydromagnetic flow from a stretching rotating disk: DTM-Padé simulation of novel nuclear MHD propulsion systems, Front. Aerospace Eng., 2 (1) (2013), 29-38.

[59] O. Mahian, H. Oztop, I. Pop, S. Mahmud, S. Wongwises, Entropy generation between two vertical cylinders in the presence of MHD flow subjected to constant wall temperature, Int. Commun. Heat Mass Transf., 44 (2013), 87–92.

[60] A.S. Eegunjobi, O.D. Makinde, Entropy generation analysis in a variable viscosity MHD channel flow with permeable walls and convective heating, Math. Prob. Eng., (2013), Article ID 630798, 12 pages.

[61] P. Vyas, N. Srivastava, Entropy analysis of generalized MHD Couette flow inside a composite duct with asymmetric convective cooling, Arabian J. Sci. Eng., 40 (2) (2015), 603-614.

[62] O.D. Makinde, A.S. Eegunjobi, M.S. Tshehla, Thermodynamics analysis of variable viscosity hydromagnetic Couette flow in a rotating system with Hall effects, Entropy, 17 (2015), 7811-7826.

[63] W.A. Khan, S.R. Gorla, Second law analysis for free convection in non-Newtonian fluids over a horizontal plate embedded in a porous medium: (prescribed heat flux), Brazilian J. Chem. Eng., 29 (3) (2012), 511-518.

[64] M. Dehsara, N. Dalir, M.R.H. Nobari, Numerical analysis of entropy generation in nanofluid over a transparent plate in porous medium in presence of solar radiation, viscous dissipation and variable magnetic field, Int. J. Comput. Methods Eng. Sci. Mech., 15 (2014), 345-355.

[65] M.H. Matin, Entropy analysis of combined heat and mass transfer over a plate embedded in a porous medium, J. Mech. Eng. Automation, 5 (3A), 26-32.

[66] E. Osausi, O.D. Makinde, Second law analysis of laminar flow in a channel filled with saturated porous media, Entropy, 7 (2) (2005), 148-160.

[67] K. Hooman, A. Ejlali, Second law analysis of laminar flow in a channel filled with saturated porous media: a numerical solution, Entropy, 7 (4) (2005), 300-307.

[68] K. Hooman, Second law analysis of thermally developing forced convection in a porous medium, Heat Transfer Res., 36 (5) (2005), 437-448.

[69] K. Hooman, Entropy energy analysis of forced convection in a porous saturated circular tube considering temperature dependent viscosity effects, Int. J. Exergy, 3 (4) (2006), 436-451.

[70] K. Slimi, Entropy generation for unsteady natural convection and radiation within a tilted saturated porous channel, Int. J. Exergy, 3 (2) (2006), 174-190.

[71] K. Hooman, F. Hooman, S.R. Mohebpour, Entropy generation for forced convection in a porous channel with isoflux or isothermal walls, Int. J. Exergy, 5 (1) (2008), 78-96.

[72] H. Heidary, M. Pirmohammadi, M. Davoudi, Control of free convection and entropy generation in inclined porous media, Heat Transf. Eng., 33 (6) (2012), 565-573.

[73] H. Dhahri, A. Boughamoura, S.B. Nasrallah, Entropy generation for pulsating flow in a cylinder filled with porous media including viscous dissipation effects, J. Porous Med., 16 (1) (2013), 60-87.

[74] L.J. Crane, Flow past a stretching sheet. Z. Angew. Math. Phys., 21 (1970), 645-647.

[75] P. Carragher, L.J. Crane, Heat transfer on a continuous stretching sheet, ZAMM- Z. Angew. Math. Mech., 62 (1982), 564-565.

[76] P.S. Gupta, A.S. Gupta, Heat and mass transfer on a stretching sheet with suction or blowing, Can. J. Chem. Eng., 55 (1977), 744–746.

[77] W.H.H. Banks, Similarity solutions of the boundary-layer equations for a stretching wall, J. Mech. Theor. Appl., 2 (1983), 375−392.

[78] Wang, C.Y., The three-dimensional flow due to stretching flat surface, Phys. Fluids, 27 (1984), 1915-1917.

[79] J. Grubka, K.M. Bobba, Heat transfer characteristics of a continuous stretching surface with variable temperature, Trans. ASME, J. Heat Transf., 107 (1985), 248–250.

[80] C.Y. Wang, Liquid film on an unsteady stretching surface, Q. Appl. Math., 48 (1990), 601-610.

[81] M.E. Ali, Heat transfer characteristics of a continuous stretching surface, Wärme-und Stofffűbertragung, 29 (1994), 227-234.

[82] K. Vajravelu, A. Hadjinicolaou, Convective heat transfer in an electrically conducting fluid at a stretching surface with uniform free stream, Int. J. Eng. Sci., 35 (1997), 1237-1244.

[83] E.M.A. Elbashbeshy, Heat transfer over a stretching surface with variable surface heat flux, J. Phys. D-Appl. Phys., 31 (1998),1951-1954.

[84] A. Sriramalu, N. Kishan, R.J. Anand, Steady flow and heat transfer of a viscous incompressible fluid flow through porous medium over a stretching sheet, J. Energy Heat Mass Transf., 23 (2001), 483-495.

[85] H.I. Andersson, Slip flow past a stretching surface, Acta Mech., 158 (2002), 121-125.

[86] C.Y. Wang, Flow due to a stretching boundary with partial slip-an exact solution of the Navier-Stokes equations, Chem. Eng. Sci., 57 (17) (2002), 3745-3747.

[87] H.S. Takhar, A.J. Chamkha, G. Nath, Flow and heat transfer on a stretching surface in a rotating fluid with a magnetic field, Int. J. Therm. Sci., 42 (2003), 23-31.

[88] I.C. Liu, A note on heat and mass transfer for a hydromagnetic flow over a stretching sheet, Int. Commun. Heat Mass Transfer, 32 (2005), 1075-1084.

[89] K. Vajravelu, J.R. Cannon, Fluid flow over a nonlinearly stretching sheet, Appl. Math. Comput., 181 (2006), 609-618.

[90] P.D. Ariel, The three-dimensional flow past a stretching sheet and the homotopy perturbation method, Comp. Math. Appl., 54 (2007), 910-925.

[91] T. Hayat, T. Javed, On analytic solution for generalized three-dimensional MHD flow over a porous stretching sheet, Phys. Lett. A, 370 (2007), 243–250.

[92] A. Mehmood, A. Ali, Analytic homotopy solution of generalized three dimensional channel flow due to uniform stretching of the plate, Acta Mech. Sin., 23 (2007), 503-510.

[93] A. Mehmood, A. Ali, Homotopy analysis of unsteady boundary layer flow adjacent to permeable stretching surface in a porous medium, Commun. Nonlinear Sci. Numer. Simul., 13 (2008), 340-349.

[94] A. Mehmood, A. Ali, H.S. Takhar, T. Shah, Unsteady three dimensional MHD boundary layer flow due to the impulsive motion of a stretching surface (Acta Mech. 146, 59-71, 2001), Acta Mech., 199 (2008), 241-249.

[95] A. Mehmood, A. Ali, T. Shah, Heat transfer analysis of unsteady boundary layer flow by homotopy analysis method, Commun. Nonlinear Sci. Numer. Simul., 13 (2008), 902-912.

[96] T. Hayat, A. Naseem, M. Farooq, A. Alsaedi, Unsteady MHD three-dimensional flow with viscous dissipation and Joule heating, Europ. Phys. J. Plus, 128 (2013), 158-173.

[97] P.D. Ariel, T. Hayat, S. Asghar, Homotopy perturbation method and axisymmetric flow over a stretching sheet, Int. J. Nonlinear Sci. Numer. Simulat., 7 (4) (2006), 399-406.

[98] C.Y. Wang, Natural convection on a vertical radially stretching sheet, J. Math. Anal. Appl., 332 (2007), 877-883.

[99] S. Shateyi, O.D. Makinde, Hydromagnetic stagnation point flow towards a radially stretching convectively heated disk, Math. Prob. Eng., (2013) Article ID 616947, 8 pages http://dx.doi.org/10.1155/2013/616947.

[100] M. Khan, A. Munir, A. Shahzad, A. Shah, Mhd flow and heat transfer of a viscous fluid over a radially stretching power-law sheet with suction/injection in a porous medium, J. Appl. Mech. Tech. Phys., 56 (2) (2015), 231–240.

[101] T. Fang, J. Zhang, Flow between two stretchable disks-An exact solution of the Navier-Stokes equations, Int. Commun. Heat Mass Transf., 35 (2008) 892–895.

[102] T. Hayat, M. Nawaz, Effect of heat transfer on magnetohydrodynamic axisymmetric flow between two stretching sheets, 65a (2010), 961 – 968.

[103] S. Munawar, A. Mehmood, A. Ali, Effects of slip on flow between two stretchable disks using optimal homotopy analysis method, Canad. J. Appl. Sci., 1 (2) (2011), 50–68.

[104] C.Y. Wang, Fluid flow due to stretching cylinder, Phys. Fluid, 31 (1988), 466-468.

[105] A. Ishak, R. Nazar, Laminar boundary layer flow along a stretching cylinder, Europ. J. Sci. Res., 36 (2009), 22–29.

[106] S. Munawar, A. Mehmood, A. Ali, Time-dependent flow and heat transfer over a stretching cylinder, Chin. J. Phys., 50 (2012), 828-848.

[107] K. Vajravelu, K.V. Prasad, S.R. Santhi, V. Umesh, Fluid flow and heat transfer over a permeable stretching cylinder, J. Appl. Fluid Mech., 7 (1) (2014), 111-120.

[108] S. Shateyi, G.T. Marewo, A new numerical approach for the laminar boundary layer flow and heat transfer along a stretching cylinder embedded in a porous medium with variable thermal conductivity, J. Appl. Math., (2013), Article ID 576453, 7 pages, http://dx.doi.org/10.1155/2013/576453.

[109] A.K. Borkakoti, A. Bharali, Hydromagnetic flow and heat transfer between two horizontal plates, the lower plate being a stretching sheet, Quart. Appl. Math., 41 (1983), 461-467.

[110] S. Munawar, A. Mehmood, A. Ali, Three-dimensional squeezing flow in a rotating channel of lower stretching porous wall, Comp. Math. Appl., 64 (2012), 1575-1586.

[111] A. H. Nayfeh, Perturbation Methods, John Wiley & Sons, New York, (2000).

[112] M.V. Dyke, Perturbation methods in fluid mechanics, The Parabolic Press, California, (1975).

[113] M.H. Holmes, Introduction to Perturbation Methods, Springer-Verlag, New York, (1995).

[114] T.Y. Na, Computational methods in engineering boundary value problem, Academic Press, New York, (1979).

[115] S.J. Liao, The proposed homotopy analysis technique for the solution of non-linear problems, Ph.D. Thesis, Shanghai Liao Tong University, (1992).

[116] P.J. Hilton, An Introduction to Homotopy Theory, Cambridge University Press, Cambridge (1953).

[117] S.J. Liao, Beyond Perturbation: Introduction to Homotopy Analysis Method, Chapman & Hall, Boca Raton, (2003).

[118] S.J. Liao, K.F. Cheung, Homotopy analysis of nonlinear progressive waves in deep water, J. Eng. Math., 45 (2003), 105 − 116.

[119] S.J. Liao, I. Pop, Explicit analytic solution for similarity boundary-layer equations, Int. J. Heat Mass Transf., 47 (1) (2004), 75 − 85.

[120] C. Wang, J.M. Zhu, S.J. Liao, I. Pop, On the explicit analytic solutions of Cheng-Chang equations, Int. J. Heat Mass Transf., 46 (10) (2003), 1855 − 1860.

[121] C. Yang, S.J. Liao, On the explicit, purely analytic solution of Von Karman swirling viscous flow, Commun. Nonlinear Sci. Numer. Simulat., 11 (1) (2006), 83 − 93.

[122] SJ. Liao, A uniformly valid analytical solution of 2D viscous flow past a semi infinite flat plate, J. Fluid Mech., 385 (1999), 101 − 128.

[123] SJ. Liao, An explicit, totally analytic approximate solution for Blasius viscous flow problems, Int. J. Nonlinear Mech., 34 (1999), 759 – 778.

[124] SJ. Liao, An analytic approximation of the drag coefficient for the viscous flow past a sphere, Int. J. Nonlinear Mech., 37 (2002), 1 − 18.

[125] SJ. Liao, A. Campo, Analytic solutions of the temperature distribution in Blasius viscous flow problems, J. Fluid Mech., 453 (2002), 411 − 425.

[126] SJ. Liao, On the analytic solution of magnetohydrodynamic flows of non-Newtonian fluids over a stretching sheet, J. Fluid Mech., 488 (2003), 189 − 212.

[127] S.J. Liao, On homotopy analysis method for nonlinear problems, Appl. Math. Comput., 147 (2004), 499 − 513.

[128] S.J. Liao, A general approach to get series solution of non-similarity boundary-layer flows, Commun. Nonlinear Sci. Numer. Simulat., 14(5) (2009), 2144 − 2159.

[129] S.J. Liao, A challenging nonlinear problem for numerical techniques, J. Comput. Appl. Math., 181 (2005), 467 − 472.

[130] S.J. Liao, A new branch of solution of boundary layer flows over an impermeable stretched plate, Int. J. Heat Mass Transfer, 48 (2005), 2529 – 2539.

[131] S.J. Liao, An analytic solution of unsteady boundary-layer flows caused by an impulsively stretching plate, Commun. Nonlinear Sci. Numer. Simulat., 11 (2006), 326 − 339.

[132] M. Sajid, I. Ahmad, T. Hayat, M. Ayub, Series solution for unsteady axisymmetric flow and heat transfer over a radially stretching sheet, Commun. Nonlinear Sci. Numer. Simulat., 13(10) (2008), 2193 − 2202.

[133] I. Ahmad, M. Sajid, T. Hayat, M. Ayub, Unsteady axisymmetric flow of a second grade fluid over a radially stretching sheet, Computer & Math. Appl., 56 (5) (2008), 1351 − 1357.

[134] M. Mustafa, T. Hayat, S. Obaidat, On heat and mass transfer in the unsteady squeezing flow between parallel plates, Meccanica, 47 (7) (2012), 1581-1589.

[135] M. Qasim, T. Hayat, S. Obaidat, Radiation effect on the mixed convection flow of a Viscoelastic fluid along an inclined stretching sheet, Z. Naturforsch., 67 a (2012), 195-202.

[136] T. Hayat, S.A. Shehzad, A. Alsaedi, Soret and Dufour effects on magnetohydrodynamic (MHD) flow of Casson fluid, Appl. Math. Mech., 33 (10) (2012), 1301-1312.

[137] S.A. Shehzad, A. Alsaedi, T. Hayat, Hydromagnetic steady flow of Maxwell fluid over a bidirectional stretching surface with prescribed surface temperature and prescribed surface heat flux, Plos One, 8 (7), e68139. doi:10.1371/journal.pone.0068139.

[138] T. Hayat, M. Qasim and Z. Abbas, Homotopy solutions for the unsteady three dimensional MHD flow and mass transfer in a porous media, Commun. Nonlinear Sci. Numer. Simulat., 15 (9) (2010), 2375-2387.

[139] S. Dinarvand, M.M. Rashidi, A reliable treatment of a homotopy analysis method for two-dimensional viscous flow in a rectangular domain bounded by two moving porous walls, Nonlinear Anal.: Real World Appl., 11 (3) (2010), 1502-1512.

[140] M.M. Rashidi, M. Keimanesh, Study of pulsatile flow in a porous annulus with the homotopy analysis method, Int. J. Numer. Meth. Heat Fluid Flow, 22 (8) (2012), 971-989.

[141] M.M. Rashidi, S.A.M Pour, T. Hayat, S. Obaidat, Analytic approximate solutions for steady flow over a rotating disk in porous medium with heat transfer by homotopy analysis method, Comput. Fluids, 54 (2012), 1–9.

[142] O.A Bég, M.M Rashidi, T.A Bég, M Asadi, Homotopy analysis of transient magneto-bio-fluid dynamics of micropolar squeeze film in a porous medium: a model for magneto-bio-rheological lubrication, J. Mech. Med. Bio., 12 (1) (2012), 1-21.

[143] M.M. Rashidi, N. Freidoonimehr, A. Hosseini, O. Anwar Bég, T.K. Hung, Homotopy simulation of nanofluid dynamics from a non-linearly stretching isothermal permeable sheet with transpiration, Meccanica, 49 (2014), 469–482.

[144] H. Xu, S.J. Liao, Series solutions of unsteady magnetohydrodynamic flow of non- ewtonian fluids caused by an impulsively stretching plate, J. non-Newtonian Fluid Mech., 129 (2005), 46 − 55.

[145] H. Xu, An explicit analytic solution for free convection about a vertical flat plate embedded in a porous media by means of homotopy analysis method, Appl. Math. Comput., 158 (2004), 433 − 443.

[146] H. Xu, S.J. Liao, Dual solutions of boundary-layer flow over an upstream moving plate, Commun. Nonlinear Sci. Numer. Simulat., 13 (2) (2008), 350 − 358.

[147] S.J. Liao, Homotopy Analysis Method in Nonlinear Differential equations, Springer, (2012).

[148] M.S. Tillack, N.B. Morley, Magnetohydrodynamics. Standard handbook for electrical engineers, 14th edition, McGraw Hill, (1998).

[149] H. Schlicting, Boundary layer theory, 6th ed., McGraw-Hill, New York, (1968).

adnan saeed butt thesis final copy

ORIGINALITY REPORT

16%	11%	8%	6%
SIMILARITY INDEX	INTERNET SOURCES	PUBLICATIONS	STUDENT PAPERS

PRIMARY SOURCES

1	Submitted to Higher Education Commission Pakistan Student Paper	2%
2	www.inderscience.com Internet Source	2%
3	Submitted to iGroup Student Paper	1%
4	Submitted to National Tsing Hua University Student Paper	1%
5	www.mdpi.com Internet Source	<1%
6	pdfs.semanticscholar.org Internet Source	<1%
7	doiserbia.nb.rs Internet Source	<1%
8	Submitted to Universiti Teknologi Petronas Student Paper	<1%
9	boundaryvalueproblems.springeropen.com	

	Internet Source	<1%
10	www.science.gov Internet Source	<1%
11	wjst.wu.ac.th Internet Source	<1%
12	Nonlinear Flow Phenomena and Homotopy Analysis, 2012. Publication	<1%
13	dl.begellhouse.com Internet Source	<1%
14	iiste.org Internet Source	<1%
15	journal-enertech.eu Internet Source	<1%
16	www.worldacademicunion.com Internet Source	<1%
17	International Journal of Numerical Methods for Heat & Fluid Flow, Volume 24, Issue 2 (2014-03-28) Publication	<1%
18	Nazim Tufail, M., and Asif Ali. "Irreversibility Analysis of MHD Flow Over an Exponentially Stretching Sheet", Heat Transfer-Asian Research, 2013.	<1%

	Publication	
19	www.emis.de Internet Source	<1%
20	nsp.naturalspublishing.com Internet Source	<1%
21	Khan, Junaid Ahmad Mustafa, M. Hayat, T.. "Numerical study on three-dimensional flow of nanofluid past a convectively heated exponentially stre", Canadian Journal of Physics, Oct 2015 Issue Publication	<1%
22	Butt, Adnan Saeed Ali, Asif. "Analysis of entropy generation effects in flow and heat transfer of viscous fluid through a porous m", International Journal of Exergy, Nov 7 2015 Issue Publication	<1%
23	Donald A. Nield, Adrian Bejan. "Convection in Porous Media", Springer Nature, 2017 Publication	<1%
24	Submitted to National Chiao-Tung University Student Paper	<1%
25	jafmonline.net Internet Source	<1%
26	www.iosrjournals.org Internet Source	<1%

27	www.m-hikari.com Internet Source	<1%
28	www.journal-enertech.eu Internet Source	<1%
29	Submitted to Midlands State University Student Paper	<1%
30	journals.plos.org Internet Source	<1%
31	Submitted to Universiti Teknologi Malaysia Student Paper	<1%
32	Hayat, T., Taseer Muhammad, S.A. Shehzad, G.Q. Chen, and Ibrahim A. Abbas. "Interaction of magnetic field in flow of Maxwell nanofluid with convective effect", Journal of Magnetism and Magnetic Materials, 2015. Publication	<1%
33	mdpi.com Internet Source	<1%
34	archive.org Internet Source	<1%
35	article.sciencepublishinggroup.com Internet Source	<1%
36	www.gigapaper.ir Internet Source	<1%

37	www.europment.org Internet Source	<1%
38	www.internationalscienceindex.org Internet Source	<1%
39	numericaltank.sjtu.edu.cn Internet Source	<1%
40	Submitted to Universiti Sains Malaysia Student Paper	<1%
41	wah.comsats.edu.pk Internet Source	<1%
42	en.wikipedia.org Internet Source	<1%
43	Aziz, Mohamed Abd El-. "Viscous dissipation effect on mixed convection flow of a micropolar fluid over an exponentially stre", Canadian Journal of Physics, April 2009 Issue Publication	<1%
44	www.ispacs.com Internet Source	<1%
45	www.segmentjournals.com Internet Source	<1%
46	dc.exa.unrc.edu.ar Internet Source	<1%
	International Journal of Numerical Methods for	

47	Heat & Fluid Flow, Volume 24, Issue 5 (2014-09-16) Publication	<1%
48	Ibáñez, Guillermo. "Entropy generation in MHD porous channel with hydrodynamic slip and convective boundary conditions", International Journal of Heat and Mass Transfer, 2015. Publication	<1%
49	Mehmood, A.. "Heat transfer analysis of three-dimensional flow in a channel of lower stretching wall", Journal of the Taiwan Institute of Chemical Engineers, 201001 Publication	<1%
50	Guven Komurgoz. "Second-Law Analysis for an Inclined Channel Containing Porous-Clear Fluid Layers by Using the Differential Transform Method", Numerical Heat Transfer Part A Applications, 01/2010 Publication	<1%
51	ajse.kfupm.edu.sa Internet Source	<1%
52	ispacs.com Internet Source	<1%
53	www.wseas.us Internet Source	<1%
54	www.researchpub.org	

	Internet Source	<1%
55	thermalscience.vinca.rs Internet Source	<1%
56	ghalambaz.ir Internet Source	<1%
57	Ramzan, M., and M. Bilal. "Three-dimensional flow of an elastico-viscous nanofluid with chemical reaction and magnetic field effects", Journal of Molecular Liquids, 2016. Publication	<1%
58	Ahmer Mehmood. "Analytic homotopy solution of generalized three-dimensional channel flow due to uniform stretching of the plate", Acta Mechanica Sinica, 09/27/2007 Publication	<1%
59	Ajibade, A.O.. "Entropy generation under the effect of suction/injection", Applied Mathematical Modelling, 201109 Publication	<1%
60	Submitted to Federal University of Technology Student Paper	<1%
61	scihost.org Internet Source	<1%
62	Ali, Farhad Khan, Ilyas Haq, Sami Ul Sha.	

	"Influence of thermal radiation on unsteady free convection MHD flow of brinkman type fluid in a poro", Mathematical Problems in Engineering, Annual 2014 Issue Publication	<1%
63	www.theo1.physik.uni-stuttgart.de Internet Source	<1%
64	scialert.net Internet Source	<1%
65	Hayat, T., M. Bilal Ashraf, and A. Alsaedi. "Small-Time Solutions for the Thin Film Flow of a Casson Fluid Due to a Suddenly Moved Plate", Journal of Aerospace Engineering, 2013. Publication	<1%
66	www.slideshare.net Internet Source	<1%
67	www.medjchem.com Internet Source	<1%
68	146.230.128.141 Internet Source	<1%
69	iasj.net Internet Source	<1%
70	www.thermalfluidscentral.org Internet Source	<1%

71	Submitted to VIT University Student Paper	<1%
72	nanoscalereslett.springeropen.com Internet Source	<1%
73	Rashidi, M.M., and N. Freidoonimehr. "Analysis of Entropy Generation in MHD Stagnation-Point in Porous Media with Heat Transfer", International Journal for Computational Methods in Engineering Science and Mechanics, 2014. Publication	<1%
74	Submitted to University Der Es Salaam Student Paper	<1%
75	Submitted to Malaviya National Institute of Technology Student Paper	<1%
76	oa.upm.es Internet Source	<1%
77	dl1.ponato.com Internet Source	<1%
78	Freidoonimehr, Navid Rostami, Behnam Ras. "Analytical modelling of three-dimensional squeezing nanofluid flow in a rotating channel on a lower ", Mathematical Problems in Engineering, Annual 2014 Issue Publication	<1%

79	Ariel, P.D.. "Axisymmetric flow due to a stretching sheet with partial slip", Computers and Mathematics with Applications, 200710 Publication	<1%
80	www.intechopen.com Internet Source	<1%
81	Submitted to Universiti Kebangsaan Malaysia Student Paper	<1%
82	www.incdfm.ro Internet Source	<1%
83	Hsiao, Kai-Long. "Viscoelastic fluid over a stretching sheet with electromagnetic effects and nonuniform heat source/s", Mathematical Problems in Engineering, Annual 2010 Issue Publication	<1%
84	Submitted to George Washington University Student Paper	<1%
85	009_djvu.txtarchive.org Internet Source	<1%
86	ijemr.net Internet Source	<1%
87	Uddin, Mohammed Jashim Beg, Osman Anwar . "Mathematical modelling of radiative hydromagnetic thermosolutal nanofluid convection slip flow in sa", Mathematical	<1%

	Problems in Engineering, Annual 2014 Issue Publication	
88	www.journalajst.com Internet Source	<1%
89	www.eudoxuspress.com Internet Source	<1%
90	apsms.org Internet Source	<1%
91	Sheikholeslami, M., H. R. Ashorynejad, G. Domairry, and I. Hashim. "Flow and Heat Transfer of Cu-Water Nanofluid between a Stretching Sheet and a Porous Surface in a Rotating System", Journal of Applied Mathematics, 2012. Publication	<1%
92	bluepenjournals.org Internet Source	<1%
93	cdn.intechopen.com Internet Source	<1%
94	Ghalambaz, M. Izadpanahi, E. Noghrehabad. "Study of the boundary layer heat transfer of nanofluids over a stretching sheet: passive control of ", Canadian Journal of Physics, July 2015 Issue Publication	<1%

95	etd.ohiolink.edu Internet Source	<1%
96	"Research Conducted by A.S. Butt and Co-Researchers Has Updated Our Knowledge about Exergy Analysis (", Science Letter, Dec 11 2015 Issue Publication	<1%
97	journal.pmf.ni.ac.rs Internet Source	<1%
98	banglajol.info Internet Source	<1%
99	studium-coaching.de Internet Source	<1%
100	Angius, Alessio Horvath, Andras Halawani. "Constructing matrix exponential distributions by moments and behavior around zero. (Research Article)", Mathematical Problems in Engineering, Annual 2014 Issue Publication	<1%
101	Lok, Y.Y.. "Non-orthogonal stagnation point flow towards a stretching sheet", International Journal of Non-Linear Mechanics, 200605 Publication	<1%
102	www.scielo.br Internet Source	<1%

103	www.iiste.org Internet Source	<1%
104	Hayat, T.. "The influence of thermal radiation on MHD flow of a second grade fluid", International Journal of Heat and Mass Transfer, 200703 Publication	<1%
105	exocomm.net Internet Source	<1%
106	dissertations.ub.rug.nl Internet Source	<1%
107	www.doiserbia.nb.rs Internet Source	<1%
108	mecano.gme.usherbrooke.ca Internet Source	<1%
109	www.insipub.com Internet Source	<1%
110	Sajid, M.. "The application of homotopy analysis method for MHD viscous flow due to a shrinking sheet", Chaos, Solitons and Fractals, 20090215 Publication	<1%
111	mat520.unime.it Internet Source	<1%

112	Submitted to Eastern Mediterranean University Student Paper	<1%
113	International Journal of Numerical Methods for Heat & Fluid Flow, Volume 23, Issue 2 (2013-05-27) Publication	<1%
114	Mahian, Omid, Hakan Oztop, Ioan Pop, Shohel Mahmud, and Somchai Wongwises. "Entropy generation between two vertical cylinders in the presence of MHD flow subjected to constant wall temperature", International Communications in Heat and Mass Transfer, 2013. Publication	<1%
115	heattransfer.asmedigitalcollection.asme.org Internet Source	<1%
116	vitalsignsreport.com Internet Source	<1%
117	lists.windowmaker.org Internet Source	<1%
118	Abd El-Aziz, Mohamed, and Tamer Nabil. "Homotopy Analysis Solution of Hydromagnetic Mixed Convection Flow Past an Exponentially Stretching Sheet with Hall Current", Mathematical Problems in Engineering, 2012. Publication	<1%

119	www.mycite.my Internet Source	<1%
120	Munawar, Sufian, Asif Ali, and Ahmer Mehmood. "Thermal analysis of the flow over an oscillatory stretching cylinder", Physica Scripta, 2012. Publication	<1%
121	pubs.sciepub.com Internet Source	<1%
122	documents.mx Internet Source	<1%
123	jacs.usv.ro Internet Source	<1%
124	Engineering Computations, Volume 29, Issue 6 (2012-08-18) Publication	<1%
125	www.mdpi.org Internet Source	<1%
126	www.scribd.com Internet Source	<1%
127	International Journal of Numerical Methods for Heat & Fluid Flow, Volume 23, Issue 5 (2013-06-08) Publication	<1%
	Submitted to Monash University Sunway	

128	Campus Malaysia Sdn Bhd Student Paper	<1%
129	ijens.org Internet Source	<1%
130	am.ippt.pan.pl Internet Source	<1%
131	Mustafa, Irfan Javed, Tariq Majeed, Abid. "Magnetohydrodynamic (MHD) mixed convection stagnation point flow of a nanofluid over a vertical plat", Canadian Journal of Physics, Nov 2015 Issue Publication	<1%
132	waset.org Internet Source	<1%
133	Famouri, M.. "Entropy generation for natural convection by heated partitions in a cavity", International Communications in Heat and Mass Transfer, 200804 Publication	<1%
134	Hayat, Tasawar, Maria Imtiaz, Ahmed Alsaedi, and Faris Alzahrani. "Effects of homogeneous–heterogeneous reactions in flow of magnetite-Fe3O4 nanoparticles by a rotating disk", Journal of Molecular Liquids, 2016. Publication	<1%
	ses.library.usyd.edu.au	

135	Internet Source	<1%
136	Rashidi, Mohammad Mehdi Ali, Mohamed Ros. "Heat and mass transfer for MHD viscoelastic fluid flow over a vertical stretching sheet with conside", Mathematical Problems in Engineering, Annual 2015 Issue Publication	<1%
137	www.astro.ku.dk Internet Source	<1%
138	freeleaks.net Internet Source	<1%
139	Anandalakshmi, R., and Tanmay Basak. "Analysis of natural convection via entropy generation approach in porous rhombic enclosures for various thermal aspect ratios", International Journal of Heat and Mass Transfer, 2013. Publication	<1%
140	Aiboud, S.. "Entropy analysis for viscoelastic magnetohydrodynamic flow over a stretching surface", International Journal of Non-Linear Mechanics, 201006 Publication	<1%
141	Yazdi, M.H. Hashim, I. Fudholi, A. Oosha. "Entropy generation analysis of power-law non-	<1%

Newtonian fluid flow caused by micropatterned moving su", Mathematical Problems in Engineering, Annual 2014 Issue
Publication

---

142 Gupta, A.K., and S. Saha Ray. "Numerical treatment for investigation of squeezing unsteady nanofluid flow between two parallel plates", Powder Technology, 2015. <1%
Publication

---

143 www.prostore.ro <1%
Internet Source

---

144 Abbas, Z. Sheikh, Mariam Sajid, M.. "Hydromagnetic stagnation point flow of a micropolar viscoelastic fluid towards a stretching/shrinkin", Canadian Journal of Physics, Oct 2014 Issue <1%
Publication

---

145 Kang, Jianhong Xia, Tongqiang Liu, Yingk. "Heat transfer and flows of thermal convection in a fluid-saturated rotating porous medium. (Research ", Mathematical Problems in Engineering, Annual 2015 Issue <1%
Publication

---

146 researchmathsci.org <1%
Internet Source

---

147 iaeme.com <1%
Internet Source

148	ourspace.uregina.ca Internet Source	<1%
149	www.internonlinearscience.org Internet Source	<1%
150	www.researchgate.net Internet Source	<1%
151	www.journalijdr.com Internet Source	<1%
152	www.vkingpub.com Internet Source	<1%
153	A Mehmood. "Unsteady boundary layer flow due to an impulsively started moving plate", Proceedings of the Institution of Mechanical Engineers Part G Journal of Aerospace Engineering, 01/01/2007 Publication	<1%
154	Bataineh, A.S.. "Homotopy analysis method for singular IVPs of Emden-Fowler type", Communications in Nonlinear Science and Numerical Simulation, 200904 Publication	<1%
155	Liao, S.. "A new analytic algorithm of Lane-Emden type equations", Applied Mathematics and Computation, 20030920 Publication	<1%

156	www.matec-conferences.org Internet Source	<1%
157	aimsciences.org Internet Source	<1%
158	article.sapub.org Internet Source	<1%
159	Srinivasacharya, D., and K. Hima Bindu. "Entropy generation in a micropolar fluid flow through an inclined channel with slip and convective boundary conditions", Energy, 2015. Publication	<1%
160	sc.hec.gov.pk Internet Source	<1%
161	sci-int.com Internet Source	<1%
162	pp.qau.edu.pk Internet Source	<1%
163	Sajid, M.. "Non-similar series solution for boundary layer flow of a third-order fluid over a stretching sheet", Applied Mathematics and Computation, 20070615 Publication	<1%
164	www.e-ijaet.org Internet Source	<1%

165	Ali, A.. "Homotopy analysis of unsteady boundary layer flow adjacent to permeable stretching surface in a porous medium", Communications in Nonlinear Science and Numerical Simulation, 200803 Publication	<1%
166	maxwellsci.com Internet Source	<1%
167	Liu, I.C.. "Heat transfer over a bidirectional stretching sheet with variable thermal conditions", International Journal of Heat and Mass Transfer, 20080715 Publication	<1%
168	www3.nd.edu Internet Source	<1%
169	ediss.uni-goettingen.de Internet Source	<1%
170	Xu, H.. "A family of new solutions on the wall jet", European Journal of Mechanics / B Fluids, 200805 Publication	<1%
171	Makinde, Oluwole Daniel Khan, Waqar Ahme. "New developments in fluid mechanics and its engineering applications.(Editorial)", Mathematical Problems in Engineering, Annual 2014 Issue	<1%

Publication

172 Noghrehabadi, Aminreza, Mohammad Reza Saffarian, Rashid Pourrajab, and Mohammad Ghalambaz. "Entropy analysis for nanofluid flow over a stretching sheet in the presence of heat generation/absorption and partial slip", Journal of Mechanical Science and Technology, 2013. <1%
Publication

173 Ahmad, Iftikhar; Ahmed, Manzoor; Abbas, Zaheer and Sajid, Muhammad. "HYDROMAGNETIC FLOW AND HEAT TRANSFER OVER A BIDIRECTIONAL STRETCHING SURFACE IN A POROUS MEDIUM", Thermal Science, 2011. <1%
Publication

174 Rastegari, M. T.; Rashidi, M. M. and Bég, O. Anwar. "HOMOTOPY ANALYSIS OF SORET AND DUFOUR EFFECTS ON FREE CONVECTION NON-NEWTONIAN FLOW IN A POROUS MEDIUM WITH THERMAL RADIATION FLUX", International Journal of Applied Mathematics & Mechanics, 2013. <1%
Publication

175 Alam, M. S.. "Diffusion-Thermo and Thermal-Diffusion Effects on Free Convective Heat and Mass Transfer Flow in A Porous Medium with <1%

Time Dependent Temperature and Concentration", International Journal of Applied Engineering Research/09734562, 20070401
Publication

176 Makinde, Oluwole Daniel. "Second Law Analysis for Variable Viscosity Hydromagnetic Boundary Layer Flow with Thermal Radiation and Newtonian Heating", Entropy, 2011. <1%
Publication

177 Kamisli, F.. "Second law analysis of a disturbed flow in a thin slit with wall suction or injection", International Journal of Heat and Mass Transfer, 20080715 <1%
Publication

178 Goldstein, R.J.. "Heat transfer-A review of 2003 literature", International Journal of Heat and Mass Transfer, 200602 <1%
Publication

179 International Journal of Numerical Methods for Heat & Fluid Flow, Volume 20, Issue 4 (2010-12-18) <1%
Publication

EXCLUDE QUOTES	OFF	EXCLUDE MATCHES	OFF
EXCLUDE BIBLIOGRAPHY	ON		